Factors limiting fast bowling performance in cricket

FACTORS LIMITING FAST BOWLING PERFORMANCE IN CRICKET

by

PAUL JAMES FELTON

A Doctoral Thesis

Submitted in partial fulfilment of the requirements for the award of Doctor of Philosophy of Loughborough University

September 2014

- ABSTRACT -

FACTORS LIMITING FAST BOWLING PERFORMANCE IN CRICKET

Paul James Felton, Loughborough University, 2014

In cricket, fast bowlers utilise the speed at which they are able to deliver the ball in order to be successful. Previous research has investigated the effect of different technique parameters on ball release speed using an experimental approach. While an experimental approach is suitable to understand the differences between bowlers it is not suitable to understand the changes required to improve a bowler's performance. The aim of this research was to investigate the factors that limit fast bowling using a theoretical approach. A 16-segment subject-specific torque-driven computer simulation model of the front foot contact phase of fast bowling was developed, with wobbling masses included within the shank, thigh and torso representations. Torque generators were included at the MTP, ankle and knee joints on the front leg, both hip and shoulder joints, and the elbow and wrist joints on the bowling arm. Subject-specific anthropometric, strength and performance data were collected from an elite fast bowler and model parameters were calculated using an angle-driven model. The torque-driven model was evaluated by matching a recorded performance with a simulation. The matching found close agreement with a difference of 4% indicating that the model was capable of reproducing realistic kinematics of the fast bowling action. Optimising the technique and initial body configuration of the fast bowler found increases in performance of 9.8% and 21.5%, respectively, where the optimal technique consisted of a more delayed bowling arm, a straighter front knee, and increased trunk flexion during the front foot contact phase, consistent with the technique employed by the fastest elite bowlers. The effects of increasing strength and varying the run-up speed were also investigated. Increasing strength by 5% was shown to improve performance by 1.3%, and varying run-up speed found an optimal run-up speed to exist.

- PUBLICATIONS -

Conference presentations:

Felton, P. and King, M. (2014). What is the effect of elbow hyperextension on ball speed in cricket fast bowling? In e*Proceedings of the 32nd Conference of the International Society of Biomechanics in Sports,*1.

Felton, P. and King, M. (2014). How does elbow hyperextension affect ball speed in cricket? In *Proceedings of the Biomechanics Interest Group of the British Association of Sport and Exercise Sciences*, 29, 10.

Felton, P., King, M., and Such, P. (2012). A biomechanical analysis of spin bowling in cricket. In *Proceedings of the Biomechanics Interest Group of the British Association of Sport and Exercise Sciences*, 27, 13.

Felton, P. and King, M. (2011). What is the effect of elbow hyperextension on ball release velocity? In *Proceedings of the Biomechanics Interest Group of the British Association of Sport and Exercise Sciences*, 26, 25.

- ACKNOWLEDGEMENTS -

I would firstly like to thank my parents, Richard and Janette, for their unwavering support and belief in all of the challenges life presents.

Secondly, I would like to thank my supervisor, Dr Mark King, for his continued guidance and support throughout this research, and for keeping me from wandering from the task in hand.

I must also acknowledge Kevin Shine, not only for the financial support of the England and Wales Cricket Board, but also for his enthusiasm and strong support in utilising this research to improve the game of cricket.

I would also like to thank everyone in the Sports Biomechanics and Motor Control Research Group and associates at Loughborough University for their assistance and friendships. There are too many to name, but I would like to reserve special thanks to Dr Fred Yeadon, Dr Sam Allen, Dr Matt Pain and Dr Michael Hiley for their thoughtful inputs and willing nature, whenever it was needed.

Finally, I would like to thank and apologise to those unfortunate enough to be my officemates during this project, Dr Martin Lewis, Dr Jon Knight, Stuart McErlain-Naylor, and Romanda Miller. The jovial nature of our friendships has certainly made the harder points of the PhD journey easier to bear.

- DEDICATION -

Edward "Ted" Wackett

(1944 – 2009)

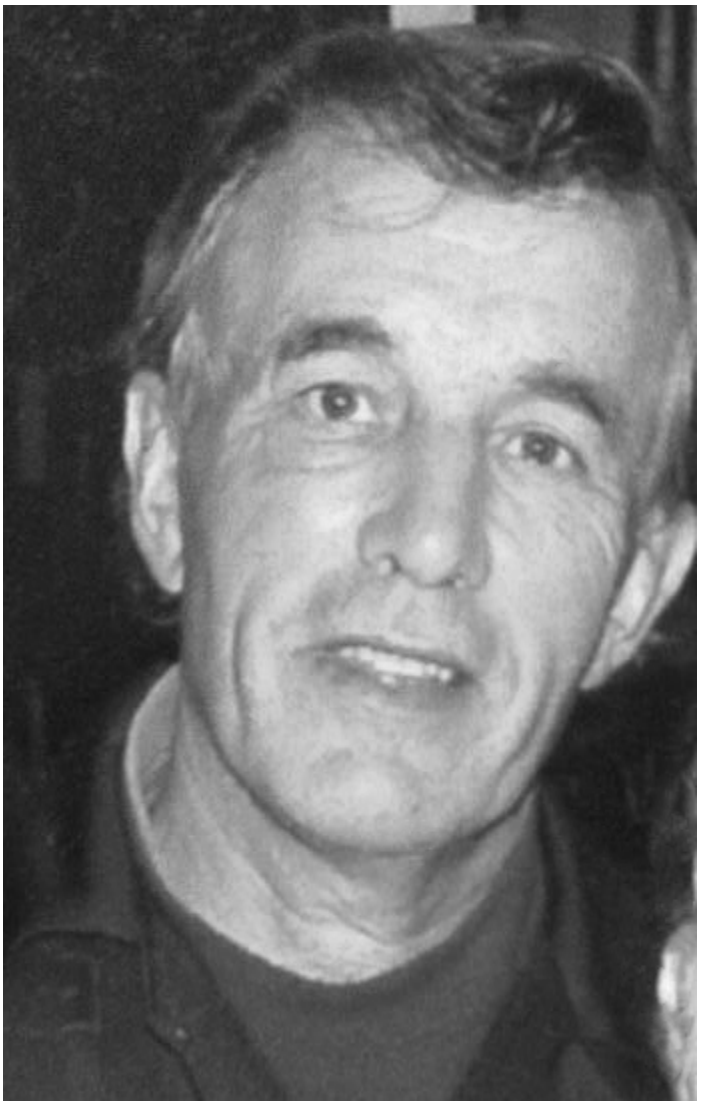

"Thank you for the hours you spent infusing the love of cricket into a 10 year old child"

- TABLE OF CONTENTS -

- LIST OF FIGURES -

- LIST OF TABLES -

- CHAPTER 1 -
INTRODUCTION

Within this chapter an introduction to cricket fast bowling is provided. The purpose of the study is outlined with reference to previous research and the research questions are posed. Finally, an overview of the thesis organisation is given along with a synopsis of each chapter.

1.1 THE AREA OF STUDY

The essence of the game of cricket entails a bowler delivering a ball towards a batsman. The aim of the game is for the batting side to score as many runs as possible before they are dismissed by the bowling side. Since 1864, when overarm bowling was introduced and legalised within the game, bowlers have split into two genres: fast bowlers and spin bowlers. Fast bowlers utilise the speed at which they are able to deliver the ball in order to minimise the batman's reaction time to interpret and select the appropriate shot. The fast bowling action (Figure 1.1) consists of a run-up, a back foot contact phase (back foot contact to front foot contact), a front foot contact phase (front foot contact to ball release), and a follow through (ball release onwards).

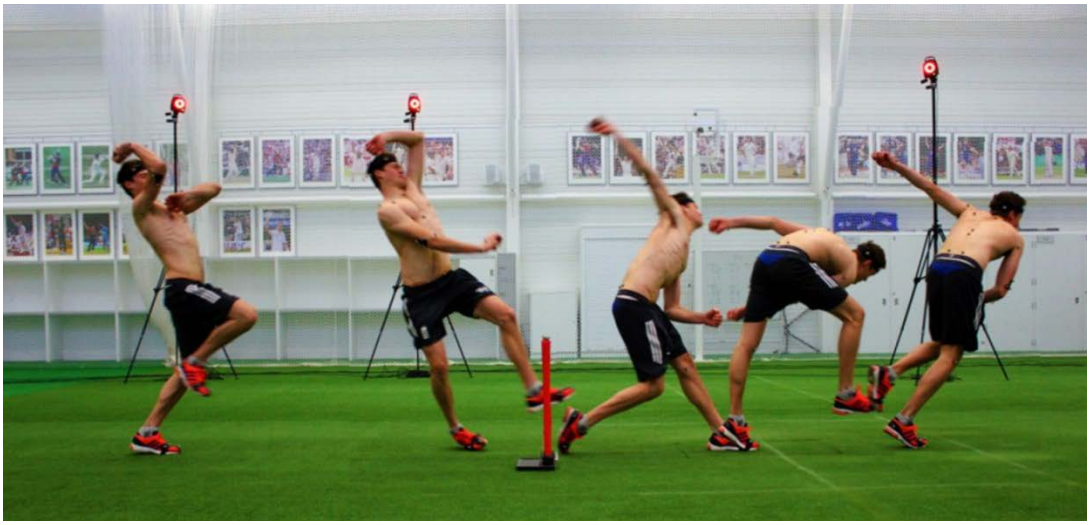

Figure 1.1. – The fast bowling action.

There are numerous experimental studies on fast bowling which have primarily focused on the relationships between ball release speed, individual technique parameters, and the forces exerted on the bowler. Investigations of individual technique parameters have concentrated on the run-up (Davis and Blanksby, 1976a; Elliott et al., 1986), the front leg (Elliott et al., 1986; Burden and Bartlett, 1990b; Portus et al., 2004), the motion of the thorax (Davis and Blanksby, 1976b; Burden and Bartlett, 1990a; Elliott et al., 1986; Portus et al., 2004) and the position of the bowling arm (Davis and Blanksby, 1976a; Elliott et al., 1986; Foster et al., 1989; Burden, 1990). A number of studies have also reported the ground reaction forces during front foot contact (Elliott et al., 1986, 1992, 1993; Foster et al., 1989; Mason et al., 1989; Saunders and Coleman, 1991; Hurrion et al., 1997a, 1997b, 2000; Portus et al., 2004). None of these studies however, attempted to link ground reaction forces with three-dimensional kinematic data of the bowling action.

The effect of individual technique parameters on ball release speed has provided contradictory arguments, most likely due to a number of technique parameters being fundamental to ball release speed rather than one. Worthington et al. (2013a) investigated the interactions between technique variables and ball release speed. It was shown that increased ball speed is linked with a faster run-up, a straight front knee at ball release, maximising thoracic flexion from front foot contact until ball release and delaying the onset of arm circumduction. Worthington et al. (2013b) also investigated the relationship between ground reaction forces and ball speed. They discovered that increased ball speeds were strongly correlated with horizontal impulse and inversely related to peak vertical ground reaction force, vertical loading rates and horizontal loading rates.

Unfortunately, since experimental based research is essentially derived from data averaged over a range of fast bowlers it is difficult to obtain a fundamental mechanical understanding of fast bowling. Therefore, the rationale of this research is to analyse the fast bowling action using a theoretical approach which will make it possible to gain an understanding of the cause and effect relationships between technique parameters, ball speed and the forces exerted

on the bowler. It will also allow the investigation of specific aspects of a fast bowler's strength or technique in order to improve performance and move towards using a subject-specific computer simulation model to directly support the coaching of elite fast bowling.

1.2 STATEMENT OF PURPOSE

A torque-driven simulation model will be developed, evaluated and then used to investigate optimum technique with regard to ball speed. A fast bowler currently within the England and Wales Cricket Board (ECB) development squad will be used to obtain subject-specific anthropometrics, strength and performance data. An angle-driven model matched to performance data will be used to determine subject-specific viscoelastic parameters. The torque-driven model will then be evaluated against performance data to ensure the model suitably represents the bowling action. Once evaluated, the model will be optimised to maximise ball speed enabling conclusions to be drawn on optimal technique.

1.3 RESEARCH QUESTIONS

Q1. How close to optimal is the technique of the bowler in this study?

A simulation model will allow an investigation into the technique of the fast bowler used within this research and its effectiveness. Subject-specific mass, inertia, anthropometry and strength data will be obtained from the bowler whilst three-dimensional kinematic data will provide a detailed representation of the technique used. A subject-specific optimal performance will be calculated by optimising the torque generator activation levels which govern the movement of the model to maximise ball release speed.

Q2. How close to optimal is the body configuration at front foot contact of the bowler in this study?

The body configuration of the bowler at front foot contact is likely to have an impact on the technique during the front foot contact phase and thus the

performance. A simulation model will be used to determine the optimal body configuration of the fast bowler used within this study and the subsequent technique employed by optimising the initial body configuration and torque generator activation levels to maximise ball release speed.

Q3. How does an increase in strength affect the performance of the bowler in this study?

A change in culture within the game of cricket has seen players train as professional athletes and spend significantly more time working on strength and conditioning in the belief that this will increase performance. There is little research however, to gauge the isolated effects that increasing strength has on ball speed within fast bowling. The torque-driven simulation model will be used to investigate the effects of increasing the strength of various muscle groups on ball speed.

Q4. How does run-up speed affect the performance of the bowler in this study?

Run-up speed has been thoroughly researched with respect to ball release speed. A positive correlation between run-up speed and ball release velocity has been found (Brees, 1989; Glazier, 2000; Ferdinands et al., 2010; Worthington et al., 2013a). Although, it has been noted that an optimum solution must exist for each individual bowler the consequences of approaching the crease too quickly are unknown. The simulation model can be used to investigate what affect increasing the approach velocity has on the bowling action up to and beyond the optimum.

1.3 CHAPTER ORGANISATION

Chapter 2 – consists of a review of the current literature regarding performance within cricket fast bowling. The review is split into two sections: experimental and theoretical research. The review of the experimental research is further split depending on whether individual or multiple variables are being linked to fast bowling, and whether the variable is kinematic, inertial

or strength related. The review of the theoretical studies is kept together due to the severe lack of this type of research in this area.

Chapter 3 – comprises relevant literature regarding all stages of constructing a simulation model. Initially, the philosophy of designing a simulation model and the available building blocks and tools for manufacturing the equations of motion are discussed. A review of the literature regarding modelling muscle is also given as well as the methods to determine subject-specific parameters. Finally, the importance of model evaluation is highlighted and model optimisation is discussed.

Chapter 4 – describes the methods and techniques used to construct a simulation model. These details include the philosophy, the body representation, the viscoelastic interfaces with external surfaces and the torque generators used.

Chapter 5 – contains the methods used to collect the performance data from an elite fast bowler and the subsequent data processing and analysis. The processes used to calculate the required model inputs such as the joint-angle time histories are also explained.

Chapter 6 – presents the methods used to determine the anthropometric and strength parameters required as inputs to both the angle and torque-driven simulation models. An explanation of the method used to determine the inertia parameters of the wobbling masses is also given.

Chapter 7 – outlines the method used to determine the model parameters required as input to the simulation model using an angle-driven model. The subsequent evaluation of the parameters using an independent trial is described and the results presented.

Chapter 8 – presents the method of evaluating the torque-driven model using the best recorded performance. The subsequent results are presented and discussed.

Chapter 9 – applies the torque-driven simulation model to answer the research questions. Fast bowling performance is optimised through adjustments to the fast bowler's initial body configuration and technique during the front contact phase of fast bowling. The results of the optimisations are presented and discussed.

Chapter 10 – a summary of the thesis is given. This includes a review of the methods used and the results obtained. Future applications of the simulation model are identified along with potential areas of improvement.

- CHAPTER 2 -

FAST BOWLING LITERATURE REVIEW

In this chapter literature from previous research investigating fast bowling in cricket has been reviewed. The review is split based on the research approach: experimental or theoretical. The experimental review is further split based on parameter type: technique (single and multiple parameter approaches discussed separately), anthropometric, or strength.

2.1 EXPERIMENTAL FAST BOWLING STUDIES

2.1.1 Individual fast bowling technique parameters vs. ball speed

The performance of a fast bowler is judged almost solely by the ball speed achieved (Bartlett et al., 1996). The greater the ball speed, the shorter the reaction time of the batsman to interpret the delivery and select an appropriate shot. The relationships between individual components of the fast bowling action and ball speed have been investigated by a number of researchers. The findings of their research is summarised below;

2.1.1.1 Run-up

The run-up has been heavily investigated with respect to ball speed with the length and speed the main focus. Each bowler has a unique run-up length usually determined by the run-up speed and anthropometrics of the bowler. Currently, there is no understanding of the optimal length of the run-up (Bartlett et al., 1996). The first study on run-up length found it was possible to release the ball at 37 ms^{-1} using a 14 pace run-up (Davis and Blanksby, 1976b). The same researchers also reported that their 6 fastest bowlers used a longer run-up (by 2.14 m) than their 6 slowest bowlers. The link however, was left unexplained. Elliott and Foster (1989) were the first to offer advice, suggesting a run-up length of between 15 and 30 m, using a controlled and rhythmical running technique.

Run-up speed has been much more thoroughly researched. Elliott and Foster (1989) proposed that a sufficient run-up speed was required to maximise the linear velocity of the body for the greatest ball speed, whilst adopting a technically correct bowling action. The percentage contribution made to ball speed by run-up speed was the focus of research by Davis and Blanksby (1976a) and Elliott et al. (1986) with values of 19% and 15% found respectively. This was calculated by subtracting the centre of mass velocity from the ball speed. Later research however, (Bartlett, 2006) suggested these findings were flawed since it assumed that all bowlers use the same technique. In reality, the percentage contribution will vary depending on technique of each individual bowler.

Brees (1989) manipulated the bowler's run-up speeds into three categories: slow, normal, and fast, and investigated the effects on ball speed, accuracy and delivery stride kinematics, whilst asking them to bowl as quickly and accurately as possible. There was a positive correlation between run-up speed and ball speed ($P < 0.05$). A negative correlation however, was found between run-up speed and accuracy ($P < 0.05$) suggesting fast bowlers chose a run-up which optimises for both speed and accuracy. However, since the slow and fast speeds were considerably different to the normal speed these findings may not accurately describe the effect of run-up variability on the ball speed of an individual during matches.

A strong correlation between the horizontal velocity of the run-up during the pre-delivery stride (5.9 ± 0.7 ms^{-1}) and ball speed ($r = 0.728$, $P < 0.05$) was also observed by Glazier et al. (2000). Ferdinands et al. (2010) similarly found run-up speed to be positively correlated with ball speed ($r = 0.580$, $P<0.05$), but also stated that other kinematic factors are required to explain the variance in ball speed among fast bowlers. However, Burden (1990) found no relationship between the velocity of the bowler at ball release and ball speed, although, it is unlikely that the speed at the point of ball release is representative of the run-up speed.

Finally, results have also been reported where run-up speed may depend on, or impact, other factors within the bowling action who may affect ball speed. Elliott and Foster (1984) discovered that fast bowlers which adopt a front-on technique are able to run-up faster and convert more of their horizontal velocity into ball speed compared to bowlers with a side-on technique (4.5 ± 0.1 ms^{-1} vs. 3.9 ± 0.1 ms^{-1}). Brees (1989) discovered that increased run-up speeds were associated with decreased flexion and lateral flexion of the trunk, as well as increased front knee flexion between front foot contact and ball release. The run-up speed has been further linked to delivery stride length and bowler physique (Marylebone CC, 1976; Elliott et al. 1986). Elliott and Foster (1989) reported that the bowler with the slowest run-up speed (3.8 ms^{-1}) also had the shortest delivery stride length (1.34 m) whilst the bowler with the quickest run-up (4.6 ms^{-1}) had the longest delivery stride (1.67 m). They also reported that bowlers approaching the crease too quickly may exhibit a reduced delivery stride length which may restrict them from bowling with a side-on action. Although, Bartlett et al. (2006) concluded that there is currently insufficient evidence to substantiate a general conclusion on the relationship between delivery stride length and run-up speed, Ferdinands et al. (2010) discovered a positive correlation ($r = 0.572$, $P = 0.001$).

2.1.1.2 Delivery Stride

There is a limited amount of research conducted on the relationship between ball speed and the technical fundamentals during the delivery stride. The Marylebone Cricket Club (1976) advises that the bowler's weight should be on the back foot at back foot contact and leaning away from the batsman to bowl fast. Wormgoor et al. (2010) discovered that there was a significant correlation between the height of the front ankle during the delivery stride and ball speed ($r = 0.44$, $P = 0.019$). It was speculated that a higher ankle promotes a backwards lean and could assist in the efficient transfer of run-up momentum over the same ankle between front foot contact and ball release resulting in a higher ball speed. This technique is similar to some javelin techniques which maximise the acceleration path of the javelin as proposed by Bartlett and Best (1988). Ferdinands et al. (2010) found a strong negative correlation between

ball speed and centre of mass acceleration during the delivery stride (r = -0.472, P = 0.006). The deceleration of the mass centre during the delivery stride was shown using a stepwise linear regression model to explain 43.1% of the variance in ball speed, and was the most important parameter associated with ball speed. Furthermore, they also reported that there was little correlation between stride length and ball speed (r = 0.113, P = 0.533).

2.1.1.3 Front Knee Technique

The relationship between ball speed and the motion of the front knee from front foot contact to ball release has been well documented. Portus et al. (2004) highlighted that bowlers who extend their front knee bowl faster than those who flexed or extended their knee less (r = 0.37, P = 0.02). Furthermore, they categorised their bowlers according to front knee classifications (flexor, flexor-extender, extender or constant brace) and, although when comparing ball release velocities between groups no significant differences were found, ball release velocities were generally quicker between extenders and flexor-extenders.

A significant correlation between ball speed and knee angle at ball release (r = 0.41) was discovered by Burden and Bartlett (1990a). Additionally, the bowlers who did not flex their front knee after front foot contact bowled significantly faster than those that did. Elliott et al. (1986) and Portus et al. (2004) have both suggested that a front knee which is extended, or extends, during the phase between front foot contact and ball release may permit a more efficient transfer of kinetic energy to the ball and assist faster ball release velocities. Elliott et al. (1986) even suggested that a front knee angle greater than 150° is sufficient to provide this benefit. The importance of the relationship between front knee angle at ball release and ball speed was further confirmed by the significant correlation (r = -0.47, P = 0.019) found by Wormgoor et al. (2010). They also reported a relatively strong relationship (r^2 = 0.27) between knee extension and ball speed indicating that the less the front knee flexes between front foot contact and ball release the faster the ball speed. Worthington et al. (2013a) also observed that a more extended front knee at ball release characterised

the fastest bowlers, as well as maintaining a straight knee from front foot contact to ball release.

Finally, when comparing bowlers of different abilities mixed results have been found with regard to the front knee. Burden and Bartlett (1990a) compared a group of elite fast bowlers against another consisting of college medium-fast bowlers, reporting that the greatest difference was the behaviour of their front knee between front foot contact and ball release. However, Stockill and Bartlett (1994) found no such difference between two groups of international and junior bowlers.

2.1.1.4 Thoracic Motion

The relationship between ball speed and the parameters associated with the trunk, including those used to classify fast bowling actions (side-on, front-on or mixed), have been investigated. These include shoulder and pelvis orientations at back foot contact, shoulder counter rotation and pelvis-shoulder separation angles. Stockill and Bartlett (1992) found no significant relationships between ball speed and these parameters, implying that action type (front on, side-on or mixed) was not important in generating ball speed.

Portus et al. (2004) discovered a significant relationship between ball speed and the timing of the maximum pelvis-shoulder separation angle during the delivery stride. For the bowlers whose maximum pelvis-shoulder separation angle occurred after front foot contact rather than before, the ball speed was significantly faster ($r = 0.34$, $P = 0.05$). Furthermore, they found a correlation between shoulder girdle rotation (shoulder forwards rotation) and ball speed prior to ball release ($r = 0.30$, $P = 0.05$). Shoulder counter rotation however, had no correlation with ball speed ($r = 0.009$, $P = 0.95$). Wormgoor et al. (2010) observed a significant negative correlation between shoulder alignment in the transverse plane at front foot contact and ball speed ($r = -0.47$, $P = 0.013$), suggesting that the smaller the shoulder alignment angle (i.e. shoulders rotated away from the batsman) at front foot contact the faster ball speed.

Trunk flexion has also been reported to provide a significant contribution to ball speed. Davis and Blanksby (1976b) and Elliott et al. (1986) calculated that trunk flexion contributed 11% and 13% to the final ball speed, respectively. Trunk flexion-extension angles have also been compared between a group of nine college bowlers and seven professional bowlers (Burden and Bartlett, 1990a). Trunk angles were similar for both groups at back foot contact and front foot contact, a difference however, was found between front foot contact and ball release. The professional bowlers had higher maximum trunk angular velocities than their college counterparts (529°s^{-1} vs. 355°s^{-1}), as well as being in a more flexed position at ball release (60° vs. 49°). Worthington et al. (2013a) suggested that fast bowlers use thoracic flexion to generate ball speed.

2.1.1.5 Bowling Arm

Although, there is little research on the bowling arm regarding its effect on ball speed, it has been reported that the action of the arm contributes 40-50% towards the final ball speed (Davis and Blanksby, 1976a; Elliott et al., 1986). Tyson (1976) suggested that the arm position at front foot contact can be used as a good predictor of ball speed, with faster bowlers delaying the onset of upper arm circumduction for as long as possible. The position of the arm at ball release has also been considered. Davis and Blanksby (1976a) concluding that quicker bowlers release the ball with the arm behind the line of the trunk (mean 158°). Worthington et al. (2013a) found that the single variable which explained the most variance in ball speed was shoulder angle at ball release. The fastest bowlers tended to have their upper arm further back relative to their thorax confirming Davis and Blanksby's (1976a) observation.

There are no reported links between ball release height and ball speed. Studies have shown that ball release height relative to standing height has varied with 114% (Elliott et al., 1992), 116% (Elliott and Foster, 1984) and 118% (Foster and Elliott, 1985) all being reported. Theoretically, ball release height is likely to be linked to delivery stride, knee angle at ball release, and the amount of trunk flexion and lateral flexion at ball release. However, no relationships have been reported between these variables.

Portus et al. (2006) investigated the relationship between elbow extension and ball speed with respect to investigating the law which permits a maximum of 15° elbow extension between the upper arm being horizontal and ball release. It was found that the group extending beyond the threshold bowled significantly faster (effect size = 1.4, p = 0.006) than the group below the threshold (39.5 ± 2.0 vs. 37.1 ± 1.4 ms^{-1}). Furthermore, research has shown that the elbow can be forced into "hyperextension" during the bowling action (Ferdinands and Kersting, 2004; Portus et al., 2006). However, the effect of elbow hyperextension on ball speed has not been identified experimentally since its effect cannot be isolated.

2.1.2 Multiple fast bowling technique parameters vs. ball speed

The majority of previous research has focussed individually on one of the previously mentioned technique parameters and ball speed. However, relatively few have focussed on a combination of these factors being behind the generation of ball speed. Loram et al. (2005) demonstrated that 85% of the variation in ball speed in school boy bowlers could be explained by the front knee kinematics and the angle at which peak shoulder torque was generated. Salter et al. (2007) reported that from four delivery stride variables 87.5% of the variance of ball speed could be predicted. However, this was for an individual bowler and was therefore subject-specific.

Worthington et al. (2013a) was the first to try and identify these parameters in a group of elite fast bowlers, and discovered that 73.6% of the variance could be explained by four technique parameters which have been previously researched individually. These parameters were run-up speed, knee angle at ball release, thoracic flexion from front foot contact until ball release and shoulder angle at front foot contact. The fastest bowlers were found to have a quicker run-up and a more extended front knee at ball release. They also had greater thoracic flexion between front foot contact and ball release, as well as appearing to delay the onset of upper arm circumduction, indicated by a larger shoulder angle at front foot contact.

2.1.3 Anthropometric measurements vs. ball speed

Although the relationships between various anthropometric measurements (height, upper limb lengths, and skinfolds) and ball speed have been researched, the results are inconclusive. Stockill and Bartlett (1994) and Glazier et al. (2000) reported that longer limb lengths contribute to a faster ball speed whereas, Loram et al. (2005) and Wormgoor et al. (2010) found that no correlations existed between ball speed and any anthropometric variables. Although longer limbs must in theory benefit some bowlers, based on the present research these measurements have a minor impact on ball speed in high performance bowlers.

2.1.4 Strength parameters vs ball speed

The relationship between joint torques and ball release speed has been scarcely investigated experimentally. Wormgoor et al. (2010) assessed the concentric and eccentric isokinetic strength of selected knee and shoulder muscle groups. They concluded that the only significant correlation was between shoulder extension peak torque and ball speed, implying the stronger the shoulder extensors are the higher ball speed. Only one delivery was analysed per bowler, however, which is a severe limitation when analysing ball speed.

2.2 THEORETICAL FAST BOWLING STUDIES

Theoretical modelling of the fast bowling action employing simulation models is still in its preliminary stages. Ferdinands et al. (2008) used a 15 segment rigid body model to investigate the causal factors associated with counter-rotation of fast bowlers. Since the paper was primarily a methodological paper to show the potential of a forward dynamic simulation model in cricket bowling, the model has major assumptions and has no optimisation approach. Therefore, nothing of note has been concluded from it except that a simulation model of fast bowling would be a useful tool to investigate optimal performance in fast bowling.

Wells et al. (2012) used a 10 segment kinematic chain model to investigate the impact of elbow extension on wrist velocity in fast bowling. The model was driven using the angle-time histories of recorded performances for twelve right handed male fast bowlers of first grade level within Australia. In order to investigate the effect elbow extension had on ball release velocity the elbow angle-time histories were amplified and the results observed. Although, it was concluded that elbow joint extension does not result in an increase in wrist joint speed in fast bowling, the use of an angle-driven model has its limitations since the implications of the manipulation of the angle-time history can lead to unrealistic joint angles, velocities or joint torques.

2.3 SUMMARY OF LITERATURE

A number of experimental studies aiming to discover the effect of an individual technique parameter on fast bowling performance have been discussed. While these experimental studies provided some insight into the mechanics of the fast bowling action, contradictory arguments exist. Although, Worthington (2013a) highlighted that more than one characteristic of the fast bowling action was significant in producing ball speed in fast bowling, questions still remain regarding the mechanical understanding of the fast bowling action. Currently, a forward dynamics model has not been used to investigate the mechanics of fast bowling. An accurate simulation model will provide a better understanding of the fast bowling action and answer questions that cannot be addressed experimentally, as well as, allowing findings from previous studies to be confirmed or refuted.

- CHAPTER 3 -
LITERATURE ON CONSTRUCTING A SIMULATION MODEL IN SPORT

This chapter describes the philosophy and process of constructing a computer simulation model. Descriptions of the elements of simulation models, such as rigid bodies and elastic structures to represent the body segments, as well as the various methods of representing the force generating capabilities of muscle are given. The methods used to determine the performance and subject-specific data are also covered, plus the model evaluation and optimisation phases.

3.1 MODEL PHILOSPHY

The complexity of a simulation model will always be a simplification of reality since the human body consists of over 200 bones and 500 muscles. The degree of complexity depends on the activity being simulated and the purpose of the study (Yeadon and King, 2008). As a general rule, the model should be as simple as possible, while being sufficiently complex to answer the questions set (Alexander, 1992).

The level of complexity is often limited by the type of activity required to be modelled. Simulation models can either be angle-driven or torque-driven. Angle-driven models use the joint angle-time histories to calculate the whole body orientation and mass centre position, as well as the required joint torques and ground reaction forces. Torque-driven simulation models use joint torques or the muscle force-time histories with the resulting kinematics and kinetics calculated.

Angle-driven models have typically been used to model more complex activities, such as the aerial phase of sports movements, since the complexity is not limited by the representation of the strength elements. Activities have ranged from diving (Miller, 1970), high jumping (Dapena, 1981), trampolining (Yeadon et al., 1990), as well as high bar circling (Yeadon and Hiley, 2000) or

long swings on the rings (Brewin et al., 2000). In angle-driven models the joint torques should be limited to avoid unrealistic movements (Yeadon and King, 2008).

Torque-driven models have been used to model relatively simple planar movements, in which the body can be represented using simplified planar two-dimensional models. Activities in which the movement remains symmetrical about the sagittal plane, such as swinging on the rings (Sprigings et al., 1998), have often been modelled as this allows the simulation model to have fewer segments and hence fewer degrees of freedom.

3.2 MODELLING BODY SEGMENTS

3.2.1 Rigid segments

Rigid segments are the fundamental building block of most whole body simulation models in sports biomechanics and can be thought of as representing the underlying structure and inertia of the human body. Each rigid segment employed within a planar model requires four parameters: length, mass, centre of mass location and moment of inertia. The number of segments used depends on the activity being modelled. Alexander (1990) used a two segment model to investigate optimum approach speed in jumps for height and distance, whereas, Hatze (1981) simulated the take-off phase in long jump using 17 segments.

The connections between rigid segments are typically modelled as frictionless joints where the ends of the two rigid segments are joined at a common point. The assumption that joints share a common point is a simplification of reality and whilst reasonable for most joints, it can be questionable at the shoulder where motion occurs at four different joints (Yeadon and King, 2008). A simple one degree of freedom pin joint (Yeadon and King, 2002) and a simple viscoelastic representation (Hiley and Yeadon, 2003) have been used in whole body models where the overall movement of the body is of interest. However, a complex finite element model has been used in models where the individual

muscle contributions towards the movement of the shoulder are of interest (van der Helm, 1994). Therefore, the complexity of each joint depends on the requirements of the study.

3.2.2 Wobbling masses

When the body undergoes high impact forces or accelerations the dynamic behaviour of the human body becomes important. In reality, the body cannot be modelled as a set of rigid bodies. During an impact, the body's skeletal structures experience forces whilst the soft tissue's acceleration is delayed (Nigg et al., 1995). In order to accommodate this complexity some rigid bodies are modified to incorporate wobbling mass elements (Gruber et al., 1998). This representation allows some of the mass (soft tissue) in a segment to move relative to the rigid element (bone). The inclusion of wobbling segments within simulations involving impacts is crucial. Pain and Challis (2006) compared a four segment model with and without wobbling masses and discovered that a model including wobbling masses reduced joint forces and torques by up to 50% and matched experimental ground reaction forces.

The most common method of modelling segments which require a wobbling mass is to split the segment into two segments. The first segment represents the rigid element (bone) to which the wobbling segment (soft tissue) is attached. The connection between the wobbling and rigid elements is then modelled using a spring. Initially, Cole et al. (1996) used a linear spring to connect the wobbling element to the rigid element. However more recently, the preferred method has used nonlinear damped passive springs to define the connection (Gruber et al., 1998; Pain and Challis, 2006).

Using wobbling masses within a simulation model increases the number of parameter values required and complicates the equations of motion. Therefore, they should only be used when necessary. It is essential however, when modelling an activity which includes an impact, that wobbling elements are included.

3.3 MODELLING THE INTERACTION WITH EXTERNAL SURFACES

Generally, two methods are used to model the interaction between an external surface, such as the ground or sports equipment, and a human body model. The first and simplest method is to model the connection as an extra “joint” so that the model rotates about a fixed point on the external surface. Unfortunately, this method has the significant disadvantage that it prevents the model being able to translate relative to the point of contact or allow a collision to occur. Therefore, a second method is more commonly used in which forces are applied at a finite number of locations using viscoelastic elements at the interface. This method has been used to model the foot-ground interface (Pain and Challis, 2001; King and Yeadon, 2004) as well as the model-equipment interface such as a high bar (Hiley and Yeadon, 2003).

The equations governing the viscoelastic interface have varied in complexity depending on the requirements of the model. Misevich and Cavanagh (1984) suggested that the force acting on a human heel during a drop jump landing depends on the deformation, and the velocity of deformation. Therefore, the heel pad has viscoelastic properties and can be modelled as a linear spring damper. In reality, the contact between surfaces is rarely linear (Nigg, 1999). However, linear springs are commonly used to model the viscoelastic interface since they offer enough complexity to model the interface successfully in simulation models investigating optimal performance (Yeadon and King, 2002; Allen, 2010; Lewis 2011). The number of connections between the surface and the model varies but is commonly three or less (Yeadon and King, 2002) although 66 points of contact were used to simulate heel-toe running (Wright et al., 1998).

The horizontal forces acting between an external surface and the body can be calculated using either a friction model or again using viscoelastic springs. Gerritsen et al. (1995) used a friction model calculating the horizontal force acting while in contact with an external surface by expressing the horizontal force as a function of the vertical force and the horizontal velocity of the point in contact. The use of viscoelastic springs is more common (Yeadon and King,

2002; Allen, 2010; Lewis 2011), however in order to ensure the horizontal force falls to zero in conjunction with the vertical force, the horizontal force should be expressed as a function of vertical force (Wilson et al., 2006).

3.4 MODELLING THE EFFECT OF MUSCLES

The movement of the skeletal system is caused by muscles converting a signal from the nervous system into force. Each signal from the nervous system fires a set of muscle fibres in which nerve impulses stimulate the flow of calcium into the sarcomeres, causing the filaments to slide (Jones et al., 2004). Sarcomeres contain two protein based structures, thin filaments called actin and thick filaments called myosin. They are constructed one on top of another and are linked using a cross bridge, where a myosin head oscillates continuously, attaching and detaching from a binding site on the actin. When they attach, a force is exerted which causes the filaments to slide past one another. The lengths of the actin and myosin filaments remain the same but increase their overlap as they slide to produce a shortening effect (Lee et al., 2010).

3.4.1 Modelling muscle

Mechanical models to replicate the force output by muscles have predominately been based on the work first suggested by Gasser and Hill (1924). They proposed using a muscle tendon complex (Figure 3.1) to divide the force producing capabilities of muscle into a contractile element (CON) and two series elastic elements: the series elastic element (SEC), and the parallel elastic element (PEC). Mathematical relationships are required for each component in order for the force (F) exerted by the muscle on the simulation model to be defined.

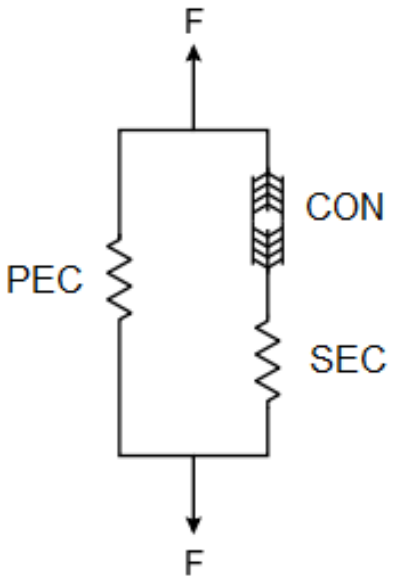

Figure 3.1 - Schematic diagram of a muscle tendon complex.

3.4.1.1 The contractile component

The contractile component plays the major role in producing the force within muscle models. The force produced by the contractile element has been expressed on the knowledge of muscle contraction both on a microscopic (Huxley, 1957) and macroscopic level (Hill, 1938).

Microscopic

On a microscopic level, Huxley (1957) combined the sliding filaments with the cross bridge theory to express muscle contraction. A Hookean spring was used to model the force within each bonded cross bridge where a first order differential equation was used to govern the number of actin-myosin cross bridge bonding reactions occurring at any time. The total force exerted by the muscle was the summation of the force contributed by each connected cross bridge.

Macroscopic

On a macroscopic level, muscle models have almost solely expressed force as a function of muscle length, muscle velocity and the neural activation of the muscle.

Force – length relationship of muscle

The force-length relationship for a muscle has been well researched. Initially, Gordon et al. (1966) used an individual sarcomere from a frog skeletal muscle to discover that the force-length relationship of an individual sarcomere was of a polygonal form (Figure 3.2).

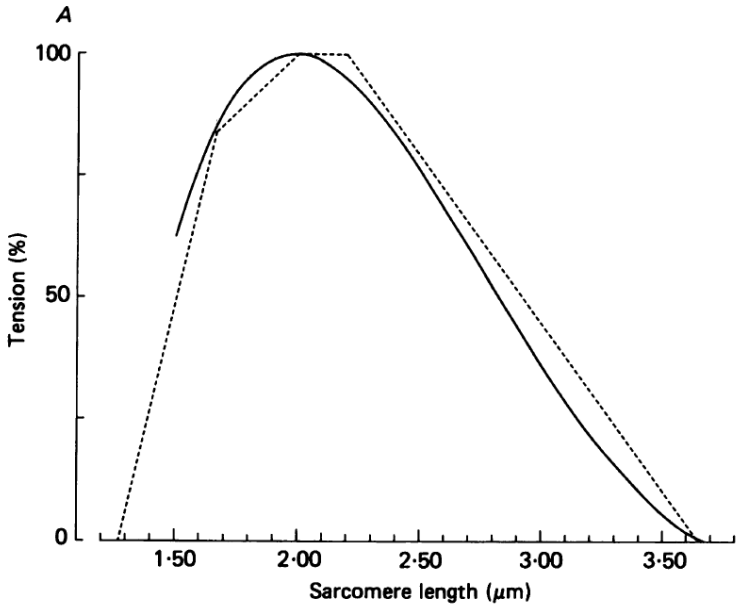

Figure 3.2. - Comparison between the length-tension curves described by Edman and Reggiani (1987) - continuous line, and Gordon et al. (1966) - dashed line. [Adapted from Edman and Reggiani, 1987]

However, the force-length relationship of a muscle in vivo has been shown to be different to the individual sarcomere initially experimented on by Gordon et al. (1966). In vivo, the force-length relationship tends to display more of a bell shaped curve (Figure 3.2) (Edman and Reggiani, 1987). The force-length relationship is therefore modelled using a simple quadratic function (King et al., 2006, Lewis, 2011) or a bell shaped curve (Audu and Davy, 1985, Allen, 2010, Jackson, 2010) within muscle models. Lewis (2011) suggested that a quadratic function provided a better representation of his measure torques.

Force – velocity relationship of muscle

The force-velocity relationship for a muscle can be split into two parts, depending on whether the muscle is lengthening (eccentric phase) or shortening (concentric phase).

A muscle begins a concentric contraction under a constant load which is less than the maximal isometric force developed by the muscle at that length (Lieber et al., 1992). As the load begins to decrease, the velocity increases to a maximum contraction velocity (V_{max}), at this velocity the muscle cannot resist any load place upon it even during maximal activation.

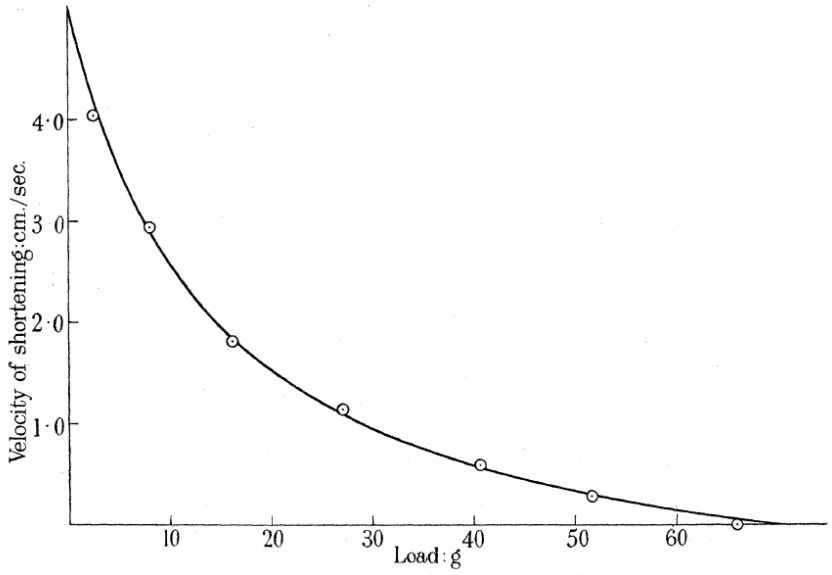

Figure 3.3. – Hill's force-velocity relationship.
(Hill, 1938, p.177)

Fenn and Marsh (1935) were the first to notice a relationship between the shortening velocity of a muscle and the force produced. Hill (1938) used an experiment on an isolated, tetanically stimulated frog skeletal muscle to describe the force-velocity relationship of a shortening muscle as a rectangular hyperbola, in which, the tetanic muscle force decreases hyperbolically with increasing speed of shortening to approach zero at maximum shortening speed (Figure 3.3).

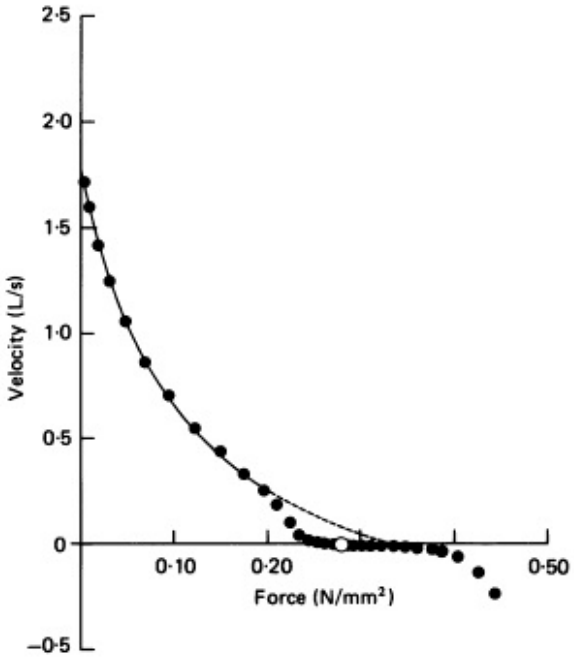

Figure 3.4. –Force-velocity relationship of shortening muscle fibres. (Edman, 1988, p.315)

Although, Edman (1988) showed that the force-velocity relationship of a shortening muscle fibre is more complicated than observing the muscle as a whole, demonstrating that muscle fibres have two distinct curve locations within their force-velocity relationship (Figure 3.4). However, since simulation models only require the force produced by the whole muscle, the use of Hill-type models to represent the force-velocity relationship of concentric contractions has been widespread (King, 1998; Wilson, 2003; Allen, 2010; Lewis, 2011).

An eccentric contraction takes place when the load on a muscle is greater than the maximum isometric force developed by the muscle at that length (Pandy and Barr, 2004). In the eccentric phase, maximum tetanic force increases rapidly, to around 1.4-2.0 times the isometric value with increasing speed of lengthening and then plateaus for higher speeds (Katz, 1939; Harry et al., 1990; Edman, 1988). Unfortunately, research on the eccentric phase in humans has shown that the increase in tetanic force compared to the isometric value does not occur. This suggests that maximal tetanic force cannot be produced during maximal voluntary eccentric contractions (Westling et al., 1990) due to neurological mechanisms reducing eccentric force to protect the body from injury. However, when the muscle is electrically stimulated an increase in force

of 21-24% is exhibited during eccentric contractions, compared to no increase in either the isometric or concentric conditions.

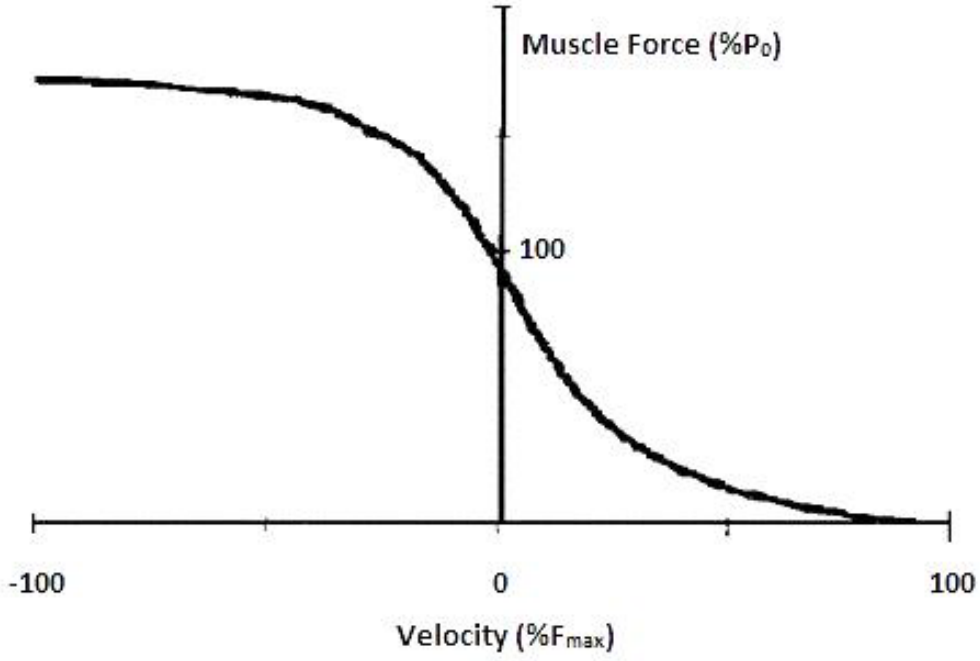

Figure 3.5. – Muscle force-velocity relationship.

The force-velocity relationship combining both the eccentric and concentric force-velocity relationships (Figure 3.5) is typically modelled using two differing hyperbolic functions. In the concentric phase, the classic Hill hyperbola (1938) is used, whilst the eccentric phase is modelled using an inverted hyperbola. When the eccentric and concentric phases swap, i.e. the velocity is 0, Hill (1938) discovered that there is a discontinuity in the slope, since the increase in tension required above the isometric maximum to produce a small velocity of lengthening, is much greater than the small drop below the isometric maximum required to produce an equal shortening velocity. Experimental investigations have shown that the slope of the force-velocity curve is 6 times (Katz, 1939) and 3.9 times (Harry et al., 1990) greater for lengthening than for slow shortening. Huxley (1957) however, predicted the slope to be 4.3 times greater using a theoretical approach.

Finally, the neural mechanism which inhibits activation levels during maximal voluntary eccentric contractions has also been included in functions modelling

the force-velocity relationship. Chow and Darling (1999) recommended this "differential activation" be included by adjusting the constants of the Hill equation. More recently, Yeadon et al. (2006) addressed the errors in the eccentric and low velocity concentric phases associated with the failure to include differential activation considerations when modelling maximal movements by using a three parameter function to mimic differential activation. Initially, a sinusoidal function was used but this function required the roots of an equation to be calculated which was computationally slow. An improved three parameter sinusoidal exponential function was introduced to speed up computational time and improve implementation within simulation models (Jackson, 2010; Forrester et al., 2011). Maximum voluntary force of a muscle is then modelled as a function of the theoretical maximum force using the Hill equation, and the differential activation function, which increases from a depressed level for high eccentric velocities to full activation for high concentric velocities (Figure 3.6).

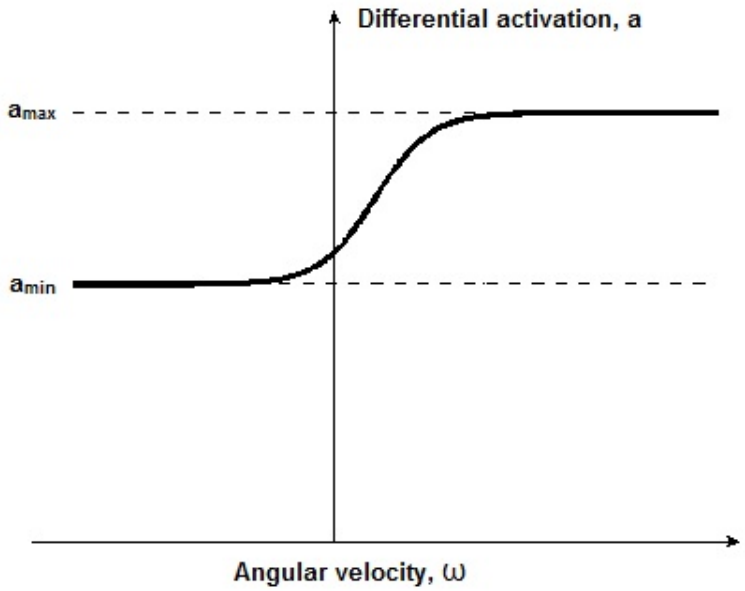

Figure 3.6 – Example of the three parameter sinusoidal exponential function used for differential activation.

Muscle activation

Muscle activation describes the level at which the muscles are activated due to the neurological signals being processed. The amount of activation ranges on a scale of 0 (no activation) to 1 (maximal activation). This function is then multiplied by the maximum voluntary force given by the force-length and force-velocity relationships to give the muscle force exerted.

Muscle activation has been modelled differently across the literature. A definition of neural control was used by Hatze (1981) to represent the activation of the contractile component by incorporating a representation of the neural executor system. Van Soest et al. (1993) simplified this approach by modifying the level of stimulus to act with a bang-bang style. More recently a ramped activation method has been used by King et al. (2006) to regulate the percentage of maximal voluntary torque exerted at a joint. This ramped activation method has been employed to control muscle activation allowing different ramp styles (Allen, 2010; Jackson, 2010; Lewis, 2011). However, it is worth noting that complex tasks may require more complicated muscle activation parameters than have been used previously.

Microscopic vs. Macroscopic

Although, microscopic models provide a much more detailed approach than macroscopic models, they are much more complicated and may require further complexity to accurately model force. Van den Bogert et al. (1998) examined modelling the force development of muscle using a cross-bridge model (microscopic) versus a Hill-type model (macroscopic). They determined that a Hill-type model was better placed to model the muscular function as long as a detailed description of the underlying process wasn’t needed. The authors conceded that the cross-bridge model required further complexity to accurately model muscle force properties, which limits its application in whole body models of human movement. Therefore, due to its simplicity and adequate accuracy, modelling the contractile component within muscle models has

almost solely employed Hill-type models (Alexander, 1990; Wilson et al., 2006; Allen, 2010).

3.4.1.2 The series elastic component

The series elastic component lies in series with the contractile component and is considered to be made up of the tendon and aponeurosis. This component exerts elastic properties within the muscle to represent the magnitude of stretching and is tasked with transferring the contractile component force to the skeleton. The force produced over the linear region is directly proportional to the series elastic stiffness. Therefore, it is common for the series elastic component to be modelled as a torsional spring with a series elastic stiffness (King, 1998; Wilson, 2003; Allen, 2010; Jackson, 2010; Lewis 2011).

The series elastic stiffness within simulation models has been calculated using experimental approaches (Hof, 1998) or been based on previous literature (King, 1998; Allen, 2010; Lewis, 2011). Hof (1998) measured the force-extension characteristics of the human tricep surae muscle using a hydraulic release ergometer. King (1998) calculated the series elastic stiffness using the muscle, tendon and moment arm lengths from the literature. Maximal joint torque was measured using an isokinetic dynamometer, whilst a 4% stretch of the tendon was assumed. Normally, it is assumed that the series elastic component stretches by around 5% at maximum isometric force (Muramatsu et al., 2001). The stiffness was then calculated using this extension and the maximal joint torques. A sensitivity analysis was also conducted which proved that the model was not sensitive to the series elastic stiffness.

This method first used by King (1998) has been used in subsequent simulation models (Wilson, 2003; Allen, 2010; Jackson, 2010; Lewis 2011) due to it being less complex and time consuming than the experimental approaches whilst maintaining accuracy.

3.4.1.3 The parallel elastic component

The parallel elastic component consists of the various connective tissues around the muscle which exerts an independent elastic force. Winter (1990) showed that the parallel elastic component force was related to the contractile component length but independent of its activation. The parallel elastic component has often been disregarded (King and Yeadon, 2004; Kong, 2004; King et al., 2006, Lewis, 2011) due to its effect being minimal during normal functional joint range of motions (Chapman, 1985). However, when it has been included the methods have been mixed with an exponential function (Hof, 1998; Allen, 2010; Jackson, 2010), a parabola (Bohm et al., 2006) and a linear function (van Soest et al., 1993) all being used.

3.4.2 Incorporating muscle models in simulation models

3.4.2.1 Individual muscles vs. torque generators

Although, the majority of muscle models are based on the model of Hill (1938), they divide into two categories; those which model individual muscles and those which use a torque generator to represent the net effect of all the muscles around that joint.

The selection of individual muscles versus torque generators is dependent on the research question the model is being developed to answer. For example, Alexander (1990) developed a model using a knee extensor torque generator to investigate the optimum take-off techniques for the high and long jump since he wasn't interested in the individual muscles. However, Nagano and Gerritsen (2001) developed a model using individual muscles to investigate the effect of strengthening particular muscles on maximal jump height. The model therefore, would not be suitable to answer the research question if it contained torque generators.

Individual muscle models have been widely used to investigate the function of individual muscles and understand human motion (Erdemir et al., 2007). Probably the most complex individual muscle model was developed by Hatze

(1981). The model consisted of 17 segments with 46 muscles to simulate the long jump take-off phase. Simpler models have been used to incorporate individual muscles; Pandy et al. (1990) modelled the body as four segments with eight muscles in order to investigate leg muscle activity. Although, Hatze (1981) claimed the parameters for each individual muscle were taken from an individual, the one overriding problem with individual muscle representations lies with the selection of realistic parameters from the wide range of measurements within the literature.

Typically, simulation studies are not concerned with the properties of the muscle and tendon and how they affect human motion but on the global performance of the joint kinematics and the techniques employed. After Alexander's (1990) early example of how a torque generator can provide satisfactory complexity to understand the problem in hand, a series of torque generator simulation model models have been developed (King, 1998; Wilson, 2003; Kong, 2004; Allen 2009; Lewis, 2010; Jackson 2010). A major advantage of modelling using torque generators rather than individual muscles is that the subject-specific strength parameters can be obtained using an isovelocity dynamometer (King et al., 2006). This leads to the assurance that the strength of the model is known to be realistic.

3.4.2.2 Monoarticular vs. Multi-articular

The human body is a complex system of monoarticular muscles, those which cross one joint and multi-articular muscles, those which cross two (biarticular) or more joints. The force produced by a muscle is considered to be a function of its length (Gordon et al., 1966), its velocity of shortening (Fenn and Marsh, 1935; Hill, 1938) and its velocity of lengthening (Katz, 1939). When the muscle is monoarticular, the length and velocity is only governed by that single joint, however if the muscle is multi-articular the length and velocity is governed by more than one joint.

Previously, torque actuators within simulation models have been incorporated at each joint with an assumption of monoarticularity (King et al., 2006; Mills et

al; 2008; Allen, 2010). This assumption has been the focus of a number of studies using individual muscle models in an attempt to establish the effect of multi-articular muscles (Pandy et al., 1990; van der Soest et al., 1993). However, the contractile component properties are often estimated from physiological measurements and as such the results aren't robust. Lewis (2011) investigated the effect of using a two joint approach to derive joint torque versus a single joint approach. He found that a two joint approach is similar to a single joint approach when the secondary joint angle does not vary too much. However, he recommended that a two joint approach should be used for plantar flexion torque when the knee joint angle varies by 45° or more, and for knee flexion/extension torque when the hip joint angle varies by 37° or more. The added complexity of a two joint approach required a 19-parameter torque generator function compared to a 9-parameter function required for a single joint approach. Therefore, it was concluded that single joint torque representations are suitable in simulation models where the joint range of movement is small, and the simulation model doesn't require the joint to maximise the work done in order to achieve the task, as, for example, is required in a vertical jump.

3.5 Model Construction

3.5.1 Generating the equations of motion

Once the complexity of the model has been decided, the equations of motion of the simulation model are formulated. A number of ways can be used to obtain the equations of motion.

3.5.1.1 First principles

The equations of motion for a simple mechanical system can be generated from first principles using Newton's Second Law (e.g. Alexander, 1990). However, this is only viable when the simulation model only consists of a small number of segments and limited complexity. For these simple planar linked models, three equations of motion are available; using Newton's second law for

each segment in two perpendicular directions, and taking moments for each segment. This allows the calculation of one and two reaction forces for each segment (Yeadon and King, 2008).

3.5.1.2 Software

Software packages are extremely useful in compiling the equations of motion for simulation models which are ever increasing in complexity. Van Soest (1992) highlighted that software packages allow the researcher to focus on the biomechanical problems they face rather than the numerical issues. However, Yeadon and Challis (1994) reminded researchers that the structure of the simulation model is still in the researcher's hands and needs to be chosen appropriately.

There are many software packages available, which can generate equations of motion for a user-defined system of rigid and elastic elements (e.g. DADS, ADAMS, AUTOLEV, SD Fast). Each package allows the user to input a relatively simple description of the model and the equations of motion are then generated, solved and integrated. Some packages, e.g. Autolev, have been more commonly used (King, 1998; Wilson, 2003; Allen, 2010; Lewis, 2011) due to their ability to generate computer source code, typically Fortran or C, for the mechanical system. This allows the user to incorporate muscle models or an optimisation routine into the basic simulation routine. Other more complex packages limit the access to the source code and prevent the user from customising the model for specific tasks.

3.5.1.3 Error Checking

However the equations of motion are calculated and customised, it is always important to check that no simple programming errors have been made. Example checks include that: energy is conserved if all damping is removed and all the muscles are switched off; the mass centre of the model follows a parabola if the forces between the simulation model and external surfaces are set to zero; impulse equals change in linear momentum; angular momentum about the mass centre is conserved in flight (Yeadon and King, 2008).

3.6 RUNNING THE SIMULATION MODEL

3.6.1 Integration methods

In order to advance the simulation model through the time steps required, a method for integrating the equations over time is used. Euler's method is the simplest process to increment a set of ordinary differential equations (equations of motion) through a time interval and uses derivative information from the beginning of the interval (Press et al., 1988). However, the Euler method requires a comparatively small step size and is not considered very stable (Press et al., 1988). Therefore, a more commonly used method is a fourth order Runge-Kutta in which four evaluations of the function are analysed per step size with the aim of meeting a predetermined accuracy with the solution with minimal computational effort (Press et al., 1988).

3.6.2 Kinematic and kinetic inputs

The initial kinematics of the performance being simulated, comprising the mass centre velocity, and the orientation and angular velocity of each segment, are required. The initial kinematics are usually calculated from recorded performances of the activity, although, it has been shown that accurate velocity estimates can be difficult to obtain (Hubbard and Alaways, 1989). The information required during the simulation is also essential. An angle-driven model needs the joint-angle time histories (Yeadon, 1990a), while a torque-driven model requires the activation time histories for each actuator in the model (Alexander, 1990). The joint-angle time histories and activation-time histories are also found using the recorded performances of the activity.

3.6.2.1 Recording kinematic data

Automatic motion analysis systems have very much become the norm over the last decade for collecting kinematic data, superseding cinematography analysis to collect position, velocities and accelerations of joint centres. The lengthy process involved and the human errors associated with manual digitization

have led to this method being used as a last resort when automatic motion analysis systems are available.

Automatic motion systems belong in one of two categories; active or passive, based on the type of markers used. Passive systems use markers that reflect light back to the sensor, while active systems use markers that emit the light for the sensors (Richards, 1999). The motion analysis systems that use passive markers tend to be used more often than those using active markers, primarily due to the ease of attaching them to the body without wires or power sources being required. These systems use a number of cameras which emit strobes of light to determine the location of the passive markers in a three dimensional volume. The passive markers are covered in a retro-reflective tape which reflects the light back in to the camera lens striking a light sensitive plate which creates a video signal. The video signal from each camera is then sent to a computer and processed to calculate the three-dimensional marker positions. Once the locations of the markers have been processed the joint kinematics can be calculated.

Richards (1999) produced a review of seven motion analysis systems (Ariel, Vicon, CODA, Elite, Motion, Peak, Qualisys, and Skill Technologies). Five of these systems were capable of reproducing a moving marker location with RMS errors of less than 2 mm and less than 1 mm for a stationary marker. It was noted that the Vicon system had the lowest RMS errors as well as having a low tracking and editing time.

3.6.2.2 Recording kinetic data

The performance ground reaction forces are commonly collected using force platforms which measure the deformation of transducers to produce a voltage proportional to the applied force (Yeadon and Challis, 1994). A force plate needs to be large enough to accommodate the contact area easily without hindering the subject's technique in trying to locate the force plate during his technique. Four transducers are used to collect the force located in each

corner of the force plate. There are two types of transducers used in force platforms; piezoelectric crystals or strain gauges (Cross, 1999).

The centre of pressure can also be calculated from the force plate by using the four transducers. The point of application of the force as well as the kinematic data allows intersegment forces and moments to be calculated (Bobbert and Schamhardt, 1990). Bobbert and Schamhardt found that using a Kistler force plate to determine the centre of pressure was accurate to ± 20 mm.

3.6.3 Subject-specific inputs

3.6.3.1 Inertia parameters

Methods to quantify body segment parameters have generally fallen into one of three categories; cadaver studies, mathematical modelling, and scanning and imagery (Robertson el al., 2004).

Cadaver studies

The inertia properties of a specific subject are difficult to obtain, ideally you would be able to isolate each individual segment and calculate its inertia properties. However, this isn't possible for a living person. Therefore, indirect attempts have been made to calculate the parameters by dissecting cadavers instead.

A number of cadaver studies have been conducted (Clauser et al., 1969; Chandler et al., 1975) but the most influential was by Dempster (1955) who not only used eight complete cadavers to provide tables for proportionally determining body segment parameters but also outlined the methods required. The cadavers were segmented before their weight, length and volume were calculated. The location of the centre of gravity was found by using a balancing technique and the moment of inertia using a pendulum technique.

The sole use of cadaver data in subject-specific simulation models is not appropriate due to need for the model to represent the subject. Therefore, statistical models have been used to relate the cadaver inertia parameters to

body measurements of the subject using regression equations (Challis and Kerwin, 1992). However, these methods are best reserved for use when only requiring average inertia parameters.

Mathematical Modelling

Mathematical models to calculate inertia parameters have been based on the work of Hanavan (1964) who made the fundamental assumptions that each segment was rigid and could be modelled as a geometric shape with uniform mass distribution.

Hanavan's work has been developed by adding more segments and using more accurate anthropometric measurements to define them. Hatze (1981) developed a 17 segment model which was based on 242 anthropometric measurements which took around 80 minutes to collect. The segments were modelled using a combination of geometrical solids using density values from Dempster (1955) and Clauser et al. (1969). Hatze concluded that owing to its accuracy (the total body mass error for the subjects tested was 0.32%), versatility and easy implementation, the model was a good way of calculating segmental parameter values. Yeadon (1990b) used a model which comprised of 40 geometrical shapes requiring 95 anthropometric measurements to define the segments which takes about 30 minutes to collect. The measurements comprise 34 lengths, 41 perimeters, 17 widths and 3 depths. Using the model, the total body mass error was 2.3%, which is considered to be reasonable.

Jensen (1978) used a method called photogrammetry, to obtain the measurements of the segments using digitised images of the subject. Although, this method has been developed, Baca (1996) developed a method to determine 220 of the 242 measurements for Hatze's model (1981), it is best to obtain the measurements directly from the subject wherever possible.

Scanning and Imagery Analysis

The anthropometric measurements can also be taken using radiation techniques to scan the living body (Brooks and Jacobs, 1975; Zatsiorsky and

Seluyanov, 1983). Gamma mass scanning was used to quantify the mass distribution by scanning incremental slices of each segment. This method allows estimations of the location of the mass centre, mass and principal moments of inertia. More expensive CT (computed tomography) and MRI scanning have also been employed to estimate segment densities and inertial parameters in vivo (Ackland et al., 1988, Mungiole and Martin, 1990). Unfortunately, due to cost, availability and ethical issues (radiation) these methods are not widely used or available.

3.6.3.2 Calculating rigid and wobbling element inertia parameters

The techniques discussed provide the inertia parameters for the segment as a whole. However, using rigid element and wobbling elements within simulation models requires each element to have its own inertia parameters which when combined together match the inertia parameters of the whole segment. Pain (1999) calculated the moments of inertia for the bone and soft tissue using a method which models the elements as geometric shapes. The mass of the wobbling and rigid elements are calculated using the values for percentage bone, muscle, and fat mass of individual limbs from Clarys and Marfell-Jones (1986). Alternatively, it is possible to estimate the bone density and latterly the bone mass by using MRI, however this method is expensive and not readily available.

3.6.3.3 Strength parameters

The strength parameters of the subject are required for the construction of a subject-specific simulation model. A number of methods have previously been used to calculate subject-specific strength parameters including invasive methods in which force transducers have been ‘buckled’ around tendons within a subject (Gregor et al., 1991; Fukashiro et al., 1995; de Vaal et al., 2010) as well as fibre optics (Komi et al., 1996; Finni et al., 1998). Unfortunately, invasive methods have severe limitations due to the nature of them, and as such aren’t appropriate within subject-specific simulation modelling. Non-invasive modern imaging techniques have also provided an insight into muscle

parameters although the technology has struggled to provide a good correlation between measurements and load.

The favourite measurement tool for collection of net joint torques at a joint has been an isokinetic dynamometer. An isovelocity dynamometer collects torque measurements as the subject works maximally against a crank moving at constant angular velocity over a range of joint angles. The effect of angular acceleration is not considered using this method as the angular velocity is kept constant. However, it is important when using an isovelocity dynamometer to also collect torque data to take into consideration the effect of the weight of the limb and crank, the acceleration and deceleration of the crank, and the difference between crank and joint angles (Yeadon and King, 2002).

Dynamometers have been heavily used to calculate subject-specific joint torque-angle velocity parameters of various joints to act as inputs to subject-specific simulation models of human movement (King, 1998; Wilson, 2003; Allen, 2010; Lewis, 2011). The torque generator parameters are found by varying each parameter of the nine parameter torque generator function (between the physiological upper and lower bounds chosen from associated literature) using a simulated annealing search algorithm in order to minimise a weighted RMS difference function between the measured joint torques taken on the dynamometer and the joint torques calculated by the nine parameter torque function (Lewis, 2011).

3.6.3.4 Viscoelastic parameters

Viscoelastic parameters are required for the springs that are included within the simulation model. Sometimes these springs represent specific elements in which it is possible to calculate the viscoelastic properties from measurements (Pain and Challis, 2001) while in other models the springs represent more than one viscoelastic element and so it is much harder to determine the parameters experimentally. Ideally, the parameters should be determined experimentally and then fixed within the model for all simulations (Gerritsen et al., 1995; Pain and Challis, 2001). When this is not possible the viscoelastic parameters can

be found through an optimisation procedure using an angle-driven or torque-driven model, allowing the viscoelastic parameters to vary until an optimum match between simulation and performance is found. For example, the viscoelastic parameters for the springs governing foot-ground contact and the connection between the rigid and wobbling elements have previously been found by using an angle-driven model (Wilson, 2003; Allen, 2010; Lewis, 2011). However, using optimisation to find the viscoelastic parameters has the potential to allow the springs to compensate for errors within the model. Although, this can be overcome by determining the viscoelastic parameters from more than one trial and then, evaluating them in a further trial (Yeadon and King, 2008).

3.7 MODEL EVALUATION AND OPTIMISATION

3.7.1 Process

Model evaluation is the most vital step in the construction of a simulation model but is often the downfall of many simulation models. Model evaluation confirms the accuracy of the assumptions made during the construction phase of the simulation model and its reliability. In order to evaluate the model, a performance under known conditions is compared with a performance of the real system with the expectation that using subject-specific parameters results in the model replicating an identical performance. The complexity and its intended aims should be taken into account when evaluating a model. For a simple model (Alexander, 1990), where general predictions are made from the simulation model, it may be suitable to show that the results are correct to the same magnitude. Alternatively, if the model is being used to investigate the factors that determine optimum performance in jumping (King et al., 2006), the model should be evaluated thoroughly (Yeadon and King, 2008).

The process of evaluating a simulation model with a recorded performance has been completed using a search algorithm to minimise a score function which compares kinematic and kinetic variables of the simulation model and real system performance (King, 1998; Allen, 2010; Lewis, 2011). The model is

considered to be accurate and reliable when the score for the evaluated simulation is satisfactory. If the comparison gives a percentage difference of less than 10%, it is often considered sufficient for applications in sports biomechanics (Yeadon and King, 2008).

Once the model has been suitably evaluated the model can be optimised. This process determines the optimal solution to a posed research question. Initially, an objective function is formulated based on the criteria of the research aims. The cost function can vary from being very simplistic, for example maximising jump height, to more complicated functions which comprise more than once function. Once the objective function is determined, realistic bounds must be determined for each of the variables than can be varied. In addition, the activation parameters of each muscle, as well as the joint angles and velocities must be constrained so that an unrealistic optimum is not achieved. In some cases, after an optimum solution has been found a sensitivity analysis is conducted. A sensitivity analysis is important to discover whether small deviations away from the optimal parameters result in similar solutions and therefore providing a confidence in the model's ability to handle changes in technique. If the model is sensitive to changes in parameters then small deviations away from the optimal technique will result in a performance that is considerably less than the optimum.

3.7.1 Optimisation algorithms

During both model evaluation and optimisation a search algorithm is employed to minimise or maximise a score function. Van Soest and Casius (2003) evaluated the performance of four key optimisation algorithms in solving 'hard' optimisation problems. A hard optimisation problem is one that can be found to share three characteristics:

1. The objective function typically has many local optima and is non-smooth or even discontinuous
2. The objective function is implicit, and as a result time consuming simulations are required for every evaluation

3. The dimensions of the optimisation parameter space cannot be kept very small

Van Soest and Casius (2003) evaluated the downhill simplex, sequential quadratic programming, simulated annealing and genetic algorithms using five separate problems for a range of initial values. They found that the downhill simplex and sequential quadratic programming algorithms were particularly poor at converging to an optimum solution in problems with a large number of parameters. The simulated annealing and genetic algorithms typically converged on solutions close to the global optimum, and were not trapped in local optima. Their results suggest that both optimisation methods are suitable for finding global optima in hard optimisation problems.

3.7.1.1 Simulated annealing algorithm

The simulated annealing algorithm (Kirkpatrick et al., 1983) is based on the thermal property of liquid metals. At high temperatures the molecules of liquid metals move freely, as the temperature begins to drop the thermal mobility of the molecules becomes restricted and they form a pure crystal, which corresponds to a state of minimum energy (Locatelli, 2000). If the cooling of the metal occurs too quickly a polycrystalline or amorphous state with a high energy and not a pure crystal is created. Locatelli, (2000) extended the simulated annealing algorithm to solve continuous global optimisation problems from the previously version used to solve combinatorial optimisation problems. The algorithm progresses by randomly creating a candidate point during every iteration and, using a random mechanism controlled by the temperature of the liquid, it decides whether to move the candidate point or remain in the current location for the next iteration.

Corana et al. (1987) found that the simulated annealing algorithm can provide a very reliable method to minimise multimodal functions but the computational cost increase linearly with the number of parameters requiring optimisation. Furthermore, Van Soest and Casius (2003) reported that the initial temperature

requires tuning to the problem otherwise the simulated annealing algorithm can take longer to converge.

3.7.1.2 Genetic algorithm

The genetic algorithm is based on the Darwinian principle of ‘survival of the fittest’ (Yang et al., 1998) and uses some of the process observed in natural evolution such as inheritance, crossover, selection and mutation (Davis et al., 1991). The aim of the genetic algorithm is to determine the parameter values of the global optima to a given problem. Each set of parameter values is represented as a chromosome where the fitness of the chromosome is determined as the solution to the problem. The general scheme of a genetic algorithm is as follows (Davis et al., 1991):

1) Generate a random initial population of n chromosomes.
2) Evaluate the fitness of each chromosome in the population.
3) Create new chromosomes by mating the current chromosomes where chromosomes are selected for breeding based on their fitness. The chromosomes with greater fitness are more likely to be bred. During the mating process crossover and mutation are applied; crossover recombines two chromosomes to generate two new chromosomes, while mutation randomly alters a single chromosome to produce a new one.
4) Evaluate the fitness of the new chromosomes.
5) Stop if the maximum number of generations has been reached; if not return to step 3.

The determination of the population size can cause two problems: if the population size is too small the genetic algorithm may not find the best solution, on the other hand if the population size is too large the computational time to determine the global optima is increased (Harik et al., 1999). A further advantage of the genetic algorithm is the ease at which it can be parallelised. Parallelising the genetic algorithm allows multiple processors to evaluate the

fitness of the population, spreading the computational requirement and decreasing the processing time significantly.

3.8 SUMMARY

The design of a simulation model should be driven by the research aims and questions to be investigated. However, choosing the correct complexity for a simulation model is not simple, and care needs to be taken to incorporate all aspects that may impact the outcomes required. These include using wobbling masses when an impact occurs, modelling the interaction between the model and an external surface using an accurate representation, and choosing the correct method of modelling the force exerted by the subject. Once the structure of the simulation model is decided, a software package should be chosen that allows the user to customise the source code to implement the method used to model the force exerted by the subject and the optimisation routine. In order to run the simulation, kinematic inputs and subject-specific parameters are required. The model should then be evaluated to confirm the accuracy, in which a difference of less than 10% is required. Finally, if the accuracy is satisfactory, the model can be used to optimise technique and used to investigate the aims of the research but care must be taken to ensure that the model remains within sensible anatomical limits and that the optimum is not sensitive to change.

- CHAPTER 4 -
CONSTRUCTION OF A COMPUTER SIMULATION MODEL OF FAST BOWLING

In this chapter, the development of a planar computer simulation model of fast bowling using Autolev^{TM} is described. A description and explanation of the structure and function of the model is also provided.

4.1 MODEL PHILOSOPHY

The computer simulation model of fast bowling was constructed using the fundamental beliefs of Alexander (1992) that computer simulation models should be as simple as possible, whilst complex enough to reproduce realistic performances. To investigate the factors limiting fast bowling performance, the simulation model required sufficient complexity to accurately model the parameters linked to increasing ball release speed. Worthington (2013a) has shown that the key performance characteristics of fast bowling occur during the front foot contact phase of fast bowling. During the front foot contact phase the movement of the fast bowling action is predominately planar, although, non-planar rotations of the pelvis and shoulders occur, as well as, side flexion of the trunk. Since modelling in three dimensions adds significant complexity, a planar simulation model was developed which incorporated sufficient detail of the non-planar movements to accurately reproduce performances of the front foot contact phase and investigate the factors limiting fast bowling performance.

4.2 BODY REPRESENTATION

The structure of the simulation model of the front foot contact phase of fast bowling was defined using rigid segments following observation and preliminary analysis of the performance data (Chapter 5). Each rigid segment had inertia properties such that they represented the body segments of a fast bowler (Section 6.1). The justification of the structure of each element in the simulation model is explained below.

4.2.1 Trunk representation

A single segment trunk was deemed to be sufficient to accurately model the motion of the torso. The head was considered to have a negligible impact on performance and was incorporated into the trunk segment. The orientation of the head was assumed to have the same orientation as the trunk.

Preliminary analysis of the fast bowling action highlighted that side flexion occurs during the front foot contact phase. In order to include this motion within the planar simulation model, the length of the trunk + head segment was allowed to vary by representing the trunk + head length as a function of the trunk orientation angle derived from the performance data (Section 5.6.3). The centre of mass position of the trunk is located as a percentage of the segment length away from the distal end. Therefore, as the segment changes length, the centre of mass position also moves accordingly.

4.2.2 Trunk orientation angle

The trunk orientation angle of the simulation model was defined using the trunk + head segment angle to the horizontal in the external coordinate system.

4.2.3 Shoulder and pelvis representation

It is common within planar simulation models to assume that the shoulder and hip joint centres are asymmetrical and connected via the trunk segment (King, 1998; Allen, 2010; Jackson 2010; Lewis, 2011). During the preliminary analysis of the fast bowling action, it was found that non planar rotations of the pelvis and shoulders occurred. Since these rotations are important to the position of the upper and lower extremities during the front foot contact phase, it was necessary to represent them within the simulation model. In order to do this, the left and right hip joint centres were connected using a massless rigid segment with variable length. The same was done for the left and right shoulder joint centres. Within the simulation, the length and orientation of the massless segments were driven as a function of the trunk orientation angle derived from the performance data (Sections 5.6.2 and 5.6.3). The trunk +

head segment was connected to the midpoint of the pelvis segment and passed through the midpoint of the shoulder segment.

4.2.4 Upper limb representation

A three segment arm consisting of an upper arm, forearm, and hand was used to model the bowling arm, since it has been reported to contribute 40 – 50% towards ball speed (Davis and Blanksby, 1976a; Elliott et al., 1986). The effect of the hand on the non-bowling arm was considered to have a negligible effect on performance. Therefore, a two segment arm consisting of upper arm and forearm + hand segments was employed.

4.2.5 Lower limb representation

The importance of the ankle, knee, and hip joints in fast bowling (Worthington, 2013a) indicates that the model should include feet, shanks, and thighs. Each foot comprised two segments, which allowed three points of contact with the ground: heel, ball, and toe.

4.3 WOBBLING MASSES

Wobbling masses were included to incorporate the effect that the impact of front foot contact has on the dynamic behaviour of the body. Five wobbling masses were attached to each end of the rigid elements representing the shanks, thighs and trunk. The inertia parameters of the segments which are represented by rigid and wobbling elements were found using a method by Allen (2010), described in Section 6.1.1. A non-linear spring damper (Pain and Challis, 2001) defined the connection between the rigid and wobbling elements:

$$R = (-k_1 \cdot |v|^3 - k_2 \cdot \dot{v}) \cdot i \qquad (4.1)$$

where v is a vector defining the position of one point from another, i is a unit vector in the direction of v, $|v|$ is the magnitude of v, $\dot{v}$ is the first differential of v, k_1 and k_2 are stiffness and damping coefficients respectively, and R is a force vector.

The wobbling masses of the torso, thigh and shank had different stiffness and damping coefficients, but the coefficients were kept consistent across both legs and both attachments of the wobbling mass.

4.4 INTERACTION WITH EXTERNAL SURFACES

4.4.1 Foot-ground interface

The horizontal and vertical forces exerted on the three points of contact on each foot by the ground were both modelled as modified linear spring dampers (Allen, 2010). In order to ensure that the vertical force was zero when the foot touched down or took off, the damping term was multiplied by the magnitude of displacement:

$$R_{yi} = -k_{1i} \cdot y_i - k_{2i} \cdot \dot{y}_i \cdot |y_i| \quad for\ i = 1{,}3 \qquad (4.2)$$

where R_y is the vertical force, y is the vertical displacement with respect to the floor, $\dot{y}_i$ is the first differential of y, k_1 and k_2 are stiffness and damping coefficients respectively, and i represents the point of contact on the foot.

In order to ensure that the horizontal force was zero prior to touchdown and after take-off the horizontal spring damper was multiplied by the vertical force:

$$R_{xi} = (-k_{3i} \cdot x_i - k_{4i} \cdot \dot{x_i}) \cdot R_{yi} \quad for\ i = 1{,}3 \qquad (4.3)$$

where R_x is the vertical force, R_y is the vertical force, x is the horizontal displacement from the initial ground contact point, $\dot{x}_i$ is the first differential of x, k_3 and k_4 are stiffness and damping coefficients respectively, and i represents the point of contact on the foot.

The total horizontal and vertical forces on each foot were the sum of these values:

$$R_x = \sum_{i=1}^{3} R_{xi} \qquad (4.4)$$

$$R_y = \sum_{i=1}^{3} R_{yi} \qquad (4.5)$$

The stiffness and damping coefficients were allowed to vary across the three points of contact on each foot since the construction of the foot and shoe was not uniform.

4.4.2 Hand-ball interface

The connection between the hand and the ball was defined using a linear spring damper:

$$R = (-k_1 \cdot v - k_2 \cdot \dot{v}) \cdot i \qquad (4.6)$$

where v is a vector defining the position of one point from another, i is a unit vector in the direction of v, $\dot{v}$ is the first differential of v, k_1 and k_2 are stiffness and damping coefficients respectively, and R is a force vector.

When the ball is in contact with the hand the stiffness and damping coefficients are extremely high in order to keep the ball fixed. Once the criteria for ball release are fulfilled (Section 8.3.2), the stiffness and damping parameters change to zero and the ball is released.

4.5 ANGLE-DRIVEN SIMULATION MODEL

The structure of the simulation model of the front foot contact phase of fast bowling described above was used within a subject-specific angle-driven simulation model to determine the model parameters. The model was driven by the joint angles, massless segment orientation, and variable length time histories obtained from performance data. This ensured that the technique used within the simulation model was close to that actually performed by the fast bowler and was perfectly suited to determining the model parameters which could not be measured experimentally. More information on the initial conditions, the required model inputs and the model parameters determined can be found in Chapter 7.

4.6 TORQUE-DRIVEN SIMULATION MODEL

In order to understand the technique of the fast bowler, a subject-specific torque-driven simulation model incorporating the previously described structure was developed. Since the aim of this study was to investigate performance within fast bowling and it was not important to understand the underlying functions of the individual muscles, monoarticular joint torque actuators were preferred to individual muscles. Monoarticular joint torque actuators were preferred to biarticular joint torque generators for two reasons. Firstly, Lewis (2011) concluded that it was suitable to use monoarticular joint torque generators in simulation models that do not require the joints to generate all the work in order to achieve the task, and secondly, it vastly reduces the complexity of the joint torque generator functions when compared to biarticular.

Flexor and extensor monoarticular joint torque generators were incorporated in the fast bowling simulation model at the front MTP joint, the front ankle, the front knee, both hips, both shoulders, the bowling arm elbow and the bowling arm wrist. The back MTP joint, back knee and non-bowling arm elbow were angle-driven since it was thought that their impact on performance was minimal.

Passive torque generators were also included in addition to the joint torque generators at the front MTP, front ankle, front knee, both hips and the bowling elbow. The passive torque generators represent the force produced by the various connective tissues around the joint which prevent the joint exceeding its anatomical range of motion.

The net torque, T_{NET} at each joint is therefore given by the following equation:

$$T_{NET} = T_F - T_E + P \qquad (4.7)$$

where T_F is the flexor torque, T_E is the extensor torque, and P is the passive torque.

4.6.1 Torque generators

The joint torque profile of each torque generator used within the simulation model of fast bowling was based on the work of Gasser and Hill (1924). A

muscle tendon complex was utilised where the contractile component represented the properties of the muscle and the series elastic component represented the properties of the tendon and aponeurosis.

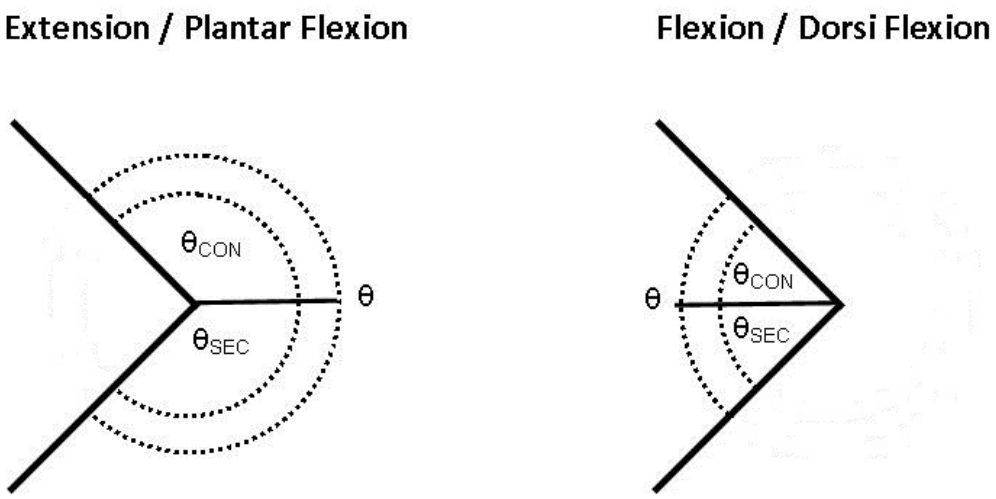

Figure 4.1. – Graphic representation of the muscle tendon complex in extension and flexion.

The relationship between the joint angle (θ), SEC angle (θ_{SEC}) and CON angle (θ_{CON}) in the muscle tendon complex observed in Figure 4.1:

$$\theta = \theta_{SEC} + \theta_{CON} \tag{4.8}$$

As the contractile and series elastic component work in series, the torque produced by the contractile component (T_{CON}) is equal to the torque produced by the series elastic component (T_{SEC}), which is equal to the torque exerted by the muscles, (T):

$$T = T_{SEC} = T_{CON} \tag{4.9}$$

The torque production properties of the contractile component depend on the contractile component angle and angular velocity. Each of the joint torque generators within this simulation model used a mathematical representation of the contractile component based on the strength of the fast bowler. In order to drive the torque-driven model, the contractile component angle and angular velocity for each of the joint torque generators is required to be determined at each time step.

Initially, at the beginning of the simulation (time = 0) the contractile component angular velocity $(\dot{\theta}_{CON})$ was assumed to be equal to the joint angular velocity $(\dot{\theta})$:

$$\dot{\theta} = \dot{\theta}_{CON} \tag{4.10}$$

During the first time step, the contractile component angle (θ_{CON}) at which the contractile component torque (T_{CON}) is equal to the series elastic component torque (T_{SEC}) is found. To achieve this, the series elastic component is assumed to operate as a non-damped linear torsional spring with series elastic stiffness (k_{SEC}), and act as a function of the series elastic component angle (θ_{SEC}):

$$\theta_{SEC} = \frac{T_{SEC}}{k_{SEC}} \tag{4.11}$$

In subsequent time steps, the contractile component angle is found by assuming constant velocity:

$$\theta_{CONnew} = \theta_{CON} + \dot{\theta}_{CON} dt \tag{4.12}$$

The series elastic component angle is then determined using Equation 4.8, before calculating the series elastic component torque using Equation 4.11. The bisection method is then used to determine the contractile angular velocity, at which the contractile component torque equals the series elastic component torque.

4.6.2 Activation levels

Since the joint torque profiles represent the maximal voluntary torque that the fast bowler can produce, the torque profiles for each joint are multiplied by an activation level to determine the applied torque; where 0.0 represents the muscle relaxed and 1.0 when the torque generator is maximally activated. A quintic function, which has zero velocity and acceleration at the end points (Yeadon and Hiley, 2000) was used to ramp up/down the activation level. The equations for the activation level when the activation is ramping up or down are shown below:

Ramp up

$$A(t) = z^3 \cdot (6z^2 - 15z + 10) \tag{4.13}$$

Ramp down

$$A(t) = 1 - z^3 \cdot (6z^2 - 15z + 10) \tag{4.14}$$

where

$$z = \frac{t - t_0}{t_1 - t_0} \tag{4.15}$$

with t_0 and t_1 representing the time (initial and final) at which the activation level reaches its end points.

Seven parameters were required to define the curve and are shown in Table 4.1. An example of an activation profile which ramps up and ramps down is shown in Figure 4.2.

Table 4.1 – Definitions of the activation level parameters

Parameter	Definition
a_0	Pre-impact activation level
a_1	Maximal/minimal activation level
a_2	Final activation level
ts_1	Start time of first ramp
tr_1	Ramp time of first ramp
ts_2	Start time of second ramp
tr_2	Ramp time of second ramp

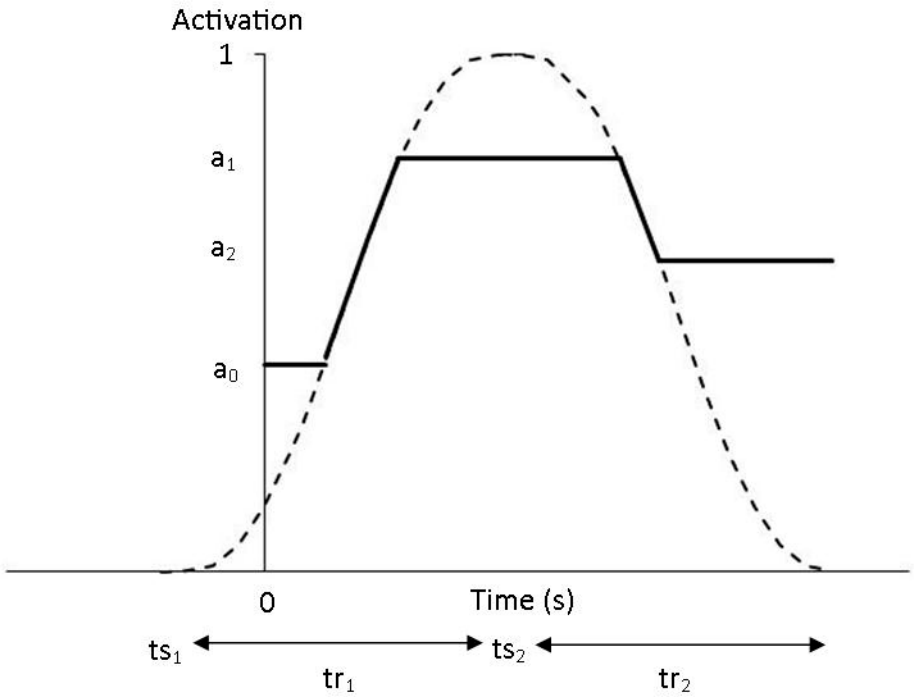

Figure 4.2 – Example of an activation level profile for a torque generator (bold line represents the activation level).

4.7 MODEL CONSTRUCTION

The Autolev^{TM} Professional Version 3.4 developed by Kane and Levinson (1985) was used to develop this simulation model. Using Kane's method, Autolev can formulate the equations of motion for multi-body constructions. The simulation model was constructed by inputting the orientation, position and generalised speeds of each segment relative to the global origin of a defined segment. The inertia parameters, internal and external forces, and the torques acting upon the system were also input. Once the equations of motion were calculated the code was output in the FORTRAN programming language, which allowed the model to be modified to include the foot-ground and hand-ball interface, as well as the profiles used to angle or torque drive the joints.

4.8 INTEGRATION ALGORITHM

The simulation advances over a designated time period using a Kutta-Merson numerical integration algorithm with a variable step size Runge-Kutta integration method (Allen, 2010).

4.9 SUMMARY

In summary, the torque-driven simulation model consists of 14 rigid segments (one with variable length), 2 massless segments with variable length, 5 wobbling masses, 9 torque-driven joints and 4 angle-driven joints, as well as, viscoelastic interactions to model the foot-ground and hand-ball interfaces (Figure 4.3).

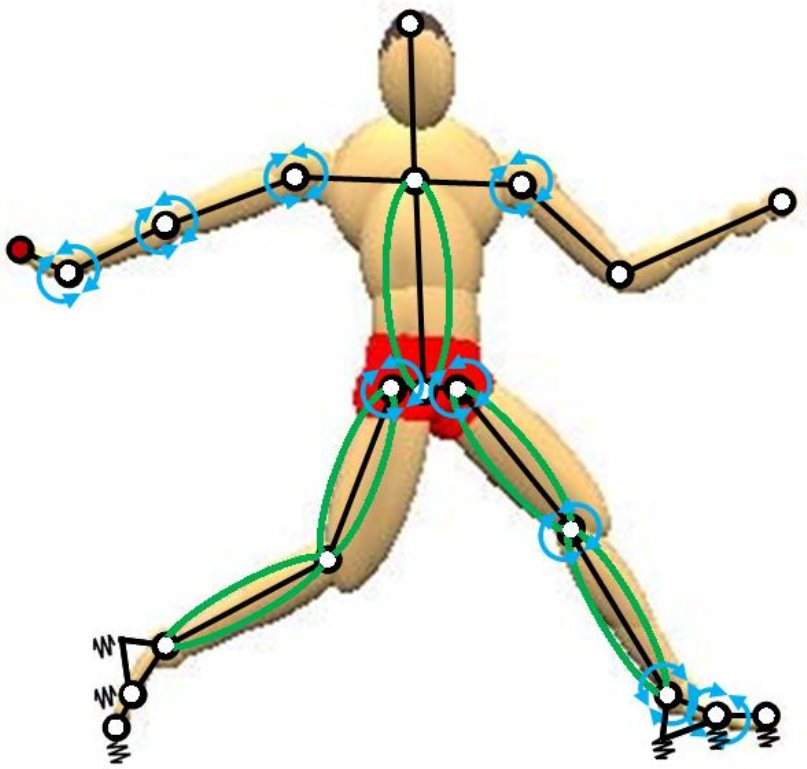

Figure 4.3. - Structure of the computer simulation model of the front foot contact phase of fast bowling.

- CHAPTER 5 -
PERFORMANCE DATA

In this chapter, a description of the protocol used to collect kinematic and kinetic data of the fast bowling action from an elite bowler is given. The analysis and processing of the recorded data are also described.

5.1 PARTICIPANT

A single male participant (age: 18 years, mass: 85.0 kg, height: 1.935 m) described as a “fast bowler” by an ECB fast bowling coach was used. He was a member of the England U19 cricket team and had been identified as having the potential to play for England within the next five years.

The bowler was deemed fit to bowl by a county physiotherapist and had been bowling regularly prior to the data collection. The testing procedures were explained to the subject in accordance with Loughborough University ethical guidelines, a pre-selection medical questionnaire was filled in, and an informed consent form was signed (Appendix 1). The subject performed a thorough warm up prior to data collection.

Ninety-five anthropometrical measurements of the participant were taken to determine the segmental inertia parameters required as the inputs to an inertia model developed by Yeadon (1990b). The measurements which include 34 lengths, 41 perimeters and 17 widths (Appendix 2) were taken by a skilled researcher. This method has been used in previous research (Wilson, 2003, Worthington, 2010) successfully, and is of little inconvenience to the participant.

5.2 DATA COLLECTION ENVIRONMENT

Kinematic and kinetic data were collected at the ECB National Cricket Performance Centre, Loughborough University, which provides an indoor practice facility allowing fast bowlers to bowl using their normal run-up on a standard sized, artificial cricket wicket. A Kistler force platform (Type 9287B –

900 x 600 mm), covered by 25 mm of artificial grass, is permanently installed within the facility and located on the popping crease.

A Vicon MX motion analysis system (OMG Plc, Oxford UK) was used to collect synchronous kinematic and kinetic data. Eighteen cameras (MX13), operating at 300 Hz were used to capture a volume covering approximately 7 x 3 x 3 m. This volume focused on the end of the run-up, the bowling action, and the follow through and was centred on the force platform (Figure 5.1). The Kistler force platform operated at 1500 Hz.

Figure 5.1. - Three dimensional data collection environment.

The system was calibrated using an Ergocal (14 mm markers) static calibration frame to define the origin and global coordinate system, and a 240 mm calibration wand (14 mm). This resulted in an image error, an RMS difference in camera pixels, of less than 0.3 pixels for all cameras which was deemed acceptable when considering the size of the volume.

In addition, two Fastec TS3 digital high speed cameras were used to capture footage at a frequency of 500 Hz. The cameras were positioned behind the bowler and to the bowling hand side. A Trackman^{TM} unit which uses Doppler radar to track the ball during flight gave instantaneous ball release velocities for each trial. The unit was located directly behind the bowling arm and was used to confirm that the bowler's ball release speeds were similar to his recorded match speeds, confirming maximal effort.

5.3 MARKERS

Fifty 14 mm retro-reflective markers were attached to the participant using a sports adhesive spray and double sided tape (Figure 5.2). Markers were positioned over bony landmarks in accordance with the marker set used by Worthington (2010).

Figure 5.2. - Marker location on participant.

An additional 15 x 15 mm marker was placed on the ball, using 3M Scotch-Lite reflective tape (Figure 5.3). This enabled ball release velocity and the moment of ball release to be calculated.

Figure 5.3. - Location of the ball marker.

5.4 PROTOCOL

The participant bowled twelve, maximal effort, stock deliveries (a normal length delivery most commonly seen in cricket), striking the force plate with his front foot. A further six stock deliveries were collected in which the back foot landed on the force plate. A trial was deemed successful if the equipment was triggered successfully, the desired foot of the bowler landed on the force plate and no markers fell off during that delivery. A “feel” score between 1 (very bad) and 10 (very good) based on the feel of the bowlers action and not the outcome was taken from the participant.

5.5 DATA ANALYSIS

The four best front and back foot bowling trials, those with the greatest ball velocity and feel scores with minimal marker loss, were selected and manually labelled within Vicon’s Nexus software (OMG Plc.).

5.5.1 Key instants

Key instants were determined manually for front foot contact and back foot contact and were identified as the first frame in which the ground reaction force was seen to increase above 25 N. When the foot did not land on the force plate, foot contact was observed to have occurred when the displacement of a marker was altered due to the interaction with the ground. Front foot flat was

considered to be the first frame in which the forefoot was on the ground. The ball release key instance was calculated using the same method as Worthington (2010). In this method, ball release is considered to have occurred when the distance between the ball marker and the wrist joint centre has increased sufficiently (>2 cm) to suggest the ball can no longer be in contact with the hand.

5.5.2 Joint centres

A BodyBuilder (OMG Plc.) model was used to calculate the joint centres. The joint centres coincided with those used within Yeadon's inertia model (1990b) and were calculated as the midpoint between a pair of markers placed medio-lateral of each joint (anterior-posterior for the shoulder). The hip joint centres were reconstructed using the "hip joint centring algorithm" (Davis et al., 1991) using markers located on the left and right anterior superior iliac spine (LASI and RASI), as well as the left and right posterior superior iliac spine (LPSI and RPSI). Joint centres for the lower and upper trunk in addition to the head and neck segments were calculated using the four pelvis markers, in addition to the markers on the distal and proximal ends of the sternum and spinous processes of L1, T10 and C7 (Roosen, 2007).

5.5.3 Joint and orientation angles

The joint angle-time histories of the thirteen joints (2 MTP, 2 ankles, 2 knees, 2 hips, 2 shoulders, 2 elbows and the bowling arm wrist), the trunk orientation angle, as well as the orientation angles of the massless pelvis and shoulder segments were calculated by projecting the coordinates of each joint centre into the sagittal plane and disregarding the coordinate in the third axis (x).

5.5.4 Variable segment lengths

The lengths of each of the segments with variable length were required during the simulation model. The segment lengths were also calculated in the sagittal plane (using the y-z coordinates) for the trunk, shoulder and pelvis.

5.6 DATA PROCESSING

5.6.1 Splining angle data

Angle-time histories from the performance data were required as an input into the angle-driven simulation model used to determine the model parameters. Quintic splines (Wood and Jennings, 1979) were fitted to the time histories of each joint angle, massless segment orientation angles and the orientation angle in order to be able to drive the simulation model at different time steps. This process fits a quintic spline defined by six spline coefficients to interpolate between discrete data points. The simulation model reads in these coefficients and uses them to calculate the angle, velocity and acceleration at each integration time step.

In addition to interpolating each angle, the quintic spline process was also used to smooth the angle data removing noise due to marker movement or errors tracking the markers. The level of smoothing was key due to the importance of keeping as much of the genuine signal as possible. Error estimates for each point were calculated as the difference between the performance data and a pseudo data set (generated by averaging coordinate values from adjacent frames) using a weighted combination of the local error variance and the global error variance. In order to achieve a balance between over smoothing and removing noise the error variances were given a weighting of 50%. Due to a danger of over fitting the data at the moment of contact (a consequence of the rapid accelerations of the points of the body associated with impacts), the error estimates were edited by changing the calculation of the pseudo data set at the moment of impact. Rather than using the pseudo data generated by averaging the coordinate values from adjacent frames, if the difference between the real data set and pseudo data set at the moment of impact was too large, the pseudo data set was replaced with the real value in the frame after impact. This method reduced the difference between the real and pseudo data values at the moment of impact and reduced the error variance, as well as the danger of over-smoothing (King, 1998). For all angles the average errors were less than 0.25°.

An example of a raw and splined angle time history for the front ankle during the front foot contact phase is displayed in Figure 5.4.

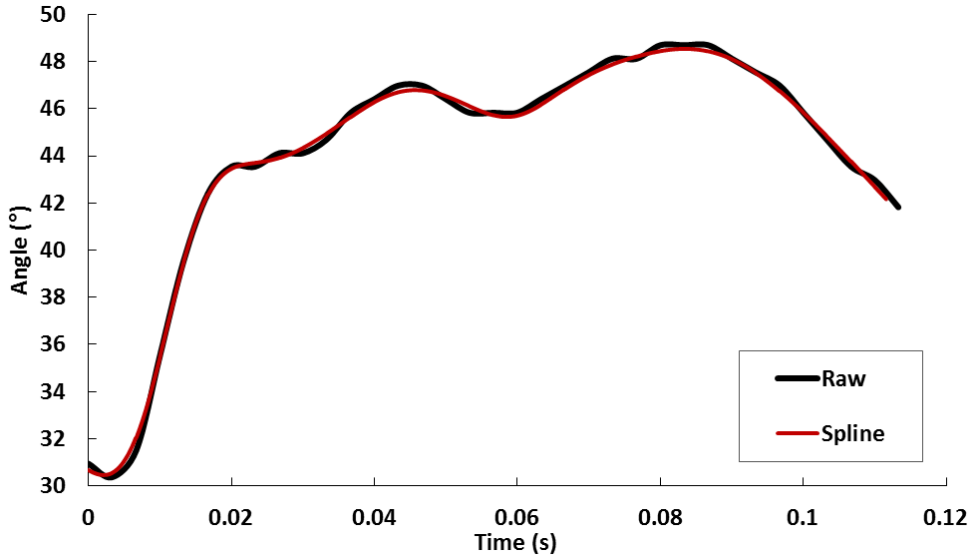

Figure 5.4 – A comparison of the raw and splined front ankle angle.

5.6.2 Massless segment angle as a function of the trunk orientation angle

In the torque-driven simulation model of fast bowling the massless segment orientation angles were required not as a function of time but as a function of an angle within the simulation model. This was done by expressing the massless segment orientation angle as a function of the trunk orientation angle. To determine this function, a third order Fourier series approximation was fitted to the coordinates from the three best recorded performances (Figure 5.5).

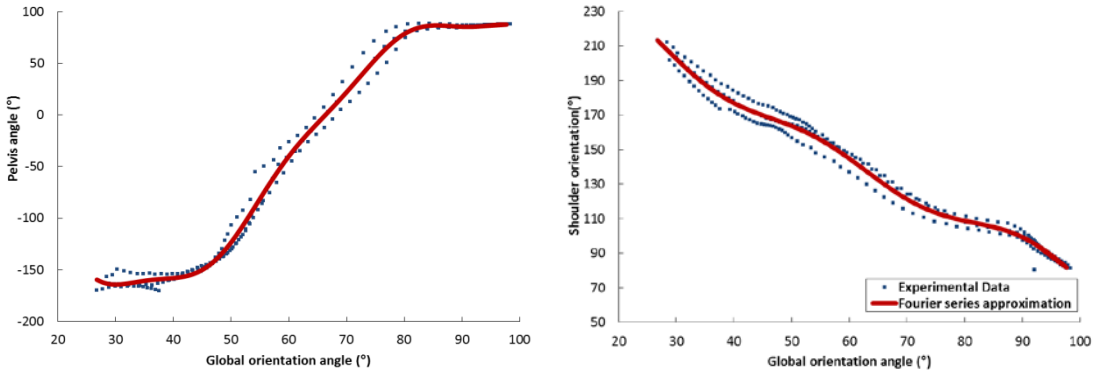

Figure 5.5. - Fourier series approximations for the pelvis and shoulder segment orientation angle as a function of the trunk orientation angle.

The root mean square error (RMSE) between the Fourier series approximation and the orientation of the massless segments was 4.3° and 7.4° for the shoulder and pelvis segments respectively, which was deemed acceptable, since the range was greater than 200° and the R^2 values were greater than 99%, indicating that the approximations provide a good fit to the data (Table 5.1).

Table 5.1. – Root mean squared error and R^2 values for the Fourier series approximations of the massless segment orientation

	RMSE (°)	**R^2 (%)**
Pelvis orientation	7.4	99.2
Shoulder orientation	4.3	99.5

5.6.3 Variable segment length as a function of the trunk orientation angle

The variable segment lengths were also required not as a function of time but as a function of an angle within the simulation model. The same method as described above for the massless segment orientation angles was used, where the trunk orientation angle was again used as the independent variable (Figure 5.6).

The root mean square error (RMSE) between the Fourier series approximations and the length of the variable segments was less than 0.01 m, with R^2 values greater than 93%, which indicates that the curves provide a good fit to the data (Table 5.2).

Table 5.2. – Root mean squared error and R^2 values for the Fourier series length approximations of the variable segment lengths

	RMSE (m)	**R^2 (%)**
Pelvis length	0.009	95.3
Shoulder length	0.005	98.4
Trunk + head length	0.009	93.1

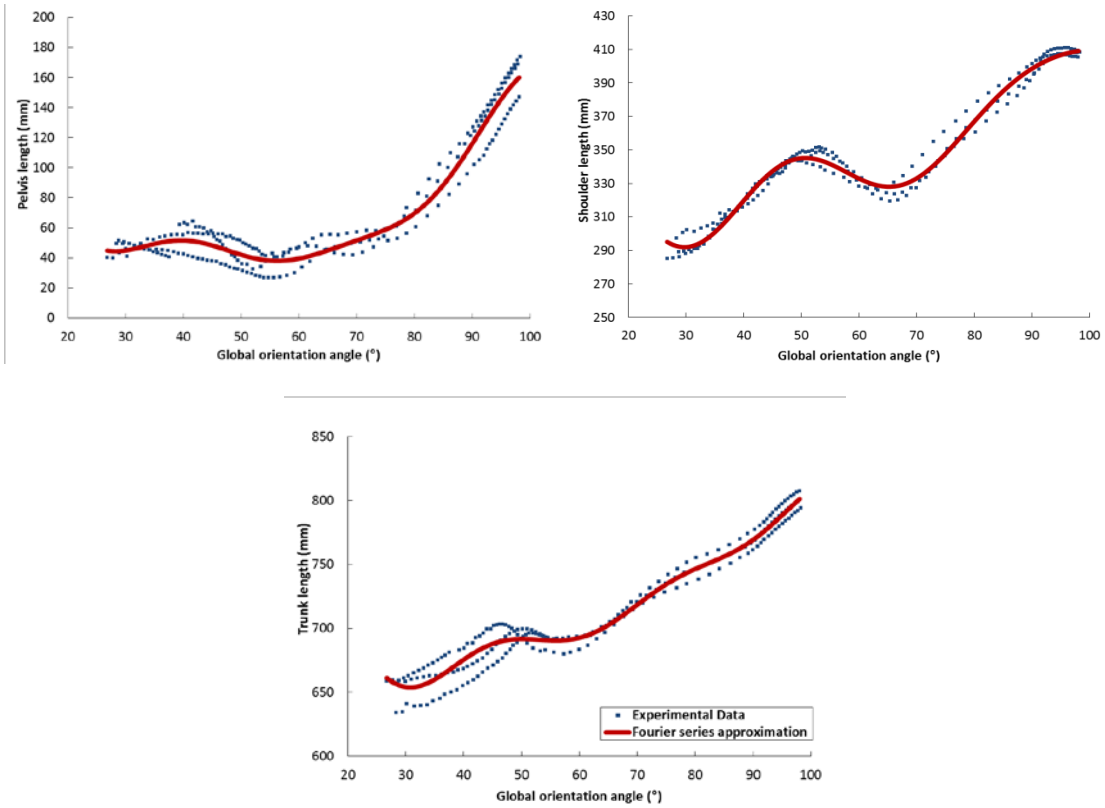

Figure 5.6. – Fourier series approximations for the pelvis, shoulder and trunk segment lengths as a function of the trunk orientation angle.

5.6.4 Force data

The force data for each trial required filtering due to the nature of the data collection environment and the activity being conducted. Since the distance between the analogue box and Vicon system was approximately 25 metres, as well as the large gain setting required on the force plate due to the size of the peak force, noise was unavoidably introduced. It was important to get the level of filtering correct as the foot-ground interface calculates force based on the displacement of the foot and shoe relative to the ground. If the data were under or over filtered, a portion of the force trace would not be governed by these factors and the simulation model could not be expected to reproduce this portion of force.

To decide on the level of filtering a spectral analysis of the horizontal and vertical force was performed on the three best recorded performances to determine the cut-off frequencies. The cut-off frequency was determined as the

point at which the signal initially decayed to zero (Figure 5.7). Any signal after this point was considered to be noise. A power spectrum was then used to calculate the percentage of the original signal accounted for by frequencies below each individual cut-off frequency (Table 5.3).

Table 5.3. – Spectral analysis for individual force traces

Trial	Direction	Visual cut-off frequency (Hz)	Signal % below cut-off frequency
1	Horizontal	73	99.8
	Vertical	60	99.7
2	Horizontal	85	99.9
	Vertical	66	99.6
3	Horizontal	81	99.9
	Vertical	73	99.6
Average	Horizontal	80	99.9
	Vertical	66	99.6

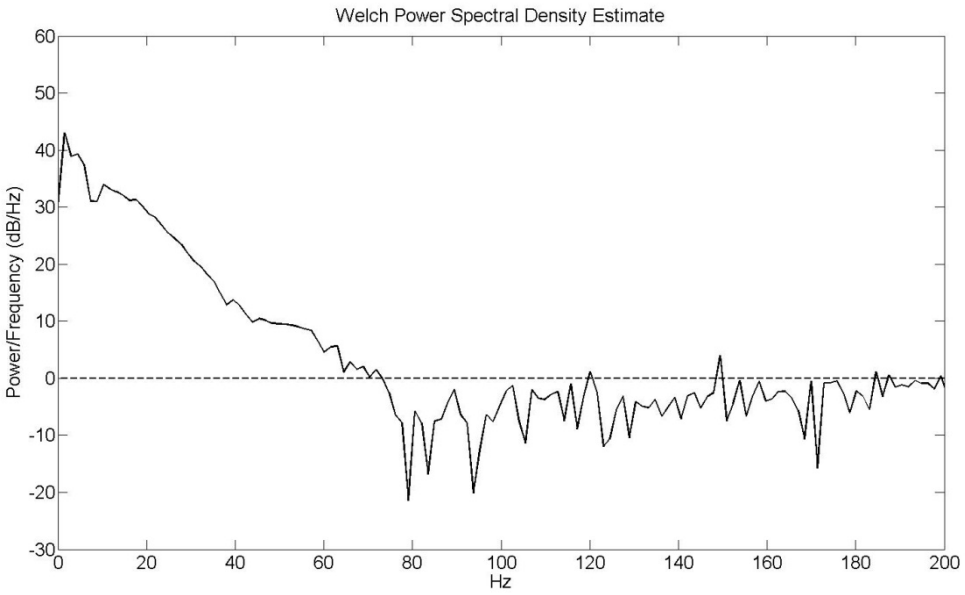

Figure 5.7. – Spectral analysis with the zero cut-off line.

Each average cut-off frequency was used to filter the data in the horizontal and vertical direction using an 8th order, zero lag, low pass, Butterworth filter. This resulted in average horizontal and vertical impulse changes below 0.01% in both directions, but noticeably smoother force traces (Figure 5.8).

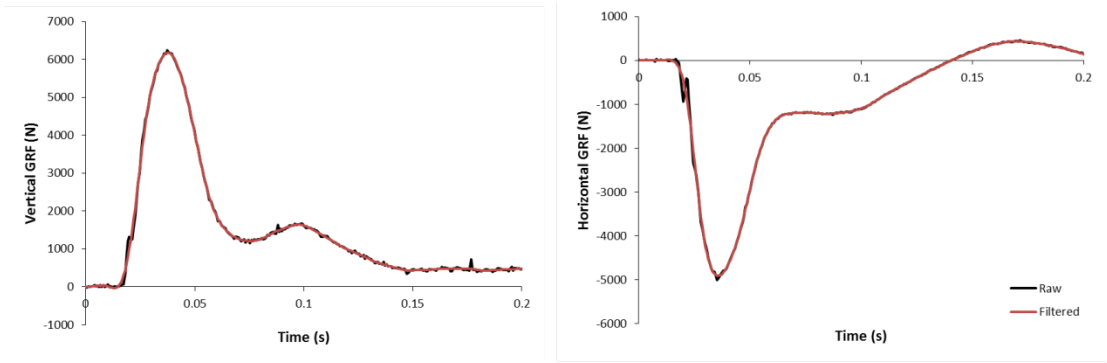

Figure 5.8. – Comparison of the raw and filtered ground reaction forces during front foot contact.

5.6.5 Centre of mass velocity

An accurate estimation of the centre of mass velocity was required as an initial condition and during model evaluation. The mass, the position of the centre of mass and the three principal moments of inertia of each segment were found using Yeadon's geometric model (1990b). These parameters were then used within Worthington's (2010) Bodybuilder code to establish the centre of mass position of the whole body in each trial.

Table 5.4 - COM velocities calculated from performance data

Trial	Direction	COM front foot contact velocity (ms^{-1})	COM ball release velocity (ms^{-1})
1	Horizontal	5.17	2.99
	Vertical	-1.42	0.50
2	Horizontal	5.37	3.24
	Vertical	-1.36	0.32
3	Horizontal	5.14	2.92
	Vertical	-1.44	0.44

In order to assess the accuracy of the centre of mass velocity (calculated by differentiating the centre of mass position), Allen (2010) calculated the difference between the impulses using the centre of mass touchdown and take-off velocities and the impulses measured from the force plate during triple jump. This process was repeated but used the centre of mass velocity at ball release rather than take-off (Table 5.4) and the impulse between the instant of front

foot contact and ball release (Table 5.5) for the three best recorded performances.

Table 5.5. – Comparison of the calculated impulse and measured impulse

Trial	Direction	Calculated impulses (N.s)	Measured impulses (N.s)	Implied difference in velocity (ms^{-1})
1	Horizontal	187.04	195.34	0.10
	Vertical	165.49	165.53	0.00
2	Horizontal	182.75	188.20	0.06
	Vertical	144.14	150.47	0.07
3	Horizontal	190.48	192.03	0.02
	Vertical	159.59	152.91	0.08
Average	Horizontal			0.06
	Vertical			0.05

Due to the implied difference in velocity between the two methods (Table 5.5), the initial centre of mass velocity was allowed to vary by 0.1 ms^{-1} in each direction to allow for the inaccuracy when calculating the centre of mass position.

5.6.6 Ball release velocity

The ball release velocity (in the horizontal and vertical directions) was calculated over a period of ten frames, starting with the instance of ball release (Worthington, 2010). No forces were considered to act on the ball in the horizontal direction and only gravity was assumed to act in the vertical direction. The ball release velocities were then calculated using the equations of constant acceleration.

5.7 SUMMARY

In this chapter the collection and processing of the performance data of the fast bowling action has been described. The determination of the variables and parameters required within the simulation model has also been given.

- CHAPTER 6 -
SUBJECT-SPECIFIC PARAMETER DETERMINATION

In this chapter, an explanation of the method used to determine the anthropometric data of the subject is given. The procedure used to determine the mass, centre of mass location and the inertia of the rigid and wobbling elements is described. The processes used to represent the strength of each joint in the simulation model are described and the determination of the associated parameters provided.

6.1 SEGMENTAL INERTIA PARAMETERS

The inertia properties of each segment of the simulation model were found using the anthropometric data described in Section 5.1 using Yeadon's inertia model (1990b). The inertia properties for each segment can be found in Appendix 3. The body fat percentage of the fast bowler within this study was determined by the Yuhasz equation (Yuhasz, 1967) which requires six skinfold measurements at the following locations: triceps, subscapular, supraspinale, abdominal, thigh, calf. The skinfold measurements were taken by a qualified researcher and the bowler's body fat percentage was calculated as 7.7%.

6.1.1 Rigid and wobbling elements

Each segment within the simulation model that was represented by a rigid element combined with a wobbling mass required separate rigid and wobbling element inertia properties, which combined formed the inertia properties of the whole segment.

In order to divide the mass of the whole segment between the rigid and wobbling elements, a method based on Clarys and Marfell-Jones' (1986) values for percentage of bone, muscle and fat mass of individual limbs was used. It was not appropriate to simply use Clarys and Marfell-Jones' values within the simulation model, since the body fat percentage of the fast bowler in

this research is much lower than the subjects used within their study (7.7 vs 34.6%). To find the separate rigid and wobbling element masses, a method described by Allen (2010), in which two previous methods used to redistribute the excess fat around the body were averaged, was employed. The first method converts the excess mass to muscle, whilst the second converts it both to bone and muscle by keeping the muscle to bone ratio constant (Pain,1999).

The centre of mass position and moment of inertia of the rigid and wobbling elements were also found using a method described by Allen (2010). In this method, the rigid segments were modelled as cylinders with uniform density. Since the rigid elements represent the bone of each segment, the density of the cylinders was equal to the density of the bone in that segment (Clarys and Marfel-Jones, 1986; Dempster 1955). Therefore, the centre of mass position coincided with the midpoint of the rigid segment and the moment of inertia could be calculated using the equation for the moment of inertia about the transverse axis. Once these were known, the centre of mass of the wobbling elements could be determined by using the equation for moments about the proximal joint and the moment of inertia by using the parallel axis theorem.

This process can be seen in Appendix 4.

6.1.2 Combining the head and rigid trunk segment

In the simulation model the trunk and head are combined as one segment. Therefore, their individual inertia properties required joining into a single rigid element. The centre of mass was found using the equation of moments about the proximal joint and the moment of inertia is by definition the sum of the two individual moments of inertia. The calculations can be seen in Appendix 5.

6.2 STRENGTH PARAMETERS

In order for the simulation model of fast bowling to be driven using torque generators at the front MTP joint, the front ankle, the front knee, both hips, both shoulders, the bowling arm elbow and the bowling arm wrist, accurate strength parameters of these joints were required for the fast bowler.

6.2.1 Ankle, knee, hip and shoulder joint torque profiles

The maximal voluntary torque of the front ankle, the front knee, the front hip and the bowling shoulder was determined experimentally using a Con-Trex MJ isovelocity dynamometer (CMV AG, Switzerland). Since bilateral symmetry was assumed, the non-bowling shoulder and back hip were considered to have the same strength as the bowling shoulder and front hip respectively.

6.2.1.1 Joint torque measurement protocol

A Con-Trex MJ isovelocity dynamometer (CMV AG, Switzerland) was used to collect movements considered as flexion and extension of the front knee, the front hip and the bowling shoulder, as well as, plantar and dorsi flexion of the front ankle. The bowler was strapped to the dynamometer in order to reduce his freedom to move, which can affect the alignment of the joint with the crank axis and subsequently the crank/joint torque relationship. The crank axis was then aligned with the functional joint centre, whilst the participant applied a torque on the crank arm. The dynamometer set-ups for the knee, ankle, hip and shoulder are shown in Figures 6.1, 6.2, 6.3 and 6.4.

Figure 6.1. - Dynamometer and participant setup for knee extension.

Figure 6.2. - Dynamometer and participant setup for ankle plantar flexion.

Figure 6.3.- Dynamometer and participant setup for hip flexion.

Figure 6.4 - Participant and dynamometer setup of shoulder flexion.

For each joint, isometric joint torque measurements were collected at 512 Hz for five seconds at six to eight joint angles throughout the participant's range of motion. During the isometric trials the participant was encouraged to start in a relaxed state before increasing his effort to reach his maximum voluntary contraction (MVC). As the joint angle was likely to vary from the crank angle due to the attachment of the participant's limb to the crank arm, a mechanical goniometer was used during the isometric trials to record a manual joint angle.

Isovelocity joint torque measurements were taken at 256 Hz. The procedure recorded joint torques using a concentric-eccentric protocol where the initial velocities were $50°s^{-1}$. The velocities were then increased in regular increments of $50°s^{-1}$, this method was chosen to avoid submaximal torques at high velocities (Yeadon et al., 2006). Maximal velocities were determined by the software used and were as follows; ankle - $300°s^{-1}$, hip - $250°s^{-1}$, shoulder - $275°s^{-1}$ (last increment was $25°s^{-1}$) and knee - $400°s^{-1}$. The participant performed one repetition of the concentric-eccentric protocol to reduce the effect of fatigue. A final isometric trial was collected at one joint angle after the isovelocity trials to confirm that the participant had not fatigued during the trial.

The passive torque component was calculated and removed from the measured torque by conducting a calibration trial in which the participant was required to stay relaxed as the crank arm passes through the range of motion. This method calculated the torque due to the gravity (weight of the system and limb), as well as the passive elements (tendons and ligaments) and was removed using the Con-Trex software. The resultant torque was the contractile component torque exerted by the participant during each isometric and isokinetic trial.

6.2.1.2 Data processing

The raw dynamometer crank torque and crank angle data were filtered using a 4^{th} order, zero lag, Butterworth, 12 Hz low pass filter. The appropriate cut-off frequency was determined by conducting a residual analysis (Winter, 1990).

The crank angle was converted to joint angle and angular velocity so that it could be used in muscle tendon complex torque generators. This was done for each joint (excluding the ankle) by fitting a linear equation to the manual goniometer data relating crank angle to joint angle collected during the isometric trials. The linear relationship was then used to calculate joint angle. Due to the difficulty measuring the ankle joint angle manually using a goniometer, the crank angle at the ankle was assumed to be equal to the joint angle plus the offset angle caused by the dynamometer attachment.

The peak torque and associated joint angle was found for every isometric trial for each joint. For each isovelocity trial the regions where crank angular velocity was between 95% and 105% of the pre-set crank velocity (Lewis 2011) were also manually determined. The concentric and eccentric isovelocity data were then chosen for the repetition in which the participant achieved their greatest torque (Figure 6.5).

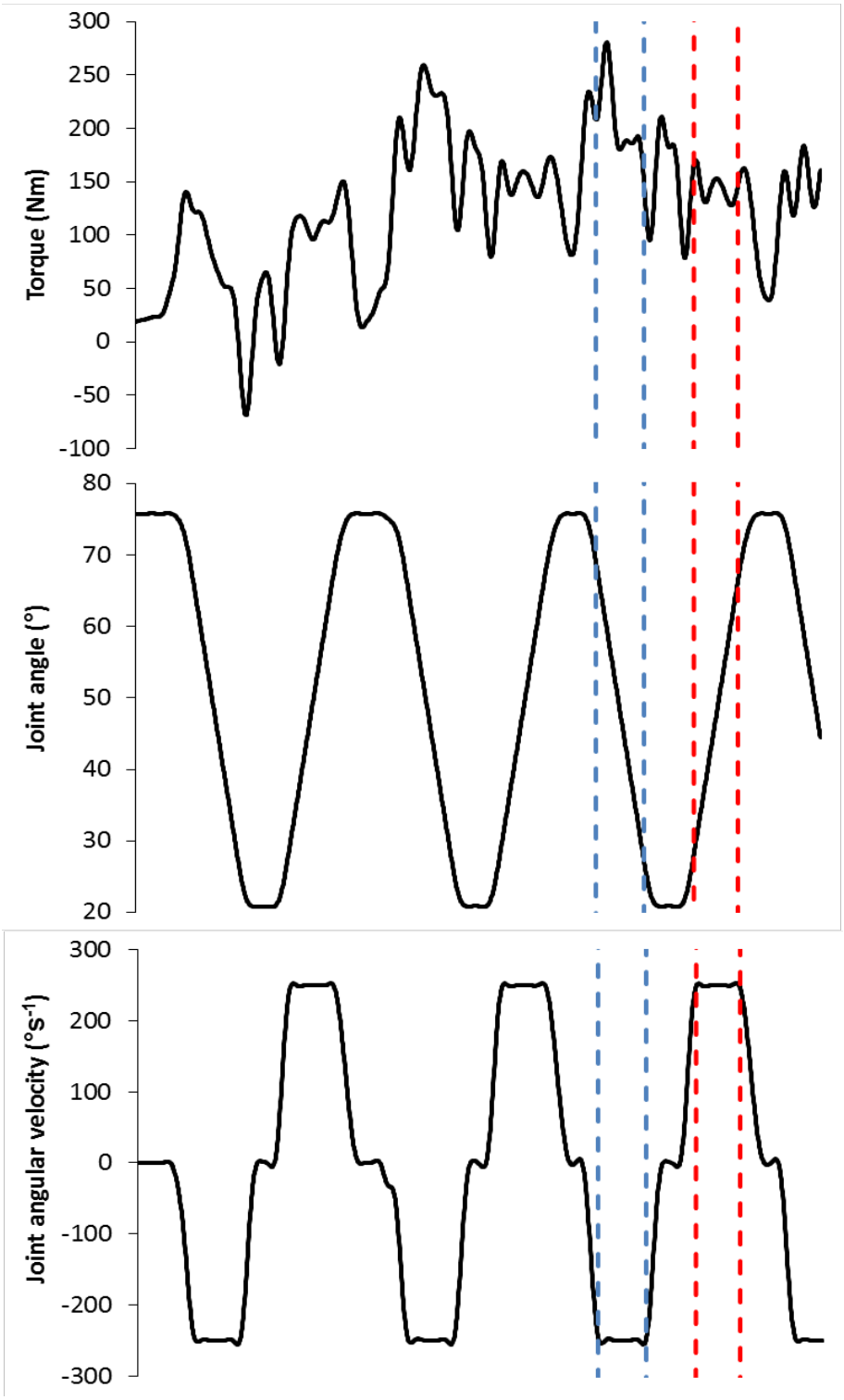

Figure 6.5. – Experimental data from an isovelocity knee extension trial showing the joint angle, angular velocity and torque. The region between the blue dashed lines is the selected maximal eccentric contractions and between the red lines the selected maximal concentric contractions.

6.2.1.3 Joint torque profile

The processed joint torque data provided the maximal voluntary torque producible at certain joint angles and angular velocities. In order to use this data within the simulation model, a torque surface defined by the relationships between torque and angle, torque and angular velocity, and differential activation and angular velocity, was used:

$$T = T_\theta(\theta) \cdot T_\omega(\omega) \cdot a(\omega) \qquad (6.1)$$

where $T_\theta(\theta)$ represents the torque calculated using the torque-angle relationship, $T_\omega(\omega)$ represents the torque calculated using the torque-angular-velocity relationship and $a(\omega)$ represents the neural inhibition of the muscles as a function of angular velocity. The mathematical relationships governing these three relationships are described below.

Torque-angle relationship

A two parameter quadratic function developed by King et al. (2006) was preferred to a bell shaped function (Audu and Davy, 1985) to describe the relationship between tetanic torque and joint angle, since Lewis (2011) found that the quadratic function provided a better representation of the measured torques.

$$T_\theta(\theta) = 1 - k_2(\theta - \theta_{opt})^2 \qquad (6.2)$$

where θ_{opt} is the optimum angle for torque production and k_2 is the width of the curve.

Previous studies (Allen, 2010; Jackson, 2010) have recalculated the torque-angle relationship when using the bell-shaped curve to be expressed as a function of the contractile component angle rather than joint angle. Lewis (2011), however, found when using the quadratic function the torque-angle relationship can be skewed by using the contractile component angle. Instead, he used the joint angle to calculate the torque-angle relationship and allowed the skew to exist between the contractile component and series elastic angles within the simulation model. This approach allowed the joint torques to be

closer matched near maximal activation when compared to those measured on the dynamometer. Therefore, the torque-angle relationship was kept as a function of joint angle.

Torque-velocity relationship

To represent the relationship between tetanic torque and contractile component angular velocity, two differing hyperbolic functions were employed depending on whether the phase was eccentric or concentric. The joint angular velocity was converted to contractile component angular velocity since King and Yeadon (2002) found that the joint angular velocity is approximately equal (or opposite and equal) to the contractile component angular velocity during periods of isovelocity.

In the concentric phase of angular velocities ω, the torque, T_ω, is represented by a rotational equivalent of the classic Hill hyperbola (1938):

$$T_\omega(\omega) = \frac{C}{(\omega_c + \omega)} - T_C \quad for\ \omega \geq 0 \qquad (6.3)$$

where

$$T_C = \frac{T_0 \omega_c}{\omega_{max}}, \qquad C = T_C(\omega_{max} + \omega_c)$$

In the eccentric phase of angular velocities, the torque is represented by an inverted hyperbola:

$$T_\omega(\omega) = \frac{E}{(\omega_E - \omega)} + T_{max} \quad for\ \omega < 0 \qquad (6.4)$$

where

$$\omega_E = \frac{(T_{max} - T_0)}{kT_0} \frac{\omega_{max}\omega_C}{(\omega_{max} + \omega_C)}, \qquad E = -(T_{max} - T_0)\omega_E$$

Four parameters are used to calculate the torque in the concentric or eccentric phases: the maximum torque in the eccentric phase, T_{max}, the isometric torque, T_0, the maximum angular velocity above which torque cannot be produced, ω_{max}, and the angular velocity of the vertical asymptote of the concentric

hyperbola, ω_C. The value of k, the ratio between the slopes of the eccentric and concentric phases, was predicted by Huxley (1957) and was set to 4.3.

Differential activation

A three parameter differential activation function was used to account for the difference between tetanic torque and maximal voluntary torque, caused by neural inhibition preventing full activation being achieved in voluntary eccentric contractions (Westing et al., 1990). A sigmoid function proposed by Forester et al (2011), in which the activation is directly defined has been employed:

$$a(\omega) = a_{min} + \frac{(a_{max} - a_{min})}{\left[1 + \exp\left(\frac{-(\omega - \omega_1)}{m}\right)\right]} \qquad (6.5)$$

where the maximum activation level, a_{max}, was assumed to be equal to 1.0, ω_1 is the midpoint of the curve and m governs the rate of activation.

6.2.1.4 Joint torque parameters

The nine parameter function (Equation 6.1) was fitted to the torque data to define the torque profile for flexion and extension of the ankle, knee, hip and shoulder, using a simulated annealing algorithm (Corana et al., 1987). The simulated annealing algorithm minimised the global difference between the torque profile and the torque data using a weighted root mean square score function (wRMS). A weighted score function was used due to the likelihood that the participant produced sub-maximal efforts thus potentially producing one-sided errors (Forrester et al., 2011).

Initial estimates of the upper and lower bounds were mostly taken from literature (Table 6.1). Although, maximum velocity movements with the limb unloaded were recorded using a Vicon Nexus motion analysis system (OMG Plc, Oxford UK) in the same data collection environment as described in Chapter 5. The participant was instructed to flex and extend as quickly as possible. This provided a lower bound prediction for the maximum joint angular velocity (Table 6.2).

Table 6.1. - Torque profile parameter bounds

Parameter	Bounds	Source
T_0	0.4 - 1.6 peak measured isometric torque	Dudley et al., 1990 Webber and Kriellers, 1997
T_{max}	$1.4\ T_0$	Dudley et al., 1990
ω_{max}	peak measured angular joint velocity	Experimental measure
ω_c	0.15 - 0.5 ω_{max}	Scovil and Ronsky, 2006
a_{min}	0.5 – 0.99	Seger and Thorstensson, 1994 Westing et al., 1990
m	0 - 1	
ω_1	-3.14 – 1.57 rad.s^{-1}	
k_2	0 – 2	Experimental measure
θ_{opt}	Based on joint range of motion	

Table 6.2. - Maximum joint angle velocities determined experimentally

Maximum joint angular velocity (rad.s^{-1})				
	Ankle	Knee	Hip	Shoulder
Flexion / Dorsi	11.4	16.8	16.6	15.0
Extension / Plantar	10.2	27.0	14.8	12.8

The nine parameters determining each joint torque profile are given in Table 6.3, as well as an example of the nine parameter joint torque function fitted to the data obtained for knee flexion (Figure 6.5).

Table 6.3 – Joint torque profile parameters

	Ankle		**Knee**		**Hip**		**Shoulder**	
	plantar	dorsi	flex	ext	flex	ext	flex	ext
$\mathbf{T_{max}}$ (Nm)	316	65	263	602	240	856	144	158
$\mathbf{T_0}$ (Nm)	226	47	188	430	172	611	103	113
$\boldsymbol{\omega_{max}}$ (rad.s^{-1})	20.1	10.6	22.0	25.8	34.4	15.4	28.9	30.0
$\boldsymbol{\omega_c}$ (rad.s^{-1})	5.10	2.42	3.35	4.74	7.83	2.30	7.74	5.15
$\mathbf{a_{min}}$	0.80	0.78	0.76	0.76	0.89	0.70	0.82	0.83
$\mathbf{m}$ (rad.s^{-1})	0.20	0.10	0.18	0.26	0.15	0.77	0.21	0.18
$\boldsymbol{\omega_1}$ (rad.s^{-1})	-0.14	-0.05	-0.06	-0.04	-0.37	1.56	-0.22	-0.22
$\mathbf{k_2}$ (rad)	2	0.64	0.264	0.8	0.29	0.3	0.2	0.3
$\boldsymbol{\theta_{opt}}$ (rad)	4.32	2.40	2.55	4.04	2.70	4.30	3.65	3.00
wRMS (Nm)	10	2	9	46	15	50	7	17
wRMS (% of $\mathbf{T_{max}}$)	4.1	3.4	4.6	10.1	7.2	8.3	5.6	13.1

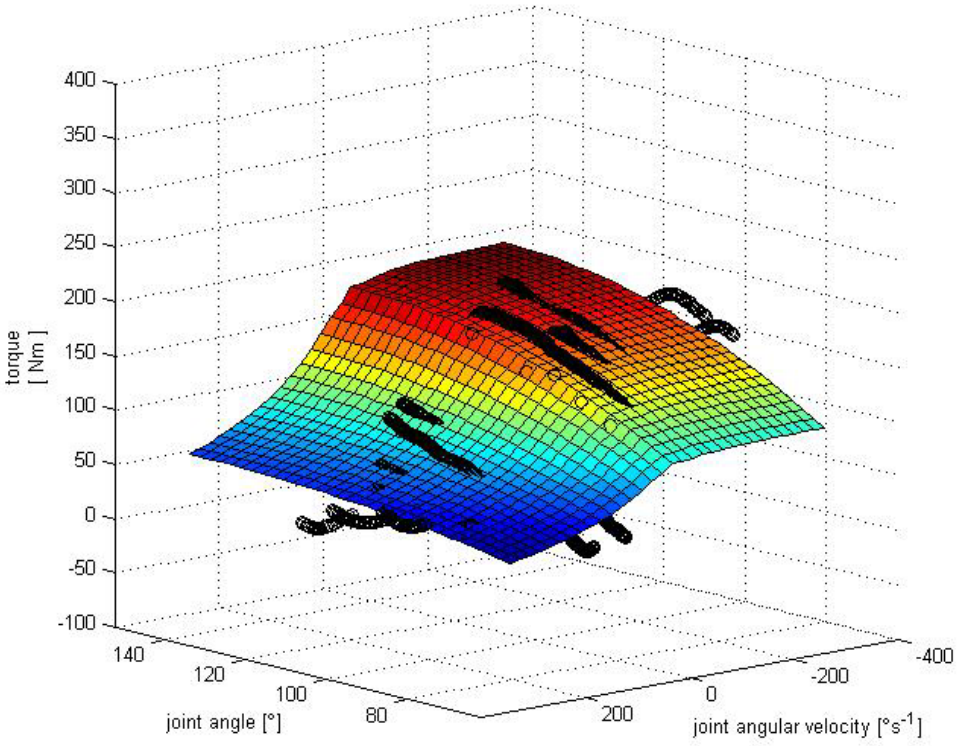

Figure 6.6. - Example of the fitted joint torque profile for knee flexion.

6.2.1.5 Series elastic component stiffness

In order to calculate the contractile component angle within the simulation model, the series elastic stiffness is required. The overall series elastic component stiffness for each joint movement is assumed to be the sum of the individual stiffness values (k_i) for the number of muscles (n) which contribute to that joint movement, since the muscles act in parallel :

$$k_{SEC} = \sum_{i=1}^{n} k_i \qquad (6.6)$$

The stiffness of each individual muscle was calculated by dividing the maximum isometric torque measured for that joint (T_{iso}) between the individual muscles depending on an estimate of their capabilities to exert force. This estimate was based on their physiological cross sectional area ($PCSA_i$) and pennation angle (α), and dividing by the associated series elastic component angle change:

$$k_i = \frac{T_{iso} \frac{d_i\ PCSA_i \cos\alpha}{\sum_{i=1}^{n}(d_i\ PCSA_i \cos\alpha)}}{\Delta\theta_{SECi}} \quad (6.7)$$

with the assumption that during maximal isometric contractions, the series elastic component is stretched by 5% (Finni and Komi, 2002), leading to a change in the series elastic component angle:

$$\Delta\theta_{SEC} = \frac{0.05\ L_{SEC}}{d} \quad (6.8)$$

where d is the moment arm of the selected muscle groups taken from the literature (Rugg et al., 1990; Spoor et al., 1990; Duda et al., 1996; Basset et al., 1990; Klein et al., 1996) and scaled to the participant using the appropriate segment length, and the length of the series elastic component (L_{SEC}) is calculated using the muscle architecture parameters (muscle belly length (L_b), tendon length (L_t), fibre length (L_f), and pennation angle (α)) found in the literature (Allard et al., 1995; Langenderfer et al., 2005) and scaled to the participant's height, using the equation of Pierrynowski (1995):

$$L_{SEC} = L_t + L_b - L_f(\cos\alpha) \quad (6.9)$$

Using this process and the muscle architecture parameters (Appendix 6), the series elastic component stiffness' have been calculated (Table 6.4).

Table 6.4. - Series elastic component stiffness parameters

Joint movement	SEC stiffness [Nm.rad^{-1}]
Plantar flexion	643
Dorsi flexion	152
Knee flexion	393
Knee extension	1008
Hip flexion	555
Hip extension	1387
Shoulder flexion	1346
Shoulder extension	1125

6.2.2 Wrist joint torque profile

The maximal voluntary flexion and extension torque of the wrist was taken from a gymnast of similar strength (Jackson, 2010). In order to account for any variability within the maximum voluntary torque between the fast bowler and gymnast, the upper bound for the activation levels for wrist flexion and extension were set to the maximum activation level found during model evaluation (Chapter 8).

Jackson (2010) used the same process as described in Section 6.2.1 to determine the wrist torque parameters (Table 6.5) and the series elastic component stiffness (Table 6.5).

Table 6.5 – Wrist torque profile parameters

	Wrist	
	flex	ext
$\mathbf{T_0}$ (Nm)	41	16
$\mathbf{T_{max}}$ (Nm)	57	22
$\boldsymbol{\omega_{max}}$ (rad.s^{-1})	36.4	37.0
$\boldsymbol{\omega_c}$ (rad.s^{-1})	5.46	5.48
$\mathbf{a_{min}}$	0.82	0.82
$\mathbf{m}$ (rad.s^{-1})	0.14	0.14
$\boldsymbol{\omega_1}$ (rad.s^{-1})	-0.16	-0.15
$\mathbf{k_2}$ (rad)	0.15	0.2
$\boldsymbol{\theta_{opt}}$ (rad)	3.8	1.59
wRMS (Nm)	8	1
wRMS (% of $\mathbf{T_{max}}$)	14	5

Table 6.6. - Series elastic component stiffness parameters

Joint movement	SEC stiffness [Nm.rad^{-1}]
Wrist flexion	37
Wrist extension	25

6.2.3 Bowling shoulder joint torque profile

Analysis of the fast bowling action revealed that the orientation of the bowling shoulder was outside the flexion/extension anatomical limit in the sagittal plane due to non-planar internal/external rotation and abduction/adduction. Therefore, it was not suitable to use the flexion/extension torque profile found within Section 6.2.1 for the bowling shoulder.

Instead, a torque function for the bowling shoulder was constructed based on the performance data. Since it was not possible to separate the flexion and extension components of the shoulder torque generator into individual components it was decided to model the net joint torque where it was assumed that the torque was always acting to extend the joint.

The extension torque was considered to be a function of the maximum voluntary torque and the activation level:

$$T = T_{MVC}(\theta, \dot{\theta}) \cdot A(t) \qquad (6.10)$$

where $T_{MVC}(\theta, \dot{\theta})$ represents the maximum voluntary torque as a function of angle and angular velocity, and $A(t)$ is the activation level.

The maximum voluntary torque has previously been defined as a function based on the torque-angle, torque-angular velocity and differential activation-angular velocity relationships (Section 6.2.1.3):

$$T_{MVC} = T_{\theta}(\theta) \cdot T_{\omega}(\omega) \cdot a(\omega) \qquad (6.11)$$

where $T_{\theta}(\theta)$ represents the torque calculated using the torque-angle relationship, $T_{\omega}(\omega)$ represents the torque calculated using the torque-angular-velocity relationship and $a(\omega)$ represents the neural inhibition of the muscles as a function of angular velocity.

As the maximal voluntary torque of the bowling shoulder in this position could not be determined using a dynamometer. The maximum voluntary torque function was modified using assumptions based on the performance data. Investigating the bowling shoulder angle-time history showed that the angle increased approximately linearly (R^2 = 0.98) during the front foot contact phase of fast bowling (Figure 6.7). The variation away from the linear relationship occurs due to the impact of the front foot with the ground and the trunk being accelerated forward, which increases the force at the shoulder.

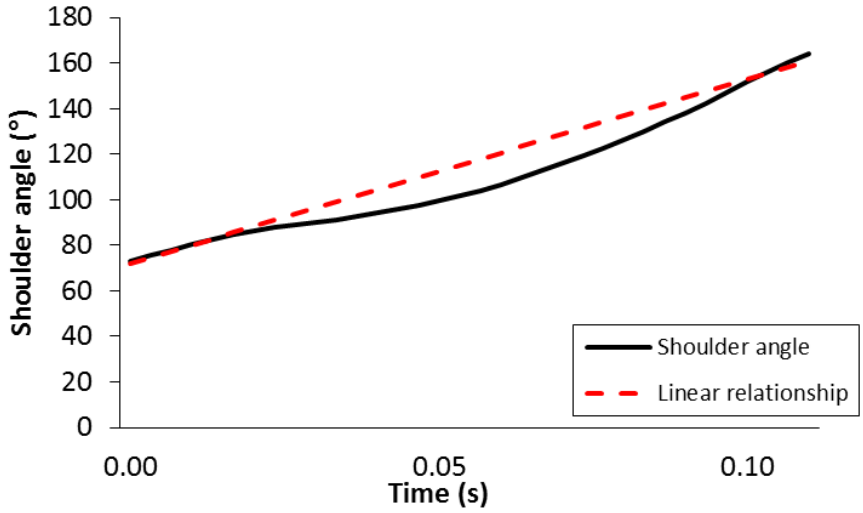

Figure 6.7. – Example of the shoulder angle-time history during the front foot contact phase of fast bowling and the interpreted linear relationship.

Since the shoulder angle-time history is approximately linear, the angular velocity by definition must be approximately constant. Assuming that the angular velocity is constant throughout the front foot contact phase of fast bowling results in the torque-angular velocity and differential activation-angular velocity relationships both being constant. Therefore, the shoulder extension joint torque can then be expressed as:

$$T = C \cdot T_\theta(\theta) \cdot A(t) \qquad (6.12)$$

where C is the constant from the product of the torque-angular velocity and differential activation-angular velocity relationships.

Since, it was not possible to deduce the torque-angle relationship; it was considered a reasonable assumption to model the torque-angle relationship as

a constant allowing any variability within the torque-angle relationship to exist within the activation level. The shoulder extension joint torque for the bowling shoulder was therefore:

$$T = \mathrm{C} \cdot A(t) \qquad (6.13)$$

where C is a constant which approximates the maximum voluntary torque of the bowling shoulder within the range of motion it goes through during the front foot contact phase of fast bowling and $A(t)$ is the activation level function described in Section 4.6.2.

In order to use this torque profile in the simulation model of fast bowling an approximation of the constant, C, was required. This was obtained by calculating the moment of the shoulder using inverse dynamics from the hand downwards for the three best trials (Figure 6.8). The shoulder torques for the three trials were seen to be very consistent. The peak torque of 71 Nm was used as the estimate of maximum voluntary torque for the bowling shoulder.

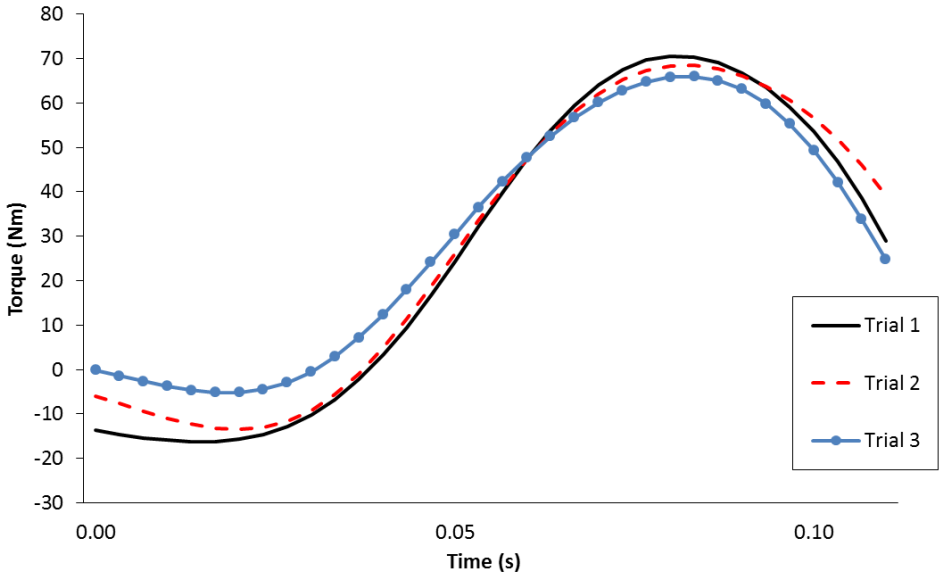

Figure 6.8 – Bowling shoulder moments calculated using inverse dynamics.

6.2.4 MTP and elbow joint torque profiles

Analysis of the performance data showed that the MTP joint was restricted by the structure of the shoe and the floor. Therefore, it was decided to assume that the contractile component at the MTP joint was zero. Similarly, the elbow

remained at its anatomical end point throughout the fast bowling action and was in hyperextension throughout. Since the contractile component for both flexion and extension would be small in this position and would have a negligible effect it was assumed to be zero.

6.3 PASSIVE PARAMETERS

The determination of the passive parameters employed at the front MTP, front ankle, front knee, front hip and the bowling elbow are detailed below.

6.3.1 Front ankle, front knee and front hip

The passive torque generators at these joints were described using the mathematical model of a 'generic subject' developed by Reiner and Edrich (1999). Passive torques of ten males was collected of comparable height, mass and age to the subject in this study, over a range of ankle, knee and hip joint angles. An exponential function was then used to relate the amount of passive torque at a joint to the angle of the joint in question, as well as the adjacent joints (in order to account for the biarticular muscles which cross both joints). Reiner and Edrich's (1999) equations for the passive torque at the ankle, knee and hip joints are shown below:

$$P_A = e^{(2.106-0.0843\theta_A-0.176\theta_K)} - e^{(-7.9763+0.01949\theta_A+0.0008\theta_K)} - 1.792 \quad (6.14)$$

$$P_K = e^{(1.800-0.046\theta_A-0.0352\theta_K+0.0217\theta_H)} - e^{(-3.971-0.0004\theta_A+0.0495\theta_K-0.0128\theta_H)} - 4.820 + e^{(2.22-0.15\theta_K)} \quad (6.15)$$

$$P_H = e^{(1.4655-0.034\theta_K-0.0750\theta_H)} - e^{(-1.3404-0.0226\theta_K+0.0305\theta_H)} + 8.072 \quad (6.16)$$

where P_A, P_K, P_H, and $\theta_A, \theta_K, \theta_H$ are the ankle, knee and hip passive torques and angles respectively.

6.3.2 Front MTP joint

Since the angle of the MTP joint is constant during the front foot contact phase of fast bowling due to the structure of the shoe and limited movement, the

parallel elastic component was modelled as a linear torsional spring which prevented the angle of the MTP joint from changing.

6.3.3 Bowling Elbow

A passive torque generator was employed at the elbow using a linear damped torsional spring, since it had been shown to provide a close agreement when modelling elbow hyperextension in previous research (Felton, 2010). The anatomical limit of the elbow was controlled using an exponential function in addition to the linear damped spring. The exponential function prevented the elbow angle, θ_E, exceeding the maximum hyperextension witnessed by the subject.

The equation for the passive torque at the elbow is:

$$P_E = -k_{es}\,(\theta_E + N\theta_E) - k_{ed}\dot{\theta_E} - p_1 e^{p_2(\theta_E + p_3)} \qquad (6.17)$$

where k_{es} and k_{ed} are the stiffness and damping coefficients of the spring at the elbow, $p_1$and p_2 are the parameters which define the exponential function limiting the anatomical range, $p_3$is the location of the anatomical limit and $N\theta_E$ is the natural length of the linear damped spring.

6.4 SUMMARY

In this chapter, the collection and determination of the subject-specific parameters has been described. The method used to determine the inertia parameters of the rigid and wobbling segments was explained. The protocol used to collect the strength data, as well as the process to fit the joint torque/angle/angular velocity relationship has been shown. Finally, the active and passive element of each joint torque profile used within the computer simulation of fast bowling has been defined.

- CHAPTER 7 -
MODEL PARAMETER DETERMINATION

In this chapter, the method for determining the model parameters using a simulated annealing algorithm together with an angle-driven model of the front foot contact phase of the fast bowling action is described. The resulting model parameters are subsequently evaluated using an independent trial.

7.1 MODEL INPUTS

The inputs for the angle-driven model described in Section 4.5, consisted of the initial conditions of the system just prior to the front foot contacting the floor, the joint-angle time histories of the MTP, both ankles, knees, hips, shoulders, and elbows as well as the bowling wrist, the massless segment orientation angle-time histories and the variable segment length-time histories (Chapter 5). The inertia properties of the segments were also required (Section 6.1). The initial conditions comprised the horizontal and vertical position of the front toe, the horizontal and vertical velocity of the centre of mass, and the orientation angle and angular velocity of the head + trunk segment.

Three maximum ball velocity bowling trials, deemed to be of a good length by the ECB Lead fast bowling coach, were chosen from the bowling data. The initial conditions for the three bowling performances are shown in (Table 7.1).

Table 7.1 – Initial conditions of the three maximum ball velocity trials

Initial Condition	Trial 1	Trial 2	Trial 3
Horizontal Front Toe Position (m)	0.826	0.669	0.457
Vertical Front Toe Position (m)	0.034	0.036	0.038
Trunk Orientation (°)	93.5	93.4	92.9
Angular Velocity ($°s^{-1}$)	179	184	161
Horizontal COM velocity (ms^{-1})	5.18	5.37	5.07
Vertical COM velocity (ms^{-1})	1.42	1.36	1.32

7.2 PARAMETER DETERMINATION

7.2.1 Initial inputs

7.2.1.1 Orientation angular velocity and COM velocity

The initial angular velocity of the trunk orientation angle, as well as the horizontal and vertical velocity of the centre of mass, were allowed to vary within the optimisation due to possible inaccuracies associated with calculating velocities (Hubbard and Alaways, 1989). The errors in the horizontal and vertical velocities of the centre of mass were calculated (Section 5.6.6) and used as the bounds in which the initial condition could vary from the measured value. The horizontal and vertical velocity was allowed to vary by ± 0.1 ms^{-1}. and the angular velocity was allowed to vary by ± 1 $rad.s^{-1}$ to account for errors in the kinematic data (King et al., 2006).

7.2.2 Model parameters

7.2.2.1 Ball position

In the simulation model the ball is attached to the hand segment, however, the distance from the wrist joint is unknown. In order to determine this, the distance of the ball from the wrist joint was allowed to vary across the three performance trials. The lower bound was taken as the smallest distance between the ball and wrist joint centre calculated in the sagittal plane from the performance data, and the upper bound was taken as the end point of the hand.

7.2.2.2 Ball release

Ball release in the angle-driven model was considered to have occurred when the simulation shoulder angle at ball release matched the performance shoulder angle at ball release. Ball release however, was considered to have occurred within the performance data when the distance between the ball marker and the wrist joint centre has sufficiently increased (>2 cm) to suggest the ball can no longer be in contact with the hand (Worthington, 2010). In reality, the force gripping the ball from the fingers decays to zero before this

point and extending the time the ball is held onto within the simulation model will cause problems when matching the simulation and performance ball release speeds. Therefore, in order to allow the simulation model to decay the force governing the ball-hand interface to zero a release window was found using the performance data defined by shoulder angle, where the lower bound was established as the last instant at which the distance between the ball marker and wrist joint centre was constant, and the upper bound was the ball release instant determined from the performance data. A parameter for each bowling trial was then used to vary the shoulder angle at which ball release occurred within this window during the optimisation process.

7.2.2.3 Ball-hand interface

The ball hand interface was modelled using a on-off approach where the ball was held in place vertically and horizontally using linear damped springs. Since the role of the springs was to hold the ball in place and limit the movement, the strength of the stiffness and damping parameters was set to 1000 Nm^{-1} and 1000 Nsm^{-1} respectively.

7.2.2.4 Front foot-ground interface

The three linear damped springs on the front foot positioned at the toe, MTP joint and the heel had individual stiffness and damping parameters. Each of the vertical stiffness parameters was allowed to vary between 0 and 100000 Nm^{-1} and the vertical damping parameters between 0 and 100000 Nsm^{-1}. Each of the horizontal stiffness parameters were varied between 0 and 20 Nm^{-1} and the horizontal damping parameters between 0 and 1 Nsm^{-1}. The horizontal parameters were a lot lower than the vertical parameters since the horizontal foot-ground interface was multiplied by vertical force to ensure the horizontal force was zero when the vertical force was zero (Section 4.4.1).

The natural length of the vertical springs was also found using this simulation model. The upper and lower bounds for the natural length of each spring were found by calculating the marker displacement before and after impact from the

performance data. Impact was deemed to have occurred when the movement of the marker at the location of each spring was seen to deviate due to impact.

7.2.2.5 Back foot-ground interface

Investigating the back foot force traces in the horizontal and vertical directions shows that the back foot has minimal force (<25 N) acting upon it during the front foot contact phase. Therefore, the vertical and horizontal stiffness parameters for the linear damped springs governing the foot-ground interface were set to 0 during the simulation period.

7.2.2.6 Wobbling-rigid element interface

The stiffness and damping of the springs at either end of the wobbling element which attach to the rigid element for the trunk, shank and thigh were determined. For each segment, the springs connecting the top and bottom of the wobbling element to the rigid element had the same parameters. Furthermore, both shank and thigh representations had the same parameters for the back and front leg. The stiffness and damping of each spring was varied between an upper and lower bound to limit the distance the wobbling mass could move from the rigid element. The spring stiffness' were allowed to vary between 0 and 5000 Nm^{-1} and the damping between 0 and 3000 Nsm^{-1}.

7.2.3 Summary

In order to find a robust set of viscoelastic parameters, the same 18 stiffness and damping parameters consisting of: three vertical stiffness', three horizontal stiffness', three vertical damping and three horizontal damping parameters on the front foot, as well as stiffness and damping values for each of the trunk, thigh and shank wobbling masses, were evaluated across each of three performance trials. The distance of the ball from the wrist joint centre and the natural length of the vertical springs on the front foot were also evaluated across each of the three performance trials. A further three parameters were included within the optimisation to vary three initial conditions. These three parameters were unique for each performance and therefore nine parameters

were required across the three performances. Finally, another unique parameter was used to determine ball release. Overall, a total of 26 optimisation parameters were used per simulation and a total of 34 parameters in the whole process.

7.3 METHOD

In order to select a robust set of parameters, three fast bowling performances were matched concurrently to determine the final parameter values. The model parameters were then evaluated on a fourth fast bowling performance.

A simulated annealing algorithm (Kirkpatrick et al., 1983) varied the model parameters in order to minimise an objective function representing the difference between the simulation and the recorded performances. A simulated annealing algorithm was chosen due to its ability to converge to a global optimum in 'hard' optimisation problems (van Soest and Casius, 2003).

The objective function used to give each set of model parameters a score was determined as the average of a performance score function applied to each of the three matched performances:

$$\bar{P} = \frac{P_1 + P_2 + P_3}{3} \qquad (7.1)$$

7.3.1 Performance score function

Each individual matching was given a score using a function comprising four components:

- S_1 - the average of the horizontal and vertical RMS differences expressed as a percentage of the peak vertical force
- S_2 - the difference in the COM velocity vector at ball release as a percentage of the relative COM velocity
- S_3 - the orientation angle RMS difference in degrees
- S_4 - the difference in the ball velocity vector at ball release expressed as a percentage of the relative ball velocity

The score function was calculated by taking the overall RMS of these four components which reduced the chances of any one of the components being neglected during the optimisation process. The components were equally weighted, where one degree was considered to be comparable to 1% difference in other measures (Yeadon and King, 2002). Thus, the performance score function for each individual performance was defined as:

$$P_i = \sqrt{\left(\frac{{S_1}^2 + {S_2}^2 + {S_3}^2 + {S_4}^2}{4}\right)} \qquad (6.2)$$

The calculations used to find the four components can be found in Appendix 7.

7.3.2 Penalties

Penalties were added to the performance score function to prevent the simulation model behaving in unrealistic manners.

Foot-ground interface

Allen et al. (2012) found that it was possible to accurately model ground reaction forces using a pin joint simulation model provided extra compliance was incorporated at the foot-ground interface. The extra compliance is required to overcome the potential weakness of pin joint simulation models that limits their ability to accurately model ground reaction forces due to the lack of compliance across the model. The magnitude of the extra compliance was found to be a crucial factor in the accuracy of the ground reaction forces, with unrestricted additional compliance providing the best match. However, this meant the model required unrealistically low stiffness and damping parameters, and therefore the accuracy of the kinematics of the performance suffered. It was shown that when the main purpose of the model is to optimise performance, the extra compliance at the floor should be minimised (<4 cm) in order to obtain the viscoelastic parameters that allow the torque-driven model to accurately match the kinematics of the performance.

In order to choose suitable limits for the movement of the front foot, it was important to understand the behaviour of the front foot both horizontally and vertically.

Vertical compression

To determine the compression within the shoe vertically during the front foot contact phase the displacement of the ankle joint centre from its initial position was assessed for the three trials to be matched (Figure 7.1).

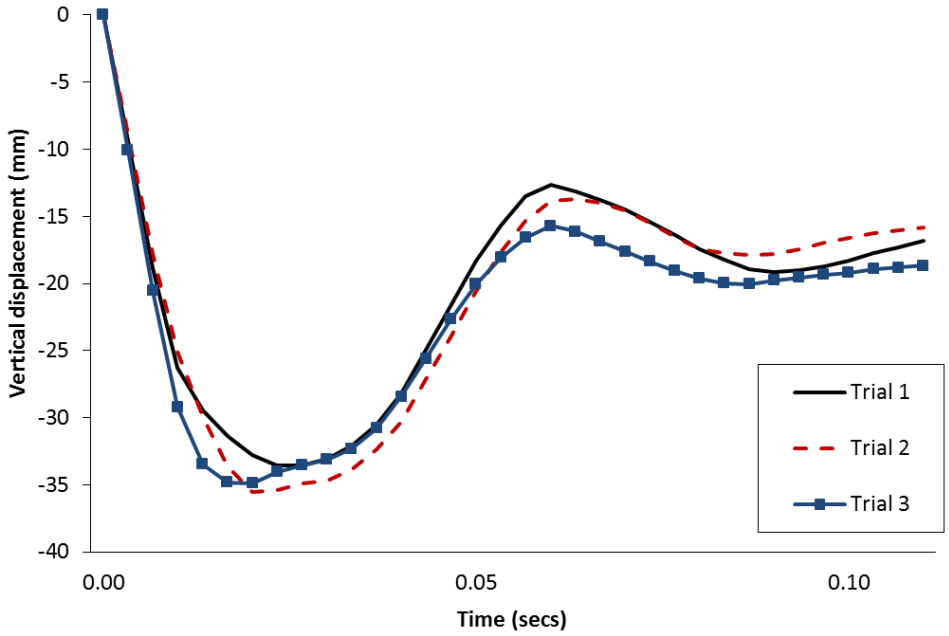

Figure 7.1 – Vertical displacement of the ankle joint.

The peak vertical compression of the foot during the contact phase is seen to be consistent across all three trials with an average of 34.7 mm.

Horizontal compression

To determine the horizontal displacement (slide) of the foot during the contact phase between front foot contact and ball release, the displacement of the ankle joint centre from the initial position was assessed for the three trials to be matched (Figure 7.2).

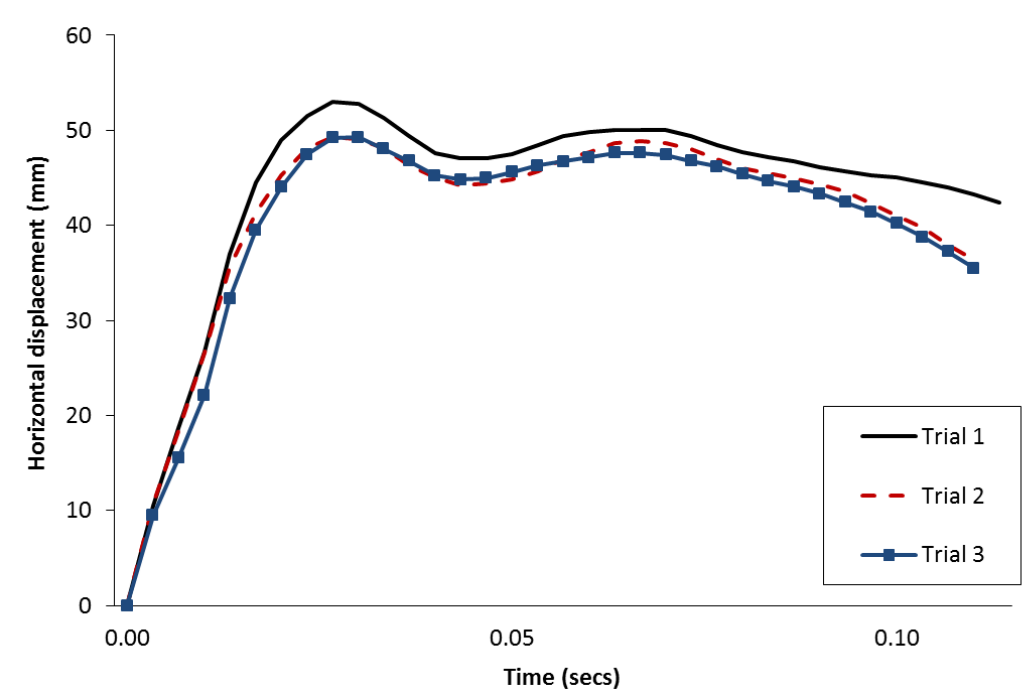

Figure 7.2 - Horizontal displacement of the ankle joint.

The peak horizontal displacement of the foot during the contact phase is seen to be consistent across all three trials with an average of 50.5 mm.

In order to take into consideration the compression in the shoe, as well as incorporating some extra compliance (<4 cm) in order to help limit the problems associated with pin joint models (Allen et al., 2012), foot movement was bound by limits of 6 cm vertically and 9 cm horizontally from the initial point of ground contact.

Penalties were also employed to ensure that the foot didn't 'bounce' in and out of contact with the ground during the simulation period as well as ensuring that the foot was still in contact with the ground at ball release.

Wobbling masses

Wobbling mass movement was limited to a maximum of 4.5 cm at the shank, 7 cm at the thigh and 10 cm at the trunk. The limits for the shank and thigh were taken from research by Lafortune et al. (1992) during loaded and unloaded knee flexion/extension which highlighted movement of external markers of up to 4.3 cm and 7.5 cm with respect to the tibia and femur, respectively. Whereas,

the limit for the trunk was taken from an investigation into the movement of the visceral mass during periodic movements (Minetti and Belli, 1994) which found displacements of 0.1 m during a hopping task. These numbers were also previously used in the simulation models of Wilson (2003) and Allen (2010).

7.4 RESULTS

When the three individual simulations were matched concurrently, a common set of viscoelastic parameters which led to a close agreement was found between the simulations and performances with an overall score of 6.5% (Table 7.2) resulting from individual scores of 7.0%, 6.6% and 6.0%. The matched viscoelastic parameters obtained in the optimisation process can be found in Appendix 8.

Table 7.2 – Combined scores for the angle-driven simulations of the three bowling trials

Component	Trial 1	Trial 2	Trial 3	Combined
GRF Force (%)	12.7	12.3	11.2	11.9
COM Velocity (%)	5.3	3.6	3.8	4.2
Trunk Orientation (°)	1.0	1.0	0.7	0.9
Ball Velocity (%)	1.8	3.3	1.7	2.3
Overall Difference (%)	**7.0**	**6.6**	**6.0**	**6.5**

The mean performance score of 6.5% can be broken down into average scores for the kinematic (COM velocity, orientation angle and ball velocity) and kinetic variables (GRF Force) of 2.5% and 11.9%, respectively. The low kinematic score of 2.5% shows that the simulation model was capable of replicating fast bowling performance of the front foot contact phase. Although, the kinetic score had larger discrepancies this was expected due to the nature of the pin joint simulation model and lack of compliance across the system (Allen et al., 2012). Furthermore, examining the force-time histories (Figures 7.3 and 7.4) showed that the key features had been maintained. Therefore, the use of the force component in the score function and the magnitude of the score values were seen as acceptable.

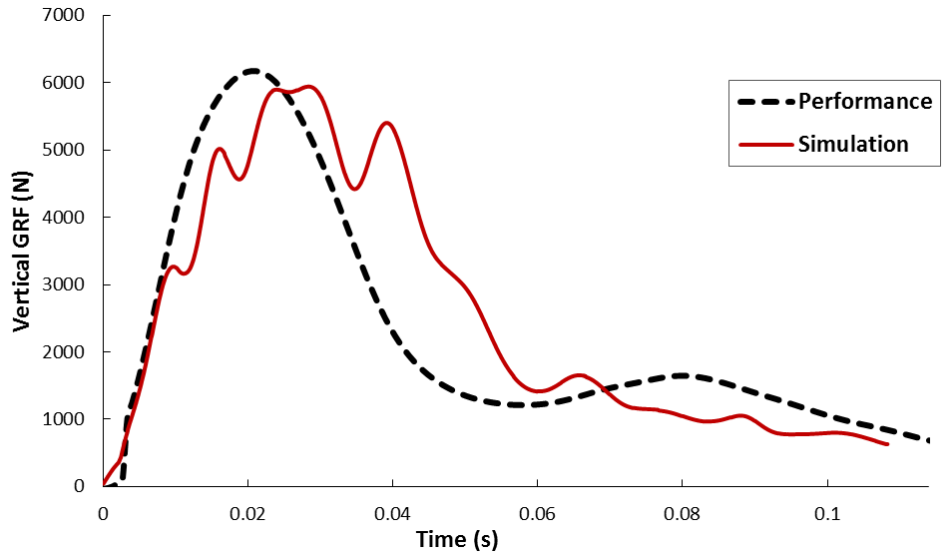

Figure 7.3 - Comparison of the vertical ground reaction forces for a simulation of the front foot contact phase vs. performance.

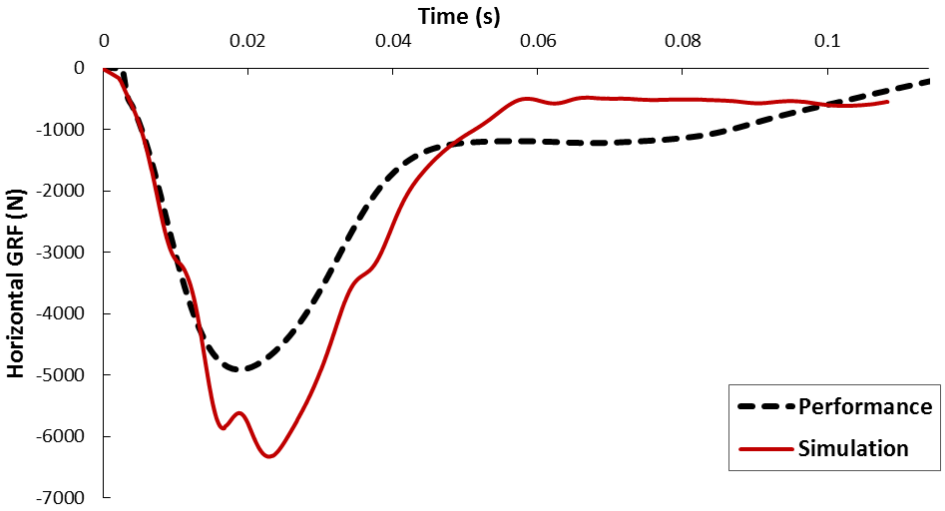

Figure 7.4 - Comparison of the horizontal ground reaction forces for a simulation of the front foot contact phase vs. performance.

7.5 EVALUATION

To ensure the validity of the viscoelastic parameters and provide a test of robustness in order to ascertain whether the simulation model could reproduce realistic human movements, and therefore be used generally to investigate fast bowling performance, an evaluation of the model was required. A fourth

bowling trial was used to evaluate the angle-driven model. The initial conditions for this bowling trial are shown in Table 7.3.

Table 7.3 – Evaluation trial initial conditions

Initial Condition	
Horizontal Front Toe Position (m)	0.753
Vertical Front Toe Position (m)	0.038
Trunk Orientation (°)	92.8
Angular Velocity (° s-1)	179
Horizontal COM velocity (ms^{-1})	5.14
Vertical COM velocity (ms^{-1})	1.44

Using the viscoelastic parameters determined from the combined matching procedure (Appendix 8), and allowing the same initial conditions to vary, the additional bowling trial was simulated and the associated score was determined. Reasonable agreement was found between the evaluation simulation trial and the recorded performance with an overall score of 6.7% (Table 7.4).

Table 7.4. – Score for the evaluation of the angle-driven model

Component	**Score**
Force (%)	11.6
COM Velocity (%)	6.5
Trunk Orientation (°)	0.9
Ball Velocity (%)	0.9
Overall Difference (%)	**6.7**

The score for the additional fast bowling trial fell within the range of scores of the three fast bowling trials simulated during the combined matching. The kinematic score (COM velocity, orientation angle and ball velocity) was again low, 2.8%, which showed that the combined matching parameters could be used to simulate the front foot contact phase of fast bowling.

Visual representations of the front foot contact phase during the recorded performance and evaluation simulation are shown in Figure 6.5, and show the close agreement between the recorded and simulated performances.

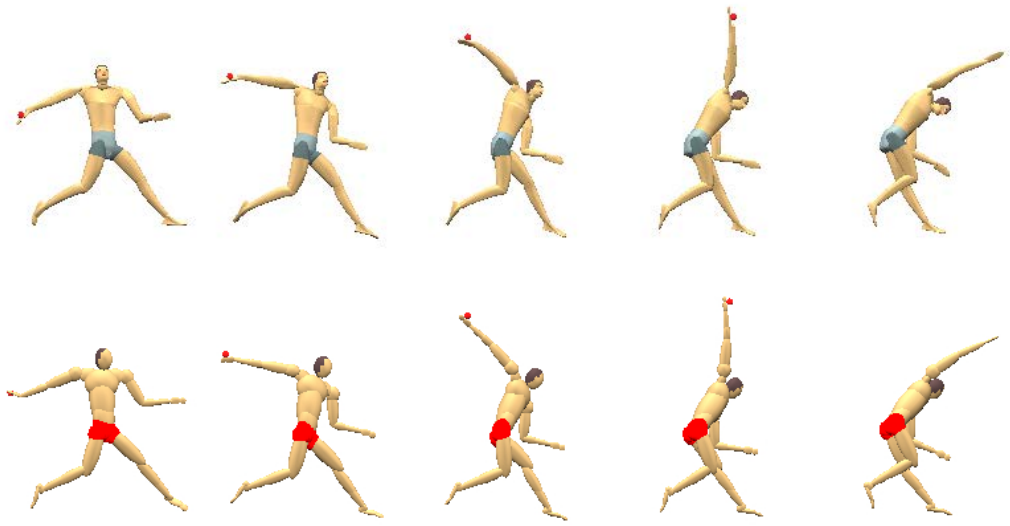

Figure 7.5 – Comparison of the front foot contact phase of fast bowling: recorded performance (upper) and angle-driven evaluation using the model parameters (lower).

7.6 SUMMARY

In this chapter, the angle-driven simulation model of fast bowling described in Section 4.6 was driven using the splined time histories of the joint angles, massless segment orientations and lengths of the variable length segments (Section 5.6) to determine a common set of model parameters. In order to select a robust set of parameters, three fast bowling performances were matched concurrently to determine the final parameter values. The model parameters were then evaluated on a fourth fast bowling performance, where the results were sufficiently accurate to enable these parameters to be used in future simulations of the front foot contact phase of fast bowling.

- CHAPTER 8 -
MODEL EVALUATION

The method for evaluating the torque-driven simulation model of the front foot contact phase of fast bowling using a genetic algorithm is described in this chapter. The results of the evaluation are reported and discussed.

8.1 MODEL INPUTS

The best recorded performance was chosen to evaluate the simulation model. The inputs for the torque-driven model consisted of the initial conditions of the body just prior to front foot contact, the joint-angle time histories of the angle-driven joints, as well as the massless segment orientations and variable segment lengths as a function of the trunk orientation angle (Section 5.6). The inertia properties of the segments were also input (Section 6.1) in addition to the model parameters determined in Chapter 7.

The initial conditions of the body comprised the horizontal and vertical position of the front toe, the horizontal and vertical velocity of the centre of mass, and the initial configuration and angular velocity of the fast bowler's body segments for the torque-driven joints. The initial conditions for the trial used during the model evaluation process are shown in Appendix 9.

8.2 MODEL VARIABLES

8.2.1 Initial inputs

The horizontal and vertical velocities of the centre of mass were allowed to vary from the recorded performance values by ±0.1 ms^{-1} (Section 5.6.6). The angle and angular velocity of the front ankle, front knee, front hip and the trunk orientation of the simulation model were allowed to vary by ± 1° and ±1 $rad.s^{-1}$ respectively. These small amounts of variation were allowed to compensate for possible inaccuracies with calculating velocities (Hubbard and Alaways, 1989),

errors due to modelling assumptions and errors in the kinematic data due to marker movement under impact (Reinschmidt,1997).

8.2.2 Ball release

Ball release was determined during the evaluation of the torque-driven model using the same method as in the angle-driven model (Section 7.2.2.2).

8.2.3 Activation profiles

For each of the active torque generators, an activation profile was used to determine the amount of flexor and extensor torque being applied at each joint as outlined in Section 4.6.2. The flexor and extensor activation profiles at each joint were able to: ramp up-ramp down, ramp down-ramp up, ramp in one direction only (if the start time of the second ramp was delayed sufficiently) or remain at the initial activation level.

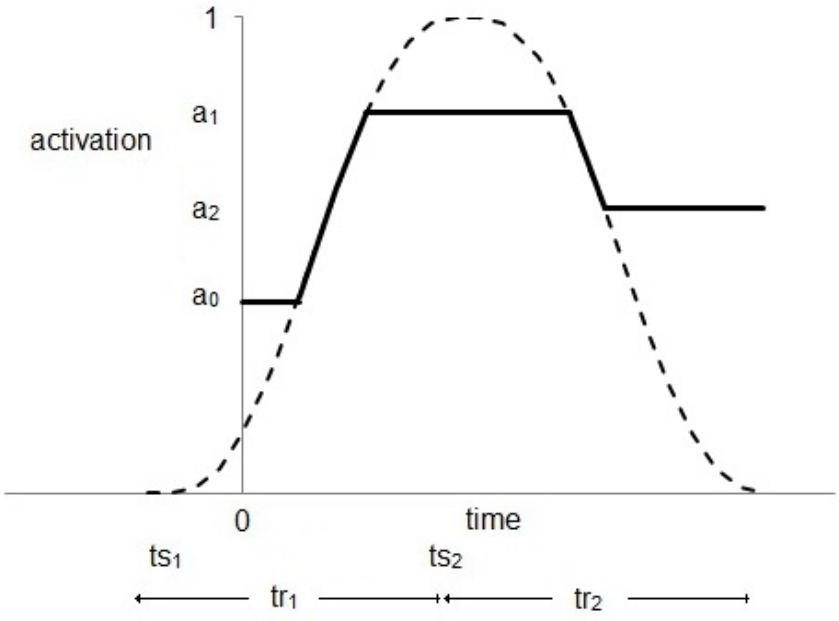

Figure 8.1 – Example of an activation level profile for a torque generator (bold line represents the activation level).

The activation profile described in Section 4.6.2 is defined by seven parameters (Figure 8.1). The lower and upper bounds of these parameters were decided based on information in the literature as outlined below.

The initial activation of the profiles governing the joints in the front leg (ankle, knee and hip) were considered to be in co-contraction since Yeadon et al. (2010) demonstrated that the muscles of the legs are activated before a landing. Co-contraction allows the muscles to be active without large joint accelerations occurring. In order to ensure the joints in the front leg were in co-contraction the initial activation level, $a_{0,}$ was bound within the range 0.25 - 0.5. Since there is non-zero activation prior to impact, the first muscle ramp can also start prior to impact. The start time of the first muscle ramp was therefore allowed to occur between 35 ms before impact and 250 ms after. The initial activation level of the back hip, the non-bowling arm shoulder and the bowling arm wrist were allowed to vary between 0-1, where the initial start time of the first ramp had the same bounds as above (-35 - 250 ms). The initial activation of the bowling shoulder was forced to be below 0.5, with the same initial start time (-35 – 200 ms).

The time for each ramp, tr_1 and tr_2, was set based on the minimum time required to ramp from zero to maximal activation for voluntary muscle contraction. Freund and Budingen (1978) observed this time to be 70 ms. The minimum time to ramp from maximal to zero is assumed to be similar, and therefore the lower bound for tr_1 and tr_2 was set to 70 ms. Theoretically, there is no upper limit for the upper bound, however it was set to 250 ms, within which time the front foot contact phase of fast bowling would have comfortably been completed.

The start time of the second ramp, ts_2, was constrained to start after the end of the first ramp to avoid rapid changes in activation level. The activation parameters and associated bounds are summarised in Table 8.1, where the bounds for the joints in co-contraction prior to impact (front ankle, front knee and front hip) are given in brackets if different to those that aren’t in co-contraction.

Table 8.1 – Definitions of the activation level parameters

Parameter	Definition	Lower bound	Upper bound
a_0	Pre-impact activation level	0.0 (0.2)	1.0 (0.5)
a_1	Maximal/minimal activation level	0.0	1.0
a_2	Final activation level	0.0	1.0
ts_1	Start time of first ramp (s)	-0.035	0.25
tr_1	Ramp time of first ramp (s)	0.07	0.25
ts_2	Start time of second ramp (s)	ts_1+tr_1	$ts_1+tr_1+0.25$
tr_2	Ramp time of second ramp (s)	0.07	0.25

8.2.4 Passive torque parameters

The stiffness of the linear torsional spring that modelled the passive torque at the front MTP joint (Section 6.3.2) was determined during model evaluation. The stiffness and damping coefficients of the linear damped spring and exponential function within the passive torque profile at the elbow (Section 6.3.3) were also found.

8.2.5 Orientation angle functions

Since the Fourier series approximations that describe both the variable segment lengths and segment orientation angles as a function of the trunk orientation angle were deduced using the three best recorded performances, the function was allowed to translate both horizontally and vertically (Figure 8.2) to provide a closer match with the best trial.

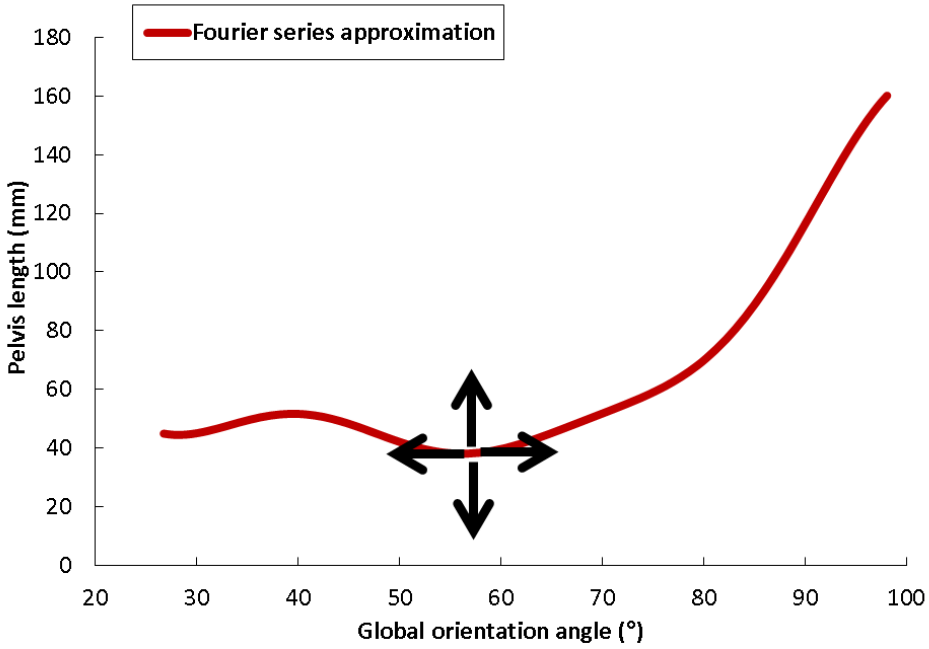

Figure 8.2 – Possible adjustments of the Fourier series approximation.

8.2.5.1 Variable segment length

The functions governing the length of each segment was able to translate ± 2 cm in the vertical direction and ± 2° in the horizontal direction. The possible segment lengths for the trunk + head, pelvis and shoulder segments are shown in Figure 8.3 below:

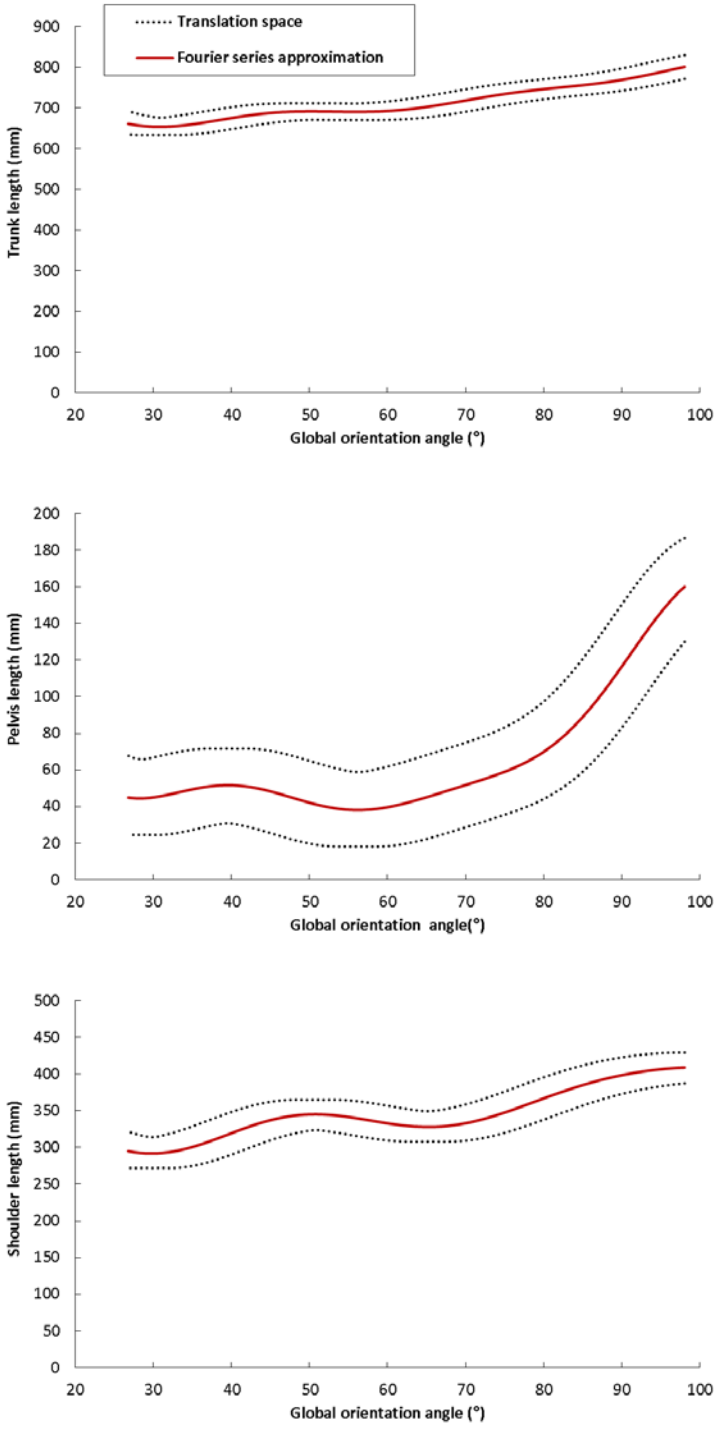

Figure 8.3 – Possible translations of the variable segment length functions.

8.2.5.1 Orientation of the massless segments

The orientation of the massless pelvis segment was able to translate ± 7.5° in the vertical direction and ± 2° in the horizontal direction. The orientation of the massless shoulder segment was able to translate ± 5° in the vertical direction

and ± 2° in the horizontal direction. The possible translations of these two orientations are shown in Figure 8.4 below:

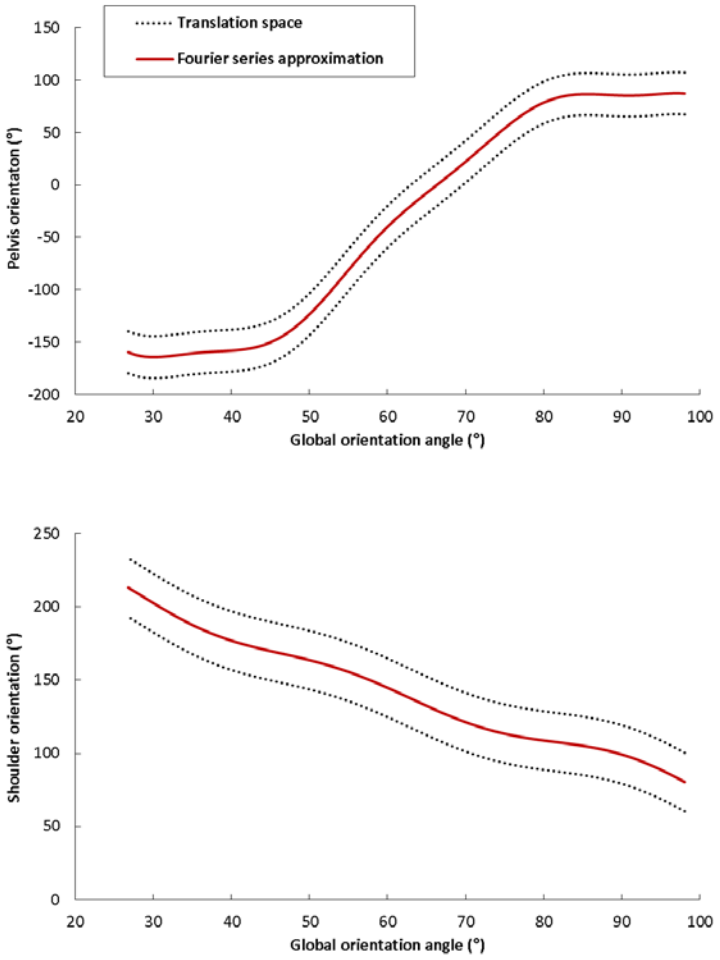

Figure 8.4 – Possible translations of the orientation of the massless segments.

8.2.6 Summary

In order to evaluate the model of fast bowling, 119 parameters were used: 10 parameters were used to vary the initial conditions of the simulation model, 91 parameters governed the activation levels of the torque generators, 10 parameters allowed the variable segment lengths and massless segment orientation angles to vary, 7 parameters determined the passive torque profiles of the front MTP and elbow joints and 1 parameter was used to determine ball release.

8.3 METHOD

In order to evaluate the simulation model of the front foot contact phase of fast bowling, an objective function was minimised using a genetic algorithm (Carroll, 2001). A genetic algorithm was chosen for the model evaluation as the code could be parallelised which greatly reduced the processing time required to determine the optimum solution.

8.3.1 Objective function

An objective function was used to give each simulation a score relating to how well the simulation matched the recorded performance which composed of six components:

- S_1 - the average of the RMS difference of the horizontal and vertical ground reaction forces expressed as a percentage of the peak vertical force
- S_2 - the difference in the COM velocity vector at ball release as a percentage of the relative COM velocity
- S_3 - the trunk orientation angle RMS difference in degrees
- S_4 - the difference in the ball velocity vector at ball release expressed as a percentage of the relative ball velocity
- S_5 - the difference in time of the front foot contact phase as a percentage of the time taken during the actual performance
- S_6 - the RMS of the RMS differences of the nine torque-driven joint angles in degrees

The overall score was calculated by taking the RMS of these six components. This reduced the chances of any one of the components being neglected during the optimisation process. The components were equally weighted, where one degree was considered to be comparable to 1% difference in other measures (Yeadon and King, 2002). Thus, the score function for each individual performance was defined as:

$$P_i = \sqrt{\left(\frac{{S_1}^2 + {S_2}^2 + {S_3}^2 + {S_4}^2 + {S_5}^2 + {S_6}^2}{6}\right)} \qquad (8.3)$$

The calculations used to find the six components can be found in Appendix 10.

8.3.2 Penalties

The score for each simulation incurred penalties if the foot-ground interface and wobbling mass movement exceeded the same bounds as described for the angle-driven model in Section 7.3.2.

In addition to these penalties, the model suffered penalties if the joint angles exceed the fast bowler's anatomical bounds. For each degree that the joint angle exceeded an anatomical bound, a one percent penalty was acquired. The bounds can be seen in Table 8.2. The limits were only in place if the model was likely to break them, hence the one sided nature of the ankle, knee, hip and elbow joints, as well as no anatomical bounds being placed on the shoulder joint. The limits were chosen based on the performance data and known anatomical constraints.

Table 8.2 – Bounds on the range of motion of the joints

Joint angle	Lower bound	Upper bound
Ankle	n/a	150°
Knee	n/a	200°
Hip	n/a	210°
Shoulder	n/a	n/a
Elbow	n/a	194°
Wrist	90°	225°

8.4 RESULTS

The simulation of the front foot phase of the fast bowling action matched well with the performance data, with an overall difference of 3.99%. Table 8.3 shows the differences between the simulation and recorded performance for each of the score components. The kinematic score (disregarding the force component) is very low, 0.87%, which suggests the simulation can accurately reproduce the kinematics of the front foot contact phase. None of the penalties

regarding the foot-ground interface, the wobbling masses or the anatomical limits of the joints were incurred during the simulation. The optimisation parameters which are associated with this simulation can be found in Appendix 11.

Table 8.3. – Difference between the performance and matched torque-driven simulations

Component	Difference
S_1 – Force (%)	9.59
S_2 – COM (%)	0.06
S_3 – Orientation (°)	0.67
S_4 – Ball velocity (%)	0.03
S_5 – Time (%)	0.19
S_6 – Joint angles (°)	1.81
Overall Difference (%)	**3.99**

Visual representations of the front foot contact phase during the recorded performance and matched torque-driven simulation are shown in Figure 8.5, and show the close agreement between the recorded performance and matched torque-driven simulation.

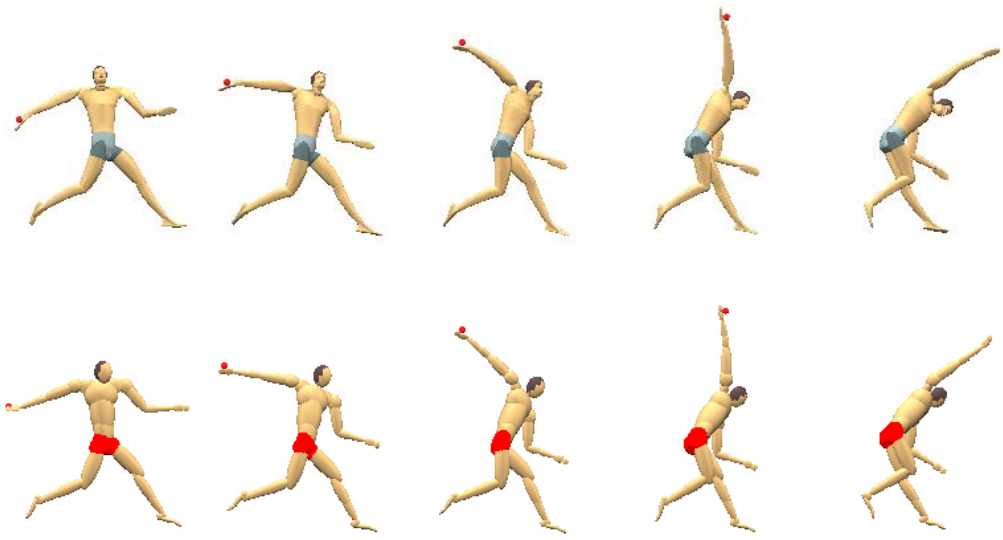

Figure 8.5 - Comparison of the front foot contact phase of fast bowling: recorded performance (upper) and torque-driven matched simulation (lower).

Due to the close agreement between the matched torque-driven model and the recorded performance, evident in the small differences within the objective

function components, it is indicated that the simulation model is capable of adequately replicating the front foot contact phase of the fast bowling action. The simulation results however, will be analysed and discussed in the following sections.

8.4.1 Centre of mass position

The centre of mass displacement time histories for the recorded performance and matched torque-driven simulation are shown in Figure 8.6 and shows a close match with RMS differences of 2.8 cm horizontally and 4.1 cm vertically. The differences are attributed to the fixed segment lengths used in the simulation model and the difference in joint angles between the simulation and performance. The centre of mass time history was not included explicity within the matching criteria.

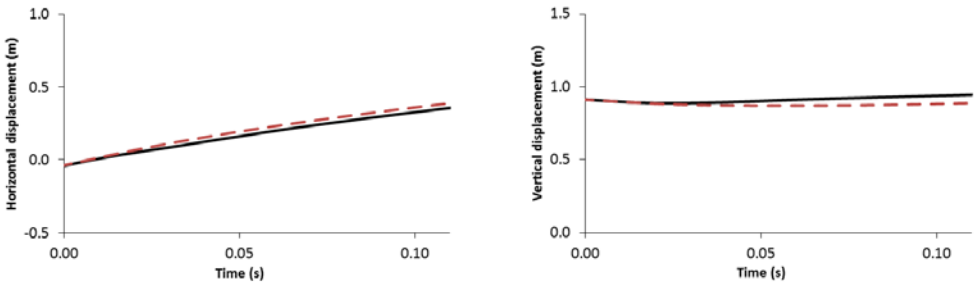

Figure 8.6 – Centre of mass displacement time histories from the matched simulation (red dashed lines) and the performance (solid black lines) of the front foot contact phase of fast bowling.

8.4.2 Joint angles

The simulated joint angles for each of the torque-driven joints are compared to the recorded performance in Figure 8.7. The individual joint angle RMS differences between the matched simulation and the recorded performance for these joints are shown in Table 8.4. Since there was no clear trend of the simulation joint angles matching more closely at one joint than at another, the individual torque generators at each joint are capable of providing the requisite torques for the simulation model to match the recorded performance.

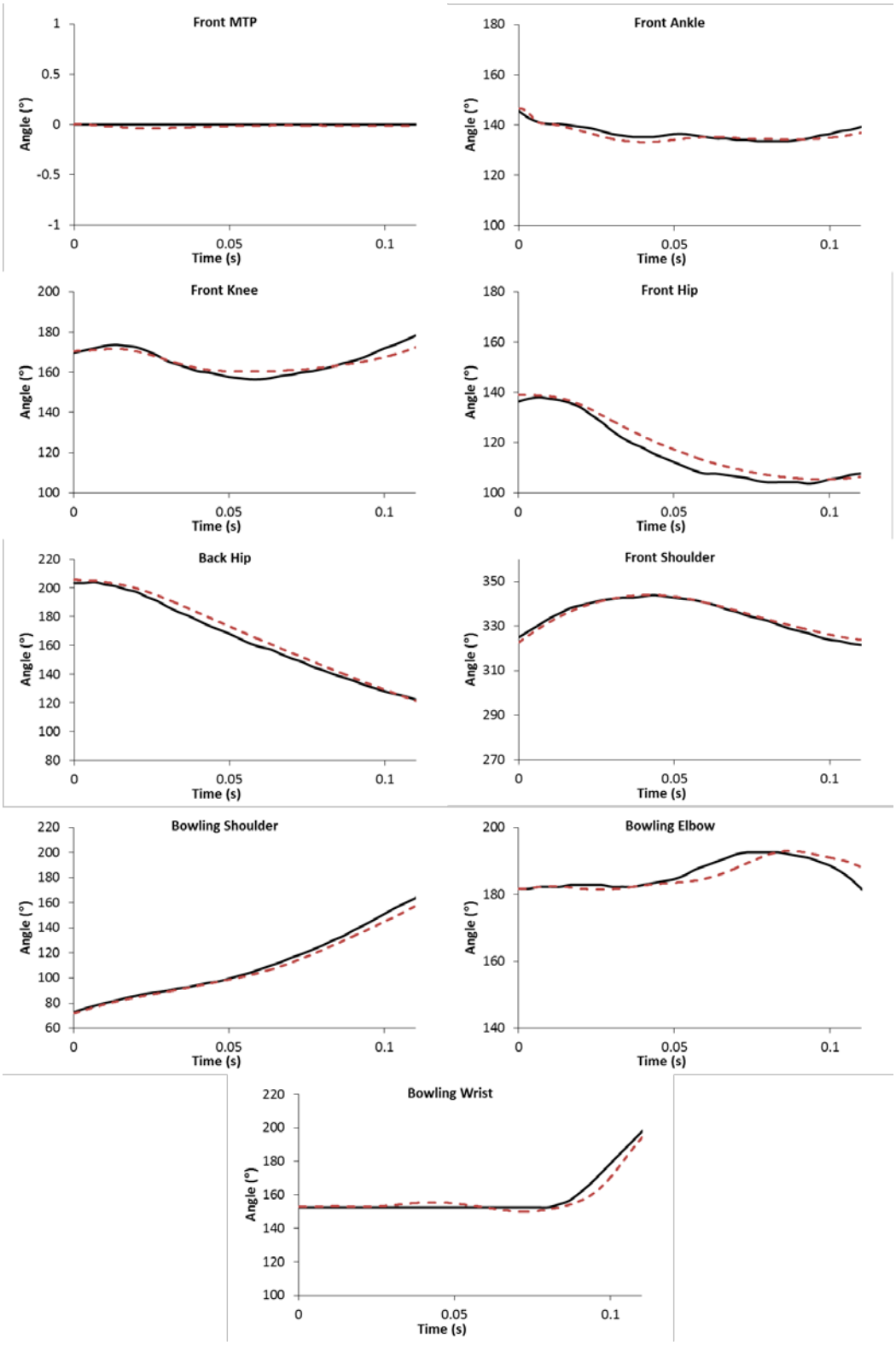

Figure 8.7 – Joint angle time histories from the matched simulation (red dashed lines) and the performance (solid black lines) of the front foot contact phase of fast bowling.

Table 8.4 – RMS differences of the torque-driven joint angles between the recorded performance and matched simulation

Joint angle	RMS Difference (°)
Front MTP	0.02
Front ankle	1.54
Front knee	2.31
Front hip	2.06
Back hip	1.79
Front shoulder	1.01
Bowling shoulder	1.14
Bowling elbow	2.67
Bowling wrist	2.20
RMS	**1.81**

The close agreement between the recorded performance and matched simulation joint angles for the front foot contact phase of fast bowling indicate that the joint torque generators included within this simulation model are strong enough to match the performance.

8.4.3 Joint torque activation profiles

The joint torque activation profiles of the seven torque generators with active elements are shown in Figure 8.8.

The level of flexor activity in the front ankle, knee and hip highlight that co-contraction is necessary prior to front foot contact in order to hold these joints in the correct configuration for landing whilst keeping the activation level of the extensor muscles high. Co-contraction was maintained throughout the front foot contact phase indicating that maximum torques at these joints were not required in order to match the performance.

The back hip activation profile has a high level of activation for the flexors, with a small amount of extensor activation. This was expected due to the back leg being driven forwards during the front foot contact phase and the onset occurring prior to front foot contact. It was expected that the front shoulder would also exhibit similar torque activation levels compared to the back hip as

the front arm is driven downwards during the front foot contact phase of fast bowling. The high level of flexor activity of the front shoulder indicates however, that the fast bowler is decelerating the rate of extension of the shoulder joint during the front foot contact phase.

Since the activation of the shoulder extensors reaches maximum activation, the estimate of the maximum voluntary torque (Section 6.2.3) may be sub-maximal. Nevertheless, the estimate of the maximum voluntary torque provides a close match between the bowling shoulder joint angle in the recorded performances and the matched simulation. Furthermore, as the duration of the maximal effort is short, 50 ms, it is not unreasonable to expect that the bowler could exert maximal effort over this period of time.

The bowling wrist activation profile indicates that a high level of activation of the extensor torque is required to hold the wrist in an extended position prior to ball release. During this stage, the flexor activation is low, before ramping up in order to flex the wrist prior to ball release.

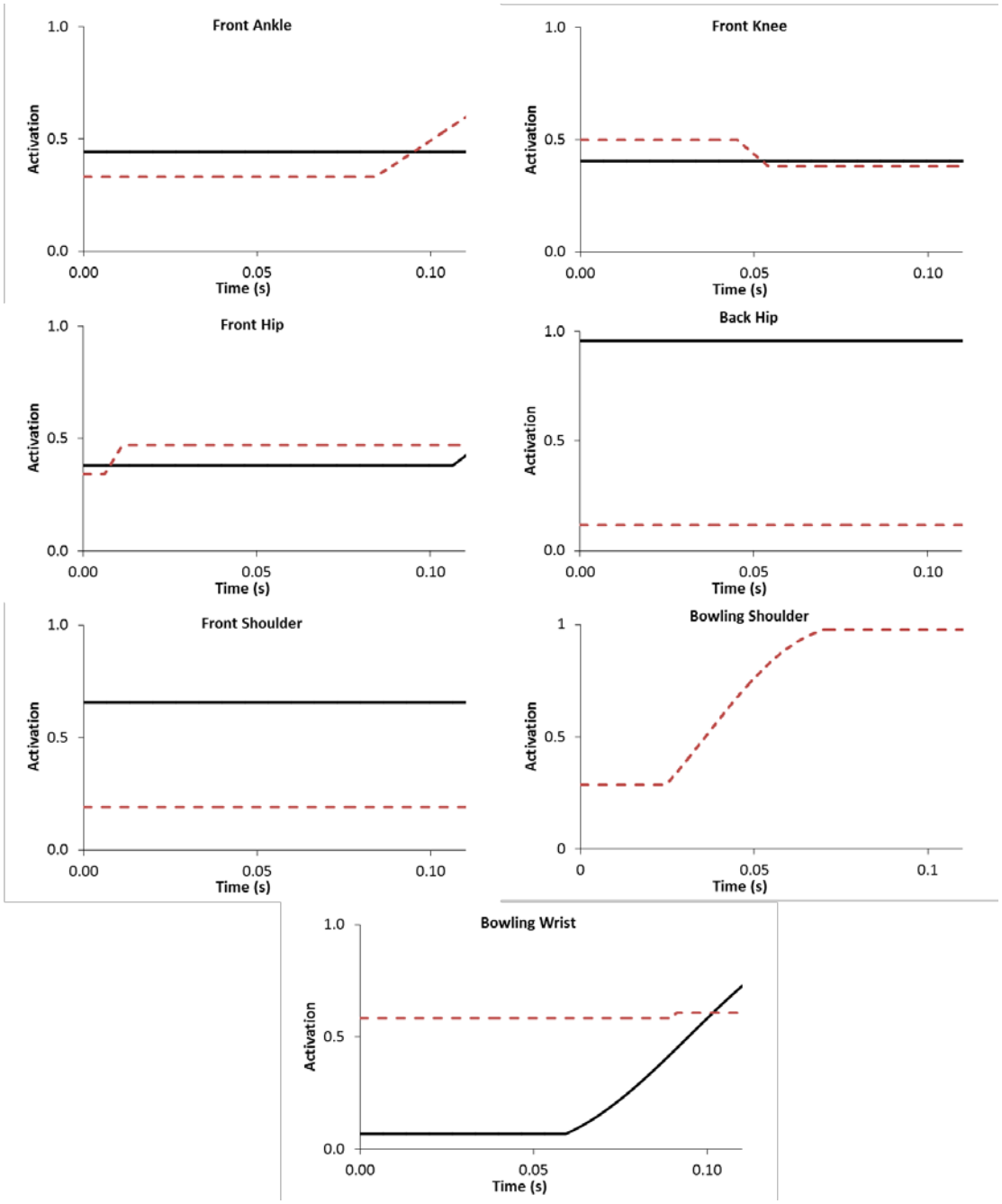

Figure 8.8 – Flexor (solid black lines) and extensor (red dashed lines) torque generator activation time histories for the matched simulation. (No flexor torque for the bowling shoulder).

8.4.4 Joint torques

The net joint torque time histories for each joint from the matched torque-driven simulation of fast bowling are shown in Figure 8.9. Positive torques represent flexion and negative torques represent extension.

The passive torques included at the front MTP and the bowling elbow joints are the sole contributors to the net joint torque in Figure 8.8. Although the magnitude of the MTP passive torque is large, this was expected since the movement of the MTP joint was restricted by the stiffness of the shoe in this region. Therefore, this passive torque really represents the torque applied by the shoe at the MTP joint and was deemed acceptable.

The passive torque at the elbow was used to model the behaviour of the elbow at the end of the range of motion during hyperextension. In order to determine whether the profile used at the elbow was acceptable, the peak passive torque was considered. The peak passive torque (≈ 50 Nm) at the elbow can be compared as the equivalent of holding a 10 kg with a straight arm, where the length of the lower arm and hand is approximately 0.5 m. Since this is more than feasible, the passive torque profile at the elbow was considered to be suitable.

The passive torque at the front ankle, knee and hip joints has been included within the net joint torque shown in Figure 8.8. As this torque was implemented to prevent the fast bowler exceeding his range of motion and was not subject-specific, it was important to check that they were behaving sensibly. Figure 8.9 shows the passive torques for the front ankle, knee and hip of the matched simulation model of fast bowling.

The three passive torques employed at the front ankle, knee and hip are relatively small (<25 Nm), which is expected since the penalties regarding exceeding the bowlers anatomical bounds were not incurred. Therefore, the passive torque profiles are not considered to have an excessive effect on the performance of the simulation model.

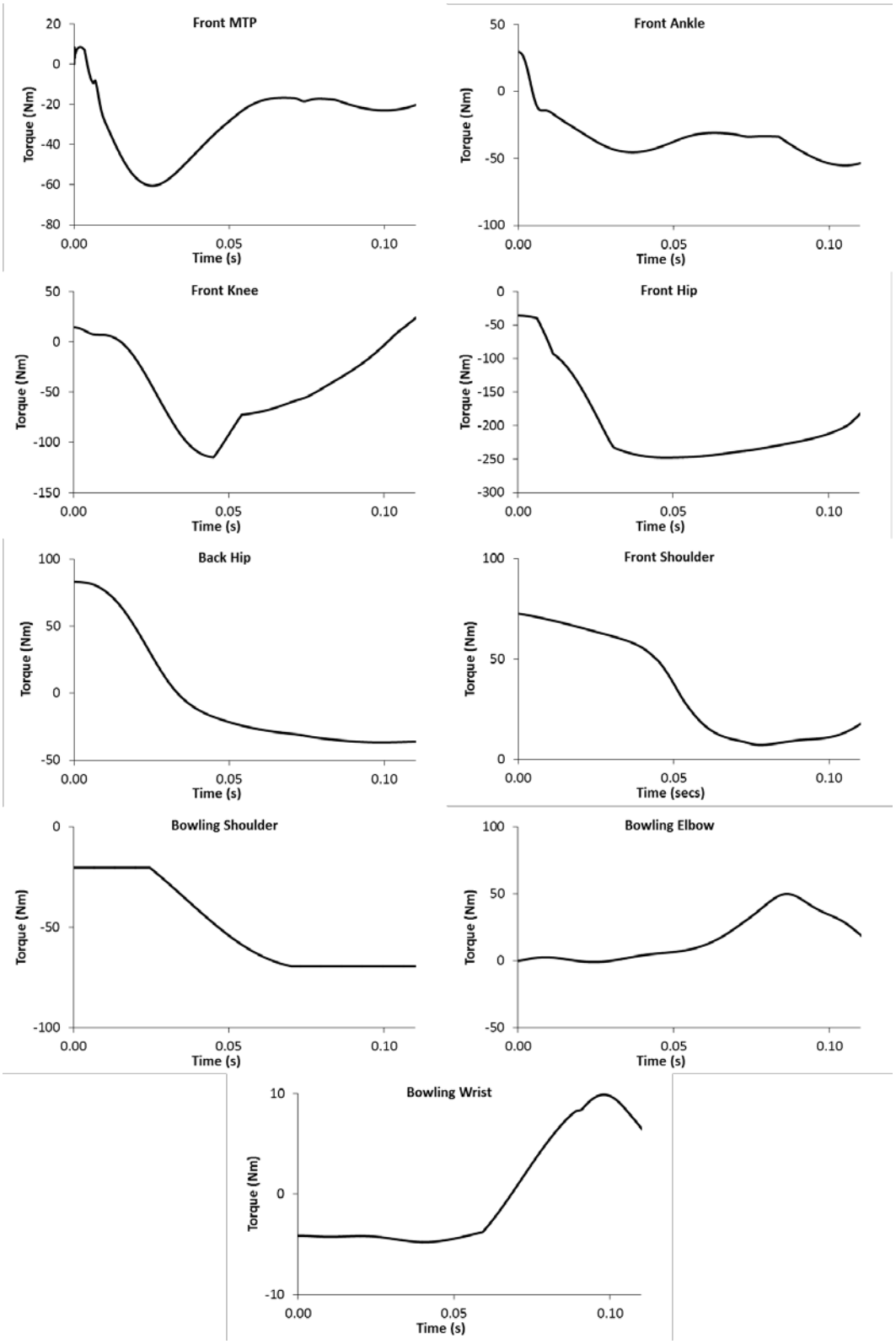

Figure 8.9 – Joint torque time histories for the matched simulation.

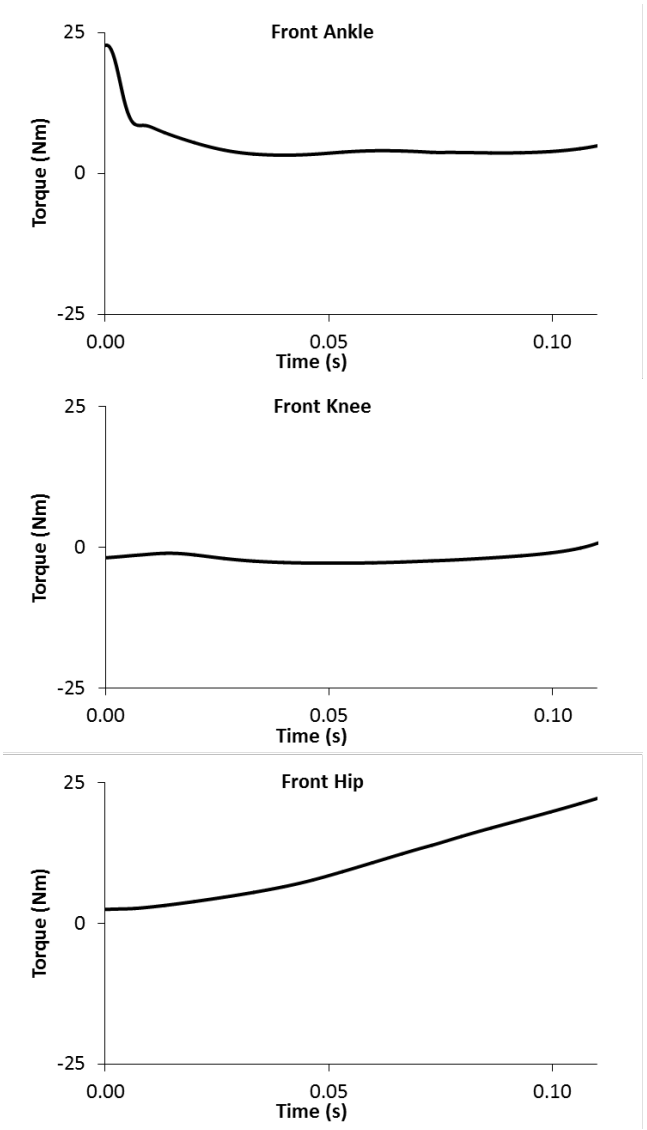

Figure 8.10 – Passive torques for the matched simulation of the front ankle, knee and hip.

8.4.5 Force

The simulated horizontal and vertical ground reaction force for the torque-driven simulation of the front contact phase of fast bowling is compared to the recorded performance in Figure 8.11.

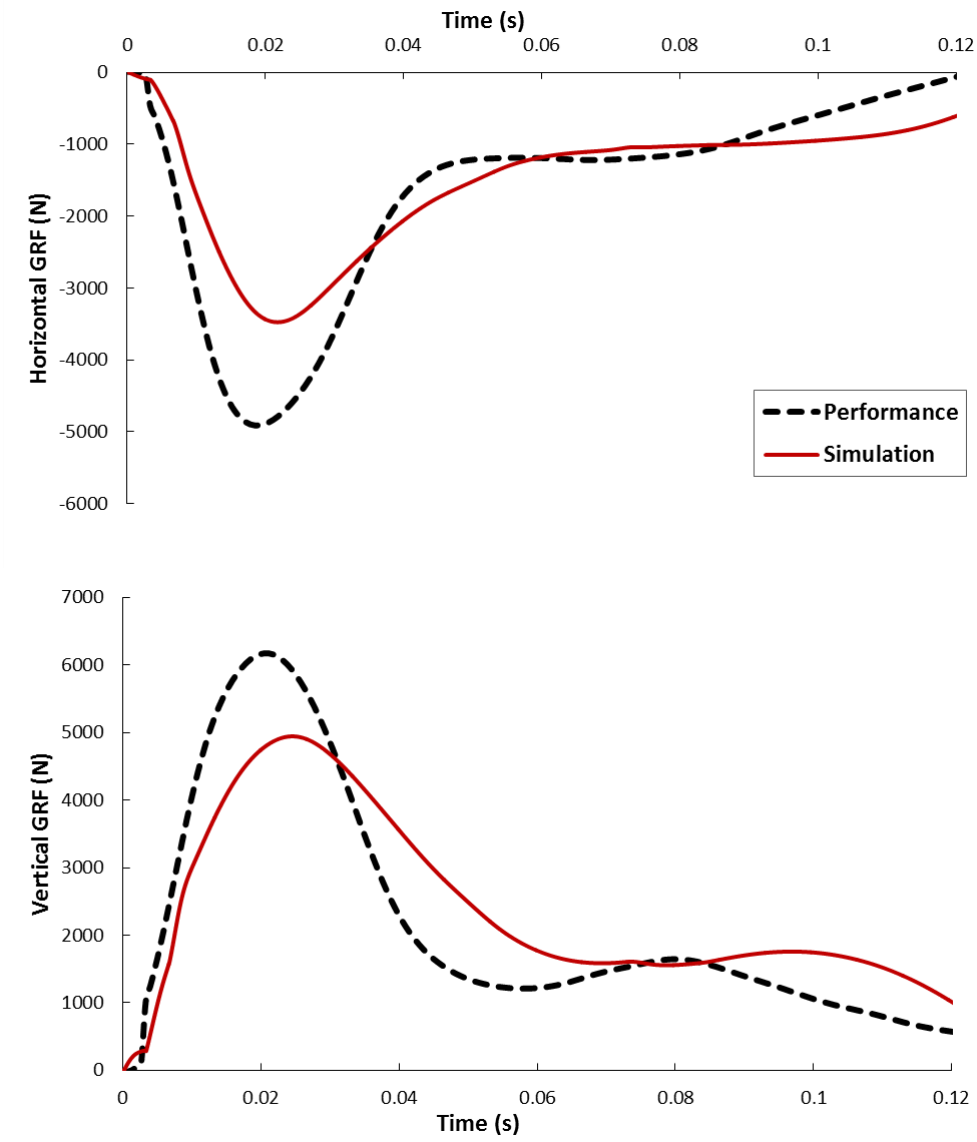

Figure 8.11 – Comparison of the ground reaction forces for the matched simulation and the recorded performance.

The average RMS difference between the matched simulation and the recorded performance ground reaction force-time histories was 9.6%. Although, this does not match as well as the kinematic variables, the error is considered small when the limitations of using pin joint models to reproduce force are considered (Allen at al., 2012). However, caution must be taken when reporting the differences in force when optimising.

8.5 SUMMARY

In this chapter, the torque-driven simulation model (Section 4.6) of the front foot contact phase of fast bowling was evaluated to ensure that it produced realistic movements. The model was driven using the flexion-extension torque profiles for the front MTP, front ankle, front knee, both hips, both shoulders, bowling arm elbow and bowling arm wrist (Sections 6.2 and 6.3), and the angle-time histories at the back MTP, back ankle, back knee and non-bowling arm elbow (Section 5.6.1). The orientation of the massless segments and the length of the variable length segments were driven as a function of the trunk orientation angle (Sections 5.6.2 and 5.6.3). A genetic algorithm (Carroll, 2001) was used to vary the torque generator activation profiles, the parameters for the front MTP and bowling elbow, the massless segment orientation and variable length-orientation angle function translation parameters and the initial conditions to minimise an objective function that was based on the difference between the matched simulation and the recorded performance. The result showed a close agreement between the recorded performance and matched simulation. Therefore, the model was deemed suitable to simulate the front foot contact phase of the fast bowling action.

- CHAPTER 9 -
MODEL APPLICATION AND PERFORMANCE ANALYSIS

The purpose for this study was to investigate the factors limiting fast bowling performance, and then use this information to identify ways to improve performance. This chapter describes the process taken in applying the model to answer specific research questions.

9.1 BALL RELEASE CRITERIA

To determine optimal performances, it was necessary to ensure that the outcome was the same. To do this, each delivery was projected towards the same landing site and ball release was defined to occur once the upper arm had passed the vertical and the horizontal distance travelled by the ball to the predicted landing site matched the recorded performance data.

9.2 OPTIMUM TECHNIQUE

In the game of cricket a fast bowler aims to bowl the ball as fast as possible towards a batsman in order to limit the time he has to react appropriately. The fastest bowlers, who can deliver the ball with the greatest velocity, tend to be the most successful. Thus, the optimal fast bowling technique is one in which the ball release speed is maximised.

The fast bowler in this current study was able to release the ball at 79.4 mph (35.3 ms^{-1}). The simulation model of the front foot contact phase of fast bowling was applied to determine whether the fast bowler could bowl the ball faster without an increase in strength?

To determine the optimal technique during the front foot contact phase of fast bowling two optimisations were carried out. The first investigated how close to optimal the technique employed by the fast bowler between front foot contact and ball release was whilst maintaining his initial body configuration from the

recorded performance. The second investigated the optimal technique whilst allowing his initial body configuration at front foot contact to vary.

The matched performance (Chapter 8) was used to investigate the optimum technique between front foot contact and ball release. The model inputs consisted of those found during Chapters 5, 6, 7 and 8.

9.2.1 How close to optimal is the technique of the bowler in this study?

A genetic algorithm (Carroll, 2001) varied the muscle activation parameters to maximise an objective function which comprised solely of the ball release speed. During the optimisation the joint angle constraints outlined in Section 8.3.2 were employed to ensure that the optimised solution did not exceed the anatomical bounds of the subject. If the range was exceeded, a penalty of -1 was incurred for each degree past the limit. A constraint was also added to limit the angular velocity of the shoulder and wrist on the bowling arm. For the shoulder, the torque profile does not use a torque-angular velocity relationship. Therefore, to prevent unrealistic angular velocities at this joint it was constrained to the maximum angular velocity found when the model was evaluated. The wrist was also constrained to the maximum angular velocity found during model evaluation as the angular velocity of the wrist at ball release in fast bowling is not maximal. Instead, fast bowlers use a sub-maximal angular velocity which allows a sufficient release window to maintain accuracy. If either of the angular velocity constraints were surpassed, a penalty of -1 was suffered for each degree per second past the limit.

Optimisation of the technique used during the front foot contact phase of fast bowling highlighted that a potential increase in ball release speed was possible. The optimised technique released the ball at 87.2 mph (38.8 ms^{-1}), an increase of 9.8%. The optimised performance incurred no penalties and the technique changes that enable the increase in ball speed to occur are investigated below.

Joint angles, torques and activation levels

The joint angle, joint torque and joint activation level, time histories for the torque-driven joints are compared for the matched simulation and the optimum performance in Figures 9.1, 9.2, and 9.3, respectively.

The activation of the extensor of the front ankle was increased whilst the flexor was decreased in the optimised performance compared to the matched simulation. As a result, the ankle remained more extended during the front foot contact phase.

The front knee also remained more extended throughout the front foot contact phase, although the peak extension joint torque was of a similar magnitude to the matched simulation. The flexor activation level ramps up during the front foot contact phase. This decreased the extension torque more rapidly than in the matched simulation and most likely occurred to prevent the knee hyperextending.

The flexors of the front hip can be seen to ramp up during the optimised performance compared to the matched simulation, this reduced the co-contraction of the front hip, which decreased the extension torque and allows trunk flexion to occur.

Although, the joint activation levels of the back hip look similar, the joint torque-time history shows an increase in the flexion torque, which leads to the back hip flexing more during the front foot contact phase.

The joint angle-time history of the front shoulder is similar. The bowling wrist has an oscillation within the angle-time history which is caused by the wrist extensors not being strong enough to hold the wrist back before it flexes. The effect on ball release speed is minimal since the wrist is in a similar position prior to flexing as the recorded performance and the angular velocity of the joint at release is similar.

The activation level-time history of the bowling shoulder extensor indicates that there is a delay in the bowling arm, which the joint-angle time history confirms.

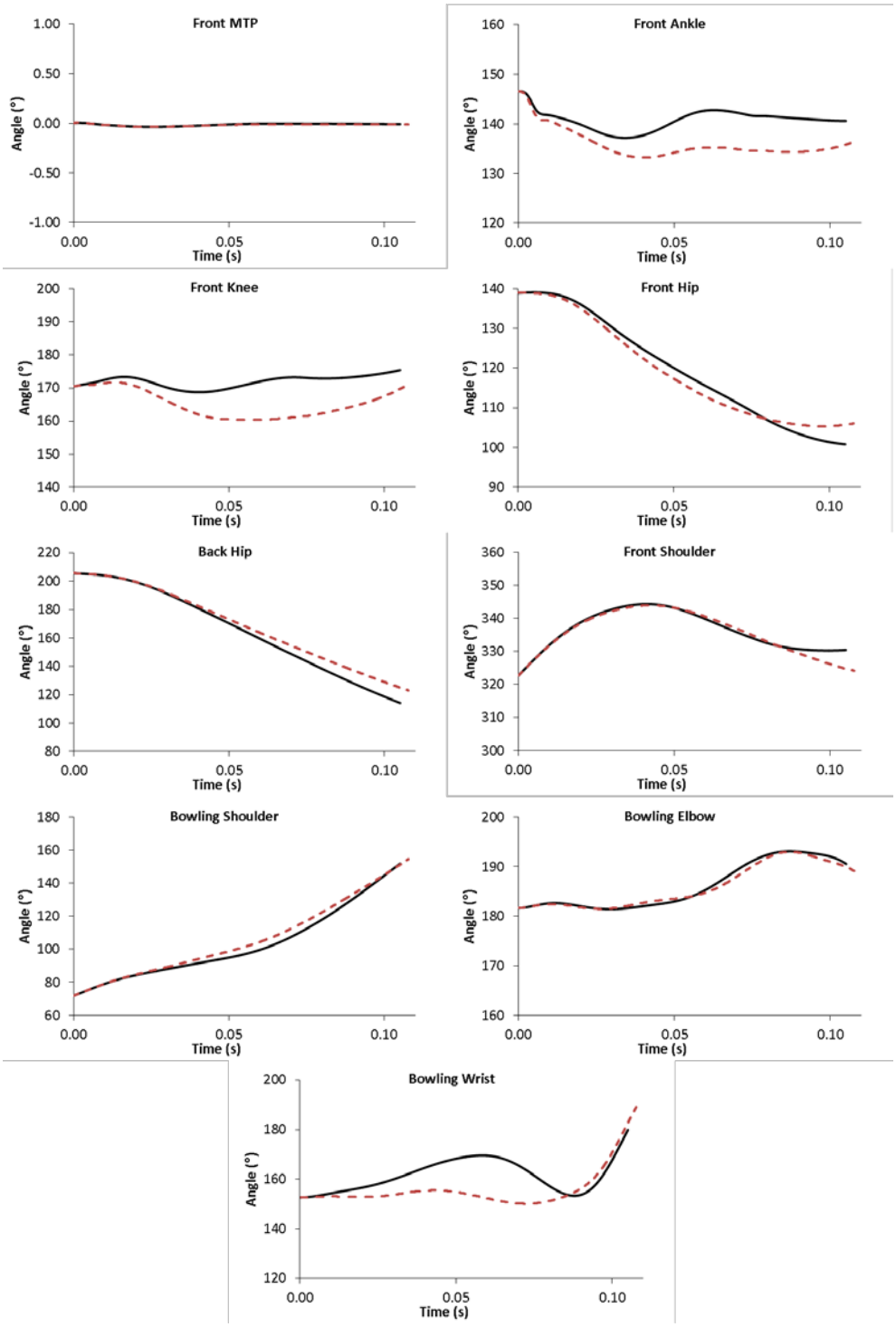

Figure 9.1 – Comparison of joint angle-time histories for: matched simulation (dashed lines) and optimised simulation (solid lines).

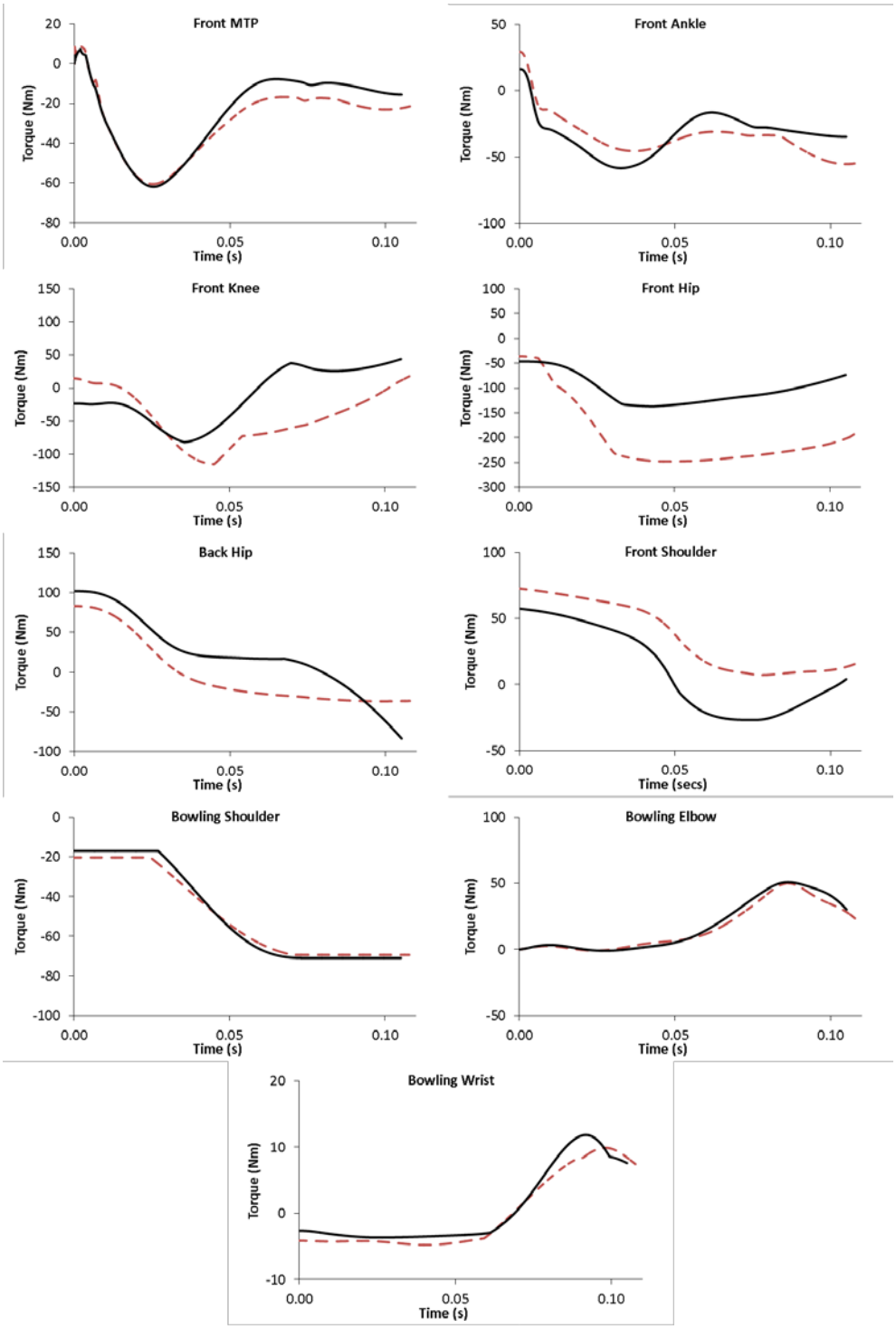

Figure 9.2 – Comparison of the joint torque-time histories for: matched simulation (dashed lines) and optimised simulation (solid lines).

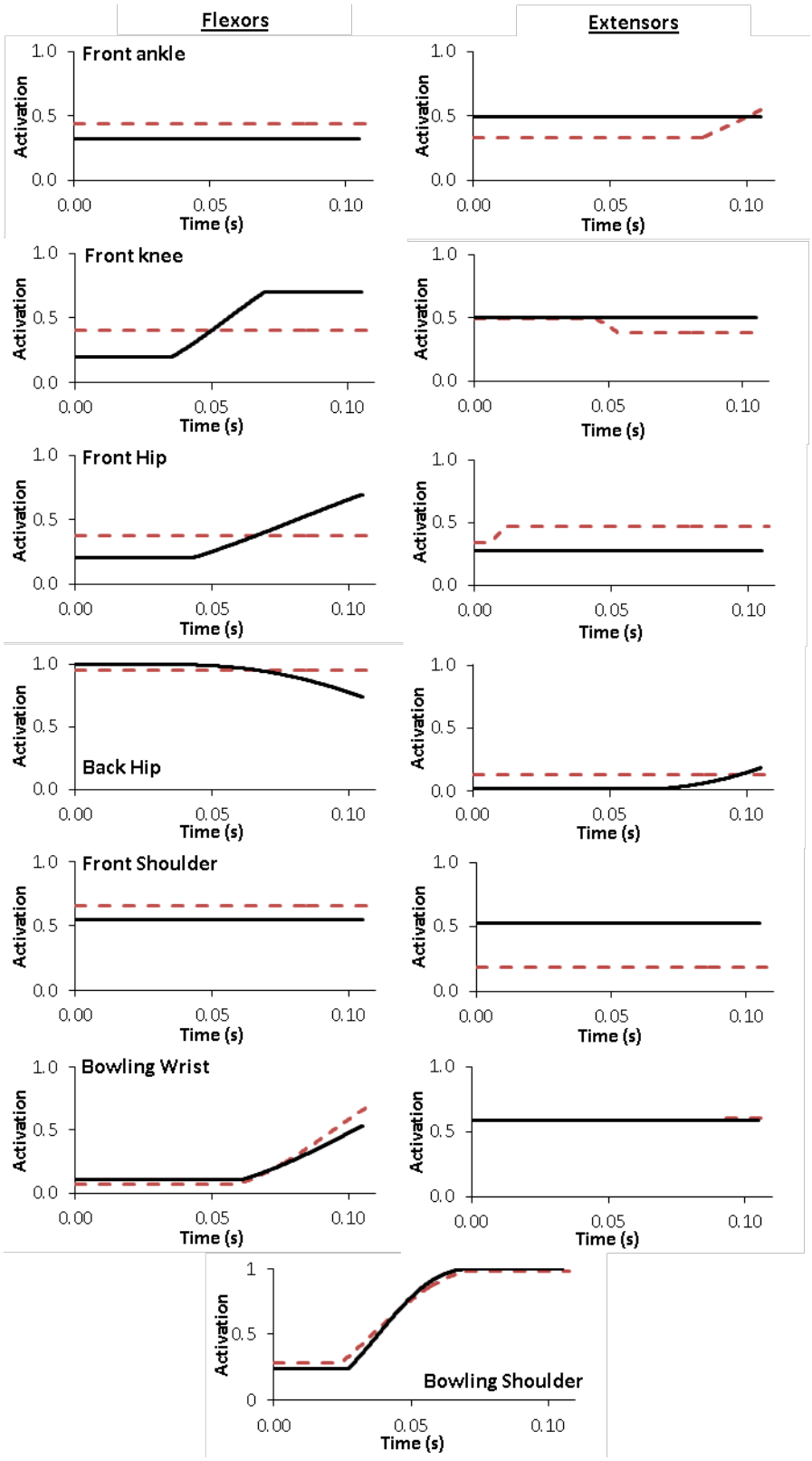

Figure 9.3 – Comparison of the torque generator activation level-time histories for: matched simulation (dashed lines) and optimised simulation (solid lines).

Force

The horizontal and vertical ground reaction force-time histories are compared for the matched and optimised simulations in Figure 9.4. The force traces are similar, although, a small increase in the peak horizontal ground reaction force can be seen. This is an indication that more extended front leg kinematics brake the body more effectively, which provides a more effective conversion of linear momentum into angular momentum about the front foot.

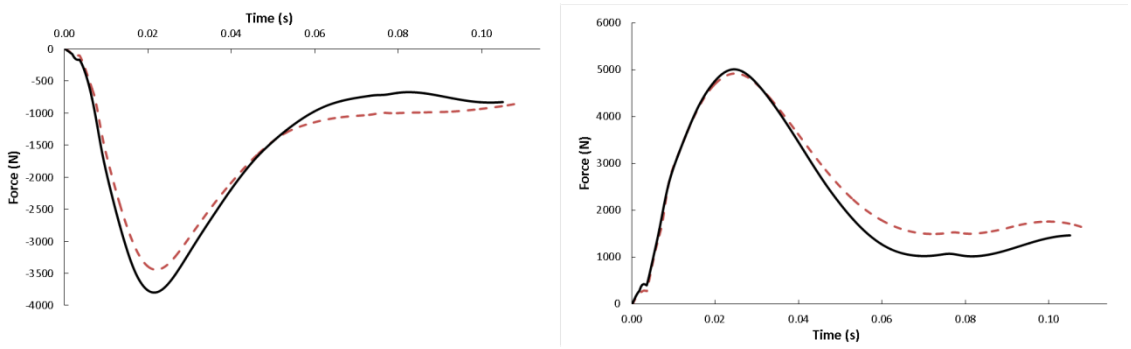

Figure 9.4 – Ground reaction forces for: matched simulation (dashed lines) and optimised simulation (solid lines).

9.2.2 How close to optimal is the body configuration at front foot contact of the bowler in this study?

A genetic algorithm (Carroll, 2001) varied 115 parameters which included; the muscle activation parameters, the initial conditions of the front ankle, knee, hip and shoulder, as well as the back hip and bowling shoulder, and the translation parameters of the trunk orientation angle functions which defined the segments with variable length and the orientation of the shoulder and pelvis segments. An objective function was maximised which comprised solely of ball release speed. During the optimisation, the joint angle constraints outlined in Section 8.3.2 were employed to ensure that the optimised solution did not exceed the anatomical bounds of the subject. If the range was exceeded, a penalty of -1 was incurred for each degree past the limit. The constraints in Section 9.2.1 to limit the angular velocity of the shoulder and wrist joints on the bowling arm were also enforced, where a penalty of -1 was suffered for each degree per second past the limit.

Optimisation of the initial body configuration and resulting technique during the front foot contact phase of fast bowling highlighted that a potential increase in ball release speed was possible. The optimised technique released the ball at 96.5 mph (42.9 ms^{-1}), an increase of 21.5%. The optimised performance incurred no penalties and the technique changes that enable the increase in ball speed to occur are investigated below.

Initial configuration

The changes in the initial configuration of the body are compared between the optimised simulation and the matched performance in Table 9.1 and can be seen visually in Figure 9.5.

Table 9.1 - Initial configuration of the bowler for the matched and optimised simulations

Angle	Matched	Optimised
Trunk orientation (°)	93.6	93.5
Front ankle (°)	146.5	144.1
Front knee (°)	170.5	172.3
Front hip (°)	138.9	140.1
Back hip (°)	205.7	202.6
Front shoulder (°)	322.7	271.9
Bowling shoulder (°)	71.8	53.9

A marked difference can be seen at the shoulders, the initial angle of the bowling shoulder is more delayed in the optimised performance compared to the matched simulation. The front shoulder can also be seen to be in a more flexed position, which is likely to aid the delay of the bowling arm.

The optimised performance also indicated that the initial configurations of the lower extremities of the fast bowler in this study are close to his optimal where the optimal has slightly more extension of the front knee and hip.

The differences in technique which occur due to the changes in the body configuration at front foot contact compared to the optimal performance of the bowler with his recorded body configuration are investigated below.

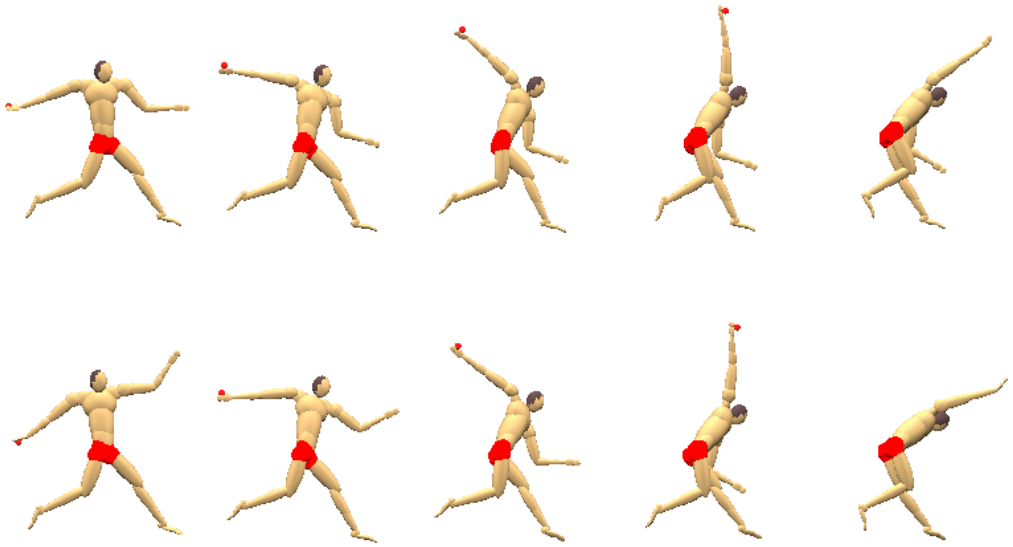

Figure 9.5 - Comparison of the matched optimisation (upper) and the optimal initial body configuration simulation (lower).

Joint angles, torques and activation levels

The joint angle, joint torque and joint activation level, time histories for the torque-driven joints are compared for the optimal technique with recorded initial body configuration and optimal technique with the optimised initial body configuration simulations in Figures 9.6, 9.7, and 9.8, respectively.

The majority of the flexor and extensor activation levels for the torque generators of the optimal initial configuration simulation are constant throughout the front foot contact phase. This indicated that the performance of the fast bowler is pre-determined by the orientation of the body at front foot contact, and the differences in the activation levels in the matched and first optimisation are due to the bowler trying to maintain a technique which is as close to the optimal technique as possible, given the sub-optimal initial body configuration.

The front ankle, knee and hip can be seen to be in co-contraction throughout the front foot contact phase, where only the ankle extensors are at the maximal pre-activation bound. In the optimal technique, co-contraction of the front ankle and knee makes the behaviour of the front leg represent a single segment.

This is likely to provide a more efficient braking of the pelvis which converts the linear momentum into angular momentum about the front foot more effectively.

The change in the configuration of the bowling shoulder resulted in an earlier activation of the extensors, although, with a slower ramp time. The front shoulder is now extended throughout the front foot contact phase. Pulling the front arm down is likely to aid trunk flexion and the rotation of the shoulders.

The behaviour of the remaining joints remained similar to the matched optimisation.

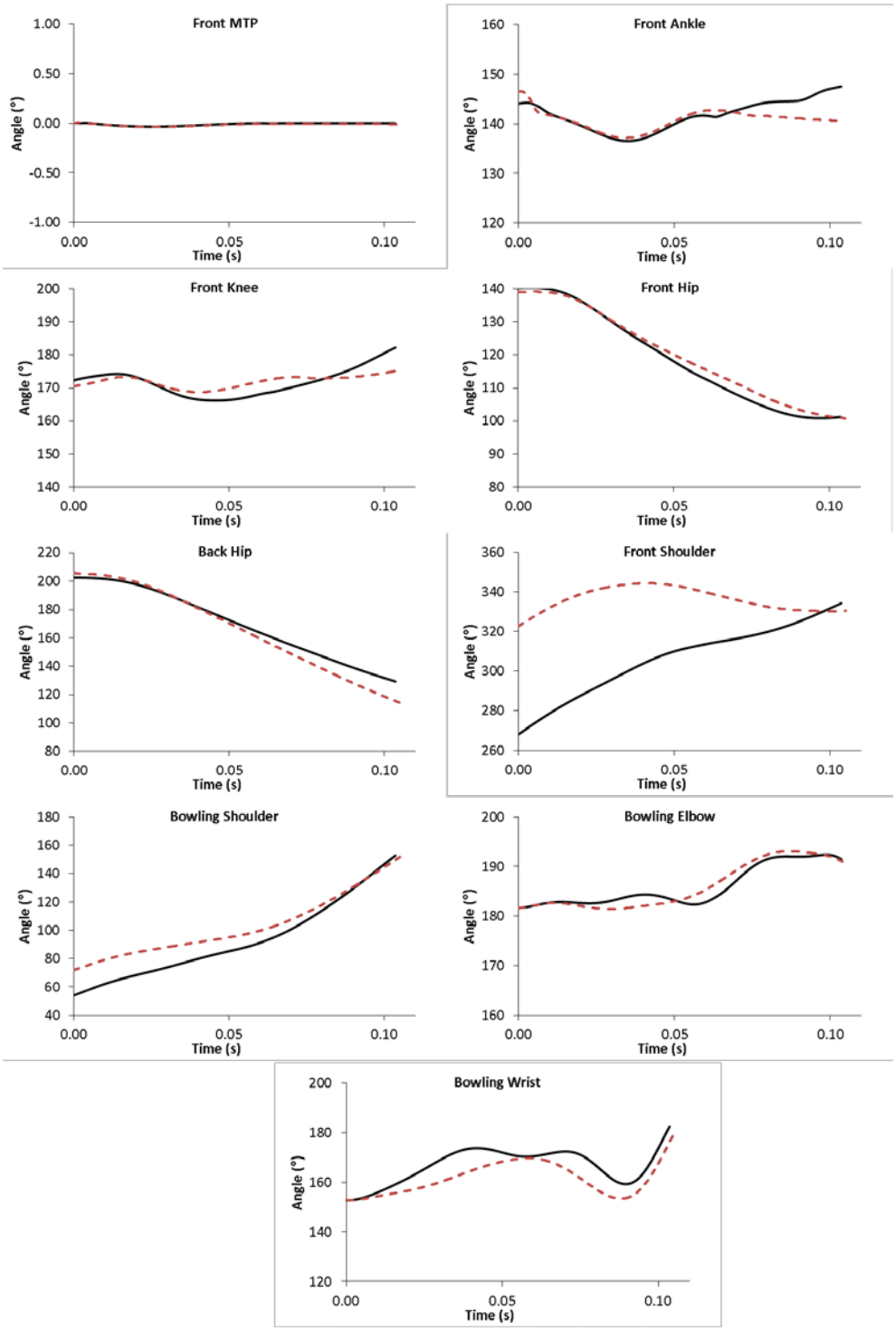

Figure 9.6 - Comparison of the joint angle-time histories for: optimal technique with recorded initial body configurations technique (dashed lines) and optimal technique with optimal initial body configuration (solid lines).

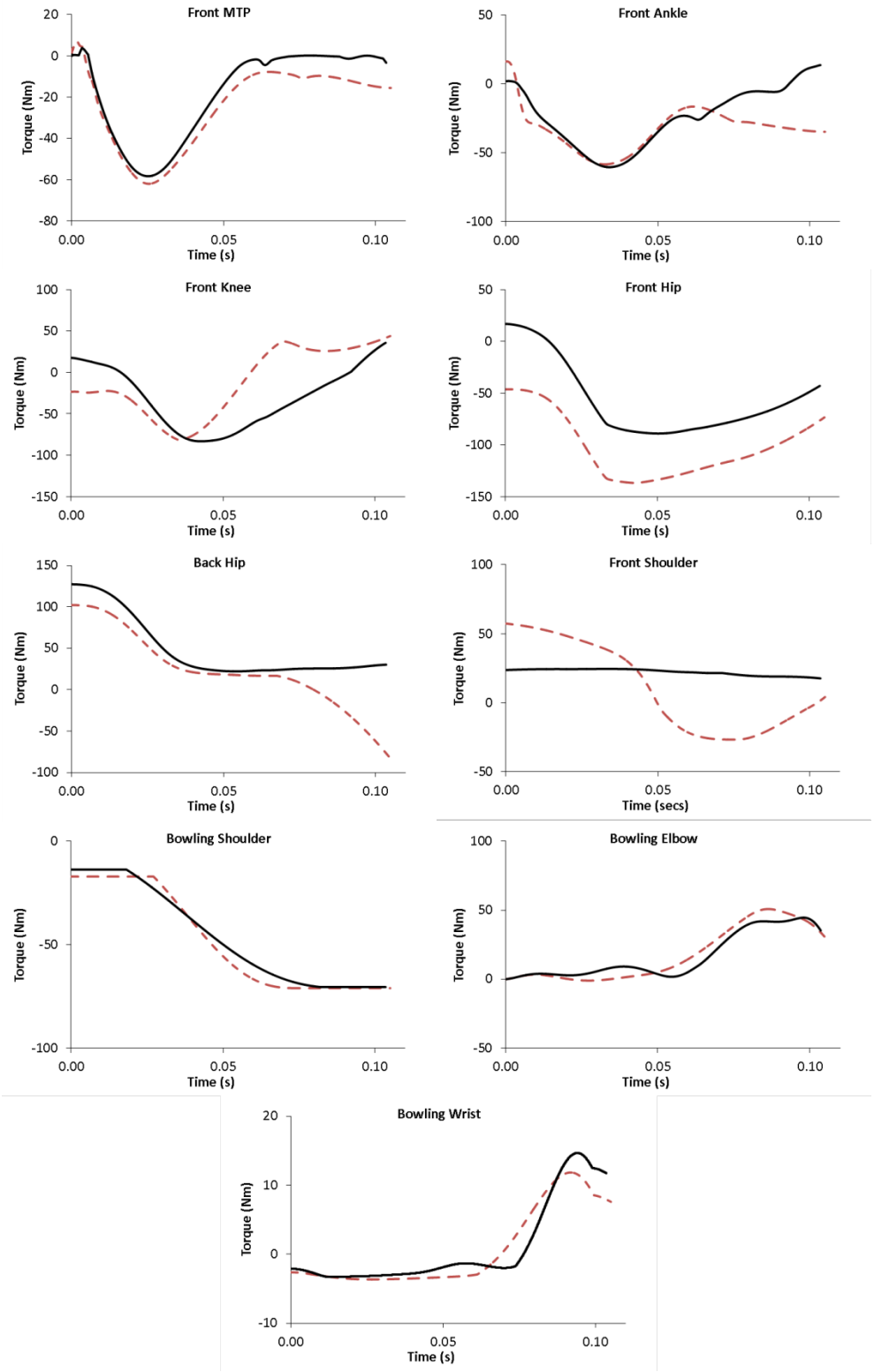

Figure 9.7 - Comparison of the joint torque-time histories for: optimal technique with recorded initial body configurations technique (dashed lines) and optimal technique with optimal initial body configuration (solid lines).

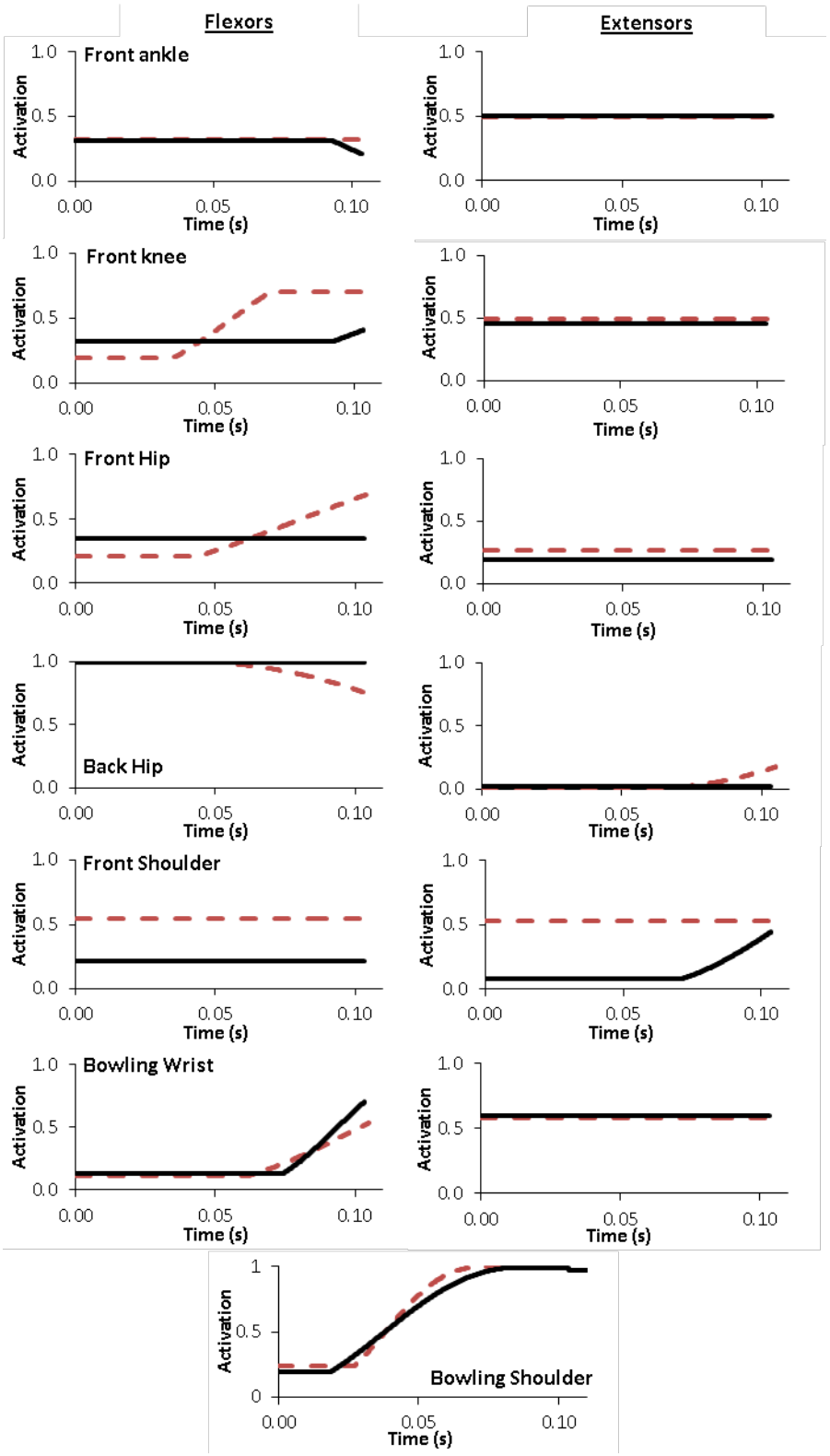

Figure 9.8 - Comparison of the joint activation level-histories for: optimal technique with recorded initial body configurations technique (dashed lines) and optimal technique with optimal initial body configuration (solid lines).

Force

The horizontal and vertical ground reaction force-time histories are compared for the optimal technique with the recorded initial body configuration and optimal technique with optimised initial body configuration simulations in Figure 9.9.

The optimal body configuration lowers the peak ground reaction force in both the horizontal and vertical directions, which appears to confirm the discovery by Worthington et al. (2013b), that a longer delivery stride decreases the peak ground reaction forces.

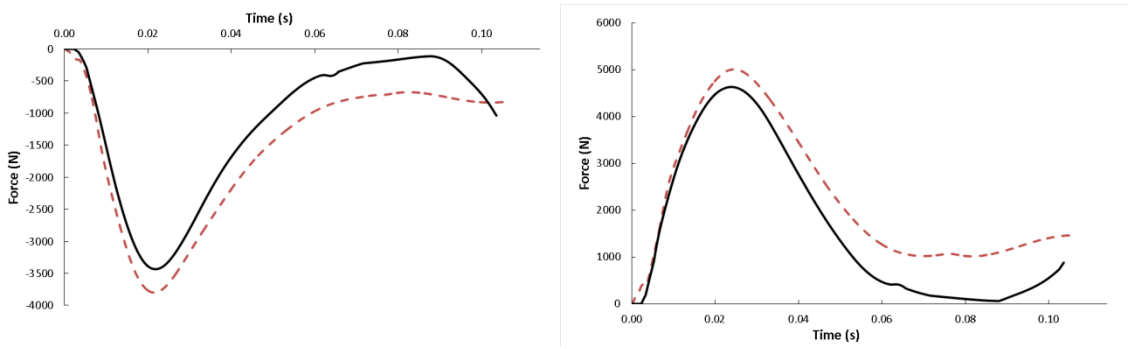

Figure 9.9 – Comparison of the ground reaction forces for: optimal technique with recorded initial body configuration (dashed lines) and optimised technique with optimal initial body configuration (solid lines).

9.2.3 Discussion

The simulation model was applied to determine two questions regarding the optimal technique during the front foot contact phase of fast bowling. The first question asked:

"How close to optimal is the technique of the bowler in this study?"

The results indicated that the fast bowler could increase his performance during the front foot contact phase by 9.8%. This was achieved by keeping the front leg straighter and also increasing the amount of trunk flexion.

The second question asked:

"How close to optimal is the body configuration at front foot contact of the bowler in this study?"

The results indicated that the fast bowler could increase his performance during the front foot contact phase by 21.5%. The most marked difference in the initial body configuration was at the shoulders, where the extension was delayed for both the front and bowling shoulder. An increase in the extension of the front knee and hip was also witnessed, which increased the delivery stride. These changes in the initial body configuration resulted in the front leg remaining straighter during the front foot contact phase, as well as an increase in the amount of trunk flexion compared to the matched performance.

The application of the simulation model of the front foot contact phase in determining the optimal technique has identified that the front leg should be kept as straight as possible between front foot contact and ball release. This is in agreement with the results found by Worthington et al. (2013a), who suggested that the fastest bowlers use their front leg to rapidly slow the linear velocity of their pelvis, which drives the thorax forward about the pelvis, providing a more efficient conversion of the linear momentum of the run-up into angular momentum about the front foot.

The amount of trunk flexion was also seen to be increased in the optimised technique. This confirms the belief of previous research (Davis and Blanksby, 1976a; Elliot et al., 1986; Burden and Bartlett, 1990a; Worthington at al., 2013a). The decrease in front hip joint torque in the optimal performance suggests that the belief stated by Worthington et al. (2013a), that increased trunk flexion is a mechanism of the bowling action used rather than as a result of muscular work in the torso, is correct. However, further investigation is required in order confidently state the reasons behind fast bowlers using trunk flexion to increase ball release speed.

The optimisation of the initial configuration of the body at front foot contact highlighted that delaying the bowling arm at front foot contact is important in increasing performance. This mechanism was first identified by Tyson (1976) but was not reported again in any studies until Worthington et al. (2013a)

identified it as one of the key parameters linked to increased ball release speeds. The reason behind the delay in the bowling arm is not known. It is probable however, that there is a relationship between the amount of trunk flexion and the delay in the bowling shoulder which maximises performance. For example, if the bowling shoulder is delayed, the trunk can flex further between front foot contact and ball release, whilst still satisfying the ball release criteria. Further investigation is required to understand this relationship and its effect on performance.

The activation levels of the optimised technique when the initial body configuration was allowed to vary indicated that the performance of the fast bowler is dependent on the initial configuration of the bowler at front foot contact and the technique that follows aims to maintain a straight front leg, which more efficiently slows the pelvis and allows more trunk flexion to occur.

The ground reaction force-time histories indicated that the larger delivery stride and straighter front knee at front foot contact lowers the peak ground reaction force in both the horizontal and vertical directions. This agrees with the conclusion of Worthington et al. (2013b) that a longer delivery stride decreases the peak ground reaction forces.

In summary, the optimal technique in order to maximise performance in fast bowling is one in which the bowler lands in a configuration which has a long delivery stride with a straight front leg, and a delayed bowling arm. The bowler should then maintain a straight front leg during the front foot contact phase and maximise trunk flexion.

9.3 STRENGTH

In recent years, the professionalism in most sports has increased and athletes have incorporated strength and conditioning programmes into their training routines. Currently, the effects of increasing strength on ball release speed in fast bowling are unknown.

The simulation model of the front foot contact phase of fast bowling was applied to determine whether the fast bowler could bowl faster with an increase in strength. The maximum isometric torques of the ankle, knee, hip and front shoulder were increased by 5% from the measured values in Section 6.2.1. The strength of the shoulders and wrist were kept the same. The bowling shoulder was not increased since the torque profile did not include torque-angle or torque-angular velocity relationships. The wrist was kept the same since it was not subject-specific and it is considered to work sub-maximally during ball release.

An optimisation was carried out to determine the effect of increasing strength on the performance of the fast bowler. The optimisation investigated the optimal technique, whilst the initial body configuration was set to that found in the previous optimisation. The remaining model inputs consisted of those found during Chapters 5, 6, 7 and 8.

9.3.1 How does an increase in strength affect the performance of the bowler in this study?

A genetic algorithm (Carroll, 2001) varied the muscle activation parameters to maximise an objective function which comprised solely of the ball release speed. During the optimisation the joint angle constraints outlined in Section 8.3.2 were employed to ensure that the optimised solution did not exceed the anatomical bounds of the subject. If the range was exceeded, a penalty of -1 was incurred for each degree past the limit. The constraints in Section 9.2.1 to limit the angular velocity of the shoulder and wrist joints on the bowling arm were also enforced, where a penalty of -1 was suffered for each degree per second past the limit.

Increasing the strength by 5% and optimising technique during the front foot contact phase showed that a potential increase in ball release speed was possible compared to the optimal technique with the bowlers specific strength. The new technique released the ball at 97.8 mph (43.5 ms^{-1}), an increase of 1.3% compared to the previous optimal technique with the bowler's strength

limitations. The optimised performance hit no penalties and the technique changes that enable the increase in ball speed to occur are investigated below.

Joint angles, torques and activation levels

The joint angle, joint torque and joint activation level, time histories for the torque-driven joints are compared for the optimal technique and optimum initial configuration simulations in Figures 9.10, 9.11, and 9.12, respectively.

The joint-angle time histories indicated that the kinematics of the optimum technique when strength is increased is similar to the previously found optimum. This is highlighted by the closeness between the majority of the joint torque-time histories and the activation level-time histories.

Increasing the strength characteristics of the fast bowler resulted in the front knee remaining slightly straighter throughout the front foot contact phase, as well as the front hip remaining extended slightly longer indicating a delay in trunk flexion. There is also a difference in the bowling shoulder, the activation ramps down at the end. This may be due to the penalties limiting the angular velocity of the shoulder or that the bowler is trying to delay the bowling shoulder at ball release. Delaying the bowling shoulder has previously been observed in experimental research by Tyson (1976) and Worthington et al. (2013a) who suggested this was the most important aspect in predicting ball release speed.

The extension of the front shoulder is also delayed, and the activation level-time history suggested that the optimal technique is to actively extend the non-bowling arm. Pulling the front arm down is likely to aid trunk flexion and the rotation of the shoulders.

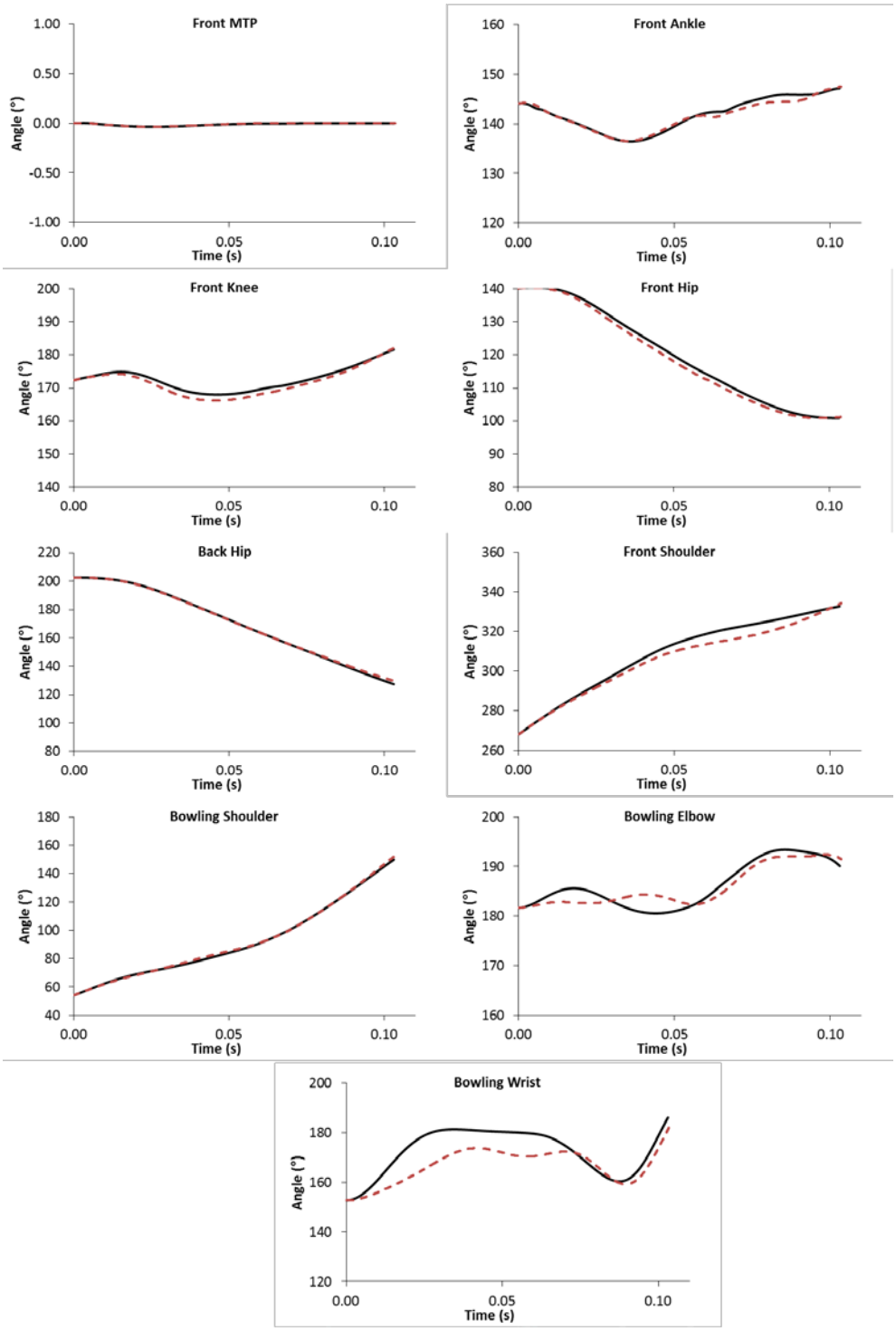

Figure 9.10 - Comparison of the joint angle-time histories for optimal technique for: actual strength (dashed lines) and increased strength (solid lines).

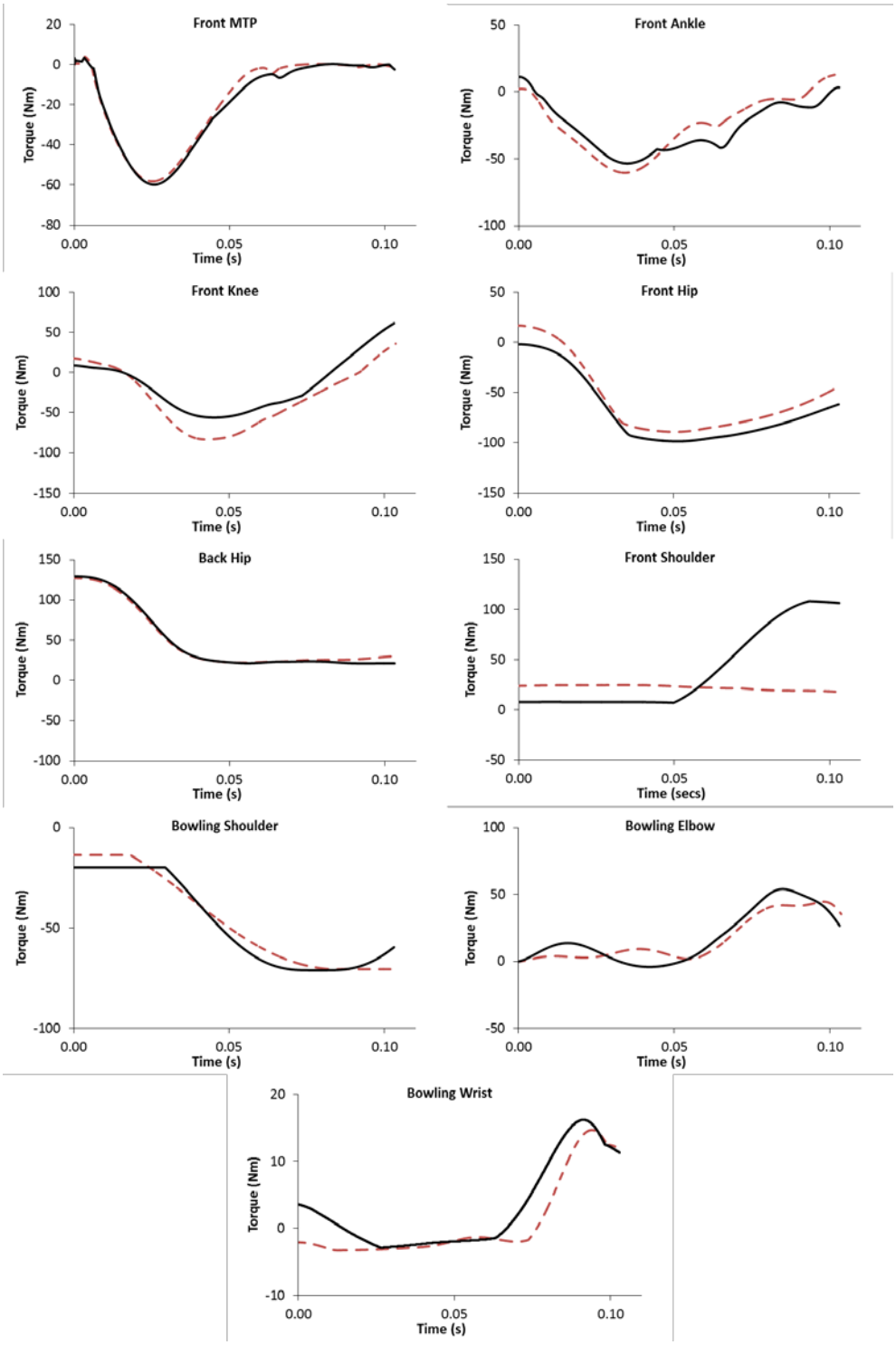

Figure 9.11 - Comparison of the joint torque-time histories for optimal technique for: actual strength (dashed lines) and increased strength (solid lines).

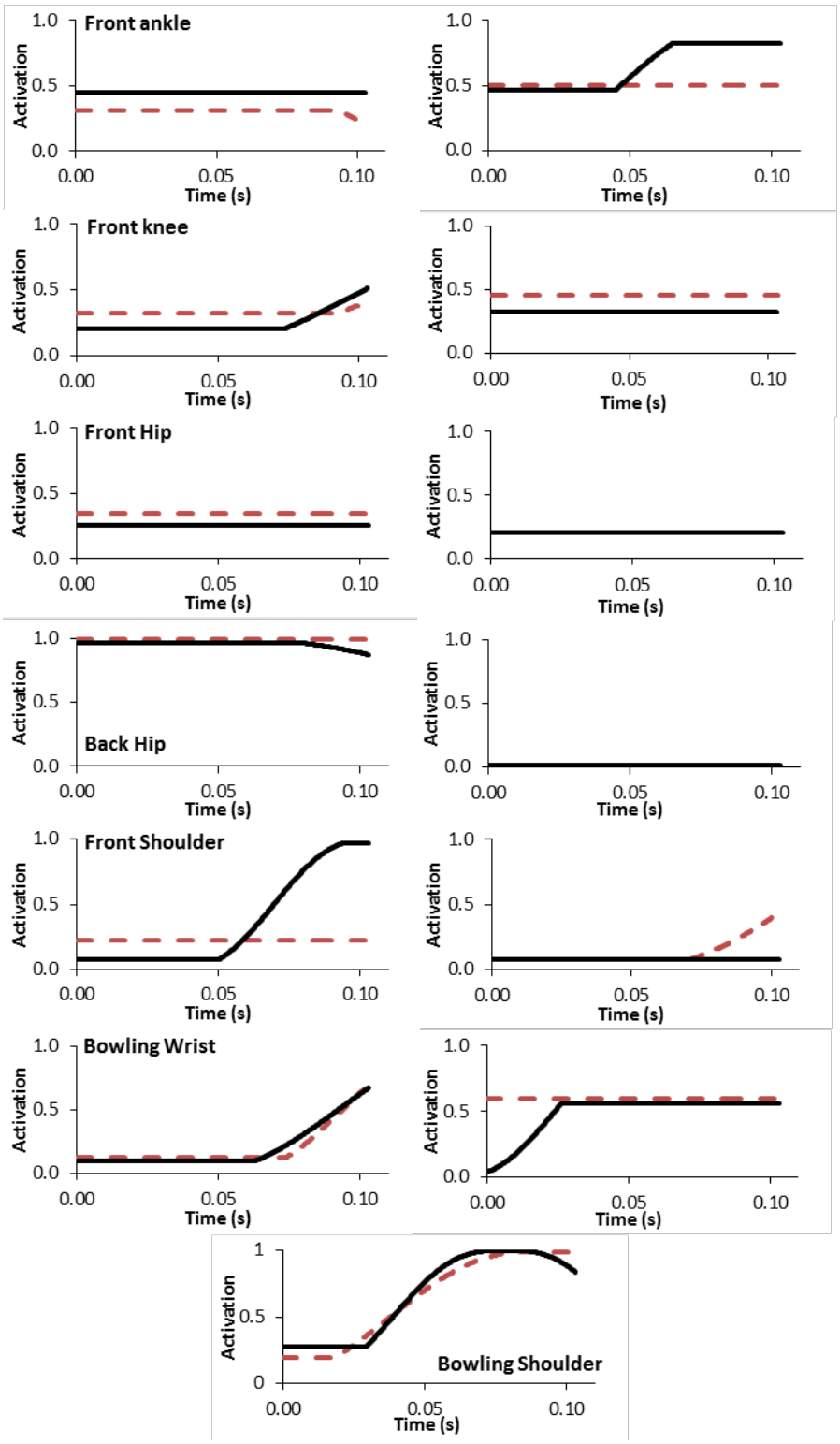

Figure 9.12 - Comparison of the joint activation level-histories for optimal technique for: actual strength (dashed lines) and increased strength (solid lines).

Force

The horizontal and vertical ground reaction force-time histories are similar when compared for actual strength and increased strength in Figure 9.13. However this was expected since the centre of mass velocity and initial body configuration at front foot contact are the same.

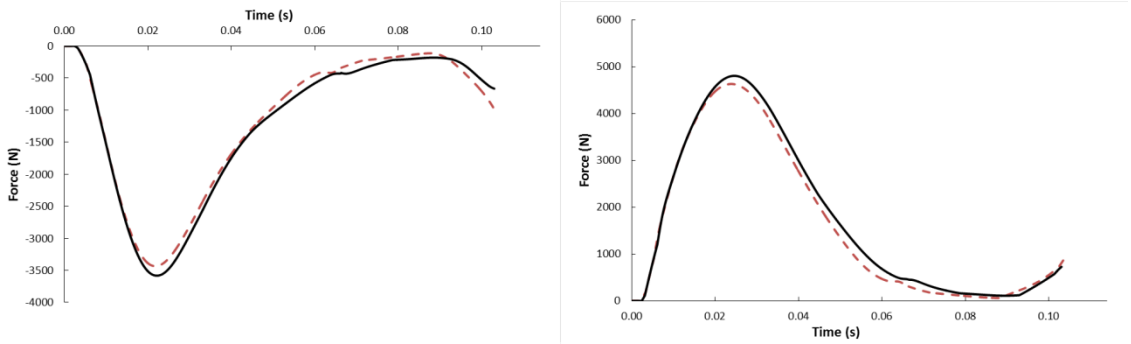

Figure 9.13 – Comparison of the ground reaction forces for optimal technique for: actual strength (dashed lines) and increased strength (solid lines).

Discussion

The simulation model was applied to determine:

How does an increase in strength affect the performance of the bowler in this study?

The results indicate that an increase in strength of 5% causes an increase in fast bowling performance of 1.3%.

The optimal technique to maximise ball release speed remained the same. However, the increase in strength allows the front leg to remain slightly straighter, trunk flexion to be delayed slightly longer, and a greater extension of the front arm to occur. These improvements appear to result in the bowling shoulder being delayed at front foot contact which has previously been seen as the biggest predictor of ball release speed in elite fast bowlers (Worthington et al., 2013).

9.4 RUN-UP SPEED

Run-up speed has been observed to be positively correlated with ball release speed in studies by Glazier et al. (2000), Elliott and Foster (1989), Ferdinands et al. (2010) and Worthington et al. (2013a). It is believed that bowlers who have a quicker run-up have a greater amount of linear momentum which can be converted into ball speed. There is likely to be an optimum run-up speed however, beyond which ball release speed decreases (Brees, 1989). The optimal is likely to exist since the required coordination to control the fast bowling action is not possible. Unsurprisingly, experimental data has been unable to identify the effects of surpassing the optimal run-up speed on fast bowling performance. Therefore, the simulation model of the front foot contact phase of fast bowling was applied to determine the effect of surpassing the optimal run-up speed on ball release speed.

Optimisations of the technique of the fast bowler were carried out at five different run-up speeds: 4.5, 5.0, 5.5, 6.0, 6.5 and 7.0 ms^{-1}. The initial body configuration of the fast bowler was taken to be the optimal body configuration for the bowler found in Section 9.2.2, and the other model inputs remained the same as the previous optimisations.

9.4.1 How does run-up speed affect the performance of the bowler in this study?

A genetic algorithm (Carroll, 2001) varied the 91 muscle activation level parameters. An objective function was maximised which comprised solely of ball release speed. During the optimisation, the joint angle constraints outlined in Section 8.3.2 were employed to ensure that the optimised solution did not exceed the anatomical bounds of the subject. If the range was exceeded, a penalty of -1 was incurred for each degree past the limit. The constraints in Section 9.2.1 to limit the angular velocity of the shoulder and wrist joints on the bowling arm were also enforced, where a penalty of -1 was suffered for each degree per second past the limit.

The optimisations with varying horizontal centre of mass velocity at front foot contact indicated that an optimum run-up speed exists (Figure 9.14), which maximises the performance of the fast bowler. The results also showed however, that the performance plateaus after this optimum rather than decreasing rapidly, as would be expected if the movement is occurring too quickly.

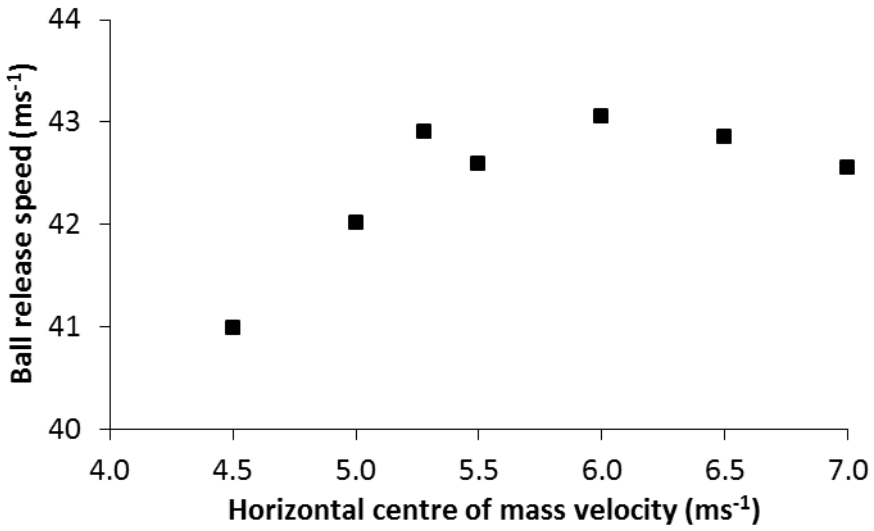

Figure 9.14 - Ball release speed of the optimisations with varying centre of mass velocity at front foot contact.

A visual representation of the optimal technique for maximising ball release speed with varying initial horizontal centre of mass velocity at front foot contact can be seen in Figure 9.15. The differences in technique can be observed to be similar for the optimised simulations at 4.5 and 6.0 ms^{-1}. The slower run-up speed caused trunk flexion to be smaller, as there is less linear momentum braking the pelvis and driving the torso forwards. However, when the run-up speed is faster than the optimum, the simulation model is forced to bend the front knee, as the model is not strong enough to keep it straight. This reduced the efficiency of the conversion of the linear momentum of the run-up to angular momentum about the front foot and resulted in a reduction in ball speed.

Figure 9.15 - Visual representation of the optimal technique for varying horizontal centre of mass velocities: (a) 4.5 ms^{-1}, (b) 6.0 ms^{-1} and (c) 7.0 ms^{-1}.

Discussion

The simulation model was applied to determine:

How does run-up speed affect the performance of the bowler in this study?

The results indicated that an increase in run-up speed would provide an increase in ball release speed. For this bowler, an increase of 0.4% is possible by increasing his horizontal centre of mass velocity from 5.28 ms^{-1} to 6 ms^{-1}. This agrees with previous research that has found that the fastest bowlers tend to have the fastest run-up speeds (Brees, 1989; Glazier, 2000; Ferdinands et al., 2010; Worthington et al., 2013a).

The impact of the horizontal centre of mass velocity increasing past this optimum appears to be small with an increase of 1 ms^{-1} causing a decrease in ball release speed of 1 mph. As the bowler is forced to bend his front knee and

reduces the efficiency of the conversion of linear momentum to angular momentum about the front foot. This simulation model is unable to determine what effect increasing the horizontal centre of mass velocity has on the back foot contact phase and the subsequent potential to allow the bowler to be in the optimal configuration at back foot contact. It is likely that this part of the fast bowling action is a limiting factor on the optimal run-up speed.

9.5 SUMMARY

In this chapter, the simulation model of fast bowling has been applied to answer the research questions regarding the limiting factors of fast bowling performance. The optimisations have shown that there was significant potential for the fast bowler to increase his ball release speed through technique and initial body configuration changes. Further optimisations have also found that an increase in strength will lead to an increase in performance, and that the optimal run-up speed is likely to be determined by the strength of the bowler to keep his front knee straight with a large delivery stride.

- CHAPTER 10 -
SUMMARY AND CONCLUSIONS

Within this final chapter, the present study is reviewed to determine whether the purpose of the research has been addressed through the development, evaluation and application of a simulation model of the front foot contact phase of fast bowling. The methods used within this study are also reviewed with the limitations and potential improvements identified. Finally, the research questions posed in the introduction (Chapter 1) are addressed and future applications of the simulation model are highlighted.

10.1 RESEARCH SUMMARY

10.1.1 Computer simulation model of fast bowling

A computer simulation model of the front contact phase of fast bowling was developed using Autolev^{TM} (Chapter 4). The planar simulation model consisted of sixteen segments, where five were represented using both rigid and wobbling elements.

Extensor and flexor torques acted at the front ankle, front knee, front hip, front shoulder, back hip and bowling arm wrist joints. A lone extensor torque acted at the shoulder on the bowling arm. Passive torque generators were incorporated at the front MTP, front ankle, front knee and front hip joints as well as the elbow on the bowling arm. The back MTP, back ankle, back knee and front elbow joints were angle-driven since it was assumed that the action of these joints during the front foot contact phase of fast bowling had minimal impact on performance. If more accuracy was required however, the torque profiles could be incorporated at these joints to simulate their effect on performance.

During the front foot contact phase of fast bowling motion occurs outside the sagittal plane. This was represented in the simulation model using a novel approach. The independent movement of the hip and shoulder joints with

respect to one another was modelled by connecting the joint centres using massless segments with variable length. The length and orientation of each segment were driven using a function of the trunk orientation angle derived from the recorded performances. Side flexion of the trunk away from the sagittal plane also occurs during the front foot contact phase of fast bowling. This was incorporated using a similar approach; the length of the trunk + head segment within the simulation model was driven as a function of the trunk orientation angle derived from the recorded performances. The results during model evaluation (Chapter 8) indicate that the simulation model accurately represents the front foot contact phase of fast bowling and thus, the methods used to represent the non-planar movements within the model are sufficient.

The interaction of the contact phase between the front foot and the ground was represented using damped linear springs. This allowed the front foot to compress vertically as well as slide and recoil horizontally. The results during the determination of the model parameters (Chapter 7) highlight that this method of representing the foot-ground interface was suitably sufficient within a simulation model of the front foot contact phase of fast bowling. The reproduction of force however, during the optimisations highlighted that the foot-ground interface may be too stiff since the vertical ground reaction force almost decays to zero when the foot is still in contact with the floor. The bowler in this research strikes the floor with his mid-foot first. Previous research (Worthington, 2010) however, has shown that some fast bowlers use a heel-striking technique. The current stiffness and damping parameters of the foot-ground interface do not provide an accurate representation of the ground reaction force if the bowler adopts a heel-striking technique. In the future, the representation of the foot-ground interface should be investigated and the method used to determine the subsequent parameters needs to include more than one subject with different front foot contact techniques.

The trunk of the fast bowler within the simulation model was represented by one segment which also incorporated the head. This representation of the trunk and head as one segment is not an accurate depiction of the spine, which can bend along its length. This representation is however, a compromise

between accuracy and simplicity which is supported by the fact the model was shown to be able to reproduce the important features of the front foot contact phase of fast bowling during model evaluation (Chapter 8). In the future, a more complex representation could be included within the model if greater accuracy is desired, although knowledge of the torque generating capacity of the spine would be required for use in a torque-driven simulation model.

One limitation of the simulation model is that the body is composed of rigid segments connected using pin joints which do not take into account the compression witnessed in real joints during an impact. Although, the foot-ground interface compensates the effect of negating joint compression within the simulation model, the error in the force traces during the determination of the model parameters and model evaluation is most likely due to this. Since the purpose of the present study was to investigate the factors limiting performance of fast bowling and the model was found to accurately reproduce these when evaluated (Chapter 8), the use of pin joints was acceptable. In the future however, if models are to accurately replicate force traces the joints of the stance leg and the spine should be modelled to incorporate these compressions.

10.1.2 Bowler specific parameters

Anthropometric, performance and strength parameters were collected from an elite fast bowler (Chapters 5 and 6).

10.1.2.1 Performance data

Performance data of eighteen, maximal effort, stock deliveries were collected from an elite fast bowler. An eighteen camera Vicon motion analysis system operating at 300 Hz was used to track fifty retro-reflective markers positioned over bony landmarks on the fast bowler. Force data were collected at 1500 Hz using a Kistler platform and was synchronised with the kinematic data using the Vicon Nexus software. Joint centres were determined from the position of these markers and the flexion/extension joint angles were calculated using the coordinates in the sagittal plane, as were the centre of mass position and

velocity, as well as the orientation of the fast bowler. A limitation of calculating the joint angles in the sagittal plane was that any non-planar movement distorts the joint angle. During the front contact phase, internal rotation of the front shoulder leads to forearm movement outside the sagittal plane. However, as the front elbow was angle-driven within the simulation model as it was expected to have minimal impact on performance, the distortion of the joint angle was allowed to exist.

10.1.2.2 Torque data

Subject-specific strength parameters for the ankle, knee, hip and shoulder joints of the fast bowler were collected on an isovelocity dynamometer (Section 6.2). Maximal voluntary joint torque, crank angle and crank angular velocity measurements were collected from movements considered as flexion and extension at each of these joints. A limitation of the method concerned the conversion of the crank angle and angular velocity to joint angle and angular velocity. In previous research, the joint angle and angular velocity has been measured by using a motion analysis system to capture the movement of markers throughout the trials since the joint kinematics can deviate substantially from the crank values (Herzog 1988; Deslandes et al., 2008). Unfortunately, it was not possible to use a motion analysis system alongside the isovelocity dynamometer. Therefore, the joint angles were measured using a mechanical goniometer during the isokinetic trials, and used to convert the crank angle of the isovelocity trials.

A further limitation of the method was that due to time constraints with the bowler, he was unfamiliar with the use of an isovelocity dynamometer. Normal practice would ensure that the bowler is capable of producing maximal effort torques by providing a familiarisation period, which involves a number of repetitions of the test procedure at each joint, before data collection commences.

Bilateral symmetry was assumed during the torque data collection to reduce the time required with the bowler. During the front contact phase of fast bowling

the front ankle, knee and hip as well as the bowling shoulder are the most important, and therefore data were collected from these joints. The back ankle and knee were angle-driven within the simulation so assuming bilateral symmetry had no impact on these two joints. The front shoulder and back hip were torque-driven, however since during model evaluation (Chapter 8) the model was capable of accurately reproducing the joint angle-time histories the assumption of bilateral symmetry is suitable. If greater accuracy is required in the future, the protocol could be modified to incorporate measurements from both sides of the body, at a cost of time to the subject.

The bowling shoulder torque profile was determined using the recorded performance, since the range of motion of the shoulder exceeds the anatomically recognised flexion/extension bounds. Unfortunately, it was not possible to determine the torque-angle or torque-angular velocity relationships for this profile. Instead, the torque profile was modelled as a constant, as the angular velocity was seen to be approximately constant during the front foot contact phase, and any variation within the torque-angle relationship was allowed to exist within the activation level. Although, this torque profile is a significant simplification of the bowling shoulder, the model evaluation process found that it was more than capable of reproducing the joint-angle time history of the bowling shoulder. In the future, a torque profile for the shoulder that incorporates the torque-angle and torque-velocity relationships of the muscles about the shoulder in this region should be developed. This is a significant task however, especially in two dimensions.

The wrist torque profile was taken from a male gymnast, and the activation levels fixed to those found during the matching process. The subsequent oscillations in the optimisations of the wrist angle highlight that limiting the wrist to the activation levels found within the matching process meant the wrist extensors were not strong enough to keep the wrist cocked. However, these oscillations were not deemed to have a major effect on the performance of the fast bowler since wrist flexion always occurred from a similar position. In the future, it would be ideal to collect wrist torque data from the fast bowler used within this simulation study and make the wrist torque profile subject-specific.

The passive torque used at the front ankle, knee and hip, within this study were not subject-specific, and instead were taken from previous literature (Reiner and Edrich, 1999). The influence on the joint torques was seen to be minimal in the matched simulation however, and therefore their use was deemed acceptable. In the future, subject-specific flexibility parameters could be collected using the dynamometer and fitting exponential functions fitted to the results (Jackson, 2010).

10.1.2.3 Anthropometric data

Subject-specific segmental inertia parameters were determined using Yeadon's inertia model (1990a). Rigid segment simulation models have used this model to calculate body segment parameters and subsequently accurately simulate human movement (Wilson et al., 2006, Allen et al., 2012).

The distribution of the mass between the rigid and wobbling elements was calculated using a method described by Allen (2010), which used values from the literature (Clarys et al., 1984). Although, the body fat percentage of the bowler was calculated using skinfolds in order to account for the difference in body composition of the subject in the literature and the bowler in this study there were unavoidable inaccuracies. To improve the accuracy of the distribution of the mass between the rigid and wobbling elements, the use of imaging techniques could be used in the future.

10.1.3 Determination of model parameters

An angle-driven model was employed to determine the model parameters using a genetic algorithm. A common set of parameters was found by matching three recorded performances concurrently. The resulting set of model parameters were then evaluated using a further recorded performance. The set of model parameters closely matched the performance data, with an overall difference of 6.7%.

10.1.4 Model Evaluation

The torque-driven simulation model of the front foot contact phase of fast bowling was matched to a recorded performance by allowing the activation level of the torque generators and the initial conditions of the front leg to vary using a genetic algorithm. The initial conditions of the front leg were allowed to vary in an attempt to account for errors in the kinematic data, and deformations within the joints which cannot be represented in a pin-joint model. A model with springs in the joint to represent the compressions which occur during impact would alleviate some of these errors in the future.

The simulations matched the recorded performance well with an overall difference of 3.99%, which was reduced to 0.87% when only the kinematic parameters of the objective function were considered. Therefore, the simulation model of the front foot contact phase of fast bowing was able to reproduce accurate kinematics of the movement and was deemed suitable to investigate the research questions.

One limitation of the simulation model was that the reproduction of the force was below the recorded performance. This is most likely due to using pin-joints and the compression of the joints across the system being incorporated within the foot-ground interface. In the future, if force traces are to match well, the joints of the limb in contact with the ground and the spine should be represented using a method which incorporates joint compression. It may also have been caused by the different orientation of the foot at ground contact where the parameters of the springs at the toe, MTP and heel were optimised for a specific orientation. In the future, the viscoelastic parameters should be determined using a number of different foot landing orientations.

10.1.5 Model Optimisation

Each optimisation of the simulation model when it was applied to investigate the research questions was processed using a parallelised genetic algorithm. Parallelising the code allowed for the processing time to be greatly reduced and the optimised solution to be found faster.

One limitation of the objective function used to discover the optimal solutions was that the robustness of the solution was not incorporated. Previously, Yeadon (2005) has provided a landscape metaphor to describe the search for optima: “The search for an optimum can be likened to the search for the highest mountain peak in a given terrain: an optimisation routine may find a local rather than a global optimum - the top of a foothill rather than the summit of the highest mountain. On the other hand, the routine may be successful in finding the top of a single pinnacle that stands on a narrow base high above the surrounding terrain. Even if this is the global optimum it is a summit that should not be attempted, since any small location error will land on a low terrain. In other words, if there is an optimum technique in javelin that is surrounded by poor performances, it is a poor strategy that strives for this in the distant hope that everything will come right on one of the attempts. The likelihood is that all the performances will be poor. A better strategy may be to find a high hilltop with a large plateau so that points even some distance away are high. There is much to be said for consistency when competing”. In the future, to determine the robustness of the optimal solution and check that the optimal solution is not surrounded by “low terrain” and therefore a poor strategy, constraints should be included within the objection function.

10.2 RESEARCH QUESTIONS

1. How close to optimal is the technique of the bowler in this study?

The optimal technique within this study was considered to be one in which ball release speed was maximised. Optimisation of the parameters governing the activation levels highlighted a potential increase of 9.8% was possible with a change in technique during the front foot contact phase.

2. How close to optimal is the body configuration at front foot contact of the bowler in this study?

A further optimisation was conducted which allowed the initial body configuration to change at front foot contact. The optimal technique was again considered to be one in which ball release speed was maximised. This

optimisation highlighted a significant increase in performance was possible. An increase of 21.5% was possible compared to the matched performance. The optimal configuration had a large delivery stride, with a straighter front knee and a delayed bowling arm. This resulted in a technique where the front leg was kept straighter, the bowling arm was delayed and trunk flexion was increased during the front foot contact phase.

Furthermore, the activation-level time histories throughout the optimised technique indicated that the performance of the fast bowler is pre-determined by the body configuration at front foot contact.

3. Does an increase in strength improve the performance of the bowler in this study?

An optimisation which increased the strength of the ankle, knee, hip and front shoulder by 5% but maintained the optimal initial body configuration from the previous optimisation found a potential increase of 1.3% mph was possible.

The optimal technique remained the same: the front leg was kept straighter, the bowling arm was delayed and trunk flexion was increased during the front foot contact phase. The increase in strength however, allowed the simulation to increase the effectiveness of this technique.

4. How does run-up speed affect the performance of the bowler in this study?

Five optimisations were run with different initial horizontal centre of mass speed at front foot contact. The results showed that an increase in the initial horizontal centre of mass at front foot contact could provide an increase in ball release speed of 0.4%. However, the simulation model was unable to determine the effect of approaching the crease too quickly.

10.3 FUTURE APPLICATIONS

Initially, the adjustment of the foot-ground interface will take place in order to simulate different orientations of the foot at front foot contact and attempt to reproduce more accurate force-time histories. This may require an adjustment

not only of the method used to determine the viscoelastic parameters but also the representation of this interface. Nevertheless, the current model has been shown to accurately reproduce the movement of a fast bowler during the front foot contact phase. Consequently, it can be used to answer questions in the future with confidence. Additional research question which may be addressed in the future include:

- How sensitive is fast bowling performance to variations in the initial conditions?
- How sensitive is fast bowling performance to noise in the muscle activation parameters?
- How does the individual strength of each joint affect fast bowling performance?
- What impact do body segment parameters have on fast bowling performance?
- How does the direction of the centre of mass velocity affect front knee kinematics?

10.4 CONCLUSIONS

The aim of this research was to identify the factors that limit fast bowling performance in cricket. A torque-driven computer simulation model was developed of the front foot contact phase of fast bowling and successfully evaluated and optimised. Subject-specific anthropometric, strength and performance data were collected from an elite fast bowler and model parameters were calculated using an angle-driven model. A recorded performance was used to evaluate the torque-driven computer simulation model and demonstrated a close match between the matched simulation and recorded performance, indicating that the model was capable of reproducing realistic kinematics of the fast bowling action. The torque-driven model was subsequently used to investigate the optimum fast bowling technique. The optimised technique employed by the simulation model agreed with features demonstrated from current elite fast bowlers and confirmed previous research

which was encouraging and a further indication of the accuracy of the model. Finally the model was used to show that increasing strength increased ball release speed and that an optimum run-up speed exists.

- REFERENCES -

Ackland, T.R., Henson, P.W., Bailey, D.A. (1988). The uniform density assumption: its effect upon the estimation of body segment inertial parameters. *Int. J. Sports Biomech*. *4*, 146-155.

Allard, P., Stokes, I.A.F., Blanchi, J. (1995). Three-dimensional analysis of human movement. Human Kinetics Publishers, Champaign.

Alexander, R.M. (1990). Optimum take-off techniques for high and long jumps. *Philosophical Transactions of the Royal Society of London*, B329, 3-10.

Alexander, R.M. (1992). Simple models of walking and jumping. *Human movement science*, 11(1), 3-9.

Allen, S.J. (2010). Optimisation of performance in the triple jump using computer simulation. *Unpublished Doctoral Thesis,* Loughborough University.

Allen, S.J., King, M.A., and Yeadon, M.R. (2012). Models incorporating pin joints are suitable for simulating performance but unsuitable for simulating internal loading. *Journal of biomechanics*, *45*(8), 1430-1436.

Audu, M.L. and Davy, D.T. (1985). The influence of muscle model complexity in musculoskeletal motion modelling. *Journal of biomechanical engineering*, 107(2), 147-157.

Baca, A. (1996). Precise determination of anthropometric dimensions by means of image processing methods for estimating human body segment parameter values. *Journal of biomechanics*, *29*(4), 563-567.

Bartlett, R.M. and Best, R.J. (1988). The biomechanics of javelin throwing: A review. *Journal of Sports Sciences*, 6, 1-38.

Bartlett, R.M., Stockill, N.P., Elliott, B.C., and Burnett, A.F. (1996). The biomechanics of fast bowling in men's cricket: A review. *Journal of Sports Sciences*, 14, 403-424.

Bassett, R.W., Browne, A.O., Morrey, B.F., and An, K.N. (1990). Glenohumeral muscle force and moment mechanics in a position of shoulder instability. *Journal of Biomechanics*, 23, 405-415.

Bartlett, R.M. (2006). Medicine and science in cricket. *Journal of Science and Medicine in Sport*, 9(6), 470-471.

Bobbert, M.F. and Schamhardt, H.C. (1990). Accuracy of determining the point of force application with piezoelectric force plates. *Journal of Biomechanics*, 23(7), 705-710.

Bohm, H., Cole, G.K., Brüggemann, G., and Ruder, H. (2006). Contribution of muscle series elasticity to maximum performance in drop jumping. *Journal of Applied Biomechanics*. 22, 3-13.

Brees, A.J. (1989). A cinematographical analysis of the effect of varying the run-up speed on ball release velocity, accuracy and body kinematics of fast bowling in cricket. *Unpublished undergraduate dissertation, Crewe and Alsager College of Higher Education.*

Brewin, M.A., Yeadon, M.R., and Kerwin, D.G. (2000). Minimising peak forces at the shoulders during backward longswings on rings. *Human Movement Science*, *19*(5), 717-736.

Brooks, C.B. and Jacobs, A.M. (1975). The gamma mass scanning technique for inertial anthropometric measurement. *Medicine and Science in Sports*, *7*(4), 290-294.

Burden, A.M. (1990). An electromyographical and cinematographical analysis of fast medium bowling in cricket. *Unpublished Master's thesis, University of Salford.*

Burden, A.M. and Bartlett, R.M. (1990a). A kinematic comparison between elite fast bowlers and college fast-medium bowlers. In *Proceedings of the Sports Biomechanics Section of the British Association of Sports Sciences, 15.*

Burden, A. M. and Bartlett, R. M. (1990b). A kinematic investigation of elite fast and fast medium cricket bowlers. In *Proceedings of the VIIIth International Symposium of the Society of Biomechanics in Sports* (pp. 41-46).

Carroll, D.L. (2001). FORTRAN genetic algorithm driver. Downloaded from: http://cuaerospace.com/carroll/ga.html.

Challis, J.H. and Kerwin, D.G. (1992). Calculating upper limb inertial parameters. *Journal of sports sciences*, *10*(3), 275-284.

Chandler, R.F., Clauser, C.E., McConville, J.T., Reynolds, H.M., and Young, J.W. (1975). Investigation of inertial properties of the human body. AMRL-TR-74-137, AD-A016-485, DOT-HS-801-430. *Aerospace Medical Research Laboratories*, Wright-Patterson Air Force Base, Ohio

Chapman, A.E. (1985). The mechanical properties of human muscle. *Exercise and Sports Sciences Reviews.* 13, 443-501.

Chow, J.W. and Darling, W.G. (1999). The maximum shortening velocity of muscle should be scaled with activation. *Journal of Applied Physiology*, 86, 1025-1031.

Clarys, J.P. and Marfell-Jones, M.J. (1986). Anthropometric prediction of component tissue masses in the minor limb segments of the human body. *Human Biology*, 761-769.

Clauser, C.E., McConville, J.T., and Young, J.W. (1969). *Weight, volume, and center of mass of segments of the human body*. ANTIOCH COLL YELLOW SPRINGS OH.

Corana, A., Marchesi, M., Martini, C., and Ridella, S. (1987). Minimizing multimodal functions of continuous variables with the "simulated annealing" algorithm. *ACM Transactions on Mathematical Software.* 13, 262-280.

Cross, R. (1999). Standing, walking, running, and jumping on a force plate. *American Journal of Physics*, 67, 304.

Dapena, J. (1981). Simulation of modified human airborne movements. *Journal of Biomechanics*, 14(2), 81-89.

Davis, K. and Blanksby, B. (1976a). The segmental components of fast bowling in cricket. *Australian Journal for Health, Physical Education and Recreation*, 71(suppl.), 6-8.

Davis, K. and Blanksby, B. (1976b). A cinematographical analysis of fast bowling in cricket. *Australian Journal for Health, Physical Education and Recreation*, 71 (suppl.), 9- 15.

Davis, R.B., Ounpuu, S., and Tyburski, D. (1991). A gait analysis data collection and reduction technique. *Human Movement Science*. 10, 575-587.

Deslandes, S., Mariot, J. P., and Serveto, S. (2008). Offset of rotation centers creates a bias in isokinetics: A virtual model including stiffness or friction. *Journal of biomechanics*, *41*(10), 2112-2120.

De Vaal, M.H., Neville, J., Scherman, J., Zilla, P., Litow, M., and Franz, T. (2010). Mechanical loadings on pectoral pacemaker implants: Correlation of in-line and transverse force of the pectoralis major. *Annals of Biomedical Engineering.* 38, 3338-3346.

Dempster, W. T. (1955). *Space Requirements of the Seated Operator: Geometric, Kinematic, and Mechanical Aspects of the Body with Special Reference to Limbs*. NTIS.

Duda, G.N., Brand, D., Freitag, S., Lierse, W., and Schneider, E. (1996). Variability of femoral muscle attachments. *Journal of Biomechanics*. 29, 1185-1190.

Dudley, G.A., Harris, R.T., Duvoisin, M.R., Hather, B.M., and Buchanan, P. (1990). Effect of voluntary vs. artificial activation on the relationship of muscle torque to speed. *Journal of Applied Physiology*. 69, 2215-2221.

Edman, K.A.P. (1988). Double-hyperbolic force-velocity relation in frog muscle fibres. *Journal of Physiology*. 404, 301-321.

Edman, K.A. and Reggiani, C. (1987). The sarcomere length-tension relation determined in short segments of intact muscle fibres of the frog. *The Journal of physiology*, *385*(1), 709-732.

Elliott, B.C. and Foster, D. (1984). A biomechanical analysis of the front-on and side-on fast bowling techniques. *Journal of Human Movement Studies*, 10, 83-94.

Elliott, B.C., Foster, D., and Gray, S. (1986). Biomechanics and physical factors affecting fast bowling. *Australian Journal of Science and Medicine in Sport*; 18, 16-21.

Elliott, B. C. and Foster, D. H. (1989). Fast bowling technique. *Send the stumps flying: The science of fast bowling.* Perth: University of Western Australia.

Elliott, B.C., Hardcastle, P.H., Burnett, A.F., and Foster, D.H. (1992). The influence of fast bowling and physical factors on radiologic features in high performance young fast bowlers. *Sports Medicine Training and Rehabilitation*, 3, 113-130.

Elliott, B.C., Davis, J.W., Khangure, M.S., Hardcastle, P. and Foster, D. (1993). Disc degeneration and the young fast bowler in cricket. *Clinical Biomechanics*, 8(5), 227-234.

Erdemir, A., McLean, S., Herzog, W., and van den Bogert, A.J. (2007). Model-based estimation of muscle forces exerted during movements. *Clinical Biomechanics.* 22, 131-154.

Felton, P.J. (2010). What is the effect of elbow hyperextension on ball release velocity? *Unpublished Masters Thesis*, Loughborough University.

Fenn, W.O. and Marsh, B.S. (1935). Muscular force at different speeds of shortening. The *Journal of Physiology*, 85, 277-297.

Ferdinands, R.E.D. and Kersting, U.G. (2004). Elbow Angle Extension and implications for the legality of the bowling action in Cricket. In A. McIntosh (Ed.), *Proceedings of Australasian Biomechanics Conference* (Vol. 5, pp. 26-27).

Ferdinands, R.E., Kersting, U.G., and Marshall, R.N. (2008). A preliminary forward solution model of cricket bowling. *International Journal of Sports Science and Engineering*, *2*(4), 211-215.

Ferdinands, R., Marshall, R.N., and Kersting, U. (2010). Centre of mass kinematics of fast bowling in cricket. *Sports Biomechanics*, *9*(3), 139-152.

Finni, T., Komi, P.V., and Lukkariniemi, J. (1998). Achilles tendon loading during walking: application of a novel optic fiber technique. *European Journal of Applied Physiology and Occupational Physiology*. 77, 289-291.

Finni, T. and Komi, P.V. (2002). Two methods for estimating tendinous tissue elongation during human movement. *Journal of Applied Biomechanics.* 18, 180-188.

Forrester, S.E., Yeadon, M.R., King, M.A., and Pain, M.T.G. (2011). Comparing different approaches for determining joint torque parameters from isovelocity dynamometer measurements. *Journal of Biomechanics*. 44, 955-961.

Foster, D. H. and Elliott, B. C. (1985). Fast bowling: An impact sport. A profile of DK Lillee. *Sports Coach*, 9(3), 3-8.

Foster, D., John, D., Elliott, B., Ackland, T. and Fitch, K. (1989). Back injuries to fast bowlers in cricket: A prospective study. *British Journal of Sports Medicine*, 23(3), 150-154.

Freund, H.J. and Büdingen, H.J. (1978). The relationship between speed and amplitude of the fastest voluntary contractions of human arm muscles. *Experimental Brain Research*, 31(1), 1-12.

Fukashiro, S., Komi, P.V., Jarvinen, M., and Miyashita, M. (1995). In vivo Achilles tendon loading during jumping in humans. *European Journal of Applied Physiology and Occupational Physiology*. 71, 453-458.

Gasser, H.S. and Hill, A.V. (1924). The dynamics of muscular contraction. *Proceedings of the Royal Society of London. Series B, Containing Papers of a Biological Character*, 96(678), 398-437.

Gerritsen, K.G., van den Bogert, A.J., and Nigg, B.M. (1995). Direct dynamics simulation of the impact phase in heel-toe running. *Journal of biomechanics*, *28*(6), 661-668.

Glazier, P.S., Paradisis, G.P., and Cooper, S.M. (2000). Anthropometric and kinematic influences on release speed in men's fast-medium bowling. *Journal of Sports Sciences*, 18, 1013-1021.

Gordon, A.M., Huxley, A.F., and Julian, F.J. (1966). The variation in isometric tension with sarcomere length in vertebrate muscle fibres. *Journal of Physiology*. 184, 170-192.

Gregor, R.J., Komi, P.V., Browning, R.C., and Jarvinen, M. (1991). A comparison of the triceps surae and residual muscle moments at the ankle during cycling. *Journal of Biomechanics*. 24, 287-297.

Gruber, K., Ruder, H., Denoth, J., and Schneider, K. (1998). A comparative study of impact dynamics: wobbling mass model versus rigid body model. *Journal of Biomechanics*, 31, 439-444.

Hanavan Jr, E.P. (1964). *A mathematical model of the human body* (No. AFIT-GA-PHYS-64-3). AIR FORCE AEROSPACE MEDICAL RESEARCH LAB WRIGHT-PATTERSON AFB OH.

Harik, G.R., Lobo, F.G., and Goldberg, D.E. (1999). The compact genetic algorithm. *IEEE Transactions on Evolutionary Computation*, 3(4), 287-297.

Herzog, W. (1988). The relation between the resultant moments at a joint and the moments measured by an isokinetic dynamometer. *Journal of Biomechanics*, *21*(1), 5-12.

Hurrion, P.D., Dyson, R., Leonard, A. and Hale, T. (1997a). The effect of athletic support location on ground reaction forces and electromyography

during the delivery stride of fast medium bowlers in cricket. In *Proceedings of the Second Annual Conference of the European College of Sports*. 778-779.

Hurrion, P.D., Dyson, R., Taylor, M. and Hale, T. (1997b). Ground reaction forces of fast-medium bowlers in cricket. In *Proceedings of the Second Annual Conference of the 140 European College of Sports Science*. 777-777.

Hurrion, P.D., Dyson, R. and Hale, T. (2000). Simultaneous measurement of back and front foot ground reaction forces during the same delivery stride of the fast-medium bowler. *Journal of Sports Sciences*, 18, 993-997.

Harry, J.D., Ward, A.W., Heglund, N.C., Morgan, D.L., and McMahon, T.A. (1990). Cross-bridge cycling theories cannot explain high-speed lengthening behaviour in frog muscle. *Biophysical Journal*. 57, 201-208.

Hatze, H. (1981). A comprehensive model for human motion simulation and its application to the takeoff phase of the long jump. *Journal of Biomechanics*. 3, 135-142.

Hiley, M.J. and Yeadon, M.R. (2003). Optimum Technique for Generating Angular Momentum in Accelerated Backward Giant Circles Prior to a Dismount. *Journal of Applied Biomechanics* ,19(2).

Hill, A.V. (1938). The heat of shortening and the dynamic constants of muscle. *Proceedings of the Royal Society*. B126, 136-195.

Hof, A.L. (1998). In vivo measurement of the series elasticity release curve of human triceps surae muscle. *Journal of Biomechanics.* 31, 793-800.

Hubbard, M. and Alaways, L.W. (1989). Rapid and accurate estimation of release conditions in the javelin throw. *Journal of Biomechanics*, *22*(6), 583-595.

Huxley, A.F. (1957). Muscle structure and theories of contraction. *Progress in Biophysics and Biophysical Chemistry*. 7, 255-318.

Jackson, M.I. (2010). The mechanics of the table contact phase of gymnastics vaulting. *Unpublished Doctoral Thesis*, Loughborough University.

Jensen, R.K. (1978). Estimation of the biomechanical properties of three body types using a photogrammetric method. *Journal of Biomechanics*, 11(8), 349-358.

Jones, D.A., Round, J.M., and De Haan, A. (2004). *Skeletal Muscle from Molecules to Movement: A Textbook of Muscle Physiotherapy for Sport, Exercise and Physiotherapy*. Churchill Livingstone.

Kane, T.R. and Levinson, D.A. (1985). *Dynamics, theory and applications*. McGraw Hill.

Katz, B. (1939). The relation between force and speed in muscular contraction. *Journal of Physiology*. **1**, 45-64.

King, M.A. (1998). Contributions to performance in dynamic jumps. *Unpublished Doctoral Thesis*, Loughborough University.

King, M.A. and Yeadon, M.R. (2002). Determining subject-specific torque parameters for use in a torque-driven simulation model of dynamic jumping. *Journal of Applied Biomechanics*, 18(3), 207-217.

King, M.A. and Yeadon, M.R. (2004). Maximising somersault rotation in tumbling. *Journal of Biomechanics*, 4, 471-477.

King, M.A., Wilson, C., and Yeadon, M.R. (2006). Evaluation of a torque-driven model of jumping for height. *Journal of Applied Biomechanics*. 22, 264-274.

Kirkpatrick, S., Gelatt, C.D., and Vecchi, M.P. (1983). Optimization by simmulated annealing. *Science*, 220(4598), 671-680.

Klein, P., Mattys, S., and Rooze, M. (1996). Moment arm length variations of selected muscles acting on talocrural and subtalar joints during movement: An in vitro study. *Journal of Biomechanics*. 1, 21-30.

Komi, P.V., Belli, A., Huttunen, V., Bonnefoy, R., Geyssant, A. and Lacour, J.R. (1996). Optic fibre as a transducer of tendomuscular forces. *European Journal of Applied Physiology and Occupational Physiology*, 72, 278-280.

Kong, P.W. (2004). Computer simulation of the take-off in springboard diving. *Unpublished Doctoral Thesis*, Loughborough University.

Lafortune, M.A., Cavanagh, P.R., Sommer Iii, H.J. and Kalenak, A. (1992). Three-dimensional kinematics of the human knee during walking. *Journal of Biomechanics*, *25*(4), 347-357.

Langenderfer, J., LaScalza, S., Mell, A., Carpenter, J.E., Kuhn, J.E., and Hughes, R. E. (2005). An EMG-driven model of the upper extremity and estimation of long head biceps force. *Computers in biology and medicine*, 35(1), 25-39.

Lee, D., Glueck, M., Khan A., Fiume, E., and Jackson, K. (2010). A survey of modeling and simulation of skeletal muscle. *ACM Transactions on Graphics*, *28*(4).

Lewis, M.G.C. (2011). Are torque-driven simulation models limited by an assumption of monoarticularity? *Unpublished Doctoral Thesis*, Loughborough University.

Lieber, R.L., Jacobson, M.D., Fazeli, B.M., Abrams, R.A., and Botte, M. J. (1992). Architecture of selected muscles of the arm and forearm: anatomy and implications for tendon transfer. *The Journal of Hand Surgery*, 17(5), 787-798.

Locatelli, M. (2000). Simulated annealing algorithms for continuous global optimization: convergence conditions. *Journal of Optimization Theory and applications*, 104(1), 121-133.

Loram, L.C., McKinon, W., Wormgoor, S., Rogers, G.G., Nowak, I., and Harden, L.M. (2005). The determinants of ball release speed in schoolboy fast-medium bowlers in cricket. *Journal of Sports Medicine and Physical Fitness*, 45, 483–490.

Marylebone Cricket Club, 1976. The M.C.C. cricket coaching book. London: William Heinemann.

Mason, B.R., Weissensteiner, J.R. and Spence, P.R. (1989). Development of a model for fast bowling in cricket. *Excel*, 6, 2-12.

Miller, D.I. (1970). A computer simulation model of the airborne phase of diving. *Unpublished Doctoral Thesis*, The Pennsylvania State University.

Mills, C., Pain, M.T., and Yeadon, M.R. (2008). The influence of simulation model complexity on the estimation of internal loading in gymnastics landings. *Journal of Biomechanics*, *41*(3), 620-628.

Minetti, A.E. and Belli, G. (1994). A model for the estimation of visceral mass displacement in periodic movements. *Journal of biomechanics*, *27*(1), 97-101.

Misevich, K. W. and Cavanagh, P. R. (1984). Material aspects of modelling shoe/foot interaction. *Sports shoes and playing surfaces. Champaign, IL: Human Kinetics*, 47-75.

Mungiole, M. and Martin, P.E. (1990). Estimating segment inertial properties: comparison of magnetic resonance imaging with existing methods. *Journal of Biomechanics*, *23*(10), 1039-1046.

Muramatsu, T., Muraoka, T., Takeshita, D., Kawakami, Y., Hirano, Y., and Fukunaga, T. (2001). Mechanical properties of tendon and aponeurosis of human gastrocnemius muscle in vivo. *Journal of Applied Physiology*, *90*(5), 1671-1678.

Nagano, A. and Gerritsen, K.G.M. (2001). Effects of neuromuscular strength training on vertical jumping performance-a computer simulation study. *Journal of Applied Biomechanics*, 17(2), 113-128.

Nigg, B.M. (1999). Mathematically determinate systems. *Biomechanics of the Musculo-skeletal System*, 458-532.

Nigg, B.M., Cole, G.K., and Bruggemann, G.P. (1995). Impact forces during heel toe running. *Journal of Applied Biomechanics*, 11(4), 407-432.

Pain, M.T.G. (1999). An analysis of human soft tissue. *Unpublished Doctoral Thesis*, Penn State University.

Pain, M.T.G. and Challis, J.H. (2001). The role of the heel pad and shank soft tissue during impacts: a further resolution of a paradox. *Journal of Biomechanics.* 34, 327-333.

Pain, M.T. and Challis, J.H. (2004). Wobbling mass influence on impact ground reaction forces: A simulation model sensitivity analysis. *Journal of Applied Biomechanics*, 20(3), 309-316.

Pain, M.T. and Challis, J.H. (2006). The influence of soft tissue movement on ground reaction forces, joint torques and joint reaction forces in drop landings. *Journal of biomechanics*, 39(1), 119-124.

Pandy, M.G., Zajac, F.E., Sim, E., and Levine, W.S. (1990). An optimal control model for maximum-height human jumping. *Journal of Biomechanics*. 23, 1185-1198.

Pandy, M.G. and Barr, R.E. (2004). Biomechanics of the musculoskeletal system. *Standard Handbook of Biomedical Engineering and Desing*.

Pierrynowski, M.R. (1995). Analytic representation of muscle line of action and geometry. In Allard, P., Stokes, I. A. F., Blanchi, J. (eds), *Three-dimensional analysis of human movement*. Human Kinetics Publishers, Champaign.

Portus, M.R., Mason, B.R., Elliott, B.C., Pfitzner, M.C., and Done, R.P. (2004). Technique factors related to ball release speed and trunk injuries in high performance cricket fast bowlers. *Sports Biomechanics*, 3(2), 263-283.

Portus, M.R., Rosemond, C.D., and Rath, D.A. (2006). Fast bowling arm actions and the illegal delivery law in men's high performance cricket matches. *Sports Biomechanics*, 5(2), 215-230.

Press, W.H., Flannery, B.P., Teukolsky, S.A., and Vetterling, W.T. (1988). Numerical Recipes. The art of Scientific Computing, Cambridge: Cambridge University Press.

Reinschmidt, C., Van Den Bogert, A. J., Lundberg, A., Nigg, B. M., Murphy, N., Stacoff, A. and Stano, A. (1997). Tibiofemoral and tibiocalcaneal motion during walking: external vs. skeletal markers. *Gait and Posture*, 6(2), 98-109.

Richards, J.G. (1999). The measurement of human motion: A comparison of commercially available systems. *Human Movement Science*, 18(5), 589-602.

Riener, R. and Edrich, T. (1999). Identification of passive elastic joint moments in the lower extremities. *Journal of biomechanics*, 32(5), 539-544.

Robertson, E., Caldwell, G. E., Gordon, D., Hamill, J., Kamen, G., and Whittlesey, S. N. (2004). Research methods in biomechanics. *Human Kinetics. ISBN X*, *73603966*.

Roosen, A. (2007). Skill reproduction in a reduced time-frame by martial athletes. *Unpublished Doctoral Thesis*, Loughborough University.

Salter, C.W., Sinclair, P.J., and Portus, M.R. (2007). The associations between fast bowling technique and ball release speed: A pilot study of the within-bowler and between-bowler approaches. *Journal of Sports Sciences*, 25, 1279–1285.

Saunders, G.C. and Coleman, S.G.S. (1991). The ground reaction forces experienced by medium-fast bowlers in cricket. *Journal of Sports Sciences*, 9, 406.

Scovil, C.Y., Ronsky, J.L. (2006). Sensitivity of a Hill-based muscle model to perturbations in model parameters. *Journal of Biomechanics*. 39, 2055-2063.

Seger, J.Y. and Thorstensson, A. (1994). Muscle strength and myoelectric activity in prepubertal and adult males and females. *European journal of applied physiology and occupational physiology*, 69(1), 81-87.

Spoor, C.W., van Leewun, J.L., Meskers, C.G., Titulaer, A.F., and Huson, A. (1990). Estimation of instantaneous moment arms of the lower-leg muscles. *Journal of Biomechanics*. 12, 1247-1259.

Sprigings, E.J., Lanovaz, J.L., Watson, L.G., and Russell, K.W. (1998). Removing swing from a handstand on rings using a properly timed backward giant circle: a simulation solution. *Journal of Biomechanics,* 31, 27-35.

Stockill, N. and Bartlett, R. (1992). A three-dimensional cinematographical analysis of the techniques of international and English County Cricket fast bowlers. *In Xth Symposium of the International Society of Biomechanics in Sports (edited by R. Rodano, G. Ferrigno and G.C. Santambrogio)*. Milan: Edi Ermes.

Stockill, N. P. and Bartlett, R. M. (1994). A temporal and kinematic comparison of junior and senior international cricket bowlers. *Journal of Biomechanics*, *27*(6), 690.

Tyson, F. (1976). *Complete Cricket Coaching*. Melbourne: Thomas Nelson Ltd.

Van Den Bogert, A.J., Gerritsen, K.G., and Cole, G.K. (1998). Human muscle modelling from a user's perspective. *Journal of Electromyography and Kinesiology*. 8, 119-124.

Van der Helm, F.C. (1994). Analysis of the kinematic and dynamic behavior of the shoulder mechanism. *Journal of biomechanics*, *27*(5), 527-550.

Van Soest, A.J. (1992). Jumping from structure to control – A simulation study of explosive movements. *Doctoral Dissertation*, University of Amsterdam.

Van Soest, A.J., Schwab, A.L. Bobbert, M.F., and Van Ingen Schenau, G.J. (1993). The influence of the biarticularity of the gastrocnemius muscle on vertical-jumping achievement. *Journal of Biomechanics*. 26, 1-8.

Van Soest, A.J. and Casius, L.J.R. (2003). The merits of parallel genetic algorithm in solving hard optimization problems. *Journal of Biomechanical Engineering*. 125, 141-146.

Webber, S., Kriellers, D. (1997). Neuromuscular factors contributing to in vivo eccentric moment generation. *Journal of Applied Physiology*. 83, 40-45.

Wells, D., Alderson, J., Middleton, K., and Donnelly, C. (2012). Assessing the accuracy of inverse kinematics in Opensim to estimate elbow flexion-extension during cricket bowling: maintain the rigid linked assumption. *ISBS-Conference Proceedings Archive*, 1(1).

Westing, S.H., Seger, J.Y., and Thorstensson, A. (1990). Effects of electrical stimulation on eccentric and concentric torque-velocity relationships during knee extension in man. *Acta Physiologica Scandinavica*. 140, 17-22.

Wilson, C. (2003). Optimisation of performance in running jumps. *Unpublished Doctoral Thesis*, Loughborough University.

Wilson, C., King, M. A., and Yeadon, M. R. (2006). Determination of subject-specific model parameters for visco-elastic elements. *Journal of Biomechanics*, 39, 1883-1890.

Winter, D.A. (1990). *Biomechanics and motor control of human movement*. Wiley, New York.

Wood, G.A. and Jennings, L.S. (1979). On the use of spline functions for data smoothing. *Journal of biomechanics*, *12*(6), 477-479.

Wormgoor, S., Harden, L., and Mckinon, W. (2010). Anthropometric, biomechanical, and isokinetic strength predictors of ball release speed in high-performance cricket fast bowlers. *Journal of sports sciences*, *28*(9), 957-965.

Worthington, P.J. (2010). A biomechanical analysis of fast bowling in cricket. *Unpublished Doctoral Thesis*, Loughborough University.

Worthington, P.J., King, M.A., and Ranson, C.A. (2013a). Relationships between fast bowling technique and ball release speed in cricket. *Journal of Applied Biomechanics, 29 (1)*, 78 - 84.

Worthington, P.J., King, M.A., and Ranson, C.A. (2013b). The influence of cricket fast bowlers' front leg technique on peak ground reaction forces. *Journal of sports sciences*, *31*(4), 434-441.

Wright, I. C., Neptune, R.R., van Den Bogert, A. J., and Nigg, B.M. (1998). Passive regulation of impact forces in heel-toe running. *Clinical Biomechanics*, *13*(7), 521-531.

Yang, J. and Honavar, V. (1998). Feature subset selection using a genetic algorithm. *Feature extraction, construction and selection*. Springer US.

Yeadon, M.R. (1990a). The simulation of aerial movement - I. The determination of orientation angles from film data. *Journal of Biomechanics*. 23, 59-66.

Yeadon, M.R. (1990b). The simulation of aerial movement - II. A mathematical inertia model of the human body. *Journal of Biomechanics*. 23, 67-74.

Yeadon, M.R. (2005). What are the limitations of experimental and theoretical approaches in sports biomechanics? *Philosophy and the sciences of exercise, health and sport: critical perspectives on research methods*. London: Routledge, 133-143.

Yeadon, M.R., Atha, J., and Hales, F.D. (1990). The simulation of aerial movement—IV. A computer simulation model. *Journal of Biomechanics*, *23*(1), 85-89.

Yeadon, M.R. and Challis, J.H. (1994). The future of performance-related sports biomechanics research. *Journal of Sports Sciences*, *12*(1), 3-32.

Yeadon, M.R. and Hiley, M.J. (2000). The mechanics of the backward giant circle on the high bar. *Human Movement Science*, *19*(2), 153-173.

Yeadon, M.R. and King, M.A. (2002). Evaluation of a torque-driven simulation model of tumbling. *Journal of Applied Biomechanics*. 18, 195-206.

Yeadon, M.R. and King, M.A. (2008). Computer simulation modelling in sport, *Biomechanical Analysis in Sport and Exercise*. Routledge, London, UK, 176-205.

Yeadon, M.R., King, M.A., and Wilson, C. (2006). Modelling the maximum voluntary joint torque/angular velocity relationship in human movement. *Journal of Biomechanics*. 39, 476-482.

Yeadon, M.R., King, M.A., Forrester, S.E., Caldwell, G.E., and Pain, M.T. (2010). The need for muscle co-contraction prior to a landing. *Journal of biomechanics*, *43*(2), 364-369.

Yuhasz, M.S. (1967). Physical Fitness and Sports Appraisal, Laboratory Manual. University of Western Ontario.

Zatsiorsky, V., and Seluyanov, V. (1983). The mass and inertia characteristics of the main segments of the human body. *Biomechanics VIII-B*, *56*(2), 1152-1159.

- APPENDIX 1 -

INFORMED CONSENT FORMS

DATA ACQUISITION FOR THE ANALYSIS OF HUMAN MOVEMENTS

LAY SUMMARY

This study comprises a biomechanical analysis of human movement. This analysis requires kinematic (how you are moving) data of the bowling action and also a number of movements that determine the range of motion of the back and shoulders.

The data of actual human movements are required to give detailed information about the current techniques used. The data collected will then be used to understand and explain techniques currently used, determine the contributions of different techniques to performance and injury as well as to optimise performance.

The kinematic data will be obtained in a number of different ways:

- Video and cinematographic recordings.
- Automatic displacement acquisition system. This is similar to being videoed but reflective markers will be taped to you and only their image recorded.
- Joint angle measurements using a goniometer.

The subject-specific parameters may be obtained from:

- Anthropometric measurements. Measuring certain arm condition(s) (such as ‘straight’ and ‘fully flexed’) with the automatic motion capture or through the use of a goniometer.

Data will be acquired in the ECB National Cricket Centre at Loughborough University. The data collection session will last no longer than two hours, with the subject actively involved for only a fraction of the total time:

- Actual performance of movements: 30 minutes
- Anthropometric measurements: 30 minutes

The study in which you have been invited to participate will involve a biomechanical analysis of your bowling action. The study will involve you being videoed, using a number of different cameras, as you bowl and carry out a number of motions which give a measure of the range of motion of your back and shoulders.

It may be necessary to shave certain areas of your body to attach monitoring equipment using adhesive tape. The data collected will be used to help increase our understanding of the mechanics of human movements.

You will perform the data collection in a suitable environment. The risk of injury during the data collection will be minimal since we will only ask you to perform movements with which you are familiar and comfortable. It is considered that no increased risks, discomforts or distresses are likely to result from the data collection of human movements above those associated with the normal performance of those movements.

The information obtained from the study will be collected and stored in adherence with the Data Protection Act. Whilst certain personal and training information will be required, you will be allocated a reference number to ensure that your identity and personal details will remain confidential. Video recordings will be stored in the video analysis room to which access is restricted to members of the biomechanics research team. The video images will be digitised and only the numerical values will be used in published work, not the images themselves. On occasion video images may be required. In such and instance we will seek your written permission to use such images and you are perfectly free to decline. Video recordings will be kept for three years after publication of the study. If you agree to take part in the study, you are free to withdraw from the study at any stage, with or without having to give any reasons. A contact name and phone number will be provided to you for use if you have any queries about any part of your participation in the study.

PRE-SELECTION MEDICAL QUESTIONNAIRE

LOUGHBOROUGH UNIVERSITY
DEPARTMENT OF PHYSICAL EDUCATION, SPORTS SCIENCE AND RECREATION MANAGEMENT

Please read through this questionnaire, BUT DO NOT ANSWER ANY OF THE QUESTIONS YET. When you have read right through, there may be questions you would prefer not to answer. Assistance will be provided if you require it to discuss any questions on this form. In this case please tick the box labelled "I wish to withdraw" immediately below. Also tick the box labelled "I wish to withdraw" if there is any other reason for you not to take part.

	tick appropriate box
I wish to withdraw	☐
I am happy to answer the questionnaire	☐

If you are happy to answer the questions posed below, please proceed. Your answers will be treated in the strictest confidence.

1. Are you at present recovering from any illness or operation? YES/NO*

2. Are you suffering from or have you suffered from or received medical treatment for any of the following conditions?

   a. Heart or circulation condition
      YES/NO*

b. High blood pressure

YES/NO*

c. Any orthopaedic problems

YES/NO*

d. Any muscular problems

YES/NO*

e. Asthma or bronchial complaints

YES/NO*

3. Are you currently taking any medication that may affect your

YES/NO*

participation in the study?

4. Are you recovering from any injury?

YES/NO*

5. Are you epileptic?

YES/NO*

6. Are you diabetic?

YES/NO*

7. Are you allergic to sticking plasters?

YES/NO*

8. Do you have any other allergies? If yes, please give details below

YES/NO*

……

……..……

……..…

……

……..…

9. Are you aware of any other condition or complaint that may be affected by participation in this study? If so, please state below;

……

……

……

……

……

……

* Delete as appropriate

INFORMED CONSENT FORM (SUBJECTS)

PURPOSE

To obtain kinematic data during human movements

PROCEDURES

The kinematic data of human movements will be obtained using:

- Video and cinematographic recordings
- Automatic displacement acquisition system
- Joint angle measurements using a goniometer

ACTIVITIES

- Bowling
- Range of motion trials

A number of trials will be requested with suitable breaks to minimise fatigue and boredom.

During the measurements two researchers will be present, at least one of whom will be of the same sex as you.

QUESTIONS

The researchers will be pleased to answer any questions you may have at any time.

WITHDRAWAL

You are free to withdraw from the study at any stage, with or without having to give any reasons.

CONFIDENTIALITY

Your identity will remain confidential in any material resulting from this work. Video recordings will be stored in the video analysis room to which access is restricted to members of the biomechanics research team. The video images will be digitised and only the numerical values will be used in published work, not the images themselves. On occasion video images may be required. In such and instance we will seek your written permission to use such images and you are perfectly free to decline. Video recordings will be kept for three years after publication of the study.

I have read the outline of the procedures which are involved in this study, and I understand what will be required by me. I have had the opportunity to ask for further information and for clarification of the demands of each of the procedures and understand what is entailed. I am aware that I have the right to withdraw from the study at any time with no obligation to give reasons for my decision. As far as I am aware I do not have any injury or infirmity which would be affected by the procedures outlined.

Name ……

Signed …… (subject)

Date ……

In the presence of:

Name ……

- APPENDIX 2 -

ANTHROPOMETRIC MEASUREMENTS FOR SEGMENTAL INERTIA PARAMETERS

TORSO

Level	hip	umbilicus	ribcage	nipple	shoulder	neck	→	nose	ear	top
Length	0	157	237	459	628	650	0	82	130	259
Perimeter	939	846	842	974		383		466	570	
Width	342	304	301	324	370					
Depth					239					

LEFT ARM

Level	shoulder	midarm	elbow	forearm	wrist	→	thumb	knuckle	nails
Length	0		353	460	645	0	53	115	216
Perimeter	469	269	262	260	175		252	208	116
Width					74		119	95	54

RIGHT ARM

Level	shoulder	midarm	elbow	forearm	wrist	→	thumb	knuckle	nails
Length	0		358	455	655	0	44	100	196
Perimeter	500	287	271	260	175		252	214	125
Width					67		110	90	53

LEFT LEG

Level	hip	crotch	midthigh	knee	calf	ankle	→	heel	arch	ball	nails
Length	0	40		443	593	935	0	21		142	215
Perimeter		576	566	382	367	221		329	261	250	163
Width										128	101
Depth								72			

RIGHT LEG

Level	hip	crotch	midthigh	knee	calf	ankle	→	heel	arch	ball	nails
Length	0	70		462	644	933	0	24		139	210
Perimeter		580	545	367	373	232		320	270	251	160
Width										127	106
Depth								69			

Height (m) 1.935 Mass (Kg) 85.0

- APPENDIX 3 -

INERTIA PARAMETERS

The inertia parameters of the fast bowler calculated using Yeadon's inertia model (1990b):

Segment	Mass (kg)	Length (m)	COM (m)	Inertia (kg m^2)
Head	4.876	0.259	0.126	0.027
Trunk	37.465	0.650	0.343	1.490
Upper arm (bowling)	3.529	0.358	0.137	0.041
Lower arm (bowling)	1.410	0.297	0.125	0.010
Hand (bowling)	0.395	0.196	0.081	0.001
Upper arm (non-bowling)	3.090	0.353	0.137	0.035
Upper arm + hand (non-bowling)	1.610	0.508	0.163	0.024
Front thigh	10.637	0.443	0.196	0.175
Front Shank	4.580	0.492	0.203	0.085
Front foot	1.148	0.215	0.081	0.003
Front toes	0.228	0.073	0.030	0.0001
Back thigh	10.854	0.462	0.200	0.193
Back Shank	4.636	0.471	0.202	0.078
Back Foot	1.133	0.210	0.079	0.003
Back toes	0.209	0.071	0.030	0.0001

NOTE:

- Centre of mass location is given from the proximal joint centre.
- Moment of inertia is given about the transverse axis through the segment's mass centre.

- APPENDIX 4 -
RIGID AND WOBBLING
ELEMENT INERTIA PROPERTIES

In this appendix the methods used to redistribute the excess body fat mass around the body are described, as well as the method used to determine the centre of mass and moment of inertia of those segments comprising a rigid and wobbling element.

RIGID AND WOBBLING ELEMENT MASS

Method 1 – Re-distributing fat as muscle

Firstly, the ratio of segment fat to total body fat was calculated using the literature Clarys and Marfell-Jones (1986):

	Trunk	**Thigh**	**Shank**
Segment fat mass % (literature)	32.7	42.6	28.8
Body fat mass % (literature)	34.6	34.6	34.6
Ratio (segment fat to total body fat)	0.94	1.23	0.83

Using the body fat percentage of the fast bowler of 7.7%, calculated using the Yuhasz equation (Yuhasz, 1967), and multiplying by the ratio of segment fat to total body fat, the fat mass percentage of each segment can be calculated:

	Trunk	**Thigh**	**Shank**
Ratio (segment fat to total body fat)	0.94	1.23	0.83
Body fat mass % (subject)	7.7	7.7	7.7
Segment fat mass % (subject)	7.3	9.5	6.4

This allows the percentage of fat left to be redistributed as muscle to be calculated by subtracting fat mass of the subject from the expected fat mass according to the literature:

	Trunk	**Thigh**	**Shank**
Segment fat mass % (literature)	32.7	42.6	28.8
Segment fat mass % (subject)	7.3	9.5	6.4
% fat to be redistributed as muscle	25.4	33.1	22.4

The percentage mass of the wobbling element is then found by adding the percentage mass of the fat mass, the muscle mass and the newly redistributed muscle mass:

	Trunk	Thigh	Shank
Segment fat mass %	7.3	9.5	6.4
Segment muscle mass %	54.3	48.3	49.5
New muscle mass %	25.4	33.1	22.4
% mass of wobbling element	87.0	90.9	78.3

The mass of the rigid and wobbling element can then be calculated by multiplying the mass of the segments by the relevant percentage for each element:

	Trunk	L Thigh	L Shank	R Thigh	R Shank
Mass of Segment (kg)	37.4	10.6	4.7	10.9	4.6
Wobbling element mass %	87.0	91.0	78.3	91.0	78.3
Rigid element mass %	13.0	9.0	21.7	9.0	21.7
Wobbling element mass (kg)	32.6	9.7	3.6	9.9	3.6
Rigid element mass (kg)	4.9	1.0	1.0	1.0	1.0

Method 2 – Maintaining muscle to bone ratio

The percentage of the subject-specific fat free mass of each segment can be calculated by subtracting the mass of the fat in each segment from 100%:

	Trunk	Thigh	Shank
Segment fat mass % (subject)	7.3	9.5	6.4
Segment fat free mass % (subject)	92.7	90.5	93.6

The ratio of bone to fat free mass according to the literature can be calculated by dividing the percentage mass of the bone in each segment by the total fat free mass of each segment:

	Trunk	Thigh	Shank
Segment bone mass % (literature)	13.1	9.0	21.7
Segment muscle mass % (literature)	54.3	48.3	49.5
Segment fat free mass % (literature)	67.4	57.3	71.2
Ratio of bone to fat free mass (literature)	0.19	0.16	0.30

The ratio of bone in fat free mass is then used to calculate the percentage of fat free mass which is made up of bone for the subject by multiplying the ratio by the segment specific fat free mass percentage:

	Trunk	Thigh	Shank
Ratio of bone in fat free mass (literature)	0.19	0.16	0.30
Segment fat free mass % (subject)	92.7	90.5	93.6
Segment bone in fat free mass % (subject)	18.0	14.2	28.5

The subject-specific percentage of fat free mass made up of muscle for each segment can then be calculated by subtracting the subject-specific bone mass percentage from the total fat free percentage:

	Trunk	Thigh	Shank
% segment fat free mass (subject)	92.7	90.5	93.6
% segment fat free mass bone (subject)	18.0	14.2	28.5
% segment fat free mass muscle (subject)	74.7	76.3	65.1

The percentage mass of the wobbling element can be calculated by adding together the subject-specific muscle and fat percentage masses:

	Trunk	Thigh	Shank
% segment mass of fat (subject)	7.3	9.5	6.4
% segment mass of muscle (subject)	74.7	76.3	65.1
% wobbling element mass	82.0	85.8	71.5

The mass of the rigid and wobbling element for each segment can then be calculated using these percentages and the segment mass:

	Trunk	L Thigh	L Shank	R Thigh	R Shank
Mass of Segment (kg)	37.4	10.6	4.7	10.9	4.6
Wobbling element mass %	82.0	85.8	71.5	85.8	71.5
Rigid element mass %	18.0	14.2	28.5	14.2	28.5
Wobbling element mass (kg)	30.7	9.1	3.3	9.3	3.3
Rigid element mass (kg)	6.7	1.5	1.3	1.6	1.3

Averaging the two methods

The input to the simulation model was taken as an average of these two methods.

For the wobbling element:

	Trunk	**L Thigh**	**L Shank**	**R Thigh**	**R Shank**
Method 1 - Wobbling element mass (kg)	32.6	9.7	3.6	9.9	3.6
Method 2 - Wobbling element mass (kg)	30.7	9.1	3.3	9.3	3.3
Average wobbling element mass (kg)	31.6	9.4	3.4	9.6	3.5

For the rigid element:

	Trunk	L Thigh	L Shank	R Thigh	R Shank
Method 1 - Rigid element mass (kg)	4.9	1.0	1.0	1.0	1.0
Method 2 - Rigid element mass (kg)	6.7	1.5	1.3	1.6	1.3
Average rigid element mass (kg)	5.8	1.2	1.1	1.3	1.2

CENTRE OF MASS AND MOMENT OF INERTIA

Table 1 – Inertia properties for the segments modelled with wobbling masses

	Trunk	L Thigh	L Shank	R Thigh	R Shank
Segment length (m)	0.65	0.44	0.49	0.46	0.47
COM position of segment from proximal joint (m)	0.34	0.20	0.20	0.20	0.20
Whole segment MOI (kg.m^2)	1.49	0.18	0.08	0.19	0.08
Mass of Segment (kg)	37.7	10.6	4.6	10.9	4.6
Mass of wobbling element (kg)	31.6	9.4	3.4	9.6	3.5
Mass of rigid element (kg)	5.8	1.2	1.1	1.3	1.2
Bone density (kg/m^3)	1100	1218	1207.5	1218	1207.5

Modelling the rigid elements as cylinders of uniform density, where the mass and length of each segment is already known and the density is taken from the literature (Table 1), the centre of mass position coincides with the midpoint of each rigid element:

	Trunk	L Thigh	L Shank	R Thigh	R Shank
COM position of rigid element from proximal joint (m)	0.33	0.22	0.25	0.23	0.24

Using the equation for the volume of a cylinder with uniform density enables the radii of the rigid element to be calculated:

$$radius = \sqrt{\frac{mass}{\pi \cdot length \cdot density}} \quad (1)$$

	Trunk	L Thigh	L Shank	R Thigh	R Shank
Radius of the rigid element (m)	0.05	0.03	0.02	0.03	0.03

The equation for the moment of inertia about the transverse axis for a cylinder with uniform density can be then be used to find the moment of inertia of the rigid element:

$$MOI_{rig} = \frac{L^2 M}{12} + \frac{r^2 M}{4} \quad (2)$$

	Trunk	L Thigh	L Shank	R Thigh	R Shank
MOI of rigid element (kg.m^2)	0.21	0.02	0.02	0.02	0.02

Using the equation for moments about the proximal joint, the centre of mass position of the wobbling element can be determined:

$$M_{seg}gd_{seg} = M_{rig}gd_{rig} + M_{wob}gd_{wob} \quad (3)$$

	Trunk	L Thigh	L Shank	R Thigh	R Shank
COM position of wobbling element from proximal joint (m)	0.32	0.20	0.19	0.20	0.19

The moment of inertia of the wobbling element for each segment can be found using the parallel axis theorem:

$$I_o = I_g + Md^2 \quad (4)$$

where the moment of inertia of the whole segment is equal to the moment of inertia of the rigid element plus the moment of inertia of the wobbling element:

$$I_{gseg} + M_{seg}{d_{seg}}^2 = I_{grig} + M_{rig}{d_{rig}}^2 + I_{gwob} + M_{wob}{d_{wob}}^2 \quad (5)$$

which leads to:

	Trunk	L Thigh	L Shank	R Thigh	R Shank
MOI of wobbling element (kg.m^2)	1.26	0.15	0.06	0.17	0.05

- APPENDIX 5 -

TRUNK + HEAD

INERTIA PROPERTIES

In this appendix the process used to calculate the combined centre of mass position and moment of inertia of the trunk + head segment is described. The individual inertia properties of the rigid trunk segment and the head segment (Table 1) are used to calculate the combined rigid segment.

Table 1 – Inertia properties of the rigid trunk and head segments

	Mass of Segment (kg)	**Segment length (m)**	**COM position of segment from proximal joint (m)**	**Whole segment MOI ($kg.m^2$)**
Trunk (rigid element)	5.8	0.65	0.33	0.21
Head	4.9	0.26	0.13	0.03

MASS

The mass of the combined rigid element is simply the mass of the rigid element of the trunk plus the mass of the head segment:

$$M_{HT} = 5.8 + 4.9 = 10.7 \text{ kg} \quad (1)$$

CENTRE OF MASS

The centre of mass position from the proximal joint was found using the equation for moments about the proximal joint:

$$COM_{HT} = \frac{m_H d_H + m_T d_T}{m_{HT}} = \frac{4.9 \cdot (0.65 + 0.13) + 5.8 \cdot 0.33}{10.7} = 0.53\, m \quad (2)$$

MOMENT OF INERTIA

The moment of inertia of the combined segment is equal to the moment of inertia of the rigid trunk element plus the moment of inertia of the head segment:

$$I_{HT} + M_{HT} {d_{HT}}^2 = I_H + M_H {d_H}^2 + I_T + M_T {d_T}^2 \quad (3)$$

which rearranged to make the moment of inertia of the combined element the subject of the equation gives:

$$I_{HT} = I_H + M_H {d_H}^2 + I_T + M_T {d_T}^2 - M_{HT} {d_{HT}}^2 \quad (4)$$

substituting in the values gives the moment of inertia of the combined segment as:

$$I_{HT} = 0.03 + 4.9 \cdot (0.65 + 0.13)^2 + 0.21 + 5.8 \cdot 0.33^2 - 10.7 \cdot 0.53^2 = 0.78\ kg.m^2 \quad (5)$$

- APPENDIX 6 -

CALCULATING SERIES ELASTIC STIFFNESS

Determining series elastic component length:

Joint action	Muscle	α (°)	L_b (mm)	L_f (mm)	L_T (mm)	L_{SEC} (mm)	Scaled L_{SEC} (mm)
Dorsi Flexion	Tibialis Anterior	9	117	99	217	236	257
	Extensor digitrum longus	11	124	101	344	369	401
	Peroneus tertius	12	85	75	112	124	134
	Extensor halluces longus	7	111	92	248	268	291
Plantar Flexion	Gastrocnemius (lateral)	11	225	88	226	365	396
	Gastrocnemius (medial)	14	248	68	207	389	423
	Soleus	26	129	49	227	312	339
	Plantaris	4	90	73	359	376	409
	Flexor hallucis longus	17	211	55	261	419	456
	Flexor digitorum longus	11	140	48	311	404	439
	Tibialis posterior	17	162	43	252	373	405
	Peroneus longus	10	159	60	304	404	439
	Peroneus brevis	8	109	64	156	202	219
Knee Flexion	Biceps femoris (long head)	7	274	101	158	332	361
	Biceps femoris (short head)	15	152	146	96	107	116
	Semitendinosus	4	288	175	196	309	336
	Semimembranosus	15	304	79	116	344	374
	Gastrocnemius (lateral)	11	225	88	226	365	396
	Gastrocnemius (medial)	14	248	68	207	389	423
	Plantaris	4	90	73	359	376	409
	Gracillis	2	322	310	148	160	174
	Sartorius	0	430	430	108	108	117
Knee Extension	Vastus lateralis	11	273	110	138	303	329
	Vastus intermedius	6	320	106	87	302	328
	Vastus medialis	10	360	112	49	299	325
	Rectus femoris	10	302	88	186	401	436

Hip Flexion	Rectus femoris	10	302	88	186	401	436
	Tensor fasciae latae	2	313	139	204	378	411
	Sartorius	0	430	430	108	108	117
	Psoas major	5	238	190	54	103	112
Hip Extension	Gluteus maximus superficial	0	171	171	409	409	445
	Biceps femoris (long head)	7	274	101	158	332	361
	Semitendinosus	4	288	175	196	309	336
	Semimembranosus	15	304	79	116	344	374
	Adductor magnus posterior	3	242	194	81	129	141
Shoulder Flexion	Biceps (long head)	0	163	146	183	200	234
	Deltoid anterior	22	126	99	26	61	71
	Coracobrachialis	27	132	78	17	79	93
	Pectoralis major (ster.)	25	171	143	47	88	103
	Pectoralis major (clav.)	17	154	137	23	46	54
Shoulder Extension	Triceps (long head)	12	208	137	200	274	321
	Deltoid posterior	18	153	120	40	79	93
	Lattisimus dorsi (superior)	25	227	184	83	144	169
	Lattisimus dorsi (middle)	19	283	185	97	205	240
	Lattisimus dorsi (inferior)	21	316	244	80.3	169	198
Wrist Flexion	Flexor carpi radialis	3	164	51	198	310	310
	Flexor carpi ulnaris	12	228	42	206	393	393
Wrist Extension	Extensor carpi ulnaris	12	228	48	174	356	356
	Extensor carpi radialis brevis	9	127	50	146	223	223
	Extensor carpi radialis longus	1	94	77	162	179	179

Determining series elastic component stiffness:

Joint action	Muscle	Scaled (mm)	PCSA (mm^2)	K ($Nm\ rad^{-1}$)	K_{SEC} ($Nm\ rad^{-1}$)
Dorsi Flexion	Tibialis Anterior	45	2040	74	152
	Extensor digitrum longus	52	1050	31	
	Peroneus tertius	42	342	20	
	Extensor halluces longus	59	485	27	
Plantar Flexion	Gastrocnemius (lateral)	61	1990	65	643
	Gastrocnemius (medial)	61	4177	126	
	Soleus	61	11868	414	
	Plantaris	61	209	7	
	Flexor hallucis longus	36	1408	13	
	Flexor digitorum longus	28	991	6	
	Tibialis posterior	11	3622	3	
	Peroneus longus	17	2144	5	
	Peroneus brevis	13	1154	3	
Knee Flexion	Biceps femoris (long head)	42	2881	94	393
	Biceps femoris (short head)	41	1024	93	
	Semitendinosus	48	938	42	
	Semimembranosus	36	3988	86	
	Gastrocnemius (lateral)	31	1990	31	
	Gastrocnemius (medial)	21	4177	28	
	Plantaris	31	209	3	
	Gracillis	23	340	7	
	Sartorius	20	365	8	
Knee Extension	Vastus lateralis	43	6880	328	1008
	Vastus intermedius	46	5368	290	
	Vastus medialis	45	4674	244	
	Rectus femoris	48	3357	146	
Hip Flexion	Rectus femoris	52	3357	292	555
	Tensor fasciae latae	45	516	36	
	Sartorius	65	365	183	

	Psoas major	16	1383	44	
Hip Extension	Gluteus maximus superficial	55	2185	269	1386
	Biceps femoris (long head)	40	2881	235	
	Semitendinosus	44	938	100	
	Semimembranosus	33	3988	205	
	Adductor magnus posterior	52	1674	7	
Shoulder Flexion	Biceps (long head)	24	157	12	1346
	Deltoid anterior	42	546	4	
	Coracobrachialis	36	167	5	
	Pectoralis major (ster.)	62	568	5	
	Pectoralis major (clav.)	62	307	3	
Shoulder Extension	Triceps (long head)	49	360	16	1125
	Deltoid posterior	53	469	5	
	Lattisimus dorsi (superior)	117	211	8	
	Lattisimus dorsi (middle)	117	258	12	
	Lattisimus dorsi (inferior)	117	261	10	
Wrist Flexion	Flexor carpi radialis	17	199	16	37
	Flexor carpi ulnaris	17	342	21	
Wrist Extension	Extensor carpi ulnaris	9	260	2	25
	Extensor carpi radialis brevis	19	273	16	
	Extensor carpi radialis longus	16	146	7	

- APPENDIX 7 -
MODEL PARAMETER
SCORE COMPONENTS

The four components used in the score function were:

Force – S_1

The force component, S_1, was the average of the overall RMS difference in the horizontal (F_Y) and vertical (F_Z) forces expressed as a percentage of the peak vertical force:

$$S_1 = \frac{RMS_{FY} + RMS_{FZ}}{2} \tag{1}$$

where

$$RMS_{FY} = \sqrt{\sum_{t_{FFC}}^{t_{BR}} \frac{t_{BR} - t_{FFC}}{intstep} \cdot \left(\frac{SimFY_t - PerFY_t}{PerFZ_{PEAK}} \cdot 100\right)^2} \tag{2}$$

and

$$RMS_{FZ} = \sqrt{\sum_{t_{FFC}}^{t_{BR}} \frac{t_{BR} - t_{FFC}}{intstep} \cdot \left(\frac{SimFZ_t - PerFZ_t}{PerFZ_{PEAK}} \cdot 100\right)^2} \tag{3}$$

Centre of mass velocity at ball release – S_2

The centre of mass velocity component, S_2, consisted of two elements:

- the RMS difference of the horizontal COM velocity (V_{COMY}) at ball release expressed as a percentage of the overall COM velocity (V_{COM})
- the RMS difference of the vertical COM velocity (V_{COMZ}) at ball release expressed as a percentage of the overall COM velocity (V_{COM})

$$S_2 = RMS_{COMY} + RMS_{COMZ} \tag{4}$$

where

$$RMS_{COMY} = 100 \cdot \sqrt{\left(\frac{\sqrt{\left(SimV_{COMY_{BR}} - PerV_{COMY_{BR}}\right)^2}}{PerV_{COM_{BR}}} \right)^2} \tag{5}$$

and

$$RMS_{COMZ} = 100 \cdot \sqrt{\left(\frac{\sqrt{\left(SimV_{COMZ_{BR}} - PerV_{COMZ_{BR}}\right)^2}}{PerV_{COM_{BR}}} \right)^2} \tag{6}$$

Trunk orientation – S_3

The trunk orientation component, S_3, was the overall RMS difference in the trunk orientation angle (θ_T) in degrees:

$$S_3 = RMS_{\theta T} \tag{7}$$

where

$$RMS_{\theta T} = \sqrt{\sum_{t_{FFC}}^{t_{BR}} \frac{t_{BR} - t_{FFC}}{intstep} \cdot \left(Sim\theta_{T_t} - Per\theta_{T_t}\right)^2} \tag{8}$$

Ball velocity at ball release – S_4

The ball velocity component, S_4, consisted of two elements:

- the RMS difference of the horizontal ball velocity (V_{BALLY}) at ball release expressed as a percentage of the overall ball velocity (V_{BALL})
- the RMS difference of the vertical ball velocity (V_{BALLZ}) at ball release expressed as a percentage of the overall ball velocity (V_{BALL})

$$S_4 = RMS_{V_{BALLY}} + RMS_{V_{BALLZ}} \tag{9}$$

where

$$RMS_{V_{BALLY}} = 100 \cdot \sqrt{\left(\frac{\sqrt{\left(SimV_{BALLY_{BR}} - PerV_{BALLY_{BR}}\right)^2}}{PerV_{BALL_{BR}}} \right)^2} \tag{10}$$

and

$$RMS_{V_{BALLZ}} = 100 \cdot \sqrt{\left(\frac{\sqrt{\left(SimV_{BALLZ_{BR}} - PerV_{BALLZ_{BR}}\right)^2}}{PerV_{BALL_{BR}}} \right)^2} \tag{11}$$

- APPENDIX 8 -

VISCOELASTIC PARAMETERS

The viscoelastic parameters governing the foot-ground interface:

Parameter	Optimised value
K_{V1} (N/m)	32219
D_{V1} (N/m^2)	22692
K_{H1} (N/m)	14.66
D_{H1} (N/m^2)	0.179
K_{V2} (N/m)	30753
D_{V2} (N/m^2)	7979
K_{H2} (N/m)	15.52
D_{H2} (N/m^2)	0.088
K_{V3} (N/m)	48719
D_{V3} (N/m^2)	6079
K_{H3} (N/m)	16.73
D_{H3} (N/m^2)	0.102

Nomenclature: K – stiffness, D – damping, V – Vertical, H – Horizontal, 1- Toe, 2- MTP, 3 - Heel

The natural length of the vertical springs on the front foot:

Spring	Length (m)
Toe	0.028
MTP	0.060
Heel	0.062

The viscoelastic parameters governing the wobbling-rigid element interface:

Parameter	Optimised value
K_S (N/m)	1821
D_S (N/m^2)	1387
K_{TH} (N/m)	1645
D_{TH} (N/m^2)	675
K_{TR} (N/m)	3227
D_{TH} (N/m^2)	1000

Nomenclature: K – stiffness, D – damping, S - Shank, TH- Thigh, TR - Trunk

The position of the ball from the proximal end of the hand segment was found to be 0.152 m.

- APPENDIX 9 -

MODEL EVALUATION - INITIAL CONDITIONS

The initial conditions for the best trial used within the model evaluation are given below:

Initial Condition	Trial
Horizontal Front Toe Position (m)	0.826
Vertical Front Toe Position (m)	0.034
Horizontal COM velocity (ms^{-1})	5.18
Vertical COM velocity (ms^{-1})	1.42
Trunk orientation angle (°)	93.5
Trunk angular velocity (° s^{-1})	179
Front MTP angle (°)	0
Front MTP angular velocity (° s^{-1})	0
Front ankle angle (°)	-35.5
Front ankle angular velocity (° s^{-1})	126
Front knee angle (°)	10
Front knee angular velocity (° s^{-1})	-230
Front hip angle (°)	50.4
Front hip angular velocity (° s^{-1})	91
Back hip angle (°)	-242.4
Back hip angular velocity (° s^{-1})	-2.6
Front shoulder angle (°)	50.9
Front shoulder angular velocity (° s^{-1})	521
Bowling shoulder angle (°)	-200
Bowling shoulder angular velocity (° s^{-1})	232
Bowling elbow angle (°)	-1.63
Bowling elbow angular velocity (° s^{-1})	-28.9
Bowling wrist angle (°)	-27.3
Bowling wrist angular velocity (° s^{-1})	0

- APPENDIX 10 -
MODEL EVALUATION
SCORE COMPONENTS

The four components used in the score function were:

Force – S_1

The force component, S_1, was the average of the overall RMS difference in the horizontal (F_Y) and vertical (F_Z) forces expressed as a percentage of the peak vertical force:

$$S_1 = \frac{RMS_{FY} + RMS_{FZ}}{2} \tag{6.12}$$

where

$$RMS_{FY} = \sqrt{\sum_{t_{FFC}}^{t_{BR}} \frac{t_{BR} - t_{FFC}}{intstep} \cdot \left(\frac{SimFY_t - PerFY_t}{PerFZ_{PEAK}} \cdot 100\right)^2} \tag{6.13}$$

and

$$RMS_{FZ} = \sqrt{\sum_{t_{FFC}}^{t_{BR}} \frac{t_{BR} - t_{FFC}}{intstep} \cdot \left(\frac{SimFZ_t - PerFZ_t}{PerFZ_{PEAK}} \cdot 100\right)^2} \tag{6.14}$$

Centre of mass velocity at ball release – S_2

The centre of mass velocity component, S_2, consisted of two elements:

- the RMS difference of the horizontal COM velocity (V_{COMY}) at ball release expressed as a percentage of the overall COM velocity (V_{COM})
- the RMS difference of the vertical COM velocity (V_{COMZ}) at ball release expressed as a percentage of the overall COM velocity (V_{COM})

$$S_2 = RMS_{COMY} + RMS_{COMZ} \tag{6.15}$$

where

$$RMS_{COMY} = 100 \cdot \sqrt{\left(\frac{\sqrt{\left(SimV_{COMY_{BR}} - PerV_{COMY_{BR}}\right)^2}}{PerV_{COM_{BR}}} \right)^2} \tag{6.16}$$

and

$$RMS_{COMZ} = 100 \cdot \sqrt{\left(\frac{\sqrt{\left(SimV_{COMZ_{BR}} - PerV_{COMZ_{BR}}\right)^2}}{PerV_{COM_{BR}}} \right)^2} \tag{6.17}$$

Trunk orientation – S_3

The trunk orientation component, S_3, was the overall RMS difference in the trunk orientation angle (θ_T) in degrees:

$$S_3 = RMS_{\theta T} \tag{6.18}$$

where

$$RMS_{\theta T} = \sqrt{\sum_{t_{FFC}}^{t_{BR}} \frac{t_{BR} - t_{FFC}}{intstep} \cdot \left(Sim\theta_{T_t} - Per\theta_{T_t}\right)^2} \tag{6.19}$$

Ball velocity at ball release – S_4

The ball velocity component, S_4, consisted of two elements:

- the RMS difference of the horizontal ball velocity (V_{BALLY}) at ball release expressed as a percentage of the overall ball velocity (V_{BALL})
- the RMS difference of the vertical ball velocity (V_{BALLZ}) at ball release expressed as a percentage of the overall ball velocity (V_{BALL})

$$S_4 = RMS_{V_{BALLY}} + RMS_{V_{BALLZ}} \tag{6.20}$$

where

$$RMS_{V_{BALLY}} = 100 \cdot \sqrt{\left(\frac{\sqrt{\left(SimV_{BALLY_{BR}} - PerV_{BALLY_{BR}}\right)^2}}{PerV_{BALL_{BR}}}\right)^2} \tag{6.21}$$

and

$$RMS_{V_{BALLZ}} = 100 \cdot \sqrt{\left(\frac{\sqrt{\left(SimV_{BALLZ_{BR}} - PerV_{BALLZ_{BR}}\right)^2}}{PerV_{BALL_{BR}}}\right)^2} \tag{6.22}$$

Time – S_5

The time component, S_5, was the percentage difference between the simulation and recorded performance front foot contact phase time, $SimT$ and $PerT$, respectively:

$$S_5 = 100 \cdot \left(\frac{SimT - PerT}{PerT}\right) \tag{6.23}$$

RMS difference of the nine torque-driven joint angles – S_6

The joint angle component, S_6, was the RMS difference, $Tor\theta_i$ between the simulation, $Sim\theta_i$ and recorded performance, $Per\theta_i$ joint angles for the nine torque-driven joints in degrees:

$$S_6 = \sqrt{\frac{\sum_1^9 (Tor\theta_i)^2}{9}} \tag{6.24}$$

where

$$Tor\theta_i = \sqrt{\sum_{t_{FFC}}^{t_{BR}} \frac{t_{BR} - t_{FFC}}{intstep} \cdot (Sim\theta_i - Per\theta_i)^2} \tag{6.25}$$

- APPENDIX 11 -

MODEL EVALUATION PARAMETERS

Torque generator activation levels:

Joint action	A_0	A_1	TS_1	TR_1	A_2	TS_2	TR_2
Dorsi flexion	0.44	0.75	0.05	0.18	0.57	0.13	0.09
Plantar flexion	0.33	0.74	0.01	0.18	0.08	0.22	0.12
Knee flexion	0.40	0.55	0.07	0.25	0.71	0.24	0.22
Knee extension	0.50	0.38	-0.03	0.14	0.81	0.02	0.21
Front hip flexion	0.38	0.86	0.04	0.15	0.85	0.23	0.11
Front hip extension	0.34	0.47	-0.02	0.07	0.27	0.17	0.09
Back hip flexion	0.96	0.12	0.20	0.13	0.98	0.06	0.09
Back hip extension	0.12	0.83	0.23	0.12	0.43	0.01	0.21
Front shoulder flexion	0.66	0.06	0.24	0.17	0.17	0.23	0.21
Front shoulder extension	0.19	0.98	0.14	0.17	0.05	0.23	0.07
Bowling shoulder extension	0.29	0.98	-0.01	0.10	0.95	0.09	0.15
Bowling wrist flexion	0.07	0.74	0.03	0.12	0.33	0.07	0.23
Bowling wrist extension	0.58	0.61	0.01	0.15	0.32	0.10	0.08

Passive torque parameters:

Parameter	
Front MTP stiffness (Nm^{-1})	95868
Bowling elbow k_{es} ($N\ rad^{-1}$)	193
Bowling elbow k_{ed} ($N\ rad^{-2}$)	0.39
Bowling elbow p_1	20
Bowling elbow p_2	30
Bowling elbow p_3 (rad)	0.24
Bowling elbow $N\theta_E$ (rad)	0.03

Initial conditions:

Parameter	
Horizontal COM velocity (ms^{-1})	5.28
Vertical COM velocity (ms^{-1})	-1.41
Trunk orientation angle (°)	93.6
Trunk orientation angular velocity ($°s^{-1}$)	228
Front ankle angle (°)	-33.5
Front ankle angular velocity ($°s^{-1}$)	105
Front knee angle (°)	9.5
Front knee angular velocity ($°s^{-1}$)	-193
Front hip angle (°)	51
Front hip angular velocity ($°s^{-1}$)	140

- APPENDIX 12 -

AUTOLEV CODE

```
% Written by Paul Felton 2014 (C)
% A torque-driven model of fast bowling consisting of 14 rigid segments, 5
wobbling masses and 2 massless segments
% Torque generators drive, front ball, front ankle, front knee, hips,
shoulders, bowling elbow and bowling wrist
% Angle drive the back knee, ankle, ball, bowling elbow
% Function drive the pelvis hip and trunk length
% Function drive the pelvis and shoulder orientation
%-------------------------------------------------------------------------
-----------------------------------
%INTITIAL DECLARATIONS
%-------------------------------------------------------------------------
-----------------------------------
NEWTONIAN N %where n2 is up, n1 is right and n3 is n1 about n2
AUTOZ on %Simplifies the output equations
%-------------------------------------------------------------------------
-----------------------------------
%DEFINING RIGID SEGMENTS
%-------------------------------------------------------------------------
-----------------------------------
BODIES a %Front MTP
BODIES b %Front Foot
BODIES c %Front Shank
BODIES d %Front Leg
BODIES e %Trunk & Head
BODIES f %Front Upperarm
BODIES g %Front Forearm & Hand
BODIES h %Bowling Upperarm
BODIES i %Bowling Forearm
BODIES j %Bowling Hand
BODIES k %Back leg
BODIES l %Back shank
BODIES m %Back foot
BODIES x %Back toes
%-------------------------------------------------------------------------
-----------------------------------
%DEFINING MASSLESS SEGMENTS
%-------------------------------------------------------------------------
-----------------------------------
BODIES r %Hips
BODIES s %Shoulders
%-------------------------------------------------------------------------
-----------------------------------
%DEFINING WOBBLING MASS SEGMENTS
%-------------------------------------------------------------------------
-----------------------------------
BODIES wc %Front Shank
BODIES wd %Front Leg
BODIES wl %Back Shank
BODIES wk %Back Leg
BODIES we %Trunk
%-------------------------------------------------------------------------
-----------------------------------
%DEFINING POINTS
%-------------------------------------------------------------------------
-----------------------------------
points o %origin
points p1 %Front Toe
points p2 %Front MTP
points p3 %Front Ankle
points p4 %Front Heel
```

```
points p5 %Front Knee
points p6 %Front Hip
points p7 %Centre of Hips
points p8 %Back Hip
points p9 %Centre of Shoulders
points p10 %Top of Head
points p11 %Front Shoulder
points p12 %Front Elbow
points p13 %Front Hand
points p14 %Bowling Shoulder
points p15 %Bowling Elbow
points p16 %Bowling Wrist
points p17 %Bowling Hand
points p18 %Back Knee
points p19 %Back Ankle
points p20 %Back Heel
points p21 %Back Toe
points p22 %Back MTP

%wobbling mass points
points p{23:32}

points CM %Centre of Mass
%-------------------------------------------------------------------------------
-----------------------------------
%DEFINING THE BALL
%-------------------------------------------------------------------------------
-----------------------------------
particles ball
%-------------------------------------------------------------------------------
-----------------------------------
%DECLARE MASSES (rigid segments)
%-------------------------------------------------------------------------------
-----------------------------------
mass a=ma
mass b=mb
mass c=mc
mass d=md
mass e=me
mass f=mf
mass g=mg
mass h=mh
mass i=mi
mass j=mj
mass k=mk
mass l=ml
mass m=mm
mass x=mx
mass ball=mball
%-------------------------------------------------------------------------------
-----------------------------------
%DECLARE MASSES (wobbling segments)
%-------------------------------------------------------------------------------
-----------------------------------
mass wc=mwc
mass wd=mwd
mass wl=mwl
mass wk=mwk
mass we=mwe
%-------------------------------------------------------------------------------
-----------------------------------
%DECLARE MASSES (massless segments)
%-------------------------------------------------------------------------------
-----------------------------------
mass r=0
mass s=0
```

```
TotM = ma+mb+mc+md+me+mf+mg+mh+mi+mj+mk+ml+mm+mx+mwc+mwd+mwl+mwk+mwe+mball
%-------------------------------------------------------------------------------
-----------------------------------
%DECLARE INERTIAS (rigid segments)
%-------------------------------------------------------------------------------
-----------------------------------
Inertia a,0,0,ia
Inertia b,0,0,ib
Inertia c,0,0,ic
Inertia d,0,0,id
Inertia e,0,0,ie
Inertia f,0,0,if
Inertia g,0,0,ig
Inertia h,0,0,ih
Inertia i,0,0,ii
Inertia j,0,0,ij
Inertia k,0,0,ik
Inertia l,0,0,il
Inertia m,0,0,im
Inertia x,0,0,ix
%-------------------------------------------------------------------------------
-----------------------------------
%DECLARE INERTIAS (wobbling segments)
%-------------------------------------------------------------------------------
-----------------------------------
Inertia wc,0,0,iwc
Inertia wd,0,0,iwd
Inertia wl,0,0,iwl
Inertia wk,0,0,iwk
Inertia we,0,0,iwe
%-------------------------------------------------------------------------------
-----------------------------------
%DECLARE INERTIAS (massless segments)
%-------------------------------------------------------------------------------
-----------------------------------
Inertia r,0,0,0
Inertia s,0,0,0
%-------------------------------------------------------------------------------
-----------------------------------
%DEFINE LENGTHS & COM POSITIONS FROM THE DISTAL END (rigid segments)
%-------------------------------------------------------------------------------
-----------------------------------
constants la,lao
constants lb1,lb2,lbo1,lbo2 %length from MTP to HEEL AND ANKLE triangle
centre of mass position (vertical and horizontal)
constants lc,lco
constants ld,ldo
constants lf,lfo
constants lg,lgo
constants lh,lho
constants li,lio
constants lj,ljo
constants lk,lko
constants ll,llo
constants lm1,lm2, lmo1,lmo2 %length from MTP to HEEL AND ANKLE triangle
centre of mass position (vertical and horizontal)
constants lx,lxo
%-------------------------------------------------------------------------------
-----------------------------------
%DEFINE LENGTHS & COM POSITIONS FROM THE DISTAL END (wobbling segments)
%-------------------------------------------------------------------------------
-----------------------------------
constants lwc,lwco
constants lwd,lwdo
constants lwl,lwlo
```

```
constants lwk,lwko
% lwe,lweo %variable as the trunk can change length defined below
%-----------------------------------------------------------------------------
-----------------------------------
%DEFINE SPRING PARAMETERS (wobbling masses) - stiffness odd numbers, damping
even
%-----------------------------------------------------------------------------
-----------------------------------
constants k1,k2 %wc parameters
constants k3,k4 %wd parameters
constants k5,k6 %wl parameters
constants k7,k8 %wk parameters
constants k9,k10 %we parameters
%-----------------------------------------------------------------------------
-----------------------------------
%DEFINE SPRING PARAMETERS (Front foot) - stiffness odd numbers, damping even
%-----------------------------------------------------------------------------
-----------------------------------
constants k11,k12,k13,k14 %TOE parameters
constants k15,k16,k17,k18 %MTP parameters
constants k19,k20,k21,k22 %HEEL parameters
%-----------------------------------------------------------------------------
-----------------------------------
%DEFINE SPRING PARAMETERS (Back foot) - stiffness odd numbers, damping even
%-----------------------------------------------------------------------------
-----------------------------------
constants k23,k24,k25,k26 %TOE parameters
constants k27,k28,k29,k30 %MTP parameters
constants k31,k32,k33,k34 %HEEL parameters
%-----------------------------------------------------------------------------
-----------------------------------
%DEFINE SPRING PARAMETERS (Ball Release)
%-----------------------------------------------------------------------------
-----------------------------------
constants k35,k36,k37,k38 %Ball release parameters
%-----------------------------------------------------------------------------
-----------------------------------
%OTHERS
%-----------------------------------------------------------------------------
-----------------------------------
constants g %gravity
variables TotVF %Total Vertical Force (Front Foot)
variables TotHF %Total Horizontal Force (Front Foot)
variables TotVB %Total Vertical Force (Back Foot)
variables TotHB %Total Horizontal Force (Back Foot)
variables thetaB,thetaF %angle of front and back foot segment
variables q{29}',u{35}',q{30:35}
%-----------------------------------------------------------------------------
-----------------------------------
%SPECIFY THE TORQUES WHICH DRIVE THE MODEL (3rd Order (two derivatives which
are edited in Fortran Code))
%-----------------------------------------------------------------------------
-----------------------------------
SPECIFIED
FMTPTOR'',FANKTOR'',FKNETOR'',FHIPTOR'',BHIPTOR'',FSHOTOR'',BWRITOR'',BELBTOR
'',BSHOTOR''
FMTPTOR=T^3
FANKTOR=T^3
FKNETOR=T^3
FHIPTOR=T^3
BHIPTOR=T^3
FSHOTOR=T^3
BWRITOR=T^3
BELBTOR=T^3
BSHOTOR=T^3
```

```
%-----------------------------------------------------------------------------
-----------------------------------
%SPECIFY THE ANGLES TO DRIVE THE MODEL (3rd Order, which are edited in
Fortran Code)
%-----------------------------------------------------------------------------
-----------------------------------
SPECIFIED AXM'',AML'',ALK'',AGF''
AXM=T^3
AML=T^3
ALK=T^3
AGF=T^3
%-----------------------------------------------------------------------------
-----------------------------------
%FORM SEGMENT ORIENTATIONS (Whole Body Orientation)
%-----------------------------------------------------------------------------
-----------------------------------
simprot(n,e,3,q3) %orientation of the trunk in global reference frame
%-----------------------------------------------------------------------------
-----------------------------------
%SPECIFY THE FUNCTION TO DRIVE THE HIP AND PELVIS ANGLE (3rd Order, which are
edited in Fortran Code)
%-----------------------------------------------------------------------------
-----------------------------------
SPECIFIED ARE'',ASE''

ARE=-1.57+T^3
ASE=1.57+T^3
%-----------------------------------------------------------------------------
-----------------------------------
%SPECIFY THE VARIABLE LENGTHS
%-----------------------------------------------------------------------------
-----------------------------------
SPECIFIED lr'',ls'',le'',leo'',lweo'',lwe'',lsr''

CONSTANTS ple1,ple2,ple3,ple4,ple5,ple6,ple7,ple8,ple9,ple10

%length of rigid trunk and head
le=ple1+ple2*cos(ple10*q3)+ple3*sin(ple10*q3)+ple4*cos(2*ple10*q3)+ple5*sin(2
*ple10*q3)+ple6*cos(3*ple10*q3)+ple7*sin(3*ple10*q3)+ple8*cos(4*ple10*q3)+ple
9*sin(4*ple10*q3)

%distance between shoulder joint centres
ls=0.4+T^3

%distance between hip joint centres
lr=0.3+T^3

%centre of mass of rigid trunk and head
leo=0.5+T^3

%distance between hips and shoulder
lsr=0.5+T^3

%Trunk wobbling mass position
lweo=0.4+T^3

%length of wobbling trunk
lwe=0.5+T^3

%-----------------------------------------------------------------------------
-----------------------------------
%FORM TRIANGLE FEET SEGMENTS
%-----------------------------------------------------------------------------
-----------------------------------
frames tb,tf %Reference frame for triangular foot
simprot (b,tf,3,thetaF) %orientation of triangle in reference frame b
```

```
simprot (m,tb,3,thetaB) %orientation of triangle in reference frame m
%-------------------------------------------------------------------------------
-----------------------------------
%FORM SEGMENT ORIENTATIONS (Massless segments)
%-------------------------------------------------------------------------------
-----------------------------------
simprot(r,e,3,ARE) %orientation of the hips about the trunk
simprot(s,e,3,ASE) %orientation of the shoulders about the trunk
%-------------------------------------------------------------------------------
-----------------------------------
%FORM SEGMENT ORIENTATIONS (Rigid segments)
%-------------------------------------------------------------------------------
-----------------------------------
%Front Leg

simprot(a,b,3,q21) %orientation of the foot about the toe
simprot(b,c,3,q22) %orientation of the shank about the foot
simprot(c,d,3,q23) %orientation of the leg about the shank
simprot(d,r,3,q24) %orientation of the hips about the leg

%Back Leg
simprot(x,m,3,AXM) %orientation of the foot about the toe
simprot(m,l,3,AML) %orientation of the shank about the foot
simprot(l,k,3,ALK) %orientation of the leg about the shank
simprot(k,r,3,q25) %orientation of the hips about the leg

%Front Arm

simprot(g,f,3,AGF) %orientation of the forearm & hand about the arm
simprot(f,s,3,q26) %orientation of the arm about the shoulders

%Bowling Arm

simprot(j,i,3,q27) %orientation of the hand about the forearm
simprot(i,h,3,q28) %orientation of the forearm about the arm
simprot(h,s,3,q29) %orientation of the arm about the shoulder

%-------------------------------------------------------------------------------
-----------------------------------
%FORM SEGMENT ORIENTATIONS (Wobbling segments)
%-------------------------------------------------------------------------------
-----------------------------------

simprot(c,wc,3,q4) %orientation of the front shank wobbling mass
simprot(d,wd,3,q7) %orientation of the front leg wobbling mass
simprot(e,we,3,q10) %orientation of the trunk wobbling mass
simprot(k,wk,3,q13) %orientation of the back leg wobbling mass
simprot(l,wl,3,q16) %orientation of the back shank wobbling mass

%-------------------------------------------------------------------------------
-----------------------------------
%POSITION VECTORS (Rigid and massless segments)
%-------------------------------------------------------------------------------
-----------------------------------

P_O_P1> = q1*N1>+q2*N2> %position from the origin to the front toe (where q1
and q2 are the coordinates (q2,q1)


P_P1_P2> = la*A1> %Position of of MTP (Front leg)
P_P2_P3> = lb1*B1> %Position of the ankle (Front leg)
P_P2_P4> = lb2*tf1> %Position of the heel (Front leg)
P_P3_P5> = lc*C1> %Position of the Knee (Front leg)
P_P5_P6> = ld*D1> %Position of the Hip Joint Centre (Front leg)
P_P6_P7> = 0.5*lr*R1> %Mid point of the hip joint centres
P_P6_P8> = lr*R1> %Position of the Hip Joint Centre (Back leg)
```

```
P_P18_P8> = lk*K1> %Position of the Hip Joint Centre (Back leg)
P_P19_P18> = ll*L1> %Position of the Knee (Back leg)
P_P22_P21> = lx*X1> %Position of of MTP (Back leg)
P_P21_P20> = lm2*tb1> %Position of the heel (Back leg)
P_P21_P19> = lm1*M1> %Position of the ankle (Back leg)

P_P7_P9> = lsr*E1> %Position of Shoulder Joint Centre
P_P7_P10> = le*E1> %Position of Head
P_P9_P11> = 0.5*ls*S1> %Position of Front Shoulder
P_P11_P12> = lf*F1> % Position of Front Elbow
P_P12_P13> = lg*G1> %Position of Front Hand
P_P9_P14> = -0.5*ls*S1> %Position of Bowling Shoulder
P_P14_P15> = lh*H1> %Position of Bowling elbow
P_P15_P16> = li*I1> %Position of Bowling wrist
P_P16_P17> = lj*J1> %Position of Bowling hand

P_P17_ball> = q19*J1>+q20*J2> %Position of the ball

P_P1_AO> = lao*A1> %Centre of mass position of toes (Front leg)
P_P2_BO> = lbo2*tf1>-lbo1*tf2> %Centre of mass position of the triangle foot
segment (Front leg)
P_P3_CO> = lco*C1> %Centre of mass position of the shank (Front leg)
P_P5_DO> = ldo*D1> %Centre of mass position of the leg (Front leg)
P_P7_EO> = (le-leo)*E1> %Centre of mass position of the trunk and head
P_P12_FO> = -lfo*F1> %Centre of mass position of the front upperarm
P_P13_GO> = -lgo*G1> %Centre of mass position of the front forearm and hand
P_P15_HO> = -lho*H1> %Centre of mass position of the bowling upperarm
P_P16_IO> = -lio*I1> %Centre of mass position of the bowling forearm
P_P17_JO> = -ljo*J1> % Centre of mass position of the bowling hand
P_P18_KO> = lko*K1> %Centre of mass position of the leg (Back leg)
P_P19_LO> = llo*L1> %Centre of mass position of the shank (Back leg)
P_P21_MO> = lmo2*tb1>-lmo1*tb2> %Centre of mass position of the triangle foot
segment (Back leg)
P_P22_XO> = lxo*X1> %Centre of mass position of toes (Back leg)

%-------------------------------------------------------------------------------
-----------------------------------
%POSITION VECTORS (wobbling segments)
%-------------------------------------------------------------------------------
-----------------------------------

P_P3_P23> = q5*C1>+q6*C2>
P_P23_wco> = lwco*wc1>
P_P23_P24> = lwc*wc1>

P_P5_P25> = q8*D1>+q9*D2>
P_P25_wdo> = lwdo*wd1>
P_P25_P26> = lwd*wd1>

P_P19_P27> = q17*L1>+q18*L2>
P_P27_wlo> = lwlo*wl1>
P_P27_P28> = lwl*wl1>

P_P18_P29> = q14*K1>+q15*K2>
P_P29_wko> = lwko*wk1>
P_P29_P30> = lwk*wk1>

P_P7_P31> = q11*E1>+q12*E2>
P_P31_weo> = lweo*we1>
P_P31_P32> = lwe*we1>

%-------------------------------------------------------------------------------
-----------------------------------
%POSITION OF POINTS RELATIVE TO O
%-------------------------------------------------------------------------------
-----------------------------------
```

```
P_O_AO> = P_O_P1>+P_P1_AO>
P_O_P2> = P_O_P1>+P_P1_P2>
P_O_BO> = P_O_P2>+P_P2_BO>
P_O_P3> = P_O_P2>+P_P2_P3>
P_O_P4> = P_O_P2>+P_P2_P4>
P_O_CO> = P_O_P3>+P_P3_CO>
P_O_P5> = P_O_P3>+P_P3_P5>
P_O_DO> = P_O_P5>+P_P5_DO>
P_O_P6> = P_O_P5>+P_P5_P6>

P_O_P7> = P_O_P6>+P_P6_P7>
P_O_P8> = P_O_P6>+P_P6_P8>
P_O_P9> = P_O_P7>+P_P7_P9>

P_O_P10> = P_O_P7>+P_P7_P10>
P_O_EO> = P_O_P7>+P_P7_EO>

P_O_P11> = P_O_P9>+P_P9_P11>
P_O_P12> = P_O_P11>+P_P11_P12>
P_O_FO> = P_O_P11>+P_P11_FO>
P_O_P13> = P_O_P12>+P_P12_P13>
P_O_GO> = P_O_P12>+P_P12_GO>
P_O_P14> = P_O_P9>+P_P9_P14>
P_O_HO> = P_O_P14>+P_P14_HO>
P_O_P15> = P_O_P14>+P_P14_P15>

P_O_P16> = P_O_P15>+P_P15_P16>
P_O_IO> = P_O_P15>+P_P15_IO>
P_O_P17> = P_O_P16>+P_P16_P17>
P_O_JO> = P_O_P16>+P_P16_JO>
P_O_ball> = P_O_P17>+P_P17_ball>

P_O_P18> = P_O_P8>+P_P8_P18>
P_O_KO> = P_O_P18>+P_P18_KO>
P_O_P19> = P_O_P18>+P_P18_P19>
P_O_LO> = P_O_P19>+P_P19_LO>
P_O_P20> = P_O_P19>+P_P19_P20>
P_O_P21> = P_O_P20>+P_P20_P21>
P_O_MO> = P_O_P21> +P_P21_MO>
P_O_P22> = P_O_P21> + P_P21_P22>
P_O_XO> = P_O_P22>+ P_P22_XO>

P_O_P23> = P_O_P3>+P_P3_P23>
P_O_WCO> = P_O_P23>+P_P23_WCO>
P_O_P24> = P_O_P23>+P_P23_P24>

P_O_P25> = P_O_P5>+P_P5_P25>
P_O_WDO> = P_O_P25>+P_P25_WDO>
P_O_P26> = P_O_P25>+P_P25_P26>

P_O_P27> = P_O_P19>+P_P19_P27>
P_O_WLO> = P_O_P27>+P_P27_WLO>
P_O_P28> = P_O_P27>+P_P27_P28>

P_O_P29> = P_O_P18>+P_P18_P29>
P_O_WKO> = P_O_P29>+P_P29_WKO>
P_O_P30> = P_O_P29>+P_P29_P30>

P_O_P31> = P_O_P7>+P_P7_P31>
P_O_WEO> = P_O_P31>+P_P31_WEO>
P_O_P32> = P_O_P31>+P_P31_P32>

%-------------------------------------------------------------------------
-----------------------------------
%POSITION OF POINTS IN THE X-Y PLANE
```

```
%-------------------------------------------------------------------------
-----------------------------------

POP1X=DOT(P_O_P1>, N1>)
POP1Y=DOT(P_O_P1>, N2>)
POP2X=DOT(P_O_P2>, N1>)
POP2Y=DOT(P_O_P2>, N2>)
POP3X=DOT(P_O_P3>, N1>)
POP3Y=DOT(P_O_P3>, N2>)
POP4X=DOT(P_O_P4>, N1>)
POP4Y=DOT(P_O_P4>, N2>)
POP5X=DOT(P_O_P5>, N1>)
POP5Y=DOT(P_O_P5>, N2>)
POP6X=DOT(P_O_P6>, N1>)
POP6Y=DOT(P_O_P6>, N2>)
POP7X=DOT(P_O_P7>, N1>)
POP7Y=DOT(P_O_P7>, N2>)
POP8X=DOT(P_O_P8>, N1>)
POP8Y=DOT(P_O_P8>, N2>)
POP9X=DOT(P_O_P9>, N1>)
POP9Y=DOT(P_O_P9>, N2>)
POP10X=DOT(P_O_P10>, N1>)
POP10Y=DOT(P_O_P10>, N2>)
POP11X=DOT(P_O_P11>, N1>)
POP11Y=DOT(P_O_P11>, N2>)
POP12X=DOT(P_O_P12>, N1>)
POP12Y=DOT(P_O_P12>, N2>)
POP13X=DOT(P_O_P13>, N1>)
POP13Y=DOT(P_O_P13>, N2>)
POP14X=DOT(P_O_P14>, N1>)
POP14Y=DOT(P_O_P14>, N2>)
POP15X=DOT(P_O_P15>, N1>)
POP15Y=DOT(P_O_P15>, N2>)
POP16X=DOT(P_O_P16>, N1>)
POP16Y=DOT(P_O_P16>, N2>)
POP17X=DOT(P_O_P17>, N1>)
POP17Y=DOT(P_O_P17>, N2>)
POP18X=DOT(P_O_P18>, N1>)
POP18Y=DOT(P_O_P18>, N2>)
POP19X=DOT(P_O_P19>, N1>)
POP19Y=DOT(P_O_P19>, N2>)
POP20X=DOT(P_O_P20>, N1>)
POP20Y=DOT(P_O_P20>, N2>)
POP21X=DOT(P_O_P21>, N1>)
POP21Y=DOT(P_O_P21>, N2>)
POP22X=DOT(P_O_P22>, N1>)
POP22Y=DOT(P_O_P22>, N2>)

POP23X=DOT(P_O_P23>, N1>)
POP23Y=DOT(P_O_P23>, N2>)
POP24X=DOT(P_O_P24>, N1>)
POP24Y=DOT(P_O_P24>, N2>)
POP25X=DOT(P_O_P25>, N1>)
POP25Y=DOT(P_O_P25>, N2>)
POP26X=DOT(P_O_P26>, N1>)
POP26Y=DOT(P_O_P26>, N2>)
POP27X=DOT(P_O_P27>, N1>)
POP27Y=DOT(P_O_P27>, N2>)
POP28X=DOT(P_O_P28>, N1>)
POP28Y=DOT(P_O_P28>, N2>)
POP29X=DOT(P_O_P29>, N1>)
POP29Y=DOT(P_O_P29>, N2>)
POP30X=DOT(P_O_P30>, N1>)
POP30Y=DOT(P_O_P30>, N2>)
POP31X=DOT(P_O_P31>, N1>)
POP31Y=DOT(P_O_P31>, N2>)
```

```
POP32X=DOT(P_O_P32>, N1>)
POP32Y=DOT(P_O_P32>, N2>)

POBALLX=DOT(P_O_BALL>, N1>)
POBALLY=DOT(P_O_BALL>, N2>)

POAOX=DOT(P_O_AO>, N1>)
POAOY=DOT(P_O_AO>, N2>)
POBOX=DOT(P_O_BO>, N1>)
POBOY=DOT(P_O_BO>, N2>)
POCOX=DOT(P_O_CO>, N1>)
POCOY=DOT(P_O_CO>, N2>)
PODOX=DOT(P_O_DO>, N1>)
PODOY=DOT(P_O_DO>, N2>)
POEOX=DOT(P_O_EO>, N1>)
POEOY=DOT(P_O_EO>, N2>)
POFOX=DOT(P_O_FO>, N1>)
POFOY=DOT(P_O_FO>, N2>)
POGOX=DOT(P_O_GO>, N1>)
POGOY=DOT(P_O_GO>, N2>)
POHOX=DOT(P_O_HO>, N1>)
POHOY=DOT(P_O_HO>, N2>)
POIOX=DOT(P_O_IO>, N1>)
POIOY=DOT(P_O_IO>, N2>)
POJOX=DOT(P_O_JO>, N1>)
POJOY=DOT(P_O_JO>, N2>)
POKOX=DOT(P_O_KO>, N1>)
POKOY=DOT(P_O_KO>, N2>)
POLOX=DOT(P_O_LO>, N1>)
POLOY=DOT(P_O_LO>, N2>)
POMOX=DOT(P_O_MO>, N1>)
POMOY=DOT(P_O_MO>, N2>)
POXOX=DOT(P_O_XO>, N1>)
POXOY=DOT(P_O_XO>, N2>)


POWCOX=DOT(P_O_WCO>, N1>)
POWCOY=DOT(P_O_WCO>, N2>)
POWDOX=DOT(P_O_WDO>, N1>)
POWDOY=DOT(P_O_WDO>, N2>)
POWEOX=DOT(P_O_WEO>, N1>)
POWEOY=DOT(P_O_WEO>, N2>)
POWKOX=DOT(P_O_WKO>, N1>)
POWKOY=DOT(P_O_WKO>, N2>)
POWLOX=DOT(P_O_WLO>, N1>)
POWLOY=DOT(P_O_WLO>, N2>)
%-------------------------------------------------------------------------------
-----------------------------------
%CENTRE OF MASS OF THE BODY
%-------------------------------------------------------------------------------
-----------------------------------

P_O_CM>=CM(O)
POCMX=DOT(P_O_CM>,N1>)
POCMY=DOT(P_O_CM>,N2>)

%-------------------------------------------------------------------------------
-----------------------------------
%KINEMATICAL DIFFERENTIAL EQUATIONS
%-------------------------------------------------------------------------------
-----------------------------------

Q1'= U1
Q2'= U2
Q3'= U3
Q4'= U4
```

```
Q5'= U5
Q6'= U6
Q7'= U7
Q8'= U8
Q9'= U9
Q10'= U10
Q11'= U11
Q12'= U12
Q13'= U13
Q14'= U14
Q15'= U15
Q16'= U16
Q17'= U17
Q18'= U18
Q19'= U19
Q20'= U20
Q21'= U21
Q22'= U22
Q23'= U23
Q24'= U24
Q25'= U25
Q26'= U26
Q27'= U27
Q28'= U28
Q29'= U29

%JOINT ANGLES
%-------------------------------------------------------------------------------
-----------------------------------

FMTPANG=q21
FANKANG=q22
FKNEANG=q23
FHIPANG=q24

BMTPANG=AXM
BANKANG=AML
BKNEANG=ALK
BHIPANG=q25

TORANG=ARE
SHOANG=ASE

FSHOANG=q26
FELBANG=AGF

BSHOANG=q29
BELBANG=q28
BWRIANG=q27

%-------------------------------------------------------------------------------
-----------------------------------
%JOINT ANGULAR VELOCITIES
%-------------------------------------------------------------------------------
-----------------------------------

FMTPW=u21
FANKW=u22
FKNEW=u23
FHIPW=u24

BMTPW=DT(BMTPANG,N)
BANKW=DT(BANKANG,N)
BKNEW=DT(BKNEANG,N)
BHIPW=u25
```

```
TORW=DT(TORANG,N)
SHOW=DT(SHOANG,N)

FSHOW=u26
FELBW=DT(FELBANG,N)

BSHOW=u29
BELBW=u28
BWRIW=u27

%-------------------------------------------------------------------------------
-----------------------------------
%ANGULAR VELOCITIES
%USE GENERALISED SPEEDS TO CALCULATE JOINT TORQUE MEASURES
%-------------------------------------------------------------------------------
-----------------------------------

W_E_N> = q3'*E3> %Angular velocity of the trunk in the GCS

W_B_A>=u21*B3> %Front toes about foot
W_C_B>=u22*C3> %Front foot about the shank
W_D_C>=u23*D3> %Front Shank about the leg
W_R_D>=u24*R3> %Front leg about the hip segment
W_M_X>=AXM'*M3>+U30*M3> %Back toes about the foot
W_L_M>=AML'*L3>+U31*L3> %Back Foot about the shank
W_K_L>=ALK'*K3>+U32*K3> %Back Shank about the leg
W_R_K>=u25*R3> %Back leg about the hip segment
W_F_G>=AGF'*F3>+U33*F3> %Front forearm about the upperarm
W_S_F>=u26*S3> %Front upperarm about the shoulder segment
W_I_J>=u27*I3> %Bowling Hand about the forearm
W_H_I>=u28*H3> %Bowling forearm about upperarm
W_S_H>=u29*S3> %Upper arm about the shoulder segment
W_E_R>=ARE'*E3>+U34*E3> %Hip segment about the trunk
W_E_S>=ASE'*E3>+U35*E3> %Shoulder segment about the trunk

W_WC_C>=q4'*WC3> %Wobbling masses
W_WD_D>=q7'*WD3>
W_WE_E>=q10'*WE3>
W_WK_K>=q13'*WK3>
W_WL_L>=q16'*WL3>

W_TF_B> = 0> %Triangle reference frame Front foot
W_TB_M> = 0> %Triangle reference frame Back foot

%-------------------------------------------------------------------------------
-----------------------------------
%ANGULAR ACCELERATIONS
%-------------------------------------------------------------------------------
-----------------------------------

ALF_E_N> = DT(W_E_N>,E)

ALF_B_A> = DT(W_B_A>,B)
ALF_C_B> = DT(W_C_B>,C)
ALF_D_C> = DT(W_D_C>,D)
ALF_R_D> = DT(W_R_D>,R)
ALF_M_X> = DT(W_M_X>,M)
ALF_L_M> = DT(W_L_M>,L)
ALF_K_L> = DT(W_K_L>,K)
ALF_R_K> = DT(W_R_K>,R)
ALF_F_G> = DT(W_F_G>,F)
ALF_S_F> = DT(W_S_F>,S)
ALF_I_J> = DT(W_I_J>,I)
ALF_H_I> = DT(W_H_I>,H)
ALF_S_H> = DT(W_S_H>,S)
```

```
ALF_E_R> = DT(W_E_R>,E)
ALF_E_S> = DT(W_E_S>,E)

ALF_WC_C> = DT(W_WC_C>,WC)
ALF_WD_D> = DT(W_WD_D>,WD)
ALF_WE_E> = DT(W_WE_E>,WE)
ALF_WK_K> = DT(W_WK_K>,WK)
ALF_WL_L> = DT(W_WL_L>,WL)

ALF_TF_B> =0>
ALF_TB_M>=0>
%-------------------------------------------------------------------------------
-----------------------------------
%LINEAR VELOCITIES
%-------------------------------------------------------------------------------
-----------------------------------

V_O_N> = 0>
V_P1_N> = DT(P_O_P1>,N)
V_P2_N> = DT(P_O_P2>,N)
V_P3_N> = DT(P_O_P3>,N)
V_P4_N> = DT(P_O_P4>,N)
V_P5_N> = DT(P_O_P5>,N)
V_P6_N> = DT(P_O_P6>,N)
V_P7_N> = DT(P_O_P7>,N)
V_P8_N> = DT(P_O_P8>,N)
V_P9_N> = DT(P_O_P9>,N)
V_P10_N> = DT(P_O_P10>,N)
V_P11_N> = DT(P_O_P11>,N)
V_P12_N> = DT(P_O_P12>,N)
V_P13_N> = DT(P_O_P13>,N)
V_P14_N> = DT(P_O_P14>,N)
V_P15_N> = DT(P_O_P15>,N)
V_P16_N> = DT(P_O_P16>,N)
V_P17_N> = DT(P_O_P17>,N)
V_P18_N> = DT(P_O_P18>,N)
V_P19_N> = DT(P_O_P19>,N)
V_P20_N> = DT(P_O_P20>,N)
V_P21_N> = DT(P_O_P21>,N)
V_P22_N> = DT(P_O_P22>,N)
V_P23_N> = DT(P_O_P23>,N)
V_P24_N> = DT(P_O_P24>,N)
V_P25_N> = DT(P_O_P25>,N)
V_P26_N> = DT(P_O_P26>,N)
V_P27_N> = DT(P_O_P27>,N)
V_P28_N> = DT(P_O_P28>,N)
V_P29_N> = DT(P_O_P29>,N)
V_P30_N> = DT(P_O_P30>,N)
V_P31_N> = DT(P_O_P31>,N)
V_P32_N> = DT(P_O_P32>,N)

v2pts(n,a,p1,ao)
v2pts(n,b,p2,bo)
v2pts(n,c,p3,co)
v2pts(n,d,p5,do)
v2pts(n,e,p7,eo)
v2pts(n,f,p11,fo)
v2pts(n,g,p12,go)
v2pts(n,h,p14,ho)
v2pts(n,i,p15,io)
v2pts(n,j,p16,jo)
v2pts(n,k,p18,ko)
v2pts(n,l,p19,lo)
v2pts(n,m,p21,mo)
v2pts(n,x,p22,xo)
```

```
V_BALL_N>=DT(P_O_BALL>,N)

V2PTS(N,WC,P23,WCO)
V2PTS(N,WD,P25,WDO)
V2PTS(N,WE,P31,WEO)
V2PTS(N,WK,P29,WKO)
V2PTS(N,WL,P27,WLO)

%-------------------------------------------------------------------------------
-----------------------------------
%CENTRE OF MASS VELOCITIES
%-------------------------------------------------------------------------------
-----------------------------------

V_CM_N> = DT(P_O_CM>,N)
VOCMX=DOT(V_CM_N>,N1>)
VOCMY=DOT(V_CM_N>,N2>)

%-------------------------------------------------------------------------------
-----------------------------------
%VELOCITY OF POINTS IN THE X-Y PLANE
%-------------------------------------------------------------------------------
-----------------------------------

VOP1X=DOT(V_P1_N>,N1>)
VOP1Y=DOT(V_P1_N>,N2>)
VOP2X=DOT(V_P2_N>,N1>)
VOP2Y=DOT(V_P2_N>,N2>)
VOP3X=DOT(V_P3_N>,N1>)
VOP3Y=DOT(V_P3_N>,N2>)
VOP4X=DOT(V_P4_N>,N1>)
VOP4Y=DOT(V_P4_N>,N2>)
VOP5X=DOT(V_P5_N>,N1>)
VOP5Y=DOT(V_P5_N>,N2>)
VOP6X=DOT(V_P6_N>,N1>)
VOP6Y=DOT(V_P6_N>,N2>)
VOP7X=DOT(V_P7_N>,N1>)
VOP7Y=DOT(V_P7_N>,N2>)
VOP8X=DOT(V_P8_N>,N1>)
VOP8Y=DOT(V_P8_N>,N2>)
VOP9X=DOT(V_P9_N>,N1>)
VOP9Y=DOT(V_P9_N>,N2>)
VOP10X=DOT(V_P10_N>,N1>)
VOP10Y=DOT(V_P10_N>,N2>)
VOP11X=DOT(V_P11_N>,N1>)
VOP11Y=DOT(V_P11_N>,N2>)
VOP12X=DOT(V_P12_N>,N1>)
VOP12Y=DOT(V_P12_N>,N2>)
VOP13X=DOT(V_P13_N>,N1>)
VOP13Y=DOT(V_P13_N>,N2>)
VOP14X=DOT(V_P14_N>,N1>)
VOP14Y=DOT(V_P14_N>,N2>)
VOP15X=DOT(V_P15_N>,N1>)
VOP15Y=DOT(V_P15_N>,N2>)
VOP16X=DOT(V_P16_N>,N1>)
VOP16Y=DOT(V_P16_N>,N2>)
VOP17X=DOT(V_P17_N>,N1>)
VOP17Y=DOT(V_P17_N>,N2>)
VOP18X=DOT(V_P18_N>,N1>)
VOP18Y=DOT(V_P18_N>,N2>)
VOP19X=DOT(V_P19_N>,N1>)
VOP19Y=DOT(V_P19_N>,N2>)
VOP20X=DOT(V_P20_N>,N1>)
VOP20Y=DOT(V_P20_N>,N2>)
VOP21X=DOT(V_P21_N>,N1>)
VOP21Y=DOT(V_P21_N>,N2>)
```

```
VOP22X=DOT(V_P22_N>,N1>)
VOP22Y=DOT(V_P22_N>,N2>)
VOP23X=DOT(V_P23_N>,N1>)
VOP23Y=DOT(V_P23_N>,N2>)
VOP24X=DOT(V_P24_N>,N1>)
VOP24Y=DOT(V_P24_N>,N2>)
VOP25X=DOT(V_P25_N>,N1>)
VOP25Y=DOT(V_P25_N>,N2>)
VOP26X=DOT(V_P26_N>,N1>)
VOP26Y=DOT(V_P26_N>,N2>)
VOP27X=DOT(V_P27_N>,N1>)
VOP27Y=DOT(V_P27_N>,N2>)
VOP28X=DOT(V_P28_N>,N1>)
VOP28Y=DOT(V_P28_N>,N2>)
VOP29X=DOT(V_P29_N>,N1>)
VOP29Y=DOT(V_P29_N>,N2>)
VOP30X=DOT(V_P30_N>,N1>)
VOP30Y=DOT(V_P30_N>,N2>)
VOP31X=DOT(V_P31_N>,N1>)
VOP31Y=DOT(V_P31_N>,N2>)
VOP32X=DOT(V_P32_N>,N1>)
VOP32Y=DOT(V_P32_N>,N2>)

VOBALLX=DOT(V_BALL_N>,N1>)
VOBALLY=DOT(V_BALL_N>,N2>)

VOBALL=SQRT(VOBALLX^2+VOBALLY^2)

VOAOX=DOT(V_AO_N>,N1>)
VOAOY=DOT(V_AO_N>,N2>)
VOBOX=DOT(V_BO_N>,N1>)
VOBOY=DOT(V_BO_N>,N2>)
VOCOX=DOT(V_CO_N>,N1>)
VOCOY=DOT(V_CO_N>,N2>)
VODOX=DOT(V_DO_N>,N1>)
VODOY=DOT(V_DO_N>,N2>)
VOEOX=DOT(V_EO_N>,N1>)
VOEOY=DOT(V_EO_N>,N2>)
VOFOX=DOT(V_FO_N>,N1>)
VOFOY=DOT(V_FO_N>,N2>)
VOGOX=DOT(V_GO_N>,N1>)
VOGOY=DOT(V_GO_N>,N2>)
VOHOX=DOT(V_HO_N>,N1>)
VOHOY=DOT(V_HO_N>,N2>)
VOIOX=DOT(V_IO_N>,N1>)
VOIOY=DOT(V_IO_N>,N2>)
VOJOX=DOT(V_JO_N>,N1>)
VOJOY=DOT(V_JO_N>,N2>)
VOKOX=DOT(V_KO_N>,N1>)
VOKOY=DOT(V_KO_N>,N2>)
VOLOX=DOT(V_LO_N>,N1>)
VOLOY=DOT(V_LO_N>,N2>)
VOMOX=DOT(V_MO_N>,N1>)
VOMOY=DOT(V_MO_N>,N2>)
VOXOX=DOT(V_XO_N>,N1>)
VOXOY=DOT(V_XO_N>,N2>)

VOWCOX=DOT(V_WCO_N>,N1>)
VOWCOY=DOT(V_WCO_N>,N2>)
VOWDOX=DOT(V_WDO_N>,N1>)
VOWDOY=DOT(V_WDO_N>,N2>)
VOWEOX=DOT(V_WEO_N>,N1>)
VOWEOY=DOT(V_WEO_N>,N2>)
VOWKOX=DOT(V_WKO_N>,N1>)
VOWKOY=DOT(V_WKO_N>,N2>)
VOWLOX=DOT(V_WLO_N>,N1>)
```

```
VOWLOY=DOT(V_WLO_N>,N2>)

%-------------------------------------------------------------------------------
-----------------------------------
%LINEAR ACCELERATIONS
%-------------------------------------------------------------------------------
-----------------------------------

A_O_N> = 0>
A_P1_N> = DT(V_P1_N>,N)
A_P2_N> = DT(V_P2_N>,N)
A_P3_N> = DT(V_P3_N>,N)
A_P4_N> = DT(V_P4_N>,N)
A_P5_N> = DT(V_P5_N>,N)
A_P6_N> = DT(V_P6_N>,N)
A_P7_N> = DT(V_P7_N>,N)
A_P8_N> = DT(V_P8_N>,N)
A_P9_N> = DT(V_P9_N>,N)
A_P10_N> = DT(V_P10_N>,N)
A_P11_N> = DT(V_P11_N>,N)
A_P12_N> = DT(V_P12_N>,N)
A_P13_N> = DT(V_P13_N>,N)
A_P14_N> = DT(V_P14_N>,N)
A_P15_N> = DT(V_P15_N>,N)
A_P16_N> = DT(V_P16_N>,N)
A_P17_N> = DT(V_P17_N>,N)
A_P18_N> = DT(V_P18_N>,N)
A_P19_N> = DT(V_P19_N>,N)
A_P20_N> = DT(V_P20_N>,N)
A_P21_N> = DT(V_P21_N>,N)
A_P22_N> = DT(V_P22_N>,N)
A_P23_N> = DT(V_P23_N>,N)
A_P24_N> = DT(V_P24_N>,N)
A_P25_N> = DT(V_P25_N>,N)
A_P26_N> = DT(V_P26_N>,N)
A_P27_N> = DT(V_P27_N>,N)
A_P28_N> = DT(V_P28_N>,N)
A_P29_N> = DT(V_P29_N>,N)
A_P30_N> = DT(V_P30_N>,N)
A_P31_N> = DT(V_P31_N>,N)
A_P32_N> = DT(V_P32_N>,N)

a2pts(n,a,p1,ao)

a2pts(n,b,p2,bo)
a2pts(n,c,p3,co)
a2pts(n,d,p5,do)
a2pts(n,e,p7,eo)
a2pts(n,f,p11,fo)
a2pts(n,g,p12,go)
a2pts(n,h,p14,ho)
a2pts(n,i,p15,io)
a2pts(n,j,p16,jo)
a2pts(n,k,p18,ko)
a2pts(n,l,p19,lo)
a2pts(n,m,p21,mo)
a2pts(n,x,p22,xo)

A_BALL_N> = DT(V_BALL_N>,N)

A2PTS(N,WC,P23,WCO)
A2PTS(N,WD,P25,WDO)
A2PTS(N,WE,P31,WEO)
A2PTS(N,WK,P29,WKO)
A2PTS(N,WL,P27,WLO)
```

```
%-------------------------------------------------------------------------------
-----------------------------------
%ANGLES FOR TORQUE CALCULATION
%-------------------------------------------------------------------------------
-----------------------------------
%CONVERT AUTOLEV ANGLES TO JOINT ANGLES

%FIND THE ROTATION OF THE THIGHS IN THE GCS IN ORDER TO CALCULATE THE HIP
ANGLE

%orientation of the Front thigh  in global reference frame
%Formula used is for ATAN2 (see wikipedia ATAN2 for info)
SPECIFIED AND',FTX',FTY'

FTX=POP5X-POP6X
FTY=POP6Y-POP5Y

AND=2*ATAN((SQRT(FTX^2+FTY^2)-FTX)/FTY)

%orientation of the Front thigh  in global reference frame

SPECIFIED ANK',BTX',BTY'

BTX=POP18X-POP8X
BTY=POP8Y-POP18Y

ANK=2*ATAN((SQRT(BTX^2+BTY^2)-BTX)/BTY)

%THE ROTATION OF THE UPPER ARMS DOESNT NEED TO BE FOUND SINCE THE SHOULDER
JOINT CENTRES
% DONT OVERTAKE ONE ANOTHER

AABF=Pi+q21
ABCF=Pi+q22
ACDF=Pi-q23

ADRF=q3+AND
AKRF=q3+ANK

AFSE=Pi+ASE+q26
AHSE=Pi+ASE+q29

AJIF=Pi-q27
AIHF=Pi-q28

%CALCULATE ANGLE FOR OPPOSITE JOINT ACTION

AABE=Pi-q21
ABCE=Pi-q22
ACDE=Pi+q23

ADRE=2*Pi-ADRF
AKRE=2*Pi-AKRF

AFSF=2*Pi-AFSE
AHSF=2*Pi-AHSE

AJIE=Pi+q27
AIHE=Pi+q28

%CONVERT AUTOLEV ANGULAR VELOCITIES TO JOINT ANGULUR VELOCITIES

WABF=DT(AABF,N)
WBCF=DT(ABCF,N)
WCDF=DT(ACDF,N)
WDRF=DT(ADRF,N)
```

```
WKRF=DT(AKRF,N)
WFSE=DT(AFSE,N)
WJIF=DT(AJIF,N)
WIHF=DT(AIHF,N)
WHSE=DT(AHSE,N)

%CALCULATE ANGULAR VELOCITIES FOR OPPOSITE JOINT ACTION

WABE=DT(AABE,N)
WBCE=DT(ABCE,N)
WCDE=DT(ACDE,N)
WDRE=DT(ADRE,N)
WKRE=DT(AKRE,N)
WFSF=DT(AFSF,N)
WJIE=DT(AJIE,N)
WIHE=DT(AIHE,N)
WHSF=DT(AHSF,N)
%-----------------------------------------------------------------------------
-----------------------------------

%-----------------------------------------------------------------------------
-----------------------------------
%SPRING POSITIONS & VECTORS (WOBBLING MASSES)
%-----------------------------------------------------------------------------
-----------------------------------

STRETCH1=MAG(P_P3_P23>)
STRETCH2=MAG(P_P5_P24>)
STRETCH3=MAG(P_P5_P25>)
STRETCH4=MAG(P_P6_P26>)
STRETCH5=MAG(P_P7_P31>)
STRETCH6=MAG(P_P9_P32>)
STRETCH7=MAG(P_P19_P27>)
STRETCH8=MAG(P_P18_P28>)
STRETCH9=MAG(P_P18_P29>)
STRETCH10=MAG(P_P8_P30>)

UVEC1>=UNITVEC(P_P3_P23>)
UVEC2>=UNITVEC(P_P5_P24>)
UVEC3>=UNITVEC(P_P5_P25>)
UVEC4>=UNITVEC(P_P6_P26>)
UVEC5>=UNITVEC(P_P7_P31>)
UVEC6>=UNITVEC(P_P9_P32>)
UVEC7>=UNITVEC(P_P19_P27>)
UVEC8>=UNITVEC(P_P18_P28>)
UVEC9>=UNITVEC(P_P18_P29>)
UVEC10>=UNITVEC(P_P8_P30>)

VELOCITY1 = DT(STRETCH1)
VELOCITY2 = DT(STRETCH2)
VELOCITY3 = DT(STRETCH3)
VELOCITY4 = DT(STRETCH4)
VELOCITY5 = DT(STRETCH5)
VELOCITY6 = DT(STRETCH6)
VELOCITY7 = DT(STRETCH7)
VELOCITY8 = DT(STRETCH8)
VELOCITY9 = DT(STRETCH9)
VELOCITY10 = DT(STRETCH10)

%FRONT FOOT

SPECIFIED RX1,RY1,RX2,RY2,RX4,RY4,RX22,RY22,RX21,RY21,RX20,RY20

RY1= -K11*POP1Y-K12*VOP1Y
RX1= (-K13*POP1X-K14*VOP1X)*RY1
```

```
RY2= -K15*POP2Y-K16*VOP2Y
RX2=(-K17*POP2X-K18*VOP2X)*RY2

RY4= -K19*POP4Y-K20*VOP4Y
RX4= (-K21*POP4X-K22*VOP4X)*RY4

TOTVF=RY1+RY2+RY4
TOTHF=RX1+RX2+RX4

%BACK FOOT

RY22= -K23*POP22Y-K24*VOP22Y
RX22= (-K25*POP22X-K26*VOP22X)*RY22

RY21= -K27*POP21Y-K28*VOP21Y
RX21=(-K29*POP21X-K30*VOP21X)*RY21

RY20= -K31*POP20Y-K32*VOP20Y
RX20= (-K33*POP20X-K34*VOP20X)*RY20

TOTVB=RY22+RY21+RY20
TOTHB=RX22+RX21+RX20

%-------------------------------------------------------------------------------
-----------------------------------
%FORCES
%-------------------------------------------------------------------------------
-----------------------------------

GRAVITY(G*N2>)

%FORCES ON THE SHOE FROM THE GROUND (FRONT FOOT)

FORCE(P1, RX1*N1>+RY1*N2>)
FORCE(P2, RX2*N1>+RY2*N2>)
FORCE(P4, RX4*N1>+RY4*N2>)

%FORCES ON THE SHOE FROM THE GROUND (BACK FOOT)

FORCE(P22, RX22*N1>+RY22*N2>)
FORCE(P21, RX21*N1>+RY21*N2>)
FORCE(P20, RX20*N1>+RY20*N2>)

%FORCES BETWEEN WOBBLING AND RIGID ELEMENTS

FORCE(P3/P23, (-K1*STRETCH1^3-K2*VELOCITY1)*UVEC1>)
FORCE(P5/P24, (-K1*STRETCH2^3-K2*VELOCITY2)*UVEC2>)
FORCE(P5/P25, (-K3*STRETCH3^3-K4*VELOCITY3)*UVEC3>)
FORCE(P6/P26, (-K3*STRETCH4^3-K4*VELOCITY4)*UVEC4>)
FORCE(P7/P31, (-K5*STRETCH5^3-K6*VELOCITY5)*UVEC5>)
FORCE(P9/P32, (-K5*STRETCH6^3-K6*VELOCITY6)*UVEC6>)
FORCE(P19/P27, (-K7*STRETCH7^3-K8*VELOCITY7)*UVEC7>)
FORCE(P18/P28, (-K7*STRETCH8^3-K8*VELOCITY8)*UVEC8>)
FORCE(P18/P29, (-K9*STRETCH9^3-K10*VELOCITY9)*UVEC9>)
FORCE(P8/P30, (-K9*STRETCH10^3-K10*VELOCITY10)*UVEC10>)

%FORCE BETWEEN HAND AND BALL (SET TO 0 AT BALL RELEASE)
FORCE(BALL/P17, (-K35*q19-k36*u19)*J1>+(-K37*q20-k38*u20)*J2>)

%JOINT TORQUES

VARIABLES BMTPTOR,BANKTOR,BKNETOR,FELBTOR,TORTOR,SHOTOR

ZEE_NOT = [BMTPTOR,BANKTOR,BKNETOR,FELBTOR,TORTOR,SHOTOR]

TORQUE(B/A, FMTPTOR*B3>)
```

```
TORQUE(C/B, FANKTOR*C3>)
TORQUE(D/C, FKNETOR*D3>)
TORQUE(R/D, FHIPTOR*R3>)

TORQUE(M/X, BMTPTOR*M3>)
TORQUE(L/M, BANKTOR*L3>)
TORQUE(K/L, BKNETOR*K3>)
TORQUE(R/K, BHIPTOR*R3>)

TORQUE(E/R, TORTOR*E3>)
TORQUE(E/S, SHOTOR*E3>)

TORQUE(S/F, FSHOTOR*S3>)
TORQUE(F/G, FELBTOR*F3>)

TORQUE(S/H, BSHOTOR*S3>)
TORQUE(H/I, BELBTOR*H3>)
TORQUE(I/J, BWRITOR*I3>)
%-------------------------------------------------------------------------------
-----------------------------------
%ENERGY
%-------------------------------------------------------------------------------
-----------------------------------
%Kinetic Energy
KECM=KE(A,B,C,D,E,F,G,H,I,J,K,L,M,X,WC,WD,WE,WK,WL,Ball)
KEA=KE(A)
KEB=KE(B)
KEC=KE(C)
KED=KE(D)
KEE=KE(E)
KEF=KE(F)
KEG=KE(G)
KEH=KE(H)
KEI=KE(I)
KEJ=KE(J)
KEK=KE(K)
KEL=KE(L)
KEM=KE(M)
KEX=KE(X)
KEWC=KE(WC)
KEWD=KE(WD)
KEWE=KE(WE)
KEWL=KE(WL)
KEWK=KE(WK)
KEBALL=KE(BALL)


%Potential Energy - Segments
PECM=-1*TotM*g*POCMY
PEA=-1*MA*G*POAOY
PEB=-1*MB*G*POBOY
PEC=-1*MC*G*POCOY
PED=-1*MD*G*PODOY
PEE=-1*ME*G*POEOY
PEF=-1*MF*G*POFOY
PEG=-1*MG*G*POGOY
PEH=-1*MH*G*POHOY
PEI=-1*MI*G*POIOY
PEJ=-1*MJ*G*POJOY
PEK=-1*MK*G*POKOY
PEL=-1*ML*G*POLOY
PEM=-1*MM*G*POMOY
PEX=-1*MX*G*POXOY
PEWC=-1*MWC*G*POWCOY
PEWD=-1*MWD*G*POWDOY
PEWE=-1*MWE*G*POWEOY
```

```
PEWK=-1*MWK*G*POWKOY
PEWL=-1*MWL*G*POWLOY
PEBALL=-1*MBALL*G*POBALLY

%Potential Energy - Wobbling mass springs

SPPEWC = 0.25*k1*(STRETCH1^4+STRETCH2^4)
SPPEWD = 0.25*k3*(STRETCH3^4+STRETCH4^4)
SPPEWE = 0.25*k5*(STRETCH5^4+STRETCH6^4)
SPPEWL = 0.25*k7*(STRETCH7^4+STRETCH8^4)
SPPEWK = 0.25*k9*(STRETCH9^4+STRETCH10^4)

%Potential Energy - Feet Springs (Needs adding in Fortran)

PEX1=Q1
PEY1=Q2
PEX2=POP2X
PEY2=POP2Y
PEX4=POP4X
PEY4=POP4Y
PEX22=POP22X
PEY22=POP22Y
PEX21=POP21X
PEY21=POP21Y
PEX20=POP20X
PEY20=POP20Y

TOTPE1
=SPPEWC+SPPEWD+SPPEWE+SPPEWL+SPPEWK+PEX1+PEY1+PEX2+PEY2+PEX4+PEY4+PEX22+PEY22
+PEX21+PEY21+PEX20+PEY20

TOTENE = TOTPE1 + KECM

%-------------------------------------------------------------------------------
-----------------------------------
%DEFINE VARIABLES TO BE EDITED IN FORTRAN
%-------------------------------------------------------------------------------
-----------------------------------
%FOOT 0 POSITIONS
CONSTANTS FF1,FF2,FF4,F22,F21,F20

%DEFINE FOOTFLAGS
FOOTFLAG1=q1
FOOTFLAG2=POP2X
FOOTFLAG4=POP4X
FOOTFLAG22=POP22X
FOOTFLAG21=POP21X
FOOTFLAG20=POP20X

%-------------------------------------------------------------------------------
-----------------------------------
%ANGULAR MOMENTUM & LINEAR MOMENTUM
%-------------------------------------------------------------------------------
-----------------------------------
AMOM>=MOMENTUM(ANGULAR,CM)
ZAMOM=DOT(AMOM>,N3>)
LMOM>=MOMENTUM(LINEAR)
XMOM=DOT(LMOM>,N1>)
YMOM=DOT(LMOM>,N2>)

%-------------------------------------------------------------------------------
-----------------------------------
%CONSTRAINTS
%-------------------------------------------------------------------------------
-----------------------------------
```

```
AUXILIARY[1]=u30
AUXILIARY[2]=u31
AUXILIARY[3]=u32
AUXILIARY[4]=u33
AUXILIARY[5]=u34
AUXILIARY[6]=u35

CONSTRAIN(AUXILIARY[u30,u31,u32,u33,u34,u35])

%-----------------------------------------------------------------------------
-----------------------------------
%EQUATIONS OF MOTION
%-----------------------------------------------------------------------------
-----------------------------------
ZERO = FR() + FRSTAR()
KANE(BMTPTOR,BANKTOR,BKNETOR,FELBTOR,TORTOR,SHOTOR)
%-----------------------------------------------------------------------------
-----------------------------------
%INPUTS - Time and Integration
%-----------------------------------------------------------------------------
-----------------------------------

INPUT TINITIAL=0, TFINAL=0.1
INPUT INTEGSTP=0.0001, PRINTINT=10
INPUT ABSERR=1.0E-08, RELERR=1.0E-07

%-----------------------------------------------------------------------------
-----------------------------------
%INPUTS - Spring Parameters
%-----------------------------------------------------------------------------
-----------------------------------

%Wobbling Mass Parameters

%FShank
INPUT K1=1.0E-07, K2=1.0E-07
%FLeg
INPUT K3=1.0E-07, K4=1.0E-07
%Trunk
INPUT K5=1.0E-07, K6=1.0E-07
%BShank
INPUT K7=1.0E-07, K8=1.0E-07
%BLeg
INPUT K9=1.0E-07, K10=1.0E-07

%Front Foot Parameters
INPUT [K11,K12,K13,K14,K15,K16,K17,K18,K19,K20,K21,K22]=1.0E-07

%Back Foot Parameters
INPUT [K23,K24,K25,K26,K27,K28,K29,K30,K31,K32,K33,K34]=1.0E-07

%Ball
INPUT [K35,K36,K37,K38] = 1.0E-07
%-----------------------------------------------------------------------------
-----------------------------------
%INPUTS - Gravity
%-----------------------------------------------------------------------------
-----------------------------------

INPUT G=-9.81

%-----------------------------------------------------------------------------
-----------------------------------
%INPUTS - Masses (Adds up to 85.163) Correct - Subject + Ball
%-----------------------------------------------------------------------------
-----------------------------------
```

```
INPUT ma = 0.228
INPUT mb = 1.148
INPUT mc = 1.1496
INPUT md = 1.2378
INPUT me = 10.6925
INPUT mf = 3.0900
INPUT mg = 1.6100
INPUT mh =  3.5292
INPUT mi = 1.4101
INPUT mj = 0.3950
INPUT mk = 1.2630
INPUT ml = 1.1637
INPUT mm = 1.133
INPUT mx = 0.209
INPUT mball = 0.163

INPUT mwc = 3.43
INPUT mwd = 9.3991
INPUT mwl = 3.4723
INPUT mwk = 9.5905
INPUT mwe = 31.6484

%-------------------------------------------------------------------------------
-----------------------------------
%INPUTS - Lengths
%-------------------------------------------------------------------------------
-----------------------------------

INPUT la = 0.0730
INPUT lb1 = 0.142,lb2 = 0.212
INPUT lc = 0.4920
INPUT ld = 0.4430
INPUT lf = 0.3530
INPUT lg = 0.508
INPUT lh = 0.358
INPUT li = 0.2970
INPUT lj = 0.1960
INPUT lk = 0.4620
INPUT ll = 0.471
INPUT lm1 = 0.139,lm2  = 0.211
INPUT lx = 0.0710
INPUT lwc = 0.4920
INPUT lwd = 0.4430
INPUT lwl = 0.471
INPUT lwk = 0.462

INPUT thetaB=0.628
INPUT thetaF=0.628

%-------------------------------------------------------------------------------
-----------------------------------
%INPUTS - COM POSITIONS FROM THE DISTAL END - (Fred's code gives proximal
from hip)
%-------------------------------------------------------------------------------
-----------------------------------

INPUT lao = 0.0433
INPUT lbo1 = 0.028,lbo2 = 0.109
INPUT lco = 0.2355
INPUT ldo = 0.231
INPUT lfo = 0.2161
INPUT lgo = 0.3453
INPUT lho = 0.2207
INPUT lio = 0.1716
INPUT ljo = 0.049
```

```
INPUT lko = 0.2215
INPUT llo = 0.246
INPUT lmo1 = 0.026,lmo2 = 0.108
INPUT lxo = 0.0411

INPUT lwco = 0.3031
INPUT lwdo = 0.2508
INPUT lwlo = 0.2801
INPUT lwko = 0.2660

%-------------------------------------------------------------------------------
----------------------------------
%INPUTS - INERTIAS
%-------------------------------------------------------------------------------
----------------------------------
INPUT ia = 0.0001
INPUT ib = 0.0008
INPUT ic = 0.0233
INPUT id = 0.0205
INPUT ie = 0.7750
INPUT if = 0.0353
INPUT ig = 0.0236
INPUT ih = 0.0412
INPUT ii = 0.0097
INPUT ij = 0.0013
INPUT ik = 0.0227
INPUT il = 0.0217
INPUT im = 0.0008
INPUT ix = 0.0001
INPUT iwc = 0.0586
INPUT iwd = 0.1539
INPUT iwl = 0.0545
INPUT iwk = 0.1686
INPUT iwe = 1.2568

%-------------------------------------------------------------------------------
----------------------------------
%INPUTS - Q's (positions and angles)
%-------------------------------------------------------------------------------
----------------------------------
%Origin to toe
INPUT Q1=1.0E-07
INPUT Q2=1.0E-07

%Origin of Trunk in GCS
INPUT Q3=90

%Wobbling Masses
INPUT Q4=1.0E-07,Q7=1.0E-07,Q10=1.0E-07,Q13=1.0E-07,Q16=1.0E-07
INPUT Q{5:6}=1.0E-07,Q{8:9}=1.0E-07,Q{11:12}=1.0E-07,Q{14:15}=1.0E-
07,Q{17:18}=1.0E-07

%Distance between Hand And Ball
INPUT Q{19:20}=1.0E-07

%Joint angles
INPUT Q21= -33 %Front foot ball
INPUT Q22= -25 %Front ankle
INPUT Q23= 10 %Front knee
INPUT Q24= 50 %Front hip
INPUT Q25= 90 %Back hip
INPUT Q26= 53 %Front shoulder
INPUT Q27= 27 %Bowling wrist
INPUT Q28= -20 %Bowling elbow
INPUT Q29= -200 %Bowling shoulder
```

```
%-------------------------------------------------------------------------------
-----------------------------------
%INPUTS - U's (velocities)
%-------------------------------------------------------------------------------
-----------------------------------
%Origin to toe
INPUT U1=1.0E-07
INPUT U2=1.0E-07

%Origin of Trunk in GCS
INPUT U3=1.0E-07

%Wobbling Masses
INPUT U4=1.0E-07,U7=1.0E-07,U10=1.0E-07,U13=1.0E-07,U16=1.0E-07
INPUT U{5:6}=1.0E-07,U{8:9}=1.0E-07,U{11:12}=1.0E-07,U{14:15}=1.0E-
07,U{17:18}=1.0E-07

%Distance between Hand And Ball
INPUT U{19:20}=1.0E-07

%Joint angular velocities
INPUT U21= 0 %Front foot ball
INPUT U22= 0 %Front ankle
INPUT U23= 0 %Front knee
INPUT U24= 0 %Front hip
INPUT U25= 0 %Back hip
INPUT U26= 0 %Front shoulder
INPUT U27= 0 %Bowling wrist
INPUT U28= 0 %Bowling elbow
INPUT U29= 0 %Bowling shoulder

%-------------------------------------------------------------------------------
-----------------------------------
%OUTPUTS
%-------------------------------------------------------------------------------
-----------------------------------

OUTPUT
T,POP1X,POP1Y,POP2X,POP2Y,POP3X,POP3Y,POP4X,POP4Y,POP5X,POP5Y,POP6X,POP6Y,POP
7X,POP7Y,POP8X,POP8Y,POP9X,POP9Y,POP10X,&
POP10Y,POP11X,POP11Y,POP12X,POP12Y,POP13X,POP13Y,POP14X,POP14Y,POP15X,POP15Y,
POP16X,POP16Y,POP17X,POP17Y,POP18X,&
POP18Y,POP19X,POP19Y,POP20X,POP20Y,POP21X,POP21Y,POP22X,POP22Y,POP23X,POP23Y,
POP24X,POP24Y,POP25X,POP25Y,POP26X,&
POP26Y,POP27X,POP27Y,POP28X,POP28Y,POP29X,POP29Y,POP30X,POP30Y,POP31X,POP31Y,
POP32X,POP32Y,POBALLX,POBALLY,POCMX,POCMY

OUTPUT
T,VOP1X,VOP1Y,VOP2X,VOP2Y,VOP3X,VOP3Y,VOP4X,VOP4Y,VOP5X,VOP5Y,VOP6X,VOP6Y,VOP
7X,VOP7Y,VOP8X,VOP8Y,VOP9X,VOP9Y,VOP10X,&
VOP10Y,VOP11X,VOP11Y,VOP12X,VOP12Y,VOP13X,VOP13Y,VOP14X,VOP14Y,VOP15X,VOP15Y,
VOP16X,VOP16Y,VOP17X,VOP17Y,VOP18X,&
VOP18Y,VOP19X,VOP19Y,VOP20X,VOP20Y,VOP21X,VOP21Y,VOP22X,VOP22Y,VOP23X,VOP23Y,
VOP24X,VOP24Y,VOP25X,VOP25Y,VOP26X,&
VOP26Y,VOP27X,VOP27Y,VOP28X,VOP28Y,VOP29X,VOP29Y,VOP30X,VOP30Y,VOP31X,VOP31Y,
VOP32X,VOP32Y,VOBALLX,VOBALLY,VOCMX,VOCMY

OUTPUT
T,POAOX,POAOY,POBOX,POBOY,POCOX,POCOY,PODOX,PODOY,POEOX,POEOY,POFOX,POFOY,POG
OX,POGOY,POHOX,POHOY,POIOX,&
POIOY,POJOX,POJOY,POKOX,POKOY,POLOX,POLOY,POMOX,POMOY,POXOX,POXOY,POWCOX,POWC
OY,POWDOX,POWDOY,POWEOX,POWEOY,POWKOX,&
POWKOY,POWLOX,POWLOY
```

```
OUTPUT
T,VOAOX,VOAOY,VOBOX,VOBOY,VOCOX,VOCOY,VODOX,VODOY,VOEOX,VOEOY,VOFOX,VOFOY,VOG
OX,VOGOY,VOHOX,VOHOY,VOIOX,&
VOIOY,VOJOX,VOJOY,VOKOX,VOKOY,VOLOX,VOLOY,VOMOX,VOMOY,VOXOX,VOXOY,VOWCOX,VOWC
OY,VOWDOX,VOWDOY,VOWEOX,VOWEOY,VOWKOX,&
VOWKOY,VOWLOX,VOWLOY

OUTPUT
T,Q1,U1,Q2,U2,Q3,U3,Q4,U4,Q5,U5,Q6,U6,Q7,U7,Q8,U8,Q9,U9,Q10,U10,Q11,U11,Q12,U
12,Q13,U13,Q14,U14,Q15,U15,Q16,U16,&
Q17,U17,Q18,U18,Q19,U19,Q20,U20,q21,u21,q23,u23,q24,u24,AXM,AXM',AML,AML',ALK
,ALK',AGF,AGF',q26,u26,q27,u27,q28,u28,&
q29,u29,ARE,ARE',ASE,ASE', q22,u22, q25, u25

OUTPUT
T,FMTPANG,FMTPW,FANKANG,FANKW,FKNEANG,FKNEW,FHIPANG,FHIPW,BMTPANG,BMTPW,BANKA
NG,BANKW,BKNEANG,BKNEW,BHIPANG,BHIPW,&
TORANG,TORW,SHOANG,SHOW,FSHOANG,FSHOW,FELBANG,FELBW,BSHOANG,BSHOW,BELBANG,BEL
BW,BWRIANG,BWRIW

OUTPUT
T,FMTPTOR,FANKTOR,FKNETOR,FHIPTOR,BMTPTOR,BANKTOR,BKNETOR,BHIPTOR,FELBTOR,FSH
OTOR,BWRITOR,BELBTOR,BSHOTOR,TORTOR,SHOTOR

OUTPUT T, RX1,RY1,RX2,RY2,RX4,RY4,RX22,RY22,RX21,RY21,RX20,RY20,
TOTHF,TOTVF,TOTHB,TOTVB

OUTPUT
T,KECM,KEA,KEB,KEC,KED,KEE,KEF,KEG,KEH,KEI,KEJ,KEK,KEL,KEM,KEX,KEWC,KEWD,KEWE
,KEWL,KEWK,KEBALL

OUTPUT
T,PECM,PEA,PEB,PEC,PED,PEE,PEF,PEG,PEH,PEI,PEJ,PEK,PEL,PEM,PEX,PEWC,PEWD,PEWE
,PEWK,PEWL,PEBALL,SPPEWC,SPPEWD,&
SPPEWE,SPPEWL,SPPEWK,PEX1,PEY1,PEX2,PEY2,PEX4,PEY4,PEX22,PEY22,PEX21,PEY21,PE
X20,PEY20,TOTPE1

OUTPUT T,ZAMOM,XMOM,YMOM, TOTENE

OUTPUT T,FOOTFLAG1,FOOTFLAG2,FOOTFLAG4,FOOTFLAG22,FOOTFLAG21,FOOTFLAG20, LSR,
LE,LWE,LS,LR

OUTPUT
T,AABF,AABE,ABCF,ABCE,ACDF,ACDE,ADRF,ADRE,AKRF,AKRE,AFSE,AFSF,AJIF,AJIE,AIHF,
AIHE,AHSE,AHSF

OUTPUT
T,WABF,WABE,WBCF,WBCE,WCDF,WCDE,WDRF,WDRE,WKRF,WKRE,WFSE,WFSF,WJIF,WJIE,WIHF,
WIHE,WHSE,WHSF

OUTPUT T, AND, ANK

%-------------------------------------------------------------------------
-----------------------------------
%UNITS
%-------------------------------------------------------------------------
-----------------------------------
UNITS T=s

UNITS  [K1,K3,K5,K7,K9,K11,K13,K15,K17,K19,K21,K23,K25,K27,K29,K31,K33,K35,K36]
= N
UNITS [K2,K4,K6,K8,K10,K12,K14,K16,K18,K20,K22,K24,K26,K28,K30,K32,K34]=N/M/S

UNITS
[ma,mb,mc,md,me,mf,mg,mh,mi,mj,mk,ml,mm,mx,mball,mwc,mwd,mwl,mwk,mwe]=KG
```

```
UNITS
[LR,LS,LE,LWE,LSR,la,lb1,lb2,lc,ld,lf,lg,lh,li,lj,lk,ll,lm1,lm2,lx,lwc,lwd,lw
l,lwk]=M

UNITS
[lao,lbo1,lbo2,lco,ldo,lfo,lgo,lho,lio,ljo,lko,llo,lmo1,lmo2,lxo,lwco,lwdo,lw
lo,lwko,lweo]=M

UNITS TOTM=M, TOTVF=N,TOTHF=N,TOTVB=N,TOTHB=N

UNITS
[POP1X,POP1Y,POP2X,POP2Y,POP3X,POP3Y,POP4X,POP4Y,POP5X,POP5Y,POP6X,POP6Y,POP7
X,POP7Y,POP8X,POP8Y,POP9X,POP9Y,POP10X,&
POP10Y,POP11X,POP11Y,POP12X,POP12Y,POP13X,POP13Y,POP14X,POP14Y,POP15X,POP15Y,
POP16X,POP16Y,POP17X,POP17Y,POP18X,&
POP18Y,POP19X,POP19Y,POP20X,POP20Y,POP21X,POP21Y,POP22X,POP22Y,POP23X,POP23Y,
POP24X,POP24Y,POP25X,POP25Y,POP26X,&
POP26Y,POP27X,POP27Y,POP28X,POP28Y,POP29X,POP29Y,POP30X,POP30Y,POP31X,POP31Y,
POP32X,POP32Y,POBALLX,POBALLY,POCMX,POCMY]=M

UNITS
[VOP1X,VOP1Y,VOP2X,VOP2Y,VOP3X,VOP3Y,VOP4X,VOP4Y,VOP5X,VOP5Y,VOP6X,VOP6Y,VOP7
X,VOP7Y,VOP8X,VOP8Y,VOP9X,VOP9Y,VOP10X,&
VOP10Y,VOP11X,VOP11Y,VOP12X,VOP12Y,VOP13X,VOP13Y,VOP14X,VOP14Y,VOP15X,VOP15Y,
VOP16X,VOP16Y,VOP17X,VOP17Y,VOP18X,&
VOP18Y,VOP19X,VOP19Y,VOP20X,VOP20Y,VOP21X,VOP21Y,VOP22X,VOP22Y,VOP23X,VOP23Y,
VOP24X,VOP24Y,VOP25X,VOP25Y,VOP26X,&
VOP26Y,VOP27X,VOP27Y,VOP28X,VOP28Y,VOP29X,VOP29Y,VOP30X,VOP30Y,VOP31X,VOP31Y,
VOP32X,VOP32Y,VOBALLX,VOBALLY,VOCMX,VOCMY]=M/S

UNITS
[POAOX,POAOY,POBOX,POBOY,POCOX,POCOY,PODOX,PODOY,POEOX,POEOY,POFOX,POFOY,POGO
X,POGOY,POHOX,POHOY,POIOX,&
POIOY,POJOX,POJOY,POKOX,POKOY,POLOX,POLOY,POMOX,POMOY,POXOX,POXOY,POWCOX,POWC
OY,POWDOX,POWDOY,POWEOX,POWEOY,POWKOX,&
POWKOY,POWLOX,POWLOY]=M

UNITS
[VOAOX,VOAOY,VOBOX,VOBOY,VOCOX,VOCOY,VODOX,VODOY,VOEOX,VOEOY,VOFOX,VOFOY,VOGO
X,VOGOY,VOHOX,VOHOY,VOIOX,&
VOIOY,VOJOX,VOJOY,VOKOX,VOKOY,VOLOX,VOLOY,VOMOX,VOMOY,VOXOX,VOXOY,VOWCOX,VOWC
OY,VOWDOX,VOWDOY,VOWEOX,VOWEOY,VOWKOX,&
VOWKOY,VOWLOX,VOWLOY]=M/S

UNITS [Q1,Q2,Q5,Q6,Q8,Q9,Q11,Q12,Q14,Q15,Q17,Q18,Q19,Q20]= M


UNITS [U1,U2,U5,U6,U8,U9,U11,U12,U14,U15,U17,U18,U19,U20]= M/S

UNITS
[Q3,Q4,Q7,Q10,Q13,Q16,Q21,Q22,Q23,Q24,AXM,AML,ALK,Q25,AGF,Q26,Q27,Q28,Q29,ARE
,ASE] = DEG

UNITS
[U3,U4,U7,U10,U13,U16,U21,U22,U23,U24,AXM',AML',ALK',U25,AGF',U26,U27,U28,U29
,ARE',ASE'] = DEG

UNITS [ia,ib,ic,id,ie,if,ig,ih,ii,ij,ik,il,im,ix,iwc,iwd,iwe,iwl,iwk] =
KG.M^2

UNITS [RX1,RY1,RX2,RY2,RX4,RY4,RX22,RY22,RX21,RY21,RX20,RY20] = N

UNITS
[FMTPTOR,FANKTOR,FKNETOR,FHIPTOR,BMTPTOR,BANKTOR,BKNETOR,BHIPTOR,FELBTOR,FSHO
TOR,BWRITOR,BELBTOR,BSHOTOR,TORTOR,SHOTOR] = NM
```

```
UNITS
[KECM,KEA,KEB,KEC,KED,KEE,KEF,KEG,KEH,KEI,KEJ,KEK,KEL,KEM,KEX,KEWC,KEWD,KEWE,
KEWL,KEWK,KEBALL] = J

UNITS
[PECM,PEA,PEB,PEC,PED,PEE,PEF,PEG,PEH,PEI,PEJ,PEK,PEL,PEM,PEX,PEWC,PEWD,PEWE,
PEWK,PEWL,PEBALL,SPPEWC,SPPEWD,&
SPPEWE,SPPEWL,SPPEWK,PEX1,PEY1,PEX2,PEY2,PEX4,PEY4,PEX22,PEY22,PEX21,PEY21,PE
X20,PEY20,TOTPE1,TOTENE] = J

UNITS [XMOM,YMOM] = KG.M/S

UNITS [ZAMOM] = KG.M^2/S

UNITS
[AABF,AABE,ABCF,ABCE,ACDF,ACDE,ADRF,ADRE,AKRF,AKRE,AFSE,AFSF,AJIF,AJIE,AIHF,A
IHE,AHSE,AHSF] = DEG

UNITS
[WABF,WABE,WBCF,WBCE,WCDF,WCDE,WDRF,WDRE,WKRF,WKRE,WFSE,WFSF,WJIF,WJIE,WIHF,W
IHE,WHSE,WHSF] = DEG

UNITS [AND,ANK] = DEG

UNITS G =m/s^2

%-------------------------------------------------------------------------------
-----------------------------------
%CODE AND SAVE
%-------------------------------------------------------------------------------
-----------------------------------
SAVE TDM.ALL
CODE DYNAMICS() TDM.FOR, SUBS

%-------------------------------------------------------------------------------
-----------------------------------
%END END END END END END END END END END END END END END END END END END END END
END END END END END END END END END
%-------------------------------------------------------------------------------
-----------------------------------
```